Flocculation Controls in a Hypertidal Estuary

UNIVERSITY OF LIVERPOOL

Thesis submitted in accordance with the requirements of the University of Liverpool for the degree of Doctor in Philosophy by

Rafael Ramírez-Mendoza

April 19, 2015

Abstract

Estuaries are ephemeral geological formations in constant change, which is being accelerated by human intervention. Fine sediments are an important characteristic of estuarine systems upon which anthropogenic and natural activities depend. An important feature of fine sediments is their cohesiveness, following which individual particles aggregate into the so-called flocs or break-up due to turbulent motions. Throughout the flocculation process (aggregation and break-up), flocs change their properties of size, density and settling velocity with consequences on suspended sediment transport, primary productivity and contamination. The prediction of possible changes in flocculation represents an important tool to help in decision making. Although some knowledge has been gained from laboratory and field investigations, the behaviour of the flocs in real conditions is still not well understood. Even though formulations to describe changes in floc dynamics have been proposed, there is a wide disparity between studies. The aim of this research is to contribute to the knowledge of the flocculation process and propose novel methods for the implementation in numerical models, via a case study in the Dee Estuary. The Dee is a hypertidal Estuary located in Liverpool Bay, with surface tidal currents over 1 $m \cdot s^{-1}$. The effects of turbulence generated by the strong tidal currents and waves on floc properties are of particular interest. The possibility of a simple formulation for the flocculation process is also investigated in order to be implemented in a state of the art coupling of hydrodynamic (POLCOMS), turbulence (GOTM) and waves (WAM) numerical models. To achieve these objectives, hourly data of grain size, volume concentration and current velocity from a mooring deployed in the Welsh Channel and water samples from a research vessel taken from 12 February to 9 March on 2008 have been used. The high sampling rate for the current velocities enables the calculation of turbulent stress, turbulent kinetic energy, shear rate, Kolmogorov microscale and dissipation. Mass concentrations were obtained from a series of water samples collected from a research vessel during the 12-14th February 2008, which were used to convert volume concentration into mass concentration.

Three hydrodynamic regimes have been distinguished from the observations: "current only" (negligible effect of waves), "combined currents-waves" (important effects from both forcings) and "wave dominant". Quarter-diurnal variability of floc size was present during the first two regimes. Observations showed aggregation of flocs

during periods of low turbulence with higher magnitude during low water slack than during high water slack. Break-up occurred concurrently with high turbulence periods during flood and ebb phases with higher magnitudes after ebb. Differences are likely due to turbulent stress asymmetries related with mixing and periodic stratification even though freshwater input was low. The "current only" regime was used to investigate the changes in floc settling velocities in relation with turbulent stress. A simple semi-empirical formulation was proposed and implemented in the numerical models. This expression depends on a single variable, which can be obtained from the turbulence model, and is both physically and mathematically correct. Model results qualitatively reproduced the neap-spring variability and the quarter-diurnal variability of floc settling velocities and suspended sediment concentration. During the "combined currents-waves" regime, waves were tidally modulated and led to enhanced aggregation and break-up, with higher floc size range than during the "current only" regime. Wave tidal modulation and quarter-diurnal variability of floc size were lost when waves were dominant. Flocs sizes exhibited a low range related to wave height. Inverse relationships between turbulent properties and median grain size were found for the three regimes, with higher scatter of data for the Kolmogorov microscale and shear rate due to different floc behaviour during flood and ebb phases. Turbulent kinetic energy showed a better relationship with floc size, which suggests its use as a floc size predictor instead of turbulent stresses.

Declaration

I certify that the work described in this thesis is my own except where otherwise stated and has not previously been submitted for any degree at this or any other university.

Rafael Ramírez-Mendoza

Contents

List of Figures

List of Tables

Acknowledgement

I would like to thank my supervisors Prof. Alejandro Souza, Dr. Laurent Amoudry and Prof. Andrew Plater, for their unlimited support, teaching, and guidance, without which this research would not have been possible. Thanks also to Dr. Jenny Brown for her role as unofficial supervisor. I was fortunate to have this team who were always committed to share their different skills and knowledge with me. I really appreciate their motivational words after meetings and PhD reviews. I have benefited throughout my study from their expertise in all aspects of this research, from data analyses, numerical modeling, scientific interpretation, conference attendance and scientific dissemination. I also developed my own skills through the rigorous peer reviews of published research that resulted in a high quality journal manuscript. I now aspire to continue collaborating with my supervisors in future research projects as my career develops.

Thanks to México, for funding this PhD through the Consejo Nacional de Ciencia y Tecnología (CONACyT) with the scholarship number 212026/306858 and to the Centro de Investigación Científica y Educación Superior de Ensenada (CICESE). In particular, to Luis Gustavo Álvarez, Guido Marinone, Luis Zavala and Miguel Lavín, for their support and believing in my capability to complete a PhD. Thanks also to the UK: National Environmental Research Council (NERC), National Capability funding to the National Oceanography Centre (NOC) and, the FORMOST (NE/E015026/1) and iCOASST (NE/J005444/1) projects, which also supported apects of my research.

Special thanks to my wife, Aglael, who always encouraged me to experience new things and face challenges. I admire her positive attitude that she has shown from the outset, even though things for her have also been difficult and stressful for her moving to the UK. She has been inspirational for me, knowing when I needed to relax and also when I needed to focus to achieve an important objective. She has patiently endured many long hours alone while I worked on my thesis. Her motivating words have given me the confidence I needed to complete this journey. There are no words to express my gratitude to her. I was only able to complete this adventure because she was here with me, making this, an achievement of both us. With all my love, thank you.

I thank to my parents for giving me the examples of dedication, hard work and honesty that have enabled me to get this far. They never pressured us (my brothers

and me) to have a professional career, but they told us two things, “do something you like to do” and “do it right”. They always mention how proud of me they are. I too am proud of them and grateful for inheriting their genes.

I also want to express my gratitude to the friends that I have made since my arrival. They have help me throughout this experience, Julio, Ruben, Rodolfo, Richard, Mark, Karen and the welcoming staff at the National Oceanography Centre have made my stay in the UK very easy and enjoyable.

Chapter 1

Introduction

1.1 Importance of Estuaries and Coastal Seas

The coastal zone has an important role because of the number of activities it supports. According to the United Nations organization (UN, 2011), the total population in coastal cities with over 750000 inhabitants is about 734 millions. However, no recent estimations have been made about the total population living in coastal areas which was considered to be between 37% and 60% by different authors (Cohen et al., 1997; Hinrichsen, 1998; Huntley et al., 2001). Huntley et al. (2001) also mentioned that 90% of the world fisheries was carried out in the coastal zone. In the United Kingdom, activities in the coastal zone include mineral resources, pipe lines, coastal based nuclear plants, wind farms, recreation areas, ports, ship routes, waste disposal and fisheries (Davidson and Buck, 1997).

Estuaries, salt marshes, dunes, and beaches are of special significance because they are the locations for ports and cities which have taken advantage of the natural shelter they provide for both inland and coastal navigation, fisheries and freshwater supply (Prandle, 2009). In addition, the strong interaction between sea, land and freshwater supply from rivers forms environments that are different from adjacent marine or freshwater systems. Even when mudflats exhibit low-diversity of species, high biodiversity can be found in the entire estuarine system: for example, over 750 species of invertebrates have been recorded in the Thames Estuary, UK (Kaiser et al., 2011). These mud flat invertebrates are important for birds, particularly migratory species, with for example 0.5 million shore birds migrating to British Isles every year. Many fish species also take advantage of the protection and food abundance for survival and use them as nurseries (Kaiser et al., 2011).

Unfortunately, human activities present a threat to estuarine ecosystems. Exploitation of biological and mineral resources, industrial and agricultural discharges are activities with high interference in marine ecosystems with sometimes immediate consequences and others after many years (Kaiser et al., 2011). In addition, climate change has consequences on sea-level-rise, wind speed, frequency and intensity of storms

(Kaiser et al., 2011). The sea level rise is of particular concern because of its impact on coastal and estuarine habitats (Cahoon et al., 2006). This has led to reconsider the important role of estuaries as protection zones. Arkema et al. (2013) modelled, for the United States of America, the risk of floods by sea level rise with and without coastal habitats and found that the damage to people and property most exposed could be decreased by half if coastal habitats were to remain fully intact. The knowledge of physical coastal processes is crucial toward good management, sustainability of the resources, and conservation of natural ecosystems.

1.2 Estuarine Processes

1.2.1 Definition and Origin

According to Pritchard (1967a), an estuary has three main characteristics: (i) it is a semi-enclosed coastal body of water, (ii) it has free communication to the open sea and (iii) fresh water supply from land that measurably dilutes sea water. The definition refers to the horizontal density gradients which result in landward subsurface flow and seaward surface flow. These are considered classic estuaries but those with little or no fresh water supply as in arid zones also exhibit these features because of the freshwater evaporation that causes longitudinal density gradients (Valle-Levinson, 2010). Estuaries began their formation after the last glacial term. Glacier melting caused carving and scraping of the valleys. Estuaries can also be formed by land subsidence and faulting (Pritchard, 1967a). After quaternary isostatic and eustatic changes in sea level played a relevant role and could even be related to the origin of submarine canyons (Steers, 1967). Morphology and dynamics of estuaries continued their major changes due to the retreat of the coast line because of the rise in sea level, the tectonic recovering and decrease of the ice cover after the end of the last glacial age (Prandle, 2009). Large flows of melted water after the glacial period excavated deep channels and in turn the deposition of available sediments (Prandle, 2009). Since their formation, estuaries have a transitional nature in their physiography form, the transition from fluvial to entirely marine and they are also transitional in time, with changes on the order of millions of years, more recent changes in the order of thousand years (glacial age) and the latest changes related with human intervention that have been played an important role (Steers, 1967). The supply and nature of fluvial sediments have changed because of the changes in the natural river flows as a result of farming, deforestation and damming. Therefore, the morphology of estuaries nowadays is the result of long-term large-scale effects together with recent consequences of human settlements and engineering works (Prandle, 2009).

1.2.2 Classification

Estuaries can be classified in different ways depending on their charachteristics. Based on tidal range, estuaries can be: (i) microtidal (<2 m range), (ii) mesotidal (2-4 m), (iii) macrotidal (4-6 m) and (iv) hypertidal (>6 m) (Archer, 2013). A geomophology classification is related with estuarine origin as: plain, fjord, bar-built, tectonic and rias. Coastal plain estuaries are the result of flooding of rivers by rising sea levels during the Pleistocene. Their width is of the order of several kilometres with depths of about 10 metres (Valle-Levinson, 2010). Fjords have depths of hundreds of metres and are narrow, also of the order of hundreds of metres resulting in a low width/depth ratio. An elongated channel and steep walls are present. Bar-built estuaries were embayments that became semi-enclosed because of the development of one or more sand bars between the coast and the sea. Some bars may develop separated from land as small islands and have more than one channel of communication between the estuary and the open sea. Faults in regions adjacent to the ocean that generated by earthquakes and fractures in the crust of the earth result in depressions which form tectonic estuaries when they are filled by the ocean. Rias are the result of a combination of processes of the drown of a river valley by sea level rise due to eustatic and tectonic changes and are common in Galicia, Spain (Evans and Prego, 2003).

There exist classifications based on waterbalance (freshwater and oceanic water supply) salinity vertical structure. However, these characteristics result in different circulation patterns which are included in hydrodynamic classifications (e.g. Hansen and Rattray, 1966; Pritchard, 1967b). Following the review by Valle-Levinson (2010), the classification is based on two hydrodynamic non-dimensional parameters which use the tidally averaged and cross-sectional averaged variables: the circulation parameter and the stratification parameter. The circulation parameter is defined as u_s/U_f. Where u_s is the near surface flow speed, which is commonly related to the freshwater discharge and of the order of 0.1 $\mathrm{m{\cdot}s^{-1}}$ while U_f is the sectional averaged flow. This flow is very small, nearly zero in estuaries where the water exchange is strong because the net flows inside and outside the estuary are similar. If the net inflow is weak, like in well-mixed and salt wedge estuaries, the magnitude of U_f will be similar to the seaward surface flow. Thus, the circulation parameter is >10 if the estuarine circulation is strong and nearly 1 if a unidirectional net outflow is present. The stratification parameter is $\delta S/S_0$, where δS is the salinity difference from top to bottom and S_0 the mean salinity over a cross-section of the estuary. A value of 1 means the stratification is as large as the mean salinity of the cross section. The stratification parameter becomes smaller as the stratification in the water column becomes weaker. The stratification parameter in most estuaries is <1.

The diffusive fraction ν_{da} can be used to represent the contributions of diffusive and advective portions of the salt flux of the estuary. The diffusive fraction is shown in

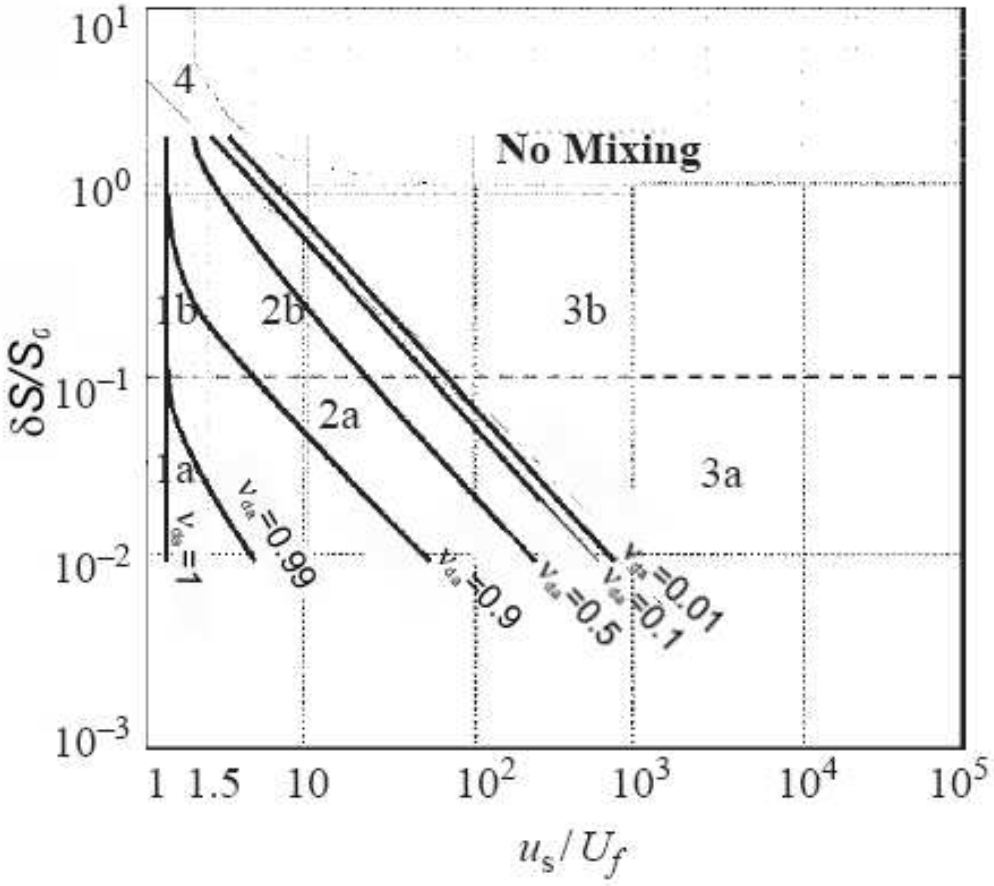

Figure 1.1: Clasification of estuaries based on the stratification $\delta S/S_0$ and circulation parameter u_s/U_f with the diffusive parameter ν_{da}. Seven estuary types can be distinguished, see text for explanation. Redrawn from (Hansen and Rattray, 1966).

figure 1.1 in terms of the circulation and stratification parameters. Type 1a estuaries are well mixed with strong tidal forcing and weak river discharge. Type 1b have large river discharge compared with tidal forcing. The diffusive processes dominate over the landward salt flow in type 1 estuaries ($\nu_{da} \approx 1$). In the type 2 estuaries the estuarine circulation is clear and the upstream salt transport has contributions of both diffusive and advective processes ($0.1 < \nu_{da} < 0.9$). Well mixed or weakly stratified are estuaries of type 2a while strongly stratified are classified as 2b estuaries. Type 3 estuaries have strong surface seaward flow and small depth averaged flows (u_s/U_f >100-1000) and commonly found in fjords. A moderate stratification is characteristic of type 3a estuaries while for type 3b the stratification is high. In type 3 estuaries the upstream transport of salt is due only to advective processes ($\nu_{da} < 0.01$). In type 4 estuaries have the flow is seaward, the stratification is high but the vertical structure is weak as in a salt wedge estuary. The trend in the ν_{ad} parameter is to converge which means both advective and diffusive processes produce salt transport.

Other non-dimensional numbers are used to classify the estuaries taking into account different processes and factors to describe the dynamics of the system, details can be found in cited references: Ekman and Kelvin numbers (Valle-Levinson, 2010), Wedderburn number (Bolaños et al., 2013), the horizontal Richardson number (Monismith et al., 1996) and the Stokes number (Souza, 2013).

1.2.3 Turbulence

Turbulence is associated with the vertical mixing of sediment in the water column. When the current increases, turbulence is produced as a result of the interaction with the bottom and stress acts over sea bed sediments. When this stress reaches a value above the critical bed shear stress, erosion takes place and sediment is taken into the water column. Therefore, turbulence characteristics are included in different flocculation prediction models (e.g., Winterwerp, 1998; Flesch et al., 1999; Ditschke and Markofsky, 2008). Following Umlauf and Burchard (2005), important quantities to ocean modelling can be defined as an ensemble mean ($\overline{u}$, $\overline{v}$) and a fluctuating part (u', v'). For the total current velocity components U, V and W in the coordinate directions x, y and z respectively:

$$U = \overline{u} + u' \tag{1.1}$$

$$V = \overline{v} + v' \tag{1.2}$$

The Navier-Stokes equations with Boussinesq approximation for fluids reduce to

$$\frac{\partial \overline{u}}{\partial t} - \nu \frac{\partial^2 \overline{u}}{\partial z^2} + \frac{\partial \overline{u'w'}}{\partial z} - f\overline{v} = -g\frac{\overline{\rho}(\zeta)}{\rho_o}\frac{\partial \zeta}{\partial x} \tag{1.3}$$

$$\frac{\partial \overline{v}}{\partial t} - \nu \frac{\partial^2 \overline{v}}{\partial z^2} + \frac{\partial \overline{v'w'}}{\partial z} + f\overline{v} = -g\frac{\overline{\rho}(\zeta)}{\rho_o}\frac{\partial \zeta}{\partial y} \tag{1.4}$$

where ν is the molecular diffusivity of momentum, f is the Corilis parameter, g is gravity acceleration, $\overline{\rho}$ averaged density, ρ_o a constant reference density from the Boussinesq approximation and ζ the elevation of the free surface. The mean buoyancy is obtained from:

$$B = -g\frac{\overline{\rho} - \rho_o}{\rho_o} \tag{1.5}$$

where the mean density follows an equation of state of the form $\overline{\rho} = \rho(T, S, P)$, with T, S and P, temperature, salinity and pressure, respectively. The turbulent fluxes in this approximation $\overline{u'w'}$ and $\overline{v'w'}$ lead to an undetermined system with more unknowns than equations in the closure problem. For the system to be solved, these fluxes need

to be determined. A widely used approach is the turbulent-viscosity hypothesis. According to this hypothesis and for simple shear flows, turbulent stresses are given by:

$$\overline{u'w'} = -\nu_t \frac{\partial U}{\partial z} \tag{1.6}$$

$$\overline{v'w'} = -\nu_t \frac{\partial V}{\partial z} \tag{1.7}$$

in which it is necessary to obtain the turbulent viscosity ν_t, in turn described as a product of an eddy velocity q and a length scale l. Several methods to achieve a specification of these quantities exist in the literature. However, different results could be obtained if different methods are used. Amoudry and Souza (2011b) have tested three turbulence closure models applied to sediment transport and morphological modelling and found different results. Nevertheless, the most common closure scheme is the k-ϵ model, where k is the turbulent kinetic energy and ϵ is the turbulent dissipation rate, both are obtained through modelled transport equations. This scheme is used in the present study and further details are given in section 4.2.

A turbulent flow in a channel can be divided in an inner region and an outer region (van Leussen, 1988). The inner region is adjacent to the bottom, covers about 10-20% of the water column and is directly affected by the bottom. The outer region covers about 80-90% of the water depth above the inner region, is indirectly affected by the bottom and influenced by conditions upstream. About 80% of the turbulence is produced in the inner region. Near to the bottom there is a thin layer called the viscous sublayer. Outside this sublayer, the inertial effects become more important until the flow is fully turbulent at a certain distance to the bottom. In a narrow buffer zone above the viscous sublayer, viscous and turbulent effects are comparable. Immediately above the buffer zone is the fully turbulent logarithmic zone where the velocity profile is logarithmic (Fig. 1.2). The logarithmic turbulent zone is described as (e.g. Tennekes and Lumley, 1972):

$$\frac{u(z)}{u_*} = \frac{1}{\kappa} ln \left(\frac{z}{z_0} \right) \tag{1.8}$$

where the rough or smooth conditions of the bed are taken into account in the roughness length z_0 and u_* the frictional velocity:

$$\tau_b = \rho {u^2}_* \tag{1.9}$$

with τ_b the turbulent shear stress at the bottom. In the outer region the deviation of the logarithmic profile is small and therefore the $k - \epsilon$ model is valid as it predicts a logarithmic velocity profile (Winterwerp and van Kesteren, 2004).

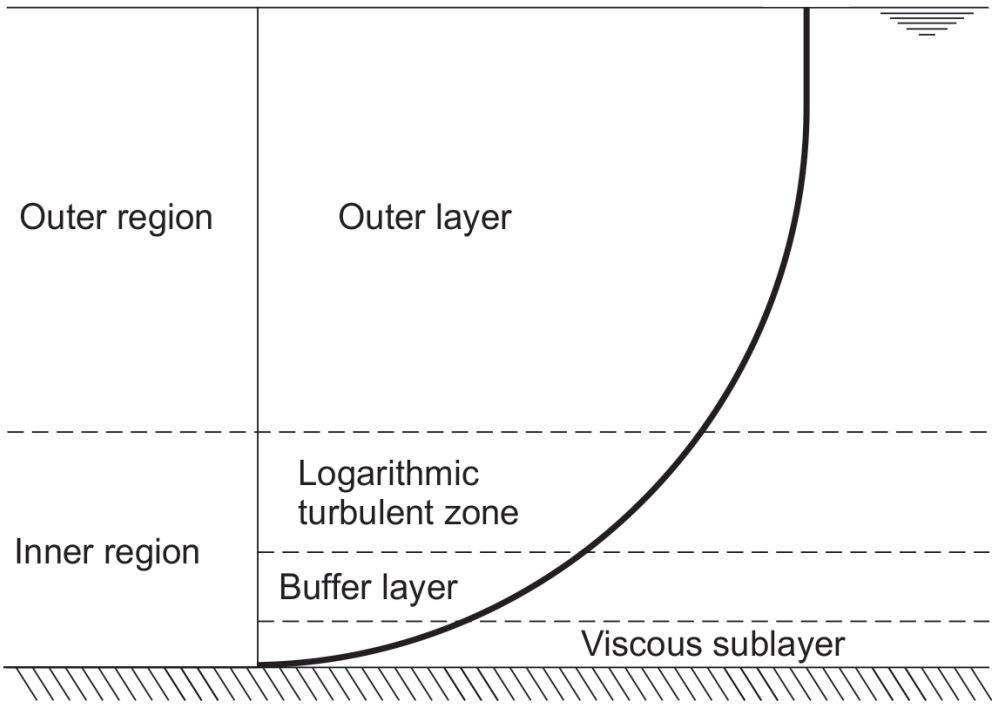

Figure 1.2: Vertical velocity profile and different zones of the boundary layer in a turbulent channel flow above a smooth bottom.

Table 1.1: Activities carried out in estuaries of the United Kingdom (Davidson and Buck, 1997).

1	Coast protection and sea defences
2	Barrage schemes
3	Power generation
4	Industrial, port and related development
5	Extraction and processing of natural gas and oil
6	Military activities
7	Waste discharge
8	Sediment extraction
9	Transport and comunication
10	Tourism and recreation
11	Wildfowling and hunting
12	Bait-collecting
13	Commercial fisheries
14	Cultivation of living resource
15	Management and killing of birds and mammals
16	Wildlife habitat management
17	Others

1.2.4 Estuaries in the United Kingdom

In the United Kingdom (UK) the coast line has many estuaries which vary in geomorphological origin, size, shape, freshwater supply and a variety of marine and coastal habitats. Altogheter, UK estuaries represent almost one-third of Western European resource (Davidson and Buck, 1997). According to the inventory of UK Estuaries (Davidson and Buck, 1997), 163 estuaries have been documented in England, Scotland, Wales and Northern Ireland covering a total of 5878.77 km^2 (Fig. 1.3). The Wash is the estuary that covers the most area with 666.54 km^2. Together, the estuaries are located along 9217.5 km of shoreline. A classification of the estuaries of England and Wales can be seen in Figure 1.4 by Prandle et al. (2006), in which the authors divided the estuaries within four major groups: Bar Built, Coastal Plain, Ria and others. A minority consists of more complex systems and difficult to fit in a particular category. The tidal range of the estuaries in UK varies from 1.2 m in Christchurch Harbour to 12.3 m in the Severn Estuary with most of the estuaries considered macrotidal in the classification of Davidson and Buck (1997). However, 34 estuaries present tidal ranges of more than 6 metres and can be considered as hypertidal and representing 20% of the total estuaries. The variety of activities related with the estuaries in UK is presented in the table 1.1 based on Davidson and Buck (1997).

In a more recent study, available data from the literature were compiled and some parameters were calculated (Manning, 2012). Data of river flow, tidal current and concentration of suspended sediments are presented in table 1.2.

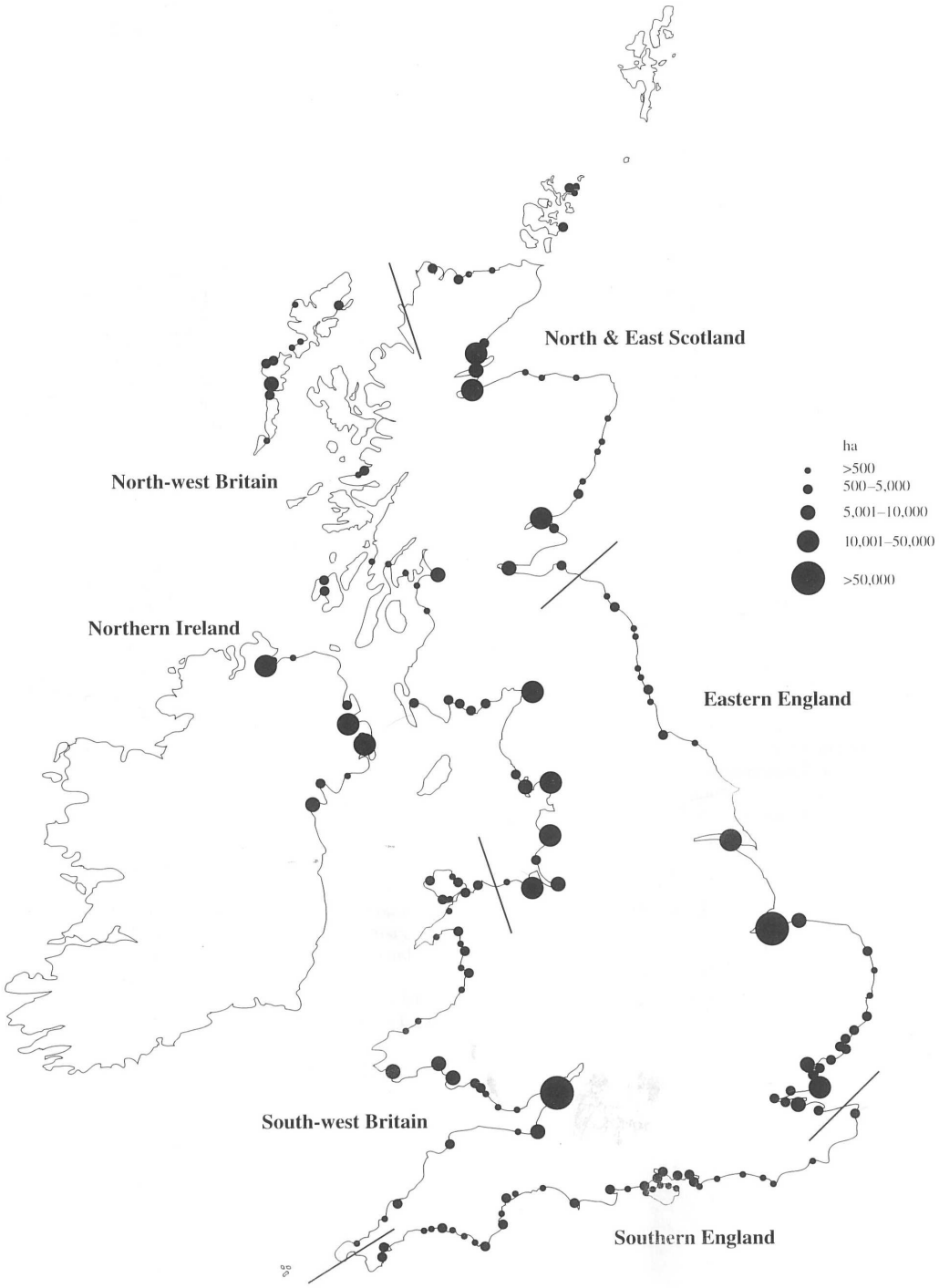

Figure 1.3: Distribution and size (1 ha=0.01 km^2) of estuaries in the United Kingdom divided by areas (Davidson and Buck, 1997).

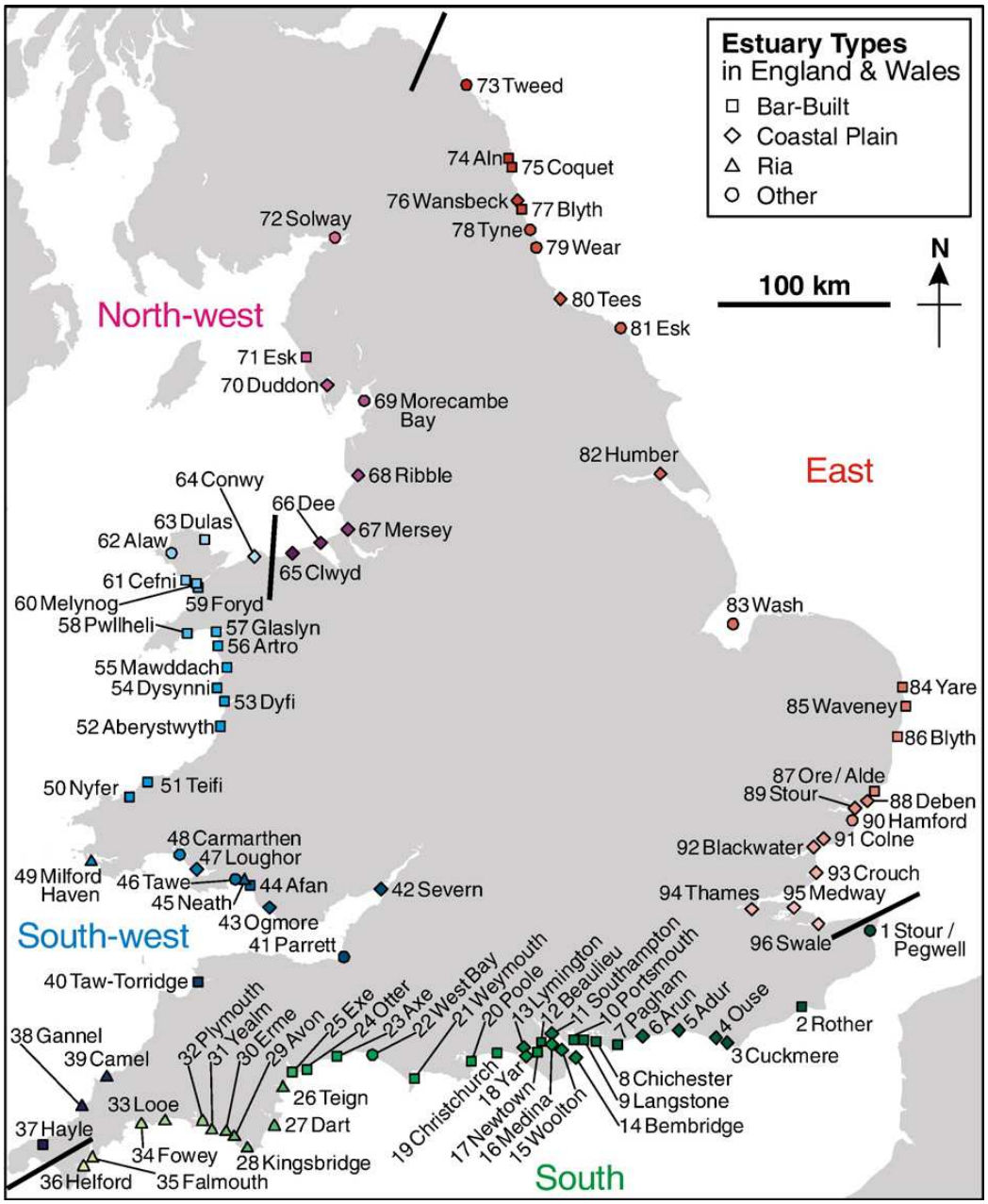

Figure 1.4: Classification of estuaries of England and Wales as presented by Prandle et al. (2006) based on data reported by Davidson and Buck (1997).

Table 1.2: Parameters calculated for estuaries in the United Kingdom using available data (Manning, 2012). Estuary numbers are consistent with numbers in figure 1.4. Kin.=Kingsbridge, Sal=Salcombe, SPM=Suspended particulate matter.

	Estuary Name	River flow $m^3 \cdot s^{-1}$	Tidal current $m \cdot s^{-1}$	SPM $mg \cdot l^{-1}$		Estuary Name	River flow $m^3 \cdot s^{-1}$	Tidal current $m \cdot s^{-1}$	SPM $mg \cdot l^{-1}$
1	Stour-Pegwell	3.24	0.66	83.83	44	Afan	18.92	1.21	506.70
2	Rother	0.52	0.71	101.90	45	Neath	37.84	1.27	584.56
3	Cuckmere	1.60	1.21	509.81	46	Tawe	11.35	1.00	281.90
4	Ouse x	3.10	1.35	707.97	47	Loughor	1.89	0.97	260.94
5	Adur	1.16	0.94	233.76	48	Carmarthen	50.76	0.89	202.30
6	Arun	4.20	1.29	612.78	51	Teifi	28.70	0.61	63.76
7	Pagham Hrb	0.10	0.68	89.70	52	Aberystwyth	6.06	1.63	1229.19
8	Chichester Hrb	0.63	0.64	75.84	53	Dovey	23.17	0.73	109.28
9	Langstone Hrb	0.40	0.65	76.81	54	Dysynni	4.51	0.69	94.36
10	Portsmouth	0.63	0.66	81.43	57	Glaslyn	5.97	0.67	87.17
11	Southampton	16.73	0.71	100.90	58	Pwllheli	0.61	0.69	92.32
12	Beaulieu	0.10	0.57	52.20	59	Foryd Bay	2.13	0.67	84.61
18	Lymington x	15.00	0.53	42.54	66	Dee	31.24	1.21	512.34
13	Bembridge x	0.22	0.56	50.10	67	Mersey	12.56	1.11	387.22
14	Wootton Crk	0.10	0.59	59.01	68	Ribble	33.33	0.93	232.26
15	Medina x	0.22	0.70	99.79	69	Morecambe	59.90	0.99	275.25
16	Newtown	0.20	0.54	44.24	70	Duddon	5.17	0.96	255.94
17	Yar	0.30	0.52	39.48	71	Esk	7.24	0.94	239.01
19	Christchurch	14.98	0.50	35.71	72	Solway	92.26	1.10	376.64
20	Poole	6.09	0.49	33.41	73	Tweed	79.65	0.66	82.86
21	Weymouth	1.90	0.56	48.84	74	Aln	3.40	0.55	47.81
23	Axe	5.34	0.60	62.52	75	Coquet	8.63	0.60	62.06
24	Otter	5.40	0.77	131.46	76	Wansbeck	3.20	0.77	130.97
25	Exe	16.23	0.65	79.48	77	Blyth NE	2.13	0.63	72.75
26	Teign	1.26	0.68	88.30	78	Tyne	45.40	0.68	88.66
27	Dart	1.26	0.70	96.05	79	Wear	11.29	0.64	75.71
28	Kin. and Sal.	11.50	0.70	97.57	80	Tees	16.90	0.67	84.99
29	Avon	3.62	0.70	98.36	81	Esk	5.90	0.70	99.10
30	Erme	2.10	0.75	119.63	82	Humber	85.65	0.84	168.79
31	Yealm	1.88	0.78	133.03	83	Wash	20.30	1.00	282.93
32	Plymouth	22.77	0.75	122.22	84	Yare	2.90	0.52	39.71
33	Looe	2.21	0.69	93.38	85	Waveney	1.82	0.55	47.54
34	Fowey	4.93	0.75	118.50	86	Blyth EA	0.50	0.49	33.61
35	Falmouth	2.13	0.90	206.52	87	Ore/Alde	0.60	0.52	40.17
36	Helford	4.77	0.78	136.31	88	Deben	0.20	0.54	44.89
37	Hayle	1.03	0.68	91.22	89	Harwich	3.05	0.60	61.33
38	Gannel	0.71	0.89	204.75	90	Hamford	0.20	0.59	57.82
39	Camel	6.12	0.83	160.57	91	Colne	1.08	0.64	74.31
40	Taw-Torridge	34.41	0.95	248.53	92	Blackwater	3.09	0.73	110.37
41	Parrett	1.21	1.06	339.04	93	Crouch	1.08	0.71	100.85
42	Severn	77.80	1.79	1651.97	94	Thames	66.32	0.91	212.63
43	Ogmore	7.57	1.14	418.14	95	Medway	11.44	0.65	79.20

1.3 The Role of Sediments

A distinctive characteristic of estuaries are the extensive mudflats composed of soft, fine, grey silt and a distinctive sulphurous odour when disturbed (Kaiser et al., 2011). Estuarine mud is a combination of deposited sediments consisting in debris and biogenic material which are unstable at the bottom resulting in rapid chemical changes related with the decomposition of organic matter which are important for the oxygen content of the bottom water, the recycling of nutrients and the amounts and nature of organic carbon (McKee et al., 2004). The chemical changes at the bottom deliver nutrients to the system. However, another important factor is light availability, which stimulates phytoplankton, the use of the dissolved inorganic nutrients, and lead to increase primary production by microbial processes (Dagg et al., 2004). This process has been identified by the presence of maxima of phytoplankton biomass and productivity in estuarine systems and are associated with the decrease in turbidity and high levels of nutrients (Dagg et al., 2004). The addition of chemical constituents to the food chain mainly depends on the size of the materials (dissolved, colloidal and particulate) from which, colloids are more important than particulates for sorption and desorption reactions but also they accumulate contaminant substances (McKee et al., 2004). These natural resources have a direct effect in all the estuarine ecosystems. Therefore, fine sediments in an estuary are related with the water quality in three aspects: turbidity, oxygen depletion, microcontaminant transport and nutrient release (Parker et al., 1994). The diversity of organisms that primarily depend on the estuarine resources are phytoplankton, zooplankton and larger organisms (polichaetes, nematodes, crustaceans, fish and molluscs). Although different distribution of organisms is found along the estuaries, it has also been suggested that their distribution depends on the availability of the mud habitat rather than the salinity levels (Kaiser et al., 2011). Thus, estuaries are a nursery ground for marine species of fish. Turbid waters may give protection to juveniles against predators.

At a larger scale, sediments in estuaries are related with many human activities (see for example table 1.1). Figure 1.5 shows the different processes in the estuaries in general. The main characteristic of the estuaries, as places of constant change, is not taken into account when the resources are used. Most of the change is related to the movement of sediments in the estuary in the processes of erosion and deposition. Sediment erosion could lead to populated areas to be unprotected against extreme weather, the disappearance of an entire ecosystem and recreation areas of economic importance. Also, the erosion can affect the stability of oil rigs, pipe and communication lines on the seabed. On the other hand, deposition of sediments could block navigation channels. Although erosion and deposition are processes occurring in a natural form, human intervention plays a relevant role in the increase or decrease of the normal rates. Either of natural or human origin, the changes affect the estuarine sediment transport.

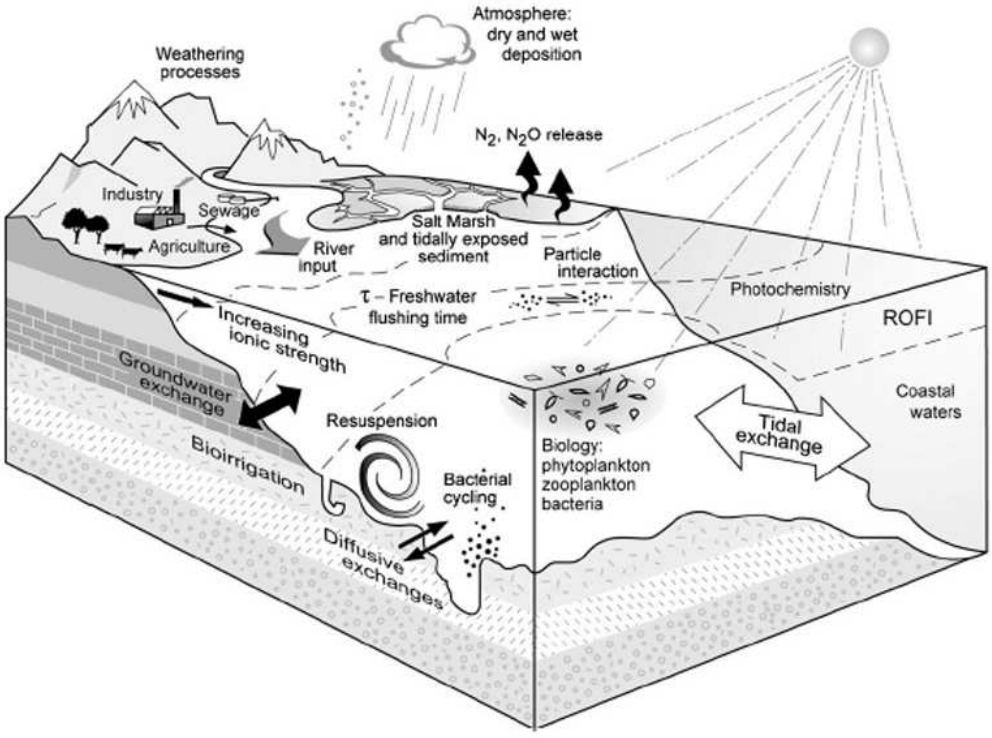

Figure 1.5: Different processes in estuaries (Geertz et al., 2012).

A good understanding of the sediment dynamics in the estuary is important for a good management of the resources. In general, the variables that need to be taken into account for sediment transport are shown in table 1.3 (Dyer, 1986).

In the particular case of estuaries, the property of cohesion leads fine sediments to form bigger particles called aggregates or flocs. However, the process is reversible and flocs can also be disaggregated. Following Winterwerp and van Kesteren (2004), in this study, the combined processes of aggregation and disaggregation of cohesive sediments is called flocculation. The flocculation process involves temporal and spatial changes of some variables in table 1.3: sediment size, shape, density and settling velocity. Floc behaviour changes due to forcings of tidal currents and stresses. In some cases, high sediment concentrations can also modify the flow. Although many studies have been made about particle flocculation, the process is still not well understood. Some studies include laboratory experiments under controlled conditions, with the use of artificial particles and are time consuming because of the difficulty to measure in the field. In recent years, the advance in new technologies has enabled to obtain longer field observations of some variables and compare the results with those of numerical models. The sediment dynamics and in particular the flocculation process will be developed in the next chapter.

Table 1.3: Important variables for sediment transport (Dyer, 1986).

Sediment size, shape, density and minaralogy of grains
Sediment settling velocity
Sediment availability
Flow depth
Water density, viscosity
Bed shear stress
Bed form wavelength, height, steepness
Maximum tidal velocity
Residual tidal velocity
Wave period, amplitude

Chapter 2

Estuarine Sediment Dynamics

This chapter provides a description of the current state of knowledge for sediment transport in general. The aim is to give an insigth of the variables and processes involved. The basics of sediment transport in general are mentioned in the next section. Section 2.2 explains the cohesive property of fine sediments with the aim of understanding the complexity between these sediments and that of cohesionless particles like sand, although it is important to note that the present work is focused on the dynamics of the flocs in an estuarine environment. This is explained in section (2.3) with an overview of the main processes and factors related with sediment flocculation. Finally, the last section (2.7) describes three different models or approximations to the prediction of the flocculation process. Most of the approximations found in the literature are modifications of these three models. The issues with the application or implementation of these models is also mentioned in the section.

2.1 Sediment transport

This section briefly reviews the basics of mainly non cohesive sediment dynamics before to continue with the complexity that flocculation adds to the process. The movement of sediment is a cyclic mechanism consisting of suspension from the bottom, transport, sedimentation and resuspension again. The transport of sediment can be classified in different ways. According to Dyer (1986), the sediment on the bottom begins its movement through rolling, continues through saltation and then as suspension. Rolling and saltation can be classified as bed load while suspension as suspended load and some sediment consisting of very fine particles, not represented in the bed, is also present as wash load (Fredsøe and Deigaard, 1992). Figure 2.1 shows the modes of sediment transport, which also distinguishes a sliding movement of gravel sediment. Particles on the bottom experience a drag force when exposed to a flowing fluid. The particles in turn disturb the flow, which accelerates over the top of the particle and causes a lowering in pressure and a difference vertically across the grain resulting in a lift force.

For the particles to start its movement, lift and drag forces should generate a larger

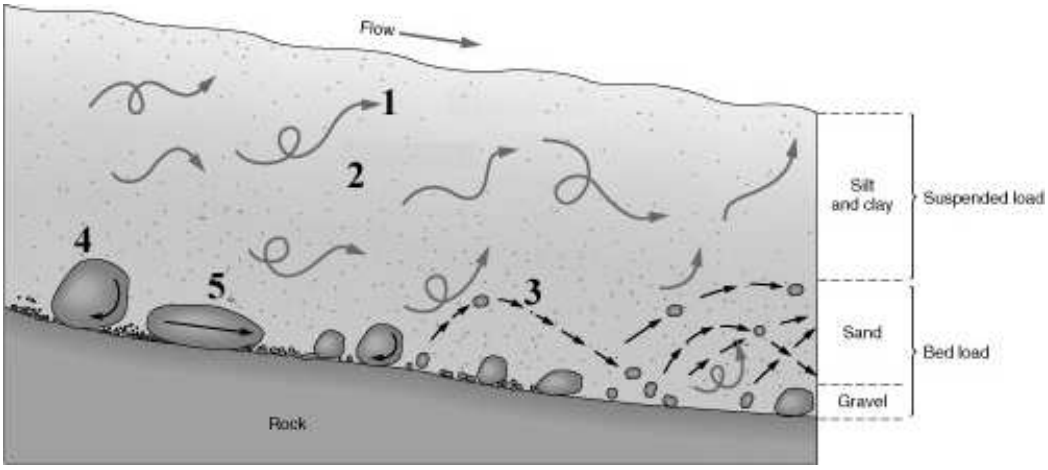

Figure 2.1: Sediment transport modes: 1) wash load, 2) suspended load, 3) saltation, 4) rolling and 5) sliding.

bottom shear stress τ than a critical threshold value τ_{cr}. This is represented in the Shields dimensionless parameter θ_c:

$$\theta_c = \frac{\tau_{cr}}{(\rho_s - \rho_w)gD} \tag{2.1}$$

where ρ_w is fluid density, ρ_s is sediment density, g is gravity acceleration and D is the particle diameter. Once sediments are in suspension, it is necessary to know their vertical concentration distribution (C_z). Assuming steady state conditions and no mean vertical velocity, the Rouse Equation (Rouse, 1937) or Vanoni-distribution (Fredsøe and Deigaard, 1992) can be used:

$$\frac{C_z}{C_a} = \left(\frac{h-z}{z} \cdot \frac{a}{h-a}\right)^{\frac{W_s}{\beta\kappa u_*}} \tag{2.2}$$

where C_a is a reference concentration measured near the bottom at a distance a, z is the height over the bottom and h the total column height. The exponent is called the Rouse number and depends on the settling velocity of the sediment W_s, β is a proporcionality constant, κ the von Karman constant and u_* is the friction velocity. The equation predicts, for example, high concentration throughout the water column for small grains and faster flow while concentration is limited near the bottom for large grains and slow flow. The sediment transport rate can be obtained as:

$$q = \int_a^h uCdz \tag{2.3}$$

Nevertheless, other parameters also play important roles. Sediments composed of grains of different sizes are not taken into account in previous formulations, each size population with different critical shear stress and therefore different vertical distribution and transport. The movement of the sediment also creates ripples at the seabed which

are capable to affect the flow. A roughness factor is commonly used to include the ripple effect. However, recent investigations have shown that the roughness factor is not sufficient to predict suspended sediment concentrations and it is also necessary to modify the sediment diffusivity (Amoudry et al., 2013). Extremely high concentrations can also modify the turbulent flow field and change its effect on the seabed. In addition, the formulations mentioned above take into account a steady state of the flow and this in nature is modified by oscillatory flows (waves) which complicates the correct assessment of suspended sediment concentrations. However, on the average and under certain assumptions, the transport of cohesionless suspended sediments can be well predicted. A different challenge is present when sediments have enough clay minerals to make sediments form aggregates which depending on the flow conditions can also be disaggregated in the process of flocculation. The diffusion-advection-settling equation for sediments is:

$$\frac{\partial C}{\partial t} + u\frac{\partial C}{\partial x} + v\frac{\partial C}{\partial y} + w\frac{\partial C}{\partial z} = \frac{\partial}{\partial z}\left(K_s\frac{\partial C}{\partial z}\right) - W_s C \tag{2.4}$$

which represents the mass balance of suspended sediments. The eddy diffusivity for the sediment K_s needs to be obtained using a closure scheme in equations 1.3 and 1.4. At first sigth the equation looks simple, but each sediment class (i) should have its own equation with corresponding concentration and settling velocity ($C^{(i)}$, ${W_s}^{(i)}$). Therefore, when sediments are cohesive, the determination of each aggregate class settling velocity and concentration becomes important for the mass balance. Moreover, boundary conditions, particularly at the bottom are crucial for the sediment availability in the water column. Therefore, deposition and erosion need to take into account cohesive sediments.

Erosion processes depend on bed sediment features such as concentration and sediment distribution, thus on consolidation processes. Biological activity is important for consolidation as it acts as stabiliser or destabiliser. Erosion due to bio-stabiliser organisms on mud flats could be several times stronger than hydrodynamic effects according to the results of Spearman and Manning (2008). Organisms also produce sticky substances that promote the aggregation of organic and inorganic particles resulting in the increase of floc size and strength (Winterwerp and van Kesteren, 2004). However, Winterwerp et al. (2006) include the effects of biological factors but their results do not appear to be affected either by this or by sediment concentration which also has been mentioned as playing an important role in the process. Nevertheless, Maggi (2009) was not able to reproduce the floc sizes until the biology factor was taken into account.

When currents are weak sediment falls to the bottom. The quantity of settled sediment determines the availability to be eroded to the water column. This depends on the inputs of sediment from rivers or a large accumulation during long periods of

low current speed. If sediment continues settling, more flocs accumulate and due to their own weight, the pore size of deposited sediments diminishes while density and shear resistance increase. This process leads to the increase of critical bed shear stress, which is an important parameter for the erosion of the sea bed. A well consolidated sea bed has a higher value of bed shear stress and more energy is needed for bed erosion. Thus the critical bed shear stress has been found to vary with depth of the sediments (e.g. Schweim and Köngeter, 2008). Other factor related with the magnitude of the shear stress is the bottom roughness which depends on the grain roughness, bed load transport and ripples. According to van Rijn (2007a) the degree of exposure of a grain with respect to the surrounding grains is also important when current acts on the sea bed.

Therefore, turbulent shear stress becomes an important parameter as it determines both the magnitude of sediment erosion from the bottom to the water column and the magnitude of sediment that can be settled. Based on experiments, the erosion rate E has been defined as (Partheniades, 1965):

$$E = M\left(\frac{\tau_b}{\tau_{ce}} - 1\right) \tag{2.5}$$

where M is an erosion rate parameter, τ_b turbulent bed shear stress and τ_{ce} a critical turbulent stress for erosion. If turbulent stresses τ_b are higher than τ_{ce} erosion takes place. More recently, Sanford and Maa (2001) proposed the following formula:

$$E = \rho_s(1 - p_c(z))E_0\left(\frac{\tau_b}{\tau_{ce}(z)} - 1\right) \tag{2.6}$$

where the porosity of the bed is included as p_c and E_0 is a site specific constant. According to Larsen et al. (2009), a value for the critical bed shear stress for erosion is $1{\times}10^{-2}$ Pa and a value for the erosion flux is of the order of $1{\times}10^{-9}$ kg·m^{-1}·s^{-1}. For Schweim and Köngeter (2008), with experiments in a laboratory and artificial particles, the shear stress value could be 0.6 Pa depending on bottom consolidation and the erosion flux was $9.4{\times}10^{-6}$ kg·m^{-2}·s^{-1}. However, bed shear stress of 2 Pa has been obtained from observations by Álvarez (2010). Therefore, sediment resuspension depends on the particular sea bed and turbulent characteristics of the study site, wich result in different values of τ_c. Turbulence damping may also be present if the vertical density is very large and modifies the turbulent structure, leading to a decrease of turbulent diffusion of sediment and reduced shear stress (Spearman and Manning, 2008).

Deposition (D_s) has been defined by Krone (1962) as:

$$D_s = \left(1 - \frac{\tau_b}{\tau_{cd}}\right) W_s C \tag{2.7}$$

where τ_{cd} is a critical stress for deposition, C is suspended sediment concentration and W_s the settling velocity of the flocs. However, results of Sanford and Halka (1993)

showed that the formulation failed to reproduce field observations from different sites and suggested a simple flux formulation:

$$D_s = W_s C \tag{2.8}$$

where W_s can be a function of time but constant in the water column. This suggest that the formulation of Krone (1962) is limited to laboratory experiments. Although there are some formulations to parameterise the settling velocity, the well-known Stokes law is commonly used:

$$W_s = \frac{g\rho_e D_f^2}{18\mu} \tag{2.9}$$

where g is gravity acceleration, ρ_e is floc density, D_f is floc diameter and μ is the dynamic viscosity of the fluid. Aggregates have been also considered to have self similar structures and lead to treat them as fractals (Kranenburg, 1994). Settling velocities taking into account this theory have been developed with constant (Winterwerp, 1998) and variable fractal numbers (Khelifa and Hill, 2006). These formulations will be shown in Chapter 5. In summary, the transport of sediment could be seen as a simple sequence of erosion, suspension, settling and deposition. However, the process is complicated because of the particle aggregation and breakup. The properties responsible for the cohesive behaviour of the particles will be explained in next section.

2.2 Cohesive Sediments

Cohesive sediments consist of granular organic and mineral solids in a liquid phase which in the marine environment are clay, silt, fine sand, organic material and occasionally gas (Winterwerp and van Kesteren, 2004). Cohesive sediment is also known as mud, for which particle sizes are smaller than 62.5 μm. In general, the silt, sand and clay parts are present in a mixture and the clay-silt fraction determines its cohesiveness: when clay-silt fraction is >0.3 the sediment is cohesive and non cohesive when the sand fraction is >0.7 (van Rijn, 2007a). Although the degree of cohesion of the sediment depends on the relation of clay particles and organic content with water chemical properties (Winterwerp and van Kesteren, 2004), the clay is the most important part and the sediment is cohesive if the clay fraction is about 5-10% (van Rijn, 2007a). The mineral fraction of sediments is composed mainly of silicates: the silt fraction (>2 μm, <63 μm) mainly of quartz, feldspar and carbonates while clay minerals (<2 μm) of kaolinite, illite, smectite and chlorite (Winterwerp and van Kesteren, 2004). The cohesion of clay minerals is due to the flat shape and size of the particles with their surface area and electrical charge interacting with ambient water. The shape of clay minerals consist mainly of two-dimensional silica tetrahedra with octahedra of aluminium-hydroxide or magnesium-hydroxide (gibbsite or brucite respectively) which

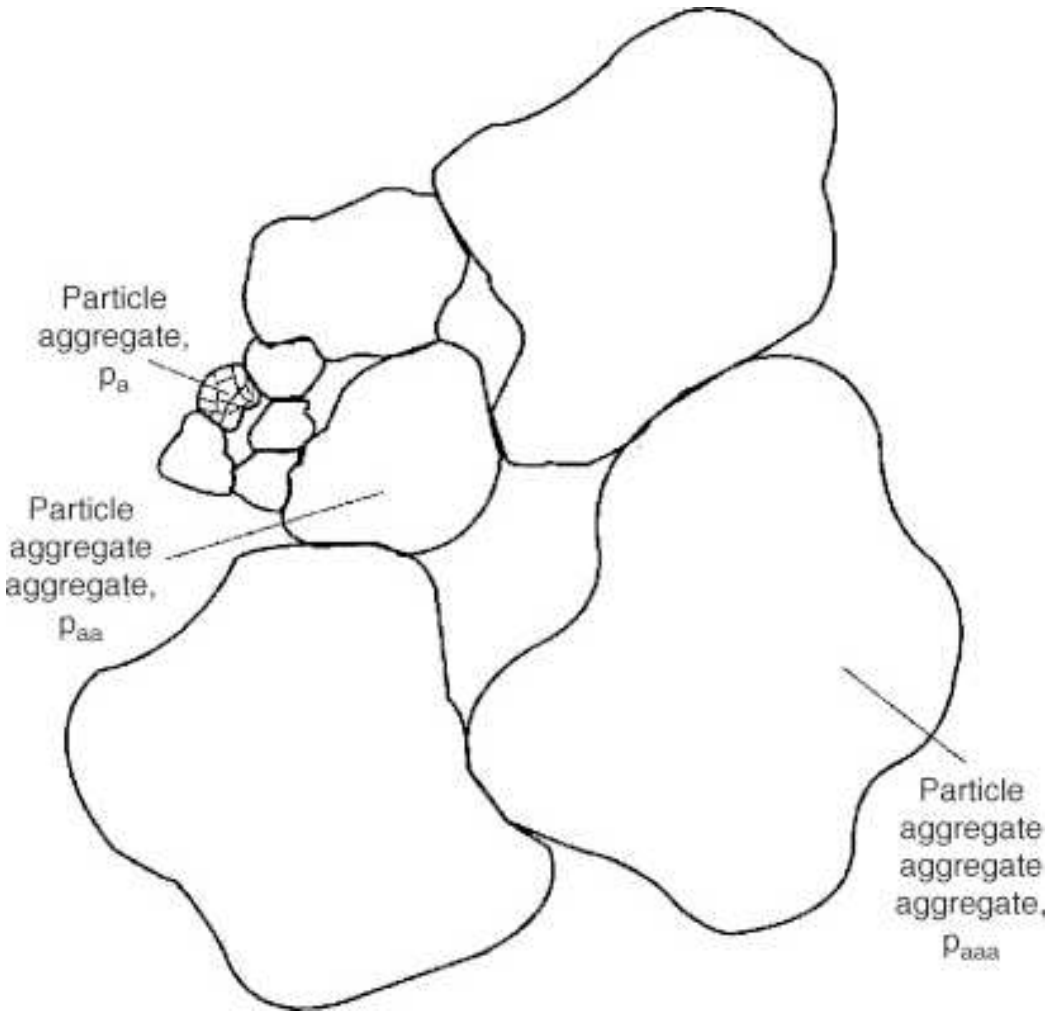

Figure 2.2: Scheme of the aggregation of particles that form flocs from the primary particles (Partheniades, 2009).

combine to form different clay minerals (Winterwerp and van Kesteren, 2004). The flat side of the particles has commonly a negative charge while the edge presents a positive charge and both interact with the ions in the water resulting in repulsive and attractive forces between particles and the latter the dominant forces in saline water and therefore a trend to flocculate (Dyer, 1986). The strength of the bond between particles depends on face to face or edge to face encounter and also on the mineralogy, pH and salinity. In the case of a face to edge attraction, particles bond is weaker and more easily broken than for the edge to edge situation (Dyer, 1986). Figure 2.2 show a drawing of the aggregation of particles that form flocs.

2.3 Flocculation process

The important consequence of the cohesion property of the sediments in sea water is that particles can be attached together and form aggregates or flocs of several times the

size of the original or primary particles and also can be disaggregated. This reversible process of aggregation and break-up of cohesive sediment is called flocculation (Dyer, 1986; Winterwerp and van Kesteren, 2004). Photographs of examples of real flocs are shown in figure 2.3. Particles need to be close enough from each other for the attraction forces to take effect. There should be enough particles for this to occur as a primary condition but a range of mechanisms may put them in close proximity. Some mechanisms that have been considered in the literature are listed below:

1. Brownian motion of the particles results in collision and formation of aggregates (Dyer, 1986; Winterwerp and van Kesteren, 2004).

2. If a velocity gradient exist particles also will collide depending on the distance between them and determined by its radii (Dyer, 1986).

3. A turbulent flow will take particles in eddies and collide to form aggregates according to Winterwerp and van Kesteren (2004) and are called "inertial encounters" by Dyer (1986) because of different particle size will react at different accelerations causing collisions. On the other hand the turbulent shear is mentioned by Winterwerp and van Kesteren (2004) as responsible of break-up of aggregates.

4. Differential settling is the result of large particles with faster settling velocity colliding with small particles falling at lower speeds (Dyer, 1986; Winterwerp and van Kesteren, 2004).

Another important factor is the collision efficiency which take into account that not all the collisions will result in aggregation (van Leussen, 1988). Although some formulations that quantify these mechanisms have been described in the literature (e.g. Partheniades, 2009), it is recognised that Brownian motion and differential settling are negligible in comparison with turbulence (e.g. Winterwerp and van Kesteren, 2004; Partheniades, 2009).

Aggregation and disagggregation are affected by sediment properties, biological activity, but mainly by turbulence variability. The changes in size and shape of the particles or flocs lead to changes in density, settling velocity and in the way they react with the environment giving a different behaviour than the non-cohesive sediment.This makes flocculation an important process in the estuarine sediment cycle. Suspended flocs can be horizontally transported or settle. Deposited flocs are subjected to consolidation and depending on the time they spend in the bottom could form a compact seabed. Although consolidation is not part of the flocculation process, it changes the threshold for the erosion and therefore the availability of flocs to the water column. Figure 2.4 shows the different processes and factors of the sediment cycle focusing in the aggregation and disaggregation of flocs as shown by Maggi (2005).

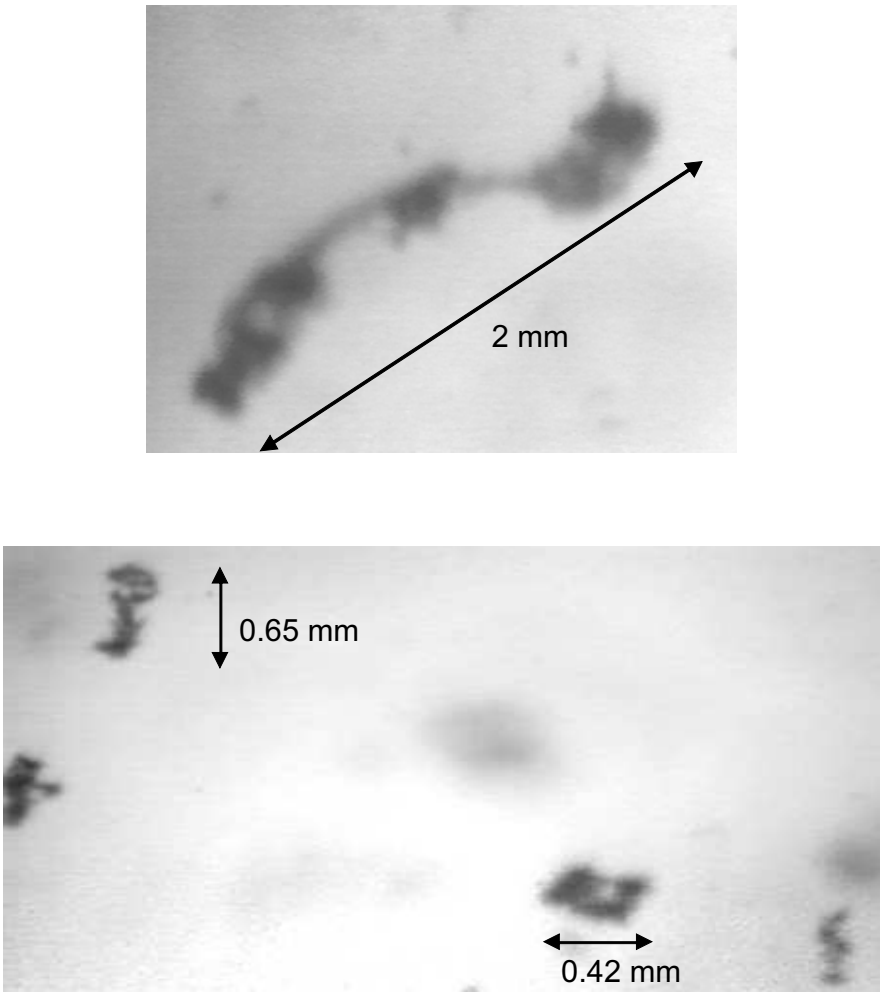

Figure 2.3: Real flocs showing the size that they can achieve and the variability of shapes. Photographs courtesy of Prof. Alejandro Souza and Dr. Andy Manning.

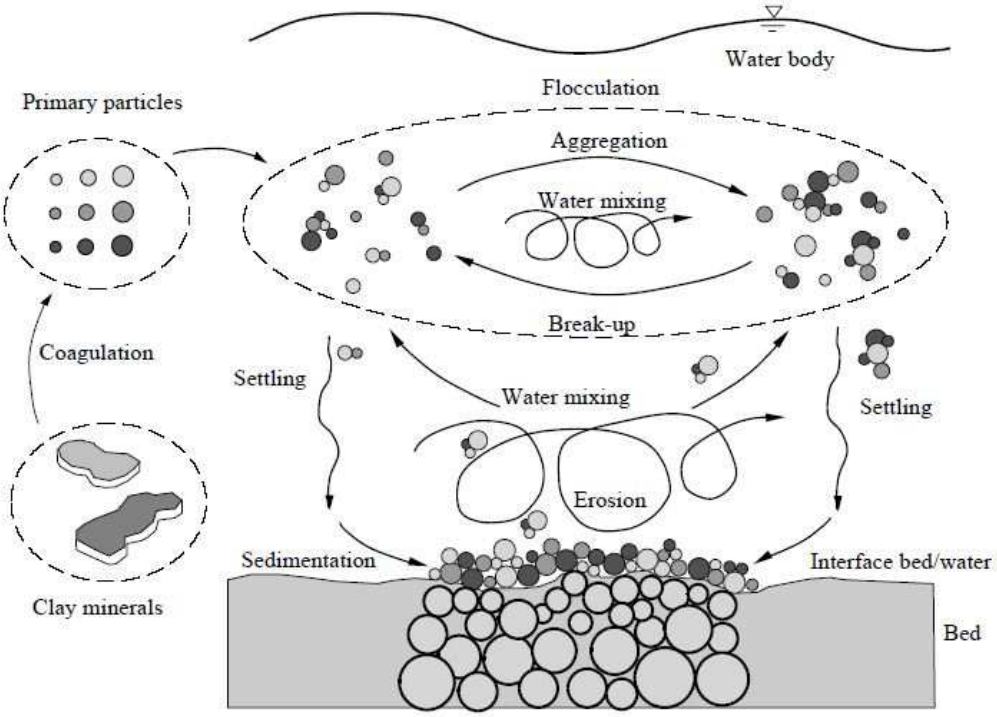

Figure 2.4: The flocculation process as shown by Maggi (2005). The clay minerals enhance the coagulation of particles resulting in the formation of flocs which depending on the turbulence (water mixing) may result in aggregation or break-up. Flocs of different sizes settle with different fall velocities and are resuspended again due to erosion of the seabed.

2.4 Hydrodynamic controls of flocculation

The turbulence produced by hydrodynamics is the main responsible of the changes in floc size. Dyer (1989) summarises early laboratory findings in his well known schematic diagram that shows an increase in grain size with a little increase in shear stress until a maximum size is reached, and then floc size starts to decrease as the shear stress continue increasing. The maximum achievable floc size at low values of shear stress seems to depend on sediment concentration (Fig 2.5). Experiments by van Leussen (1994) also confirm the conceptual behaviour described by Dyer (1989), although some differences were found between artificial particles and natural samples at low stress values (Fig. 2.7). The author pointed out the importance of the scaling factors to extrapolate the experimental results to estuaries. Also based on experiments in laboratory, with concentrations in the range of 80-200 $g \cdot m^{-3}$, Manning and Dyer (1999) found that an increase in floc concentration at low shear stress resulted in increase of floc size while the increase of both floc concentration and shear stress caused aggregate disruption. The lowest shear stress calculated by the authors was 0.1 Pa and therefore no floc behaviour was reported. Experiments have shown that aggregation is enhanced because of the increase in floc collisions with the availability of suspended flocs at low stress values. A threshold of size is achieved if shear stress continues increasing and break-up becomes the dominant process.

A good knowledge have been acquired from laboratory experiments but the questions still remain about floc behaviour in the dynamic estuarine natural environment, i.e. how the floc size changes in relation with tidal currents, concentration, salinity? Using field measurements of current velocity, floc size and suspended concentration, Manning (2008) calculated shear stresses as low as 0.02 Pa and settling velocities for a wide range of concentrations. The results were in agreement with the conceptual diagram of Dyer (1989), including a zone of floc aggregation at low shear stress up to a value of approximately 0.4 Pa. Manning (2008) also presented time series of suspended particulate matter and turbulent stress for a tidal cycle in the Tamar estuary, UK. The highest concentrations occurred during flood and ebb phases but with a time lag with the maximum turbulent stresses. Resulting settling velocity coincided with high concentration and low stress mainly during ebb phase while high stress, about an hour later, showed low settling velocity and concentration (Fig. 2.8). This behaviour is maybe due to large flocs being resuspended and aggregated or advected from the upper parts of the estuary in high concentrations and then disaggregated when stress becomes large. A less clear signal was found during the flood phase.

Longer observations of floc size and turbulence were carried out by Fugate and Friedrichs (2003) for different sites in the Chesapeake Bay, USA (Fig. 2.9). Besides hydrodynamics and biology factors, the authors identified the important role of suspended fine sediments in the water column on the flocculation process. In the region near the

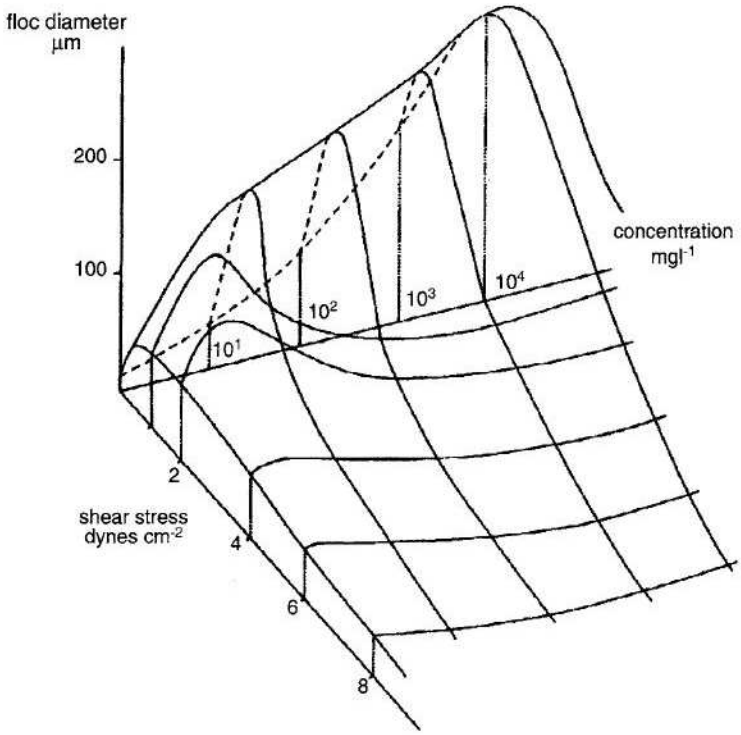

Figure 2.5: Conceptual diagram by Dyer (1989). Floc size dependent on sediment concentration and turbulence.

surface particle size were controlled by stochastic events such as advection and boat wake which affected the turbulent related processes. Near the bed, flocs in the energetic York River, were positively correlated to the Kolmogorov microscale. The biologically dominated Chesapeake Bay showed an opposite relationship due to the strong large aggregates being suspended. The third site, Elizabeth River, was characterised by low energy conditions and porous flocs larger than the Kolmogorov microscale. According to the authors, floc size was not controlled by sediment concentration and both were affected by hydrodynamic conditions.

More recently Yuan et al. (2008) found an increase in floc size coinciding with periods of high turbulent kinetic energy (Fig. 2.10). Different floc behaviour was found by Fettweis et al. (2012) with the increase in turbulent kinetic energy during extreme events. The authors explained the differences as a result of different composition of sediment advected by a storm from the north-east while other storm from the south-west enhanced the flocculation of sediments at the study site. An important difference between the works by Yuan et al. (2008) and Fettweis et al. (2012) is that turbulent kinetic energy is lower in the former than in the latter, although the measurements were not at the same level above the sea bed. However, different floc size response to high energy conditions is clear between the two studies and more research is needed to understand the processes involved. Another important result by Fettweis et al. (2012)

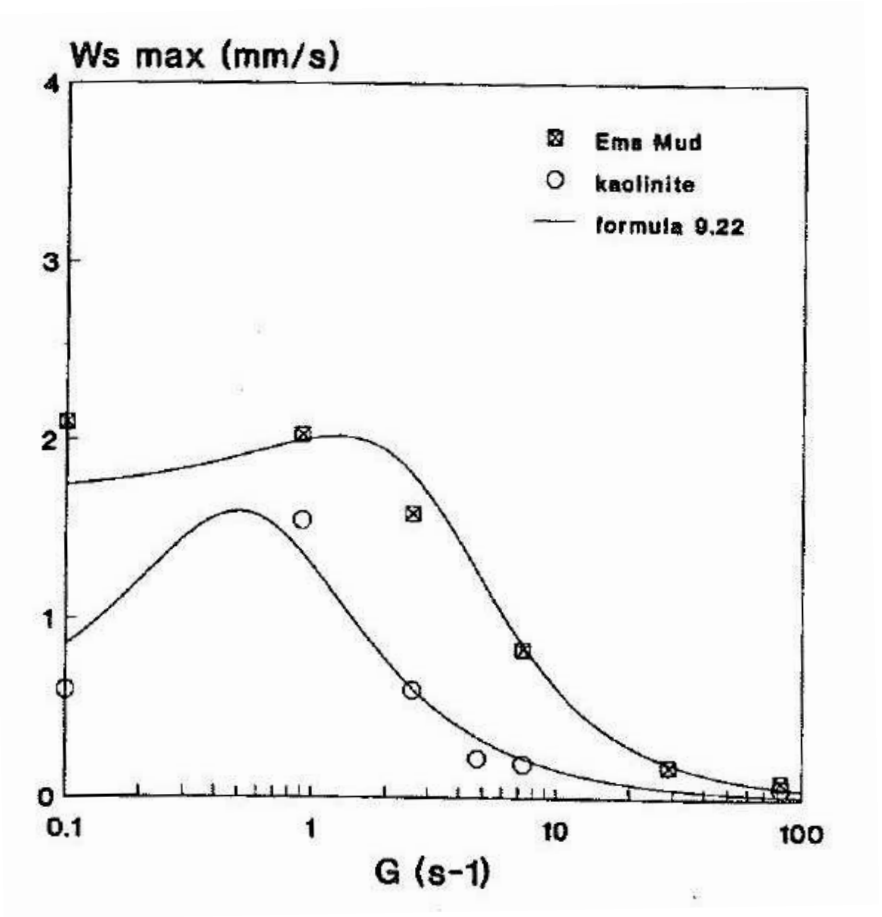

Figure 2.6: Results from experiments (markers) and a semiempirical formulation (lines) (van Leussen, 1994). G is the turbulent shear rate.

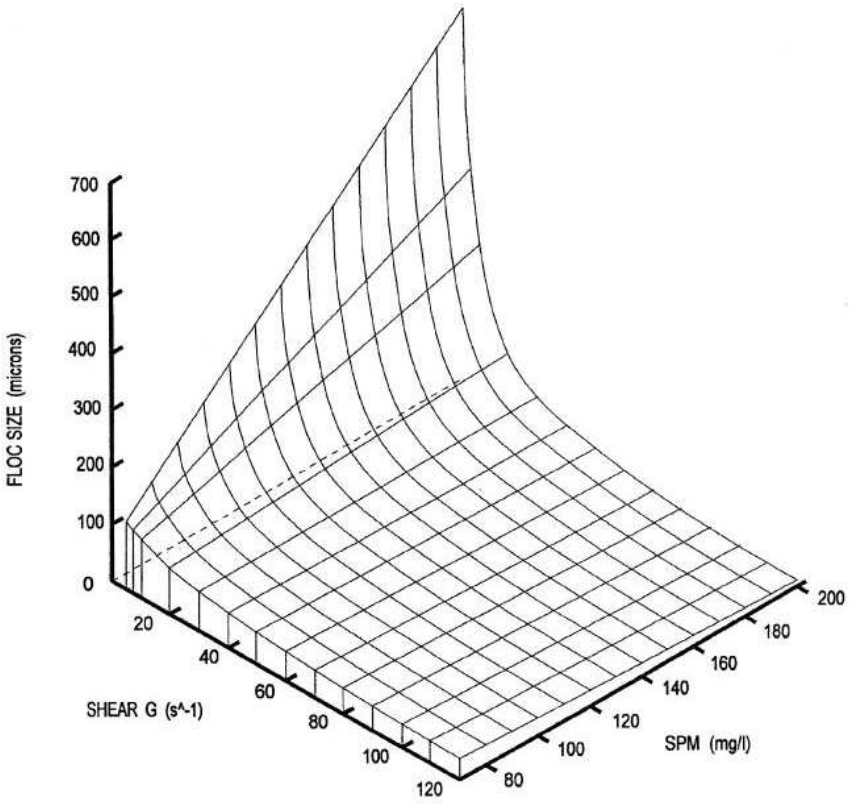

Figure 2.7: Relationship between turbulence shear and floc size using a formulation based on experiments of settling velocity (Manning and Dyer, 1999).

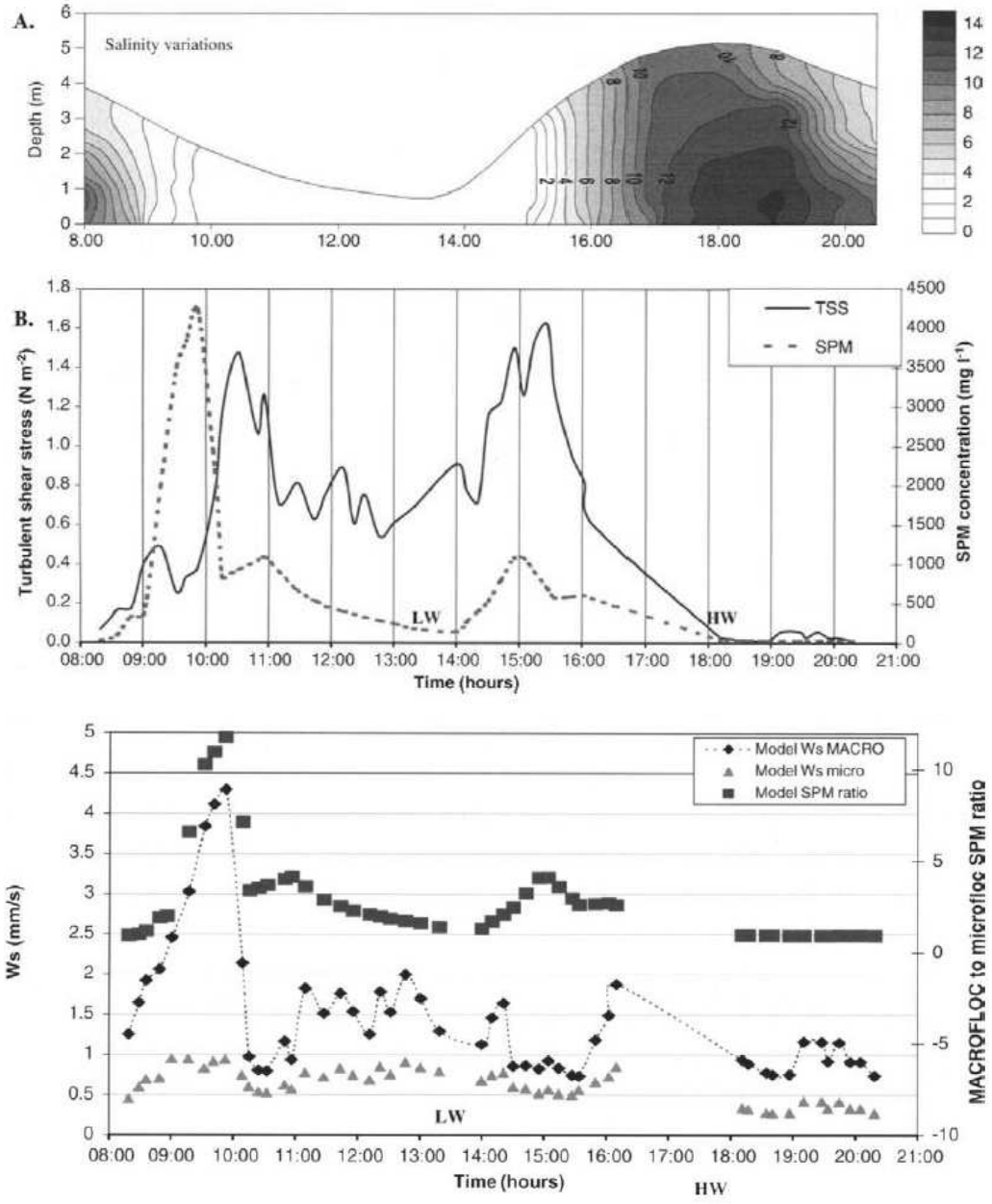

Figure 2.8: A and B are results from observations in the Tamar estuary, UK by Manning (2008). Settling velocities (Ws) in bottom panel from a formulation based on observations. Maxima in suspended particulate matter concentration (SPM) happened before maxima of turbulent shear stress (TSS). Before hour 10:00, the maximum in SPM resulted in maximum of settling velocity. After 10:00, TSS increase and settling velocity decrease. This behaviour seems to be the result of floc aggregation followed by a fast break-up period. No time series of measured settling velocities and floc size were shown by the author.

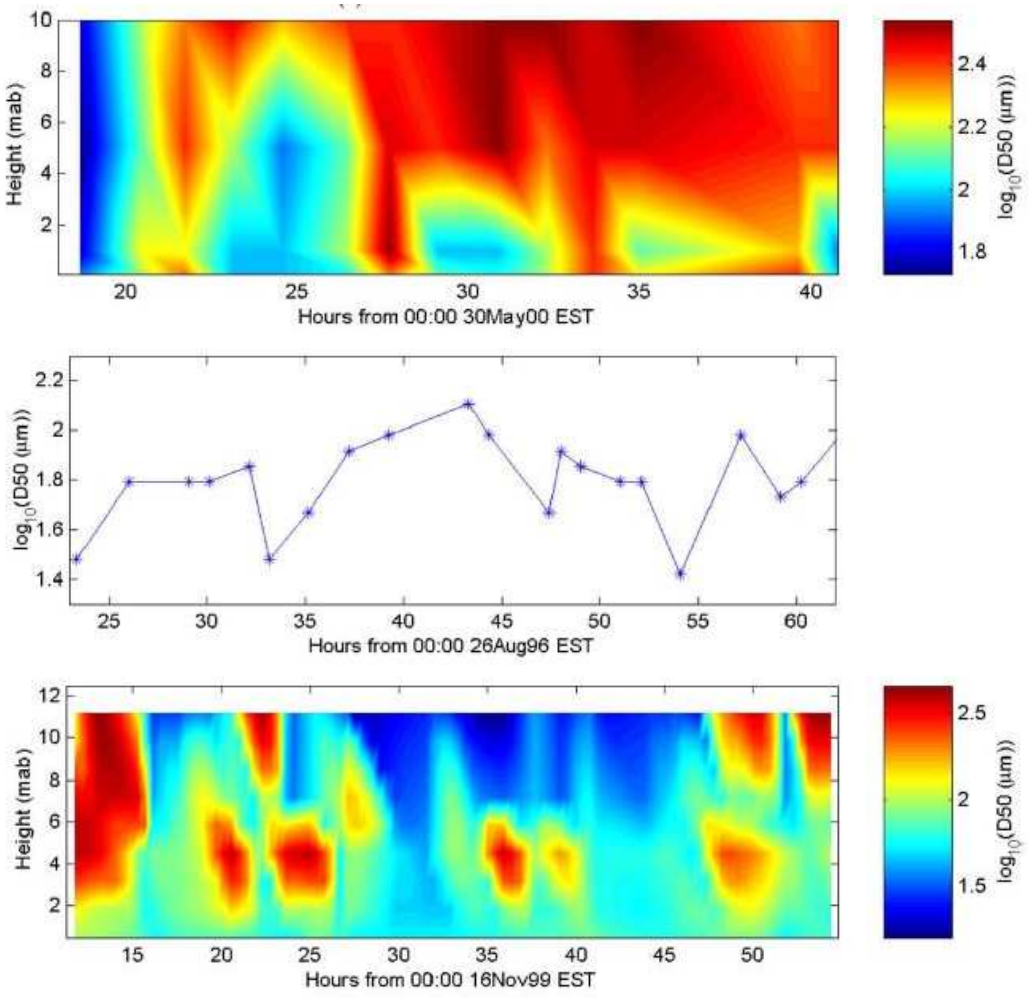

Figure 2.9: Median floc size as measured by Fugate and Friedrichs (2003). Top panel: York River. Middle panel: Chesapeake Bay. Bottom panel: Elizabeth River. Tidal range is similar at the three sites. Surface currents at York and Chesapeake are 1 $m \cdot s^{-1}$ while Elizabeth River is 0.5 $m \cdot s^{-1}$. Bottom sediments are different in the three sites and also present different bioturbation which appears to affect suspended sediments.

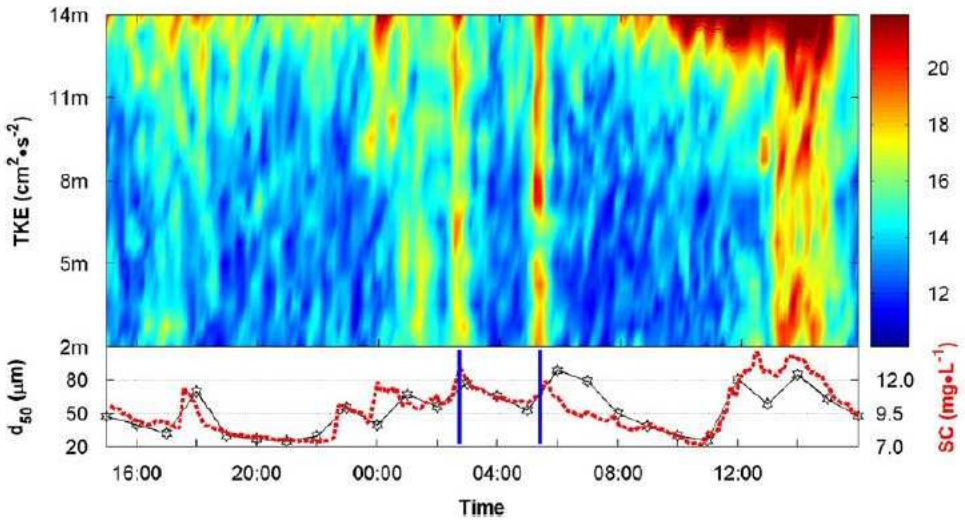

Figure 2.10: Observations of turbulent kinetic energy (TKE), median floc size (d_{50}) and suspended sediment concentration (SSC) by Yuan et al. (2008). Increase in floc size and concentration is clearly observed at periods of high TKE.

is the clear difference in the relationship between flocs and turbulent kinetic energy in normal conditions for the flood and ebb phases (Fig. 2.11). Winterwerp et al. (2006) measured the changes in floc size in the Scheldt estuary, UK, during a tidal cycle. They obtained floc sizes of about 300 μm at periods of low stress while at high stress floc sizes diminished to about 100 μm (Fig. 2.12). Also, interesting results were reported by Braithwaite et al. (2012) consisting in peak current velocity almost coinciding with the smallest flocs while largest flocs with the minimum current. The authors argue that the explanation maybe aggregation and disaggregation of flocs (Fig. 2.13). These results represent a rapid floc response to the hydrodynamic conditions.

The floc size has also been related to the Kolmogorov microscale of turbulence (e.g. Winterwerp and van Kesteren, 2004). This scale refers to the smallest eddies in a turbulent flow and had led to the assumption that flocs cannot grow larger than this scale because they would be subjected to higher shear rates resulting in disaggregation. Results have shown good agreement with this assumption with values smaller than the Kolmogorov microscale (e.g. Verney et al., 2009, and references there in). However, other studies have found floc sizes both smaller and larger than the Kolmogorov microscale. Larger flocs that are maybe the result of biological activity were found by Cross et al. (2013) while flocs of one order of magnitude smaller than the Kolmogorov microscale due to strong turbulence have been reported by Fettweis et al. (2006). These results show that the Kolmogorov microscale may be used to give an insight of the effect of turbulence on grain size and also the possible presence of other factors playing an important role.

The field studies confirm the important role of the hydrodynamics in the flocculation

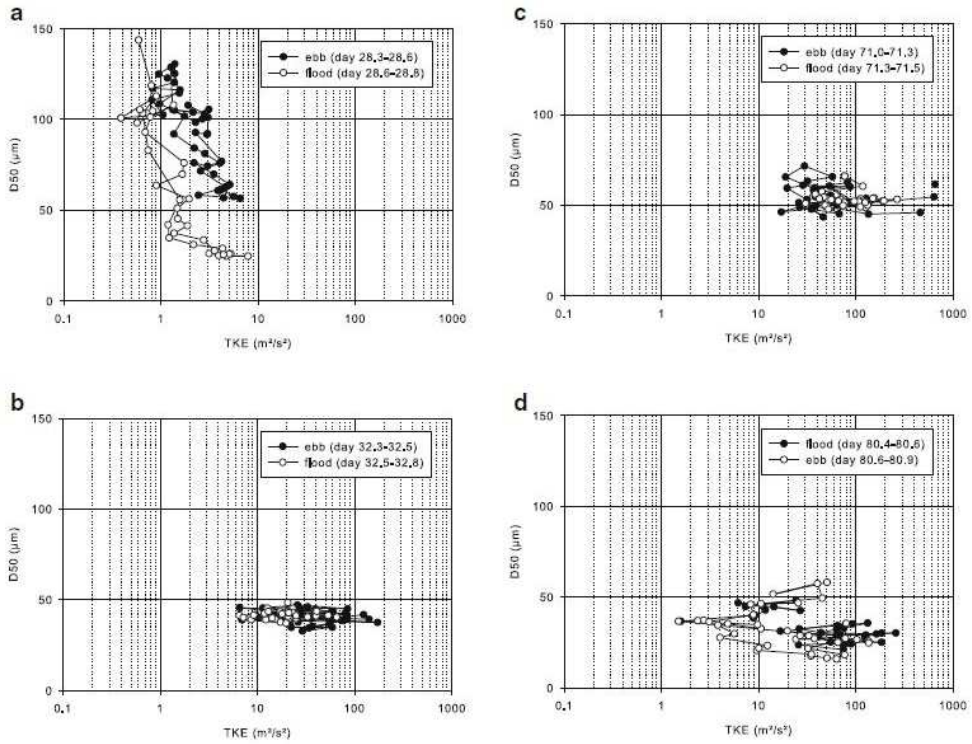

Figure 2.11: Turbulent kinetic energy (TKE) median floc size (D50). a) neap tide, b) and c) during north-east storms, and d) during a south-west storm. From Fettweis et al. (2012).

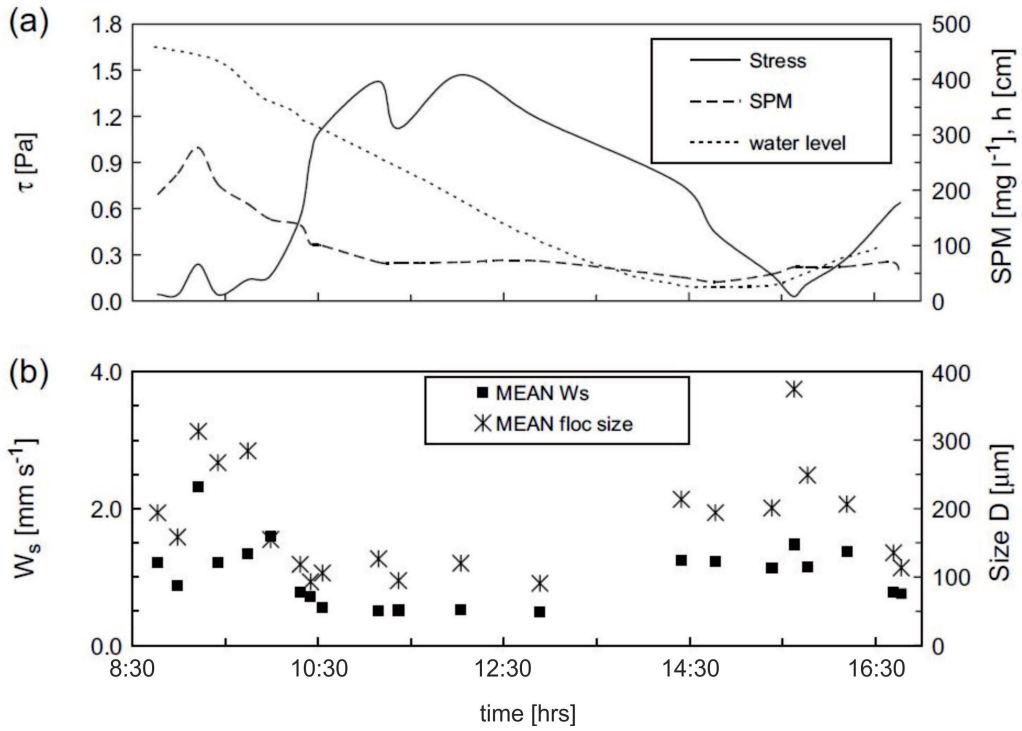

Figure 2.12: Observations by Winterwerp et al. (2006) showing large flocs with high settling velocity (W_s) coinciding with low turbulent stress (τ). A transition zone seems to appear during the increase of turbulent stress until the maximum is reached and flocs showed their minimum size.

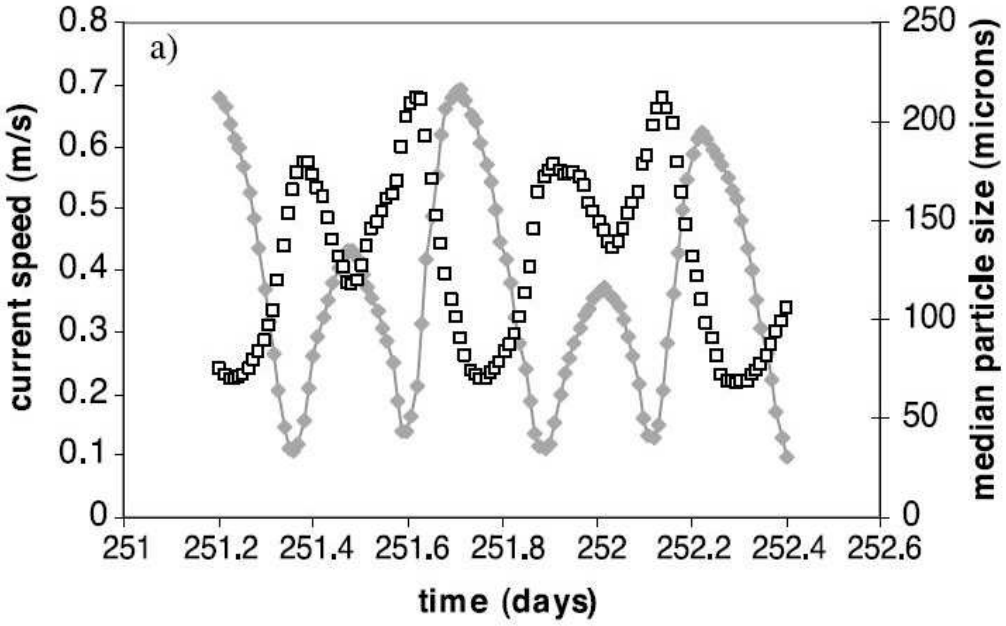

Figure 2.13: Current speed (gray line and symbols) and median floc size (open squares) from measurements by Braithwaite et al. (2012).

process. The *in situ* measurements have also identified the importance of other factors directly related with flocculation such as salinity, erosion, organic matter, advection, sediment composition and bottom heterogeneity. However, due to the many factors involved in field measurements, these are not conclusive of the floc behaviour. Moreover, instruments to measure floc size are in a developing stage and results seem to be only qualitative based on some comparative studies (e.g., Eisma et al., 1996; Mikkelsen et al., 2005; Reynolds et al., 2010). The most common result of the flocculation process is that flocs break-up when turbulence is high while aggregation takes place when turbulence is low but specific knowledge of the role of different factors are still unknown. Long term studies are needed to include changes throughout tidal phases and cycles, fortnightly cycles, seasonal changes and extreme events. Despite the gaps in flocculation process knowledge, several attempts have been made to the sediment transport of cohesive sediments taking into account important floc features such as settling velocity and floc density.

2.5 Settling Velocity

From the previous section, it can be seen that important consequences of floc aggregation and break-up are the changes in settling velocity and effective or excess density. The effective density is defined as the density of the floc without water density. This make its measurement difficult and is calculated from other variables or models based on measurements of settling velocity and using either the Stokes law or a modification of the same law (e.g. Tambo and Watanabe, 1979; McCave, 1984; Kranenburg, 1994; Khelifa and Hill, 2006; Manning, 2008; Markussen and Andersen, 2013). The results of these studies have shown that effective density decrease if the floc size increase. Figure 2.14 from Markussen and Andersen (2013) shows examples of calculated efective densities from different studies. Different results have also shown that in general, a positive relationship exist between settling velocity and grain size. Winterwerp (1998) reports diameters from 10 to 1000 microns and settling velocities ranging 0.1 to 10 $mm \cdot s^{-1}$. Manning (2008) found that the magnitude of the settling velocity seems to depend on concentration when flocs have sizes above 160 μm, below this size the settling velocity behaviour is the same for any concentration. The settling velocity increases with increasing concentration until it reaches a limit due to the hindered settling, where settling velocity decreases again (Winterwerp, 2002), although the quantitative values of settling velocity are particular to the study site, the limit appears to be the same, approximately 3 $g \cdot l^{-1}$. Nevertheless, a common feature of the settling velocity is the wide scattering in the relationship with floc size. As expected, the resulting effective densities are present also the same scattering. This issue is again addressed in section 4.1.1 with examples from Khelifa and Hill (2006) and Strom and Keyvani (2011).

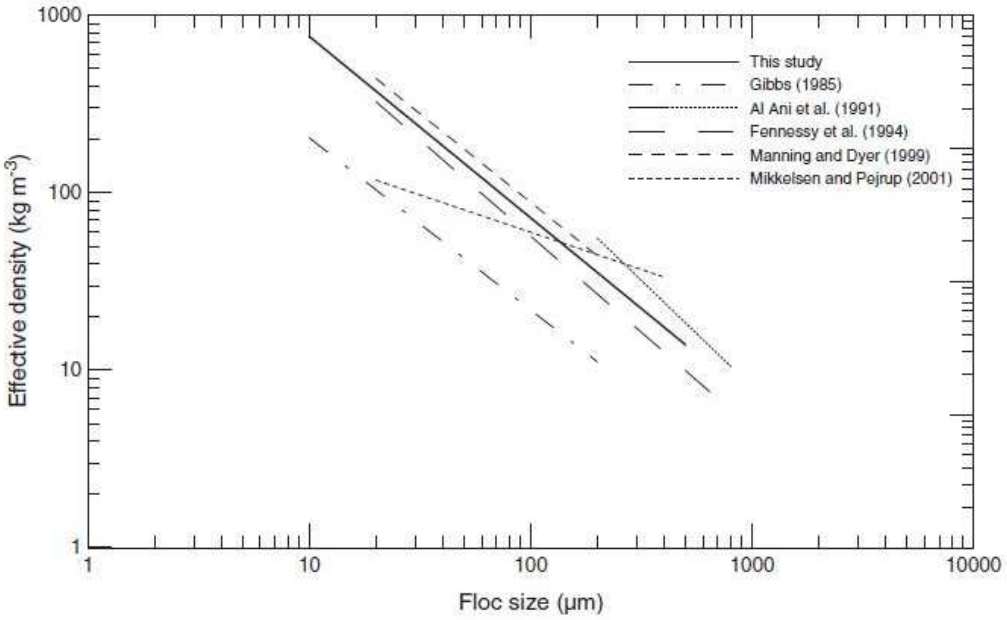

Figure 2.14: Comparison of effective densities as presented by Markussen and Andersen (2013). The authors also proposed a method to calculate effective density which results are marked "This study" in the figure.

2.6 Other Factors

Other factors could be taken into account in the process. Experiments by Al-Ani et al. (1991) showed maxima of floc sizes at salinities of 10-15 ppt. The effect of salinity appeared to enhance floc growth in observations by He et al. (2008) while Winterwerp et al. (2006) found that salinity promotes the formation of aggregates in conditions of weak currents. Fine sediment behaviour in the presence of salt is governed by physico-chemical processes and different values of salinity for flocculation have suggested in the range 1-7 ppt (van Leussen, 1988). Biology effects, which also play an important role have already been mentioned in section 2.1.

2.7 Approaches to flocculation prediction

The essential problem in the flocculation process is the parameterisation of the changes in floc size. The processes involved have been introduced in previous sections. However, it is important to notice the magnitude and scope of the problem. The spatial and temporal changes of these processes in nature play an important role in the change of floc size. Starting from the seabed and when turbulent stresses are strong, floc break-up is important resulting in small particles, but the stress magnitude is not the same throughout the water column and a different magnitude of break-up is expected at each water level. When turbulent stresses diminish, different magnitude of floc aggregation

is expected at different levels. In addition, turbulent stresses present longitudinal and lateral changes in the estuary. The turbulent stresses temporal changes are also important on the order of hours (tidal phases) and days (spring-neap tides). Seasonal changes also have an effect on the biology factor, river supply and storms. All these factors affect the floc size and make their description an important goal for sediment transport studies.

Approaches for the prediction of flocculation should include as many factors as required. For example, the sediment availability on the sea bed and the degree of consolidation, sediment properties like composition, initial floc size, porosity, density, settling velocity, physical processes like turbulence, liquefaction, aggregation, break-up and the temporal and space changes mentioned above. The transport of mass, as in equation 2.4 has been modified by Winterwerp and van Kesteren (2004) in order to include the particular concentration of each sediment class changing the concentration C by $C^{(i)}$ where i represents each sediment class concentration. Nevertheless, the problem of quantifying these concentration relies on the changes of size. The mass concentration of small flocs will diminish if some of them aggregate to form large flocs which will increase their corresponding mass concentration. Winterwerp (1998) proposed a formulation for the rate of change of the floc diameter which still has important parameters to obtain like the floc settling velocity. The author proposes a formulation for the settling velocity that incorporates the concept of flocs as fractal structures by Kranenburg (1994). A formulation may be very complete in the variables included, but it may be difficult to apply if it depends on parameters not commonly obtained from field measurements and if it has many free calibration parameters. For a formulation to be suitable, it should be as simple as possible without losing its capabilities of prediction.

The last step of a formulation is the implementation in three dimensional numerical models. The first aim of the implementation in a numerical model is to take advantage of the capabilities to manage different physical processes and variables which can help in the understanding of the flocculation process. Secondly, the prediction of the process can help in more accurate calculations of sediment transport rates which imply a better knowledge of erosion and deposition rates resulting in a better management of the estuary resources. Simple formulations to include cohesive sediments in widely used numerical models obtain settling velocities as function of only sediment concentration and one of them also salinity (Amoudry and Souza, 2011a). In this section three different models based on different formulations and complexity are briefly explained. At present, most of the formulations found in flocculation literature are either modifications of the formulation in section 2.7.3 or include the fractal structure of flocs. Multiclass models that use this concept can also be found in the literature (e.g. Verney et al., 2011; Maerz et al., 2011; Mietta et al., 2011) but still need comparisons with field

observations. For example, the multimodal model by Lee et al. (2014) showed good agreement with observations, but it need to be applied to different hydrodynamic conditions to include the spring-neap tidal variability and test how difficult is the calibration of the six parameters required in the formulations.

2.7.1 Settling velocity as a function of turbulent stress and suspended particulate matter (Manning, 2008)

This formulation is based on *in situ* measurements from three different estuaries. The sediments are divided into two populations, macro flocs (diameter>160 μm) and micro flocs (diameter<160 μm). Regression analysis was made for the different variables and sediment classes to measure their importance in the process. The author considers settling velocity ($W_{s_{macro}}$), sediment concentration (SPM) and turbulent stresses (τ) to be the most relevant characteristics in the process.

The settling velocity of the macro flocs depends on both turbulence and SPM concentration. The results were divided in three turbulent stress zones

between 0.04 and 0.7 Pa:

$$W_{s_{macro}} = 0.644 + 0.000471SPM + 9.36\tau - 13.1\tau^2 \qquad R^2 = 0.93 \tag{2.10}$$

between 0.6 and 1.5 Pa:

$$W_{s_{macro}} = 3.96 + 0.000346SPM - 4.38\tau + 1.33\tau^2 \qquad R^2 = 0.9 \tag{2.11}$$

between 1.4 and 5 Pa:

$$W_{s_{macro}} = 1.18 + 0.000302SPM - 0.491\tau + 0.057\tau^2 \qquad R^2 = 0.99 \tag{2.12}$$

The major contribution (66%) to the variability was obtained from the concentration, while the remaining 34% was due to the turbulent parameters. For the micro floc population there was no dependency on concentration

between 0.04 and 0.55 Pa:

$$W_{s_{micro}} = 0.244 + 3.25\tau - 3.71\tau^2 \qquad R^2 = 0.75 \tag{2.13}$$

between 0.51 and 10 Pa:

$$W_{s_{micro}} = 0.65\tau^{-0.541} \qquad R^2 = 0.73 \tag{2.14}$$

As a measure of the macro floc and micro floc distribution, an SPM_{ratio} was computed dividing the percentages macro by micro, and the regression analysis revealed a dependency only on the SPM concentration:

$$SPM_{ratio} = 0.815 + 3.2 \times 10^{-3} SPM - 1.4 \times 10^{-7} SPM^2 \qquad R^2 = 0.73 \tag{2.15}$$

All algorithms are combined to obtain a mass settling flux (MSF) formulation:

$$\begin{aligned} MSF &= \left[\left(1 - \frac{1}{1 + SPM_{ratio}}\right)(SPM \times W_{s_{macro}})\right] \\ &\quad + \left[\frac{1}{1 + SPM_{ratio}}(SPM \times W_{s_{micro}})\right] \end{aligned} \tag{2.16}$$

The formulation was compared against observational data during a tidal cycle. Time series of measured hydrodynamics and floc spectra were used for the formulations and the results showed good agreement for the mass settling flux. The results were also compared with those from the use of constant settling velocities and the percentage of the observations described for these later velocities was below 40% while using this formulation was over 90%. According to the results "it is the combined τ-SPM effect which governs, both spatially and temporally, how a specific concentration of suspended flocculated cohesive sediment is composed (...) and then ultimately settles".

A significant advantage of this formulation is its simplicity, since just two variables are needed, turbulence and SPM concentration. However, it depends on the availability of measured floc sizes. It also has to be tested in different locations, in the whole water column and with long term measurements.

2.7.2 The flocculation factor (van Rijn, 2007a, van Rijn, 2007b)

The settling velocity W_s and the critical bed shear stress $\tau_{cr,bed}$ are factors in which the effects of flocculation and cohesion of particles are taken into account. The settling velocity is computed through a proportional relationship between a flocculation factor ϕ_{floc}, a hindered factor ϕ_{hs}, and a settling velocity of single suspended particles in clear water $W_{s,o}$:

$$W_s = \phi_{floc} \phi_{hs} W_{s,o} \tag{2.17}$$

with

$$\phi_{floc} = \left[4 log_{10}\left(\frac{2C}{C_{gel}}\right)\right]^{\alpha} \tag{2.18}$$

where $\alpha = (D_{sand}/D_{50}) - 1$. Thus, the flocculation factor depends on the ratios between sediment concentration (C) and gelling concentration (C_{gel}), and between

the size of the sand grains D_{sand} and the mean of the total population D_{50}. This factor increases if the size of the flocs decreases from 62 to 16 μm. From experimental results the hindered factor for fine sediments can be represented by a power relationship $\phi_{hs} = (1-0.65C/C_{gel})^5$. In high concentrations, sediment particles have a stratification effect which is included in a factor ϕ_d. This has a damping effect on eddy viscosity and diffusivity and therefore on sediment concentration.

On the sea bed, the cohesion of particles has an effect on the critical bed shear stress. The bed shear stress is obtained by:

$$\tau_{cr,bed} = \phi_{bo}\phi_{packing}\phi_{cohesive}\tau_{cr,o} \tag{2.19}$$

where ϕ_{bo} is the biological and organic factor defined by the user. The particle-particle interaction with the effects of binding and clay coating is included in the cohesive factor $\phi_{cohesive}$ and depends on the particle size. The packing or bulk density effect in $\phi_{packing}$ depends on the gelling volume concentration.

The formulation has shown good agreement with observations in spite of free parameters. Time averaged concentrations were obtained from these formulations and observations. The results were quantitatively very similar when a discharge from land was included in the sediment transport (Grasmeijer et al., 2011). In the same study, but at a different location, qualitative results showed an expected horizontal distribution of suspended sediments. However, the formulations need to be used in different locations to test the sensitivity of the free parameters. Therefore, the calibration of many unknown parameters may be difficult. Also, there are no specific results shown about concentration profiles or time series near the bottom, where the gradients are largest.

2.7.3 Flocs as fractals (Winterwerp, 1998)

In this formulation, the growth rate of mud flocs with D being their characteristic diameter is used:

$$\frac{dD}{dt} = k_A C G D^{4-n_f} \tag{2.20}$$

where

$$k_A = \frac{3e_c\pi e_d D_p^{n_f-3}}{2f_s n_f \rho_s} = k'_A \frac{D_p^{n_f-3}}{n_f \rho_s} \tag{2.21}$$

with k'_A a dimensionless coefficient, e_c a parameter to account for the particle collisions resulting in aggregation, e_d a parameter for diffusion, C the mass concentration, f_s a shape factor, n_f the floc's fractal dimension, D_p the diameter of the primary particles. As a turbulence based model, this formulation strongly depends on the dissipation parameter G defined as:

$$G = \sqrt{\frac{\epsilon}{\nu}} = \frac{\nu}{\eta^2} \tag{2.22}$$

with η the Kolmogorov microscale of turbulence and the dissipation rate $\epsilon = 2\nu\overline{s_{ij}s_{ij}} = 15\nu\overline{(\partial u_1{}'/\partial x_1)^2}$, where s_{ij} is the turbulent rate of strain and u' the turbulent velocity fluctuation.

For the break-up process, the following formulation was obtained:

$$\frac{dD}{dt} = \frac{ae_b}{n_f} DG \left(\frac{D - D_p}{D_p}\right)^p \left(\frac{\mu G}{F_y/D^2}\right)^q = -k_B G^{q+1}(D - D_p)^p D^{2q+1} \tag{2.23}$$

where a, p, q are coefficients to be determined, μ the dynamic viscosity of the fluid and F_y the yield strength of flocs. Thus k_B is defined as:

$$k_B = \frac{ae_b}{n_f} D_p^{-p} \left(\frac{\mu}{F_y}\right)^q = \frac{k'_B}{n_f} D_p^{-p} \left(\frac{\mu}{F_y}\right)^q \tag{2.24}$$

and again k'_B is a dimensionless coefficient.

In a simple linear combination, the flocculation model is:

$$\frac{dD}{dt} = \frac{k'_A}{n_f}\frac{c}{\rho_s} G D_p^{n_f - 3} D^{4-n_f} - \frac{k'_B}{n_f}\left(\frac{\mu}{F_y}\right)^q G^{q+1} D_p^{-p} D^{2q+1}(D - D_p)^p \tag{2.25}$$

The validation was made on a simplified version with some assumptions. The equilibrium diameter is proportional to η, the fractal dimension of flocs n_f=2 and observations lead to the assumption that the settling velocity is proportional to D. Therefore the coefficients p and q were obtained. Through experiments in a settling column, the values of k_A and k_B were also computed. The floc size evolution obtained from the formulations and measured in the settling column was compared and a good agreement was found for the equilibrium floc size. However, for the settling velocity, the results were as expected but the comparison was made with few measurements.

In a later study and with some modifications the results of the formulations were compared with field observations (Winterwerp, 2002). The effect of hindered settling was included when the settling velocity was calculated. Vertical time series of observed and modelled concentrations using a constant settling velocity were compared. The use of a constant settling velocity showed an almost mixed distribution without the observed variability and just one short resuspension event. The full model showed qualitatively better results with larger concentrations near the bottom and increasing towards the surface. Individual profiles also showed the behaviour of the concentration but were quantitatively different. The author recommends its formulation to be used in the study of processes instead of application in an operational numerical model because of its complexity in terms of implementation and the need for several parameterisations.

2.8 Aims of the Study

Throughout experiments and field studies, some knowledge has been obtained about the behaviour of the flocs in marine environment. However, several issues are still to be addressed. In general, most of the research that has been done is time limited. Longer studies are needed to cover the changes in floc size due to tidal, fortnightly, seasonal and extreme events. Also, changes in short term as tidal phases have been poorly studied and appears to be important in the relationship of the floc behaviour and turbulence properties. The effects of the high waves have been considered more important on sediment transport than the conditions without waves. Moreover, contrasting effects of storms have been found for the same site. The combination of effects of strong currents, as in a hypertidal estuary, and the waves in an estuary where cohesive sediments are dominant has not been studied.

The different studies have confirmed that the flocculation process is mainly dependant on the turbulence produced by tidal currents. Although sediment concentration, settling velocity and effective density also play an important role, results seem to approximate to simple relationships like $W_s = A \cdot D^B$. Therefore, it is possible that a simple relationship between flocs and turbulence properties can be found in order to be implemented in full three dimensional numerical models. Existing formulations have a number of issues difficult to solve. From the examples mentioned in previous section, they include a number of variables to be measured or parameterised and coefficients for calibration. This is a major problem since some variables cannot be measured during long terms. Studies that include the flocculation formulations in a numerical three-dimensional model are scarce. A version of the model described in section 2.7.1 was implemented in a 3D hydrodynamic numerical model in an un-coupled way for only one tidal cycle (Baugh and Manning, 2007). Kombiadou and Krestenitis (2012) implemented a floc model based in the method described in section 2.7.3. Although simulations lasted from months to one year, the results showed strong differences with observations and waves were not included because the minimum depth was about 20m.

The formulation in section 2.7.1 is based on SPM. τ, and W_s measurements but results seems to be site specific and longer measurements are needed to calibrate and test the formulations. Although the formulation on section 2.7.3 is physically well based, it requires many variables, parameters and coefficients to be determined. The formulations in section 2.7.2 have been applied in a 3D numerical model by Grasmeijer et al. (2011) but the results are not yet convincing. The main gol of any flocculation formulation should be its applicability in a numerical model to obtain a good prediction of the sediment transport. A significant advance has been achieved in hydrodynamic models with good predictions of tidal currents. Therefore, the relationship between flocculation and hydrodynamics (turbulence) could be used as a first approximation of the prediction of floc behaviour.

The present study contributes to the understanding of the flocculation process in a highly energetic estuary, focusing on its relation with the hydrodynamics as the main forcing factor. The main question that is addressed in this study is to gain a better knowledge of floc behaviour and how flocs react to different hydrodynamic conditions. In particular:

1) What is the effect of the strong currents and the resulting turbulence on the flocs?

2) Can we predict the floc behaviour by means of including the findings in a numerical model?

3) What is the contribution of the waves to the flocculation process?

4) Is there any particular hydrodynamic forcing capable to describe the floc behaviour?

The chapter 3 of this study gives a description of the study area with the work that has been done and is relevant for the flocculation process. Chapter 4 describes how and which instruments were used to obtain measurements, the analysis procedure and the numerical models in which the findings were applied. Chapter 5 presents the results from observations and numerical models following a classical approach. Chapter 6 describes the new findings on the flocculation process in the Dee estuary through an analysis of the different hydrodynamic regimes. In chapter 7, the most important findings of the study are discussed and finally, in chapter 8 the concluding remarks are presented along with suggestions for future work.

Chapter 3

Study Area

3.1 Liverpool Bay

Liverpool Bay is located on the northwest coast of England and the north coast of Wales. It is a semi-enclosed section of the Irish Sea (Fig. 3.1) in which many of the activities mentioned in section 1.2.4 and table 1.1 take place, see for example figure 3.2. It is a shallow area with depths of less than 70 m at the western boundary, which diminishes gradually landward near the east and south sides (Fig. 3.1). Four main rivers supply freshwater to Liverpool Bay (Clwyd, Dee, Mersey and Ribble) at a rate of 233 $m^3 \cdot s^{-1}$ and an annual contribution of $7.3x10^9$ m^3 (Phelps et al., 2013). However, according to Polton et al. (2011), the variability of the fluxes from the rivers can be over 300 $m^3 \cdot s^{-1}$ in a day, with no clear seasonal cycle and short periods of high intensity rainfalls on daily or weekly basis. The interaction of sea and freshwater establishes a quasi-stable offshore gradient of salinity without significant seasonal change while for temperature, stronger gradients are present onshore during summer and offshore during winter (Polton et al., 2011).

The tidal wave propagates from the Irish Sea and takes the form of a standing wave in Liverpool Bay which has a large semidiurnal range of more than 8 metres during spring tides (Simpson et al., 1991; Simpson et al., 2002; Howlett et al., 2011). Tidal currents are asymmetric with largest flood currents of about 1.2 $m \cdot s^{-1}$ during spring tides. Even when there is strong tidal mixing, the stratification in the bay is controlled by the buoyancy effects of the fresh water from rivers (Verspecht et al., 2009a). The combination of strong tidal forcing and the longitudinal density gradient results in periodic stratification due to tidal straining (Simpson et al., 1990). In Liverpool Bay during ebb, surface light water is advected over denser water, resulting in stratification of the water column while during flood differential advection pushes denser water over lighter water, resulting in convection which intensifies tidal mixing (Simpson and Sharples, 1991).

In a study using 11 years of tide and wave data and modelling, Brown et al. (2010) found surge levels of 2.41 m in Liverpool Bay due to tide-surge interaction, however

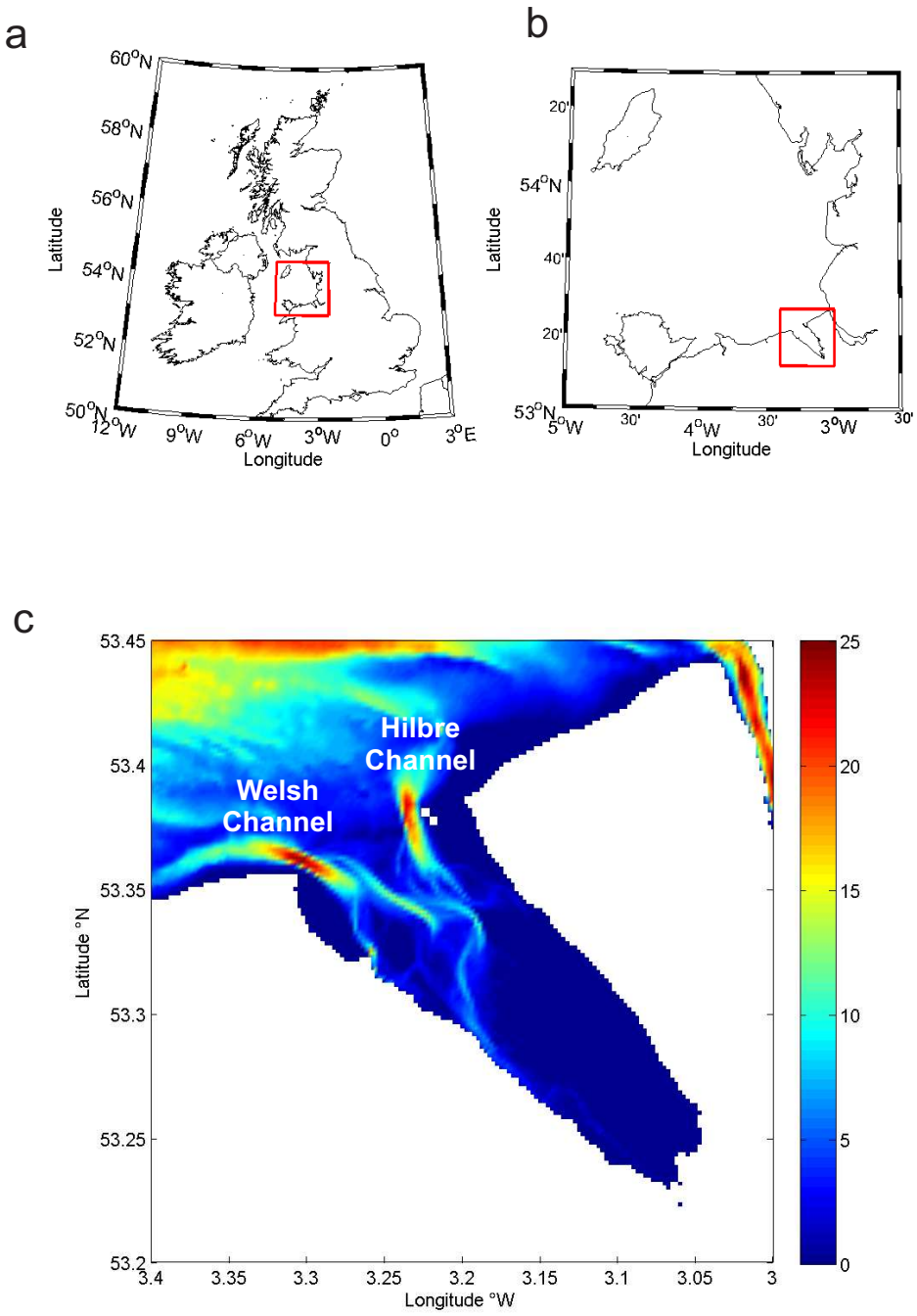

Figure 3.1: Location of the study site. a) United Kingdom, Liverpool Bay in red square, b) Liverpool Bay with the Dee Estuary in red square, and c) Dee Estuary and channels, Welsh to the west and Hilbre to the east of the entrance. Depths in metres above mean sea level.

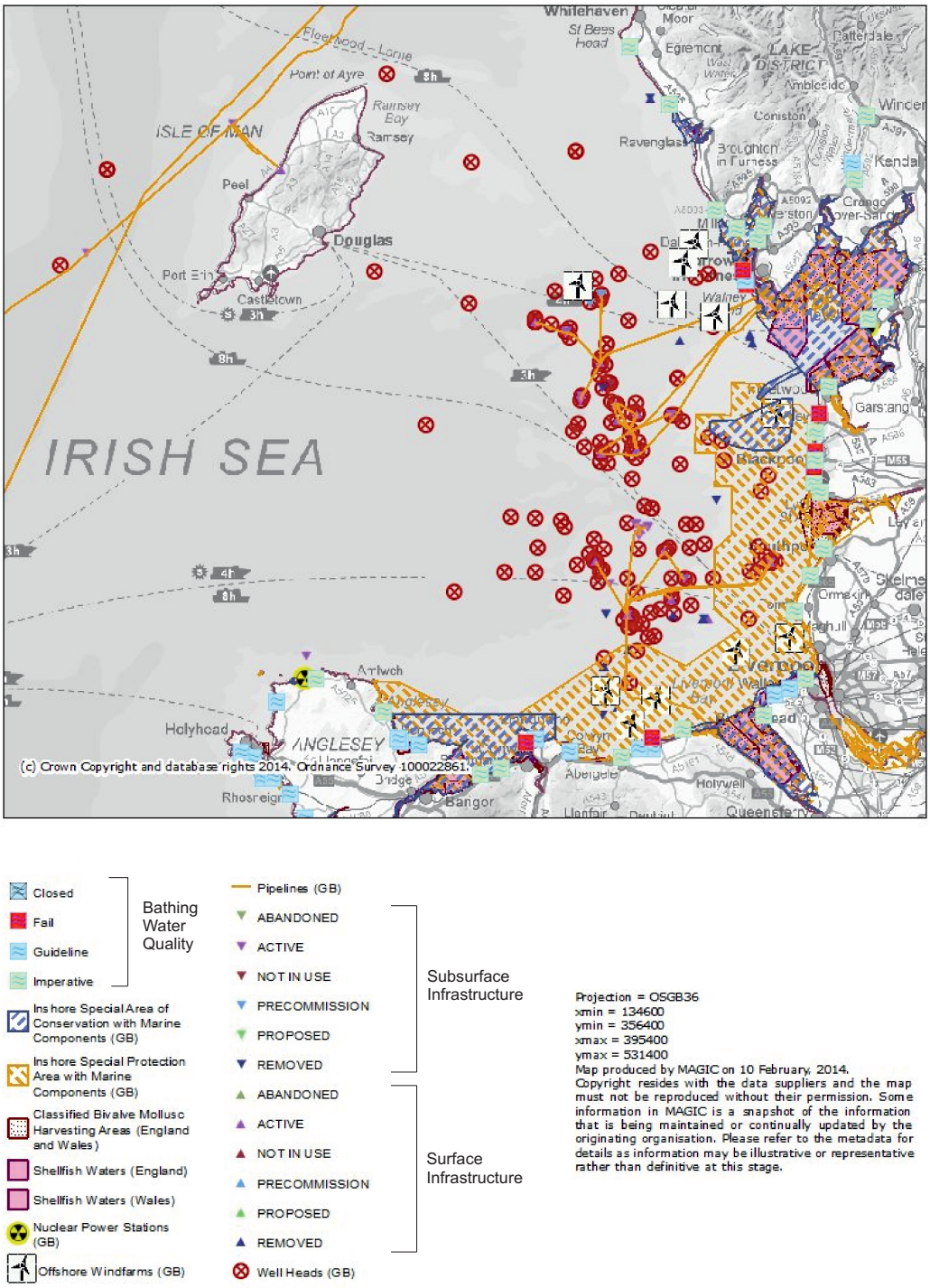

Figure 3.2: Example of different activities carried out in Liverpool Bay coastal zone (www.magic.defra.gov.uk). Subsurface and surface infrastructure are part of the oil and gas industry and include manifolds, tees, anchors, platforms, buoys.

there was no coincidence of the largest surges with high tidal levels and therefore no important high water level was recorded. The worst extreme conditions recorded were 5.1 m high water and offshore 4.8 m wave height. No clear patterns in intensity and frequency of the extreme events were found by the authors. Combining observations and modelling, Wolf et al. (2011) showed that waves in Liverpool Bay are strongly related to the local westerly winds and storms during winter. The higher wave events are limited by the fetch and come from the north-west while swell wave energy is not important because there is no propagation from the North Atlantic. Based in an multi-year observation period of 2003-2006, Wolf et al. (2011) found average and maximum wave heights of 0.9 m and 4.6 m respectively.

A distribution of sea bed sediments is showed on figure 3.3. The patterns reflect the exposure of the sea bed to sorting processes due to bottom stress by wind, storm surges, waves and tidal currents. The temporal and spatial variability of the bottom stress results in variability of the sediment imported, deposited or exported. The areas with low stress show almost stable fine-grained muddy sediments which have been deposited with very low currents (Holmes and Tappin, 2005).

Krivtsov et al. (2008) carried out a study in Liverpool Bay consisting of measurements of suspended sediments. Surface concentrations of about 24 $mg{\cdot}l^{-1}$ in winter and about 5 $mg{\cdot}l^{-1}$ in summer were found to the northwest of the entrance of the Dee and Mersey estuaries. Both surface and near-bed sediments consisted of particles of about 100 μm with mostly unimodal distribution. However, the authors also mentioned that sampling results at the same station may be different if taken at different stages of the tide. Although there is a clear offshore increase in particle size, the distribution is complicated by a number of processes such as advection, resuspension, sedimentation and flocculation (Krivtsov et al., 2008).

Sediment transport is closely related to the east-west tidal currents (Souza and Lane, 2013). However, density-driven flow influences the long-term residual resulting in a depth varying north-south flow (Brown et al., 2013) which is in agreement with previous findings by Halliwell (1973). Souza and Lane (2013) used a Lagrangian particle tracking module coupled to POLCOMS model (the latter is used in this study and described in section 4.2.1) in the Liverpool Bay and compare sediment transport with tidal forcing only and including freshwater supply from rivers. In the first case, their results showed sediment pathways in an east-west direction. In the more realistic case, near-bed coarse sediment is advected southwards but fine sediments reflect the density-driven circulation northward near the surface and south-east direction near the bed reaching the Mersey Estuary in 15 days. Therefore, current residuals and sediment transport respond to the topography and diverges from Formby Point to the north and south (Plater and Grenville, 2010). Figure 3.4a shows the pathways of sediment transport in the east part of the Liverpool Bay. Figure 3.4b and 3.4c show some results

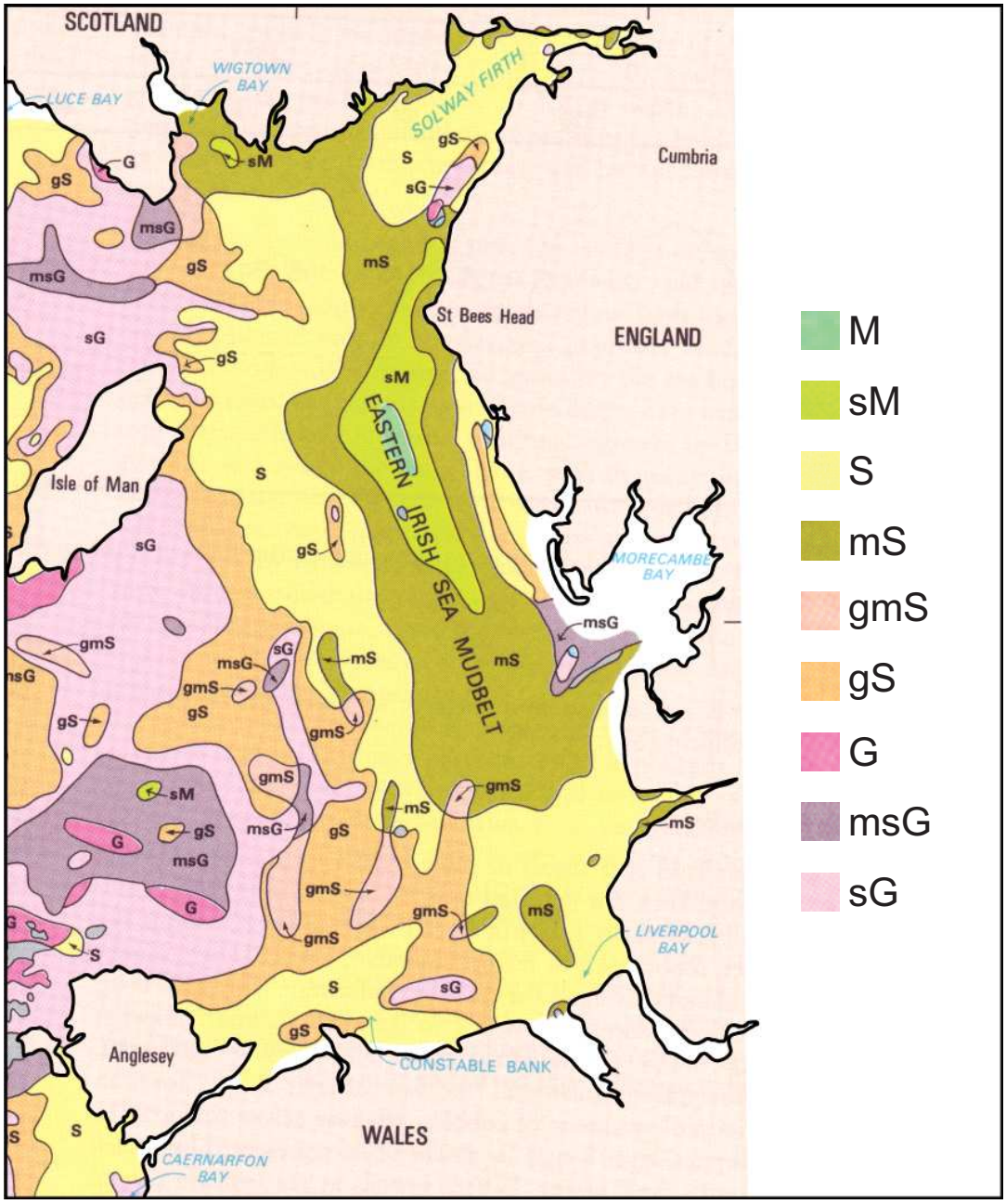

Figure 3.3: Sea bed sediment distribution from the British Geological Survey (BGS, 1996). M-mud, sM-sandy mud, S-sand, mS-muddy sand, gmS-gravelly muddy sand, gS-gravelly sand, G-gravel, msG-muddy sandy gravel, sG-sandy gravel.

of Souza and Lane (2013). Nevertheless, figure 3.5 shows evidence that coarse sediment is transported out of the estuary as bed load (Pye and Blott, 2010).

3.2 Dee Estuary

3.2.1 Morphology

Based on topography, the Dee is a coastal plain estuary situated at the southeast corner of the Liverpool Bay (Fig. 3.1b). It is believed that the Dee Estuary started its formation with the drowning of a river valley after the last glacial maximum (Steers, 1967), dated by Fairbanks (1989) about 18000 years ago. Natural and anthropogenic factors have led to accretion in the estuary and formation of very shallow areas of saltmarshes (Marker, 1967). However, some recent analysis indicate that the estuary is nearly in morphological equilibrium and sedimentation and flood dominance may decrease in the future (Moore et al., 2009). The Dee is funnel shaped with length of 30 km and a maximum width at the mouth of 8.5 km. A narrow channel comes from the shallow canalised part of the river at the south-west side of the estuary until Flint and continues on this side for about 10 km at Greenfield where it deviates to the central part and finally bifurcates before entering Liverpool Bay (Fig. 3.6). The north-east or Hilbre channel is almost oriented north-south while the south-west channel is nearly east-west orientated. Most of the inner part of the estuary is at mean sea level and only the central channel has a depth about 5 m below mean sea level. The depth increases towards the channels to 22 and 24 m for the Hilbre and Welsh channels respectively, and the central part has only about 2 m depth. The channels finish with depths diminishing to less than 5 m in the outside part of the estuary where the isobaths start to have the bathymetry of the bay. Most of these features can be seen in figure 3.6 from Moore (2009).

3.2.2 Hydrodynamics

The main hydrodynamic characteristic of the Dee Estuary is its high tidal range, e.g. 10 metres during spring tides at Hilbre Island (Bolaños et al., 2013). The classical tidal classification of estuaries proposed by Davies (1964) only set a lower limit for macrotidal systems of 4 m range at spring tide. Nevertheless, areas with high tide and extreme, short-term variability can be also distinguished from 6 m of tidal range and are called hypertidal systems (Archer, 2013). The tidal range makes the estuary tidally dominated with currents of more than 1 $m{\cdot}s^{-1}$ on the surface and nearly 0.5 $m{\cdot}s^{-1}$ near the sea bed. Tidal asymmetry is also present in the estuary with flood dominance on sandy and muddy shallow areas, although ebb dominance has been found in the channels but with less intensity (Moore et al., 2009). Flood dominance leads to stronger currents and bottom shear during flood than during ebb, which typically results in net resuspension

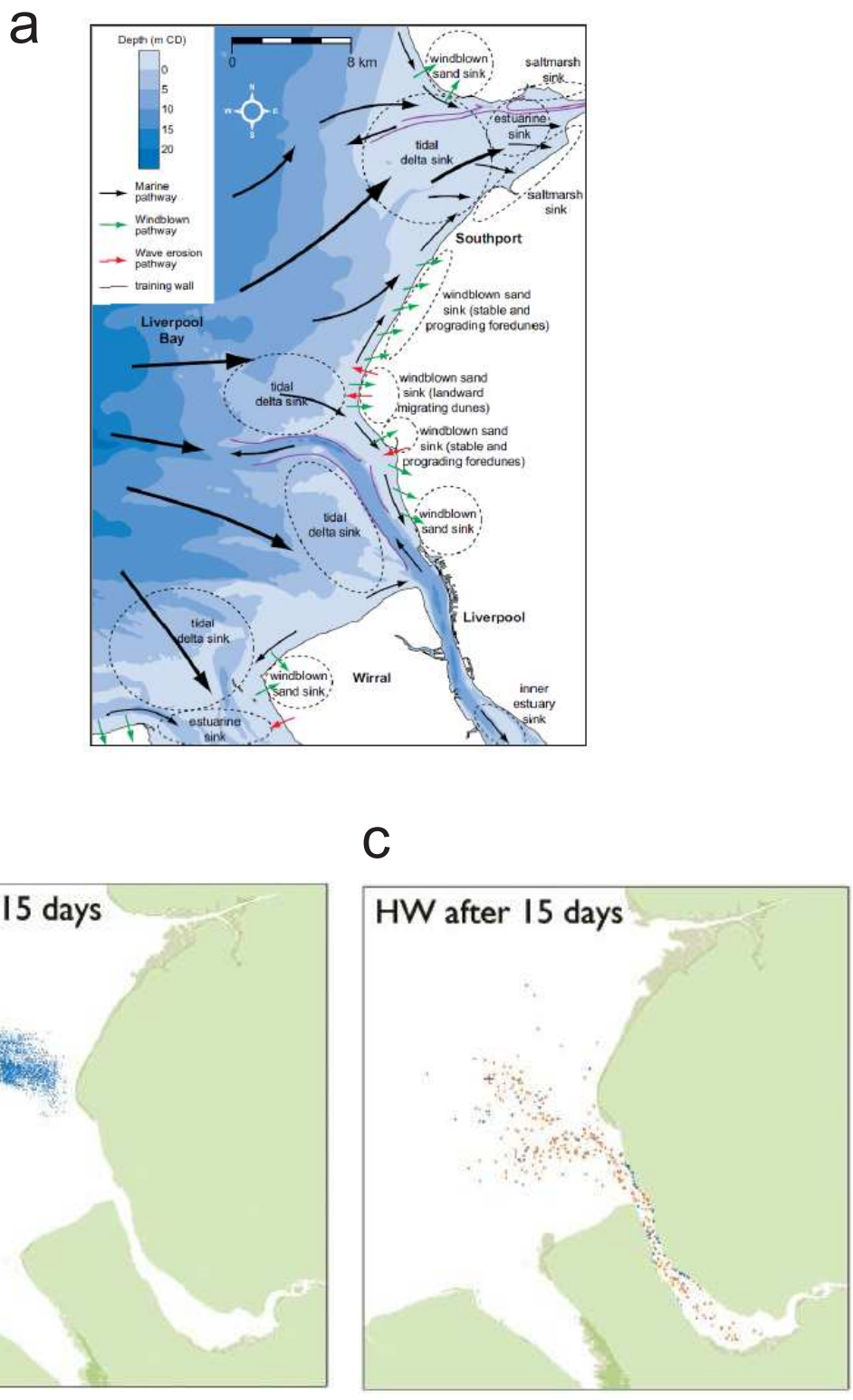

Figure 3.4: Sediment pathways and transport in Liverpool Bay. a) Generalized sediment transport (Pye and Blott, 2010), b) modelling results with muddy sand using tidal forcing only and c) modelling results including freshwater river supply from (Souza and Lane, 2013). + symbols are the release point. Blue and red points are bed and suspended sediments respectively.

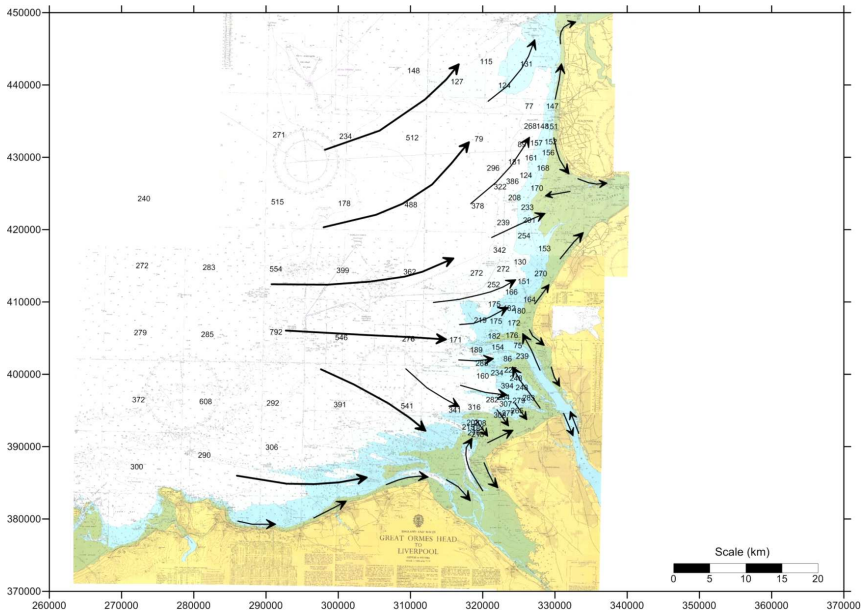

Figure 3.5: Sediment pathways inferred from the primary sand mode (Pye and Blott, 2010).

and transport of sediments into the estuary.

The baroclinicity in the estuary has an important role despite the low average river discharge. Bolaños et al. (2013) quantified different non-dimensional numbers and found that stratification, tidal straining, wind and friction all play a role in both channels although at different levels. This was supported with salinity vertical measurements which showed stratification during low tide followed by the intrusion of a salt wedge during the flood period (Fig. 3.7). Bolaños et al. (2013) also showed different residual circulation which lead to classify the Hilbre Channel as baroclinic and the Welsh Channel as barotropic. In an extended study, Brown et al. (2014) showed the time-varying characteristics of both channels. For the Welsh Channel, the residual spring tide is more important than the baroclinicity. During neap tides storm events influence the baroclinic tidal residual. During spring tides, strong winds and high waves have little effect on the dominant tidal residual. Also, waves have an influence on the stratification reducing the baroclinically induced residual. Conversely, in the Hilbre Channel baroclinicity is more important and is only exceeded by wind in cases of storm events showing that the tide is much less significant than other processes (Brown et al., 2014). Moreover, both channels seems to have different cross-channel residual circulation, with the Welsh Channel horizontally sheared while the Hilbre Channel shows a two layer exchange flow. These characteristics make it difficult to find a specific classification in terms of hydrodynamics, however, it can be stated that the Dee Estuary has two channels with different behaviour, each of which may be classified independently.

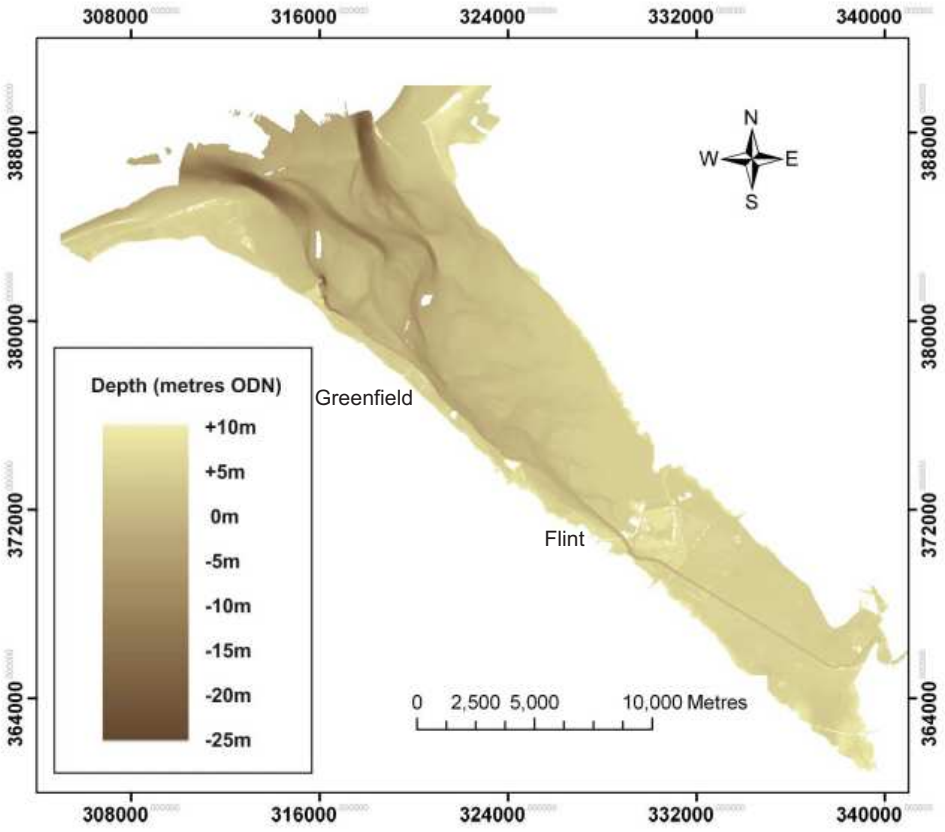

Figure 3.6: Dee Estuary bathymetry of 2003 (Moore, 2009). Depths relative to Ordnance Datum Newlyn (ODN). Coordinates of British National Grid. From the southeast, the straight section is a canalized part that ends at the west side of the estuary at Flint. The channel continues on this side until at Greenfield the main channel deviates to the central part of the estuary where bifurcates before to enter Liverpool Bay.

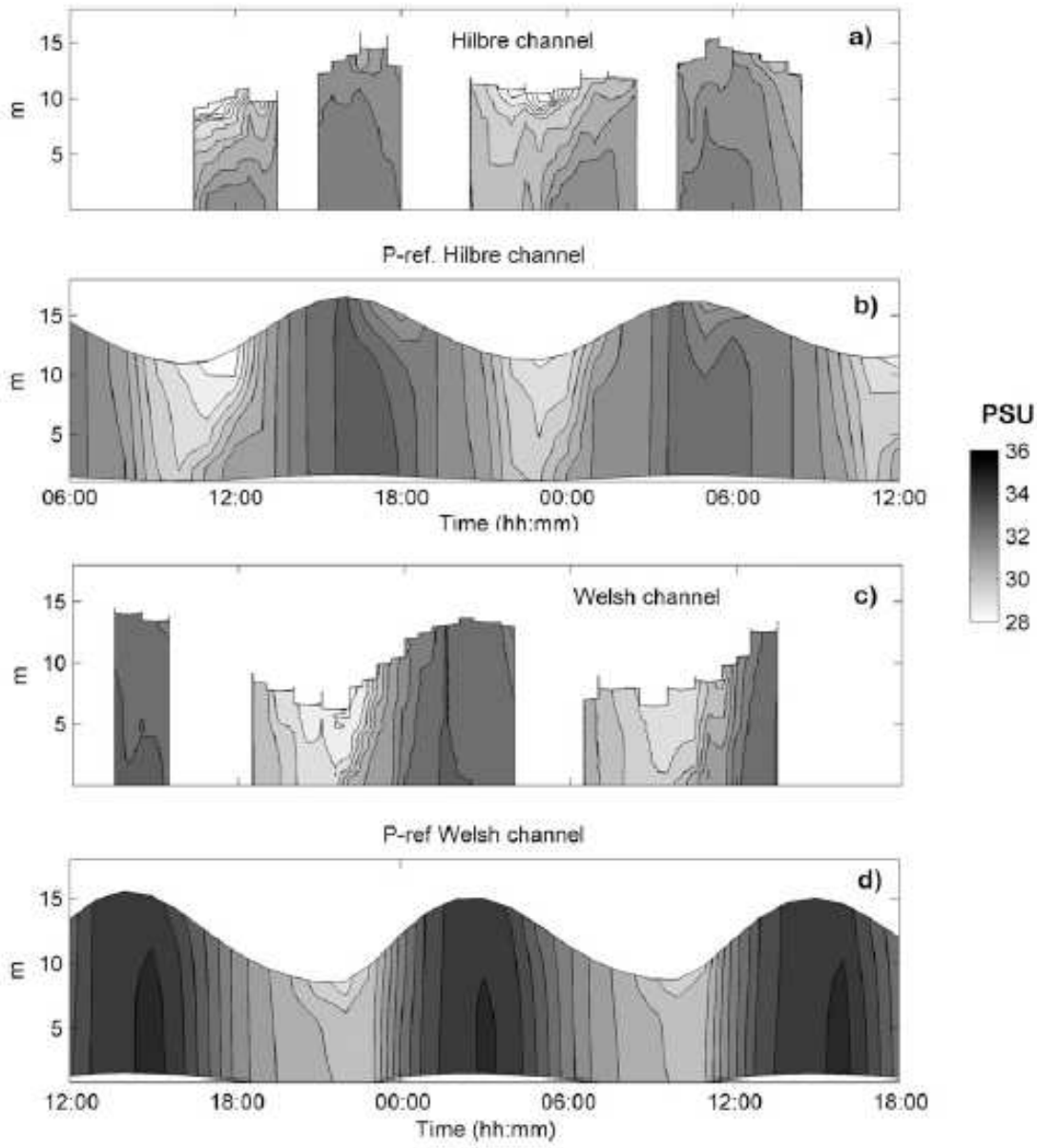

Figure 3.7: Salinity measured in the Hilbre (a) and Welsh (c) channels along with numerical simulations for the Hilbre (b) and Welsh channels (d) (Bolaños et al., 2013).

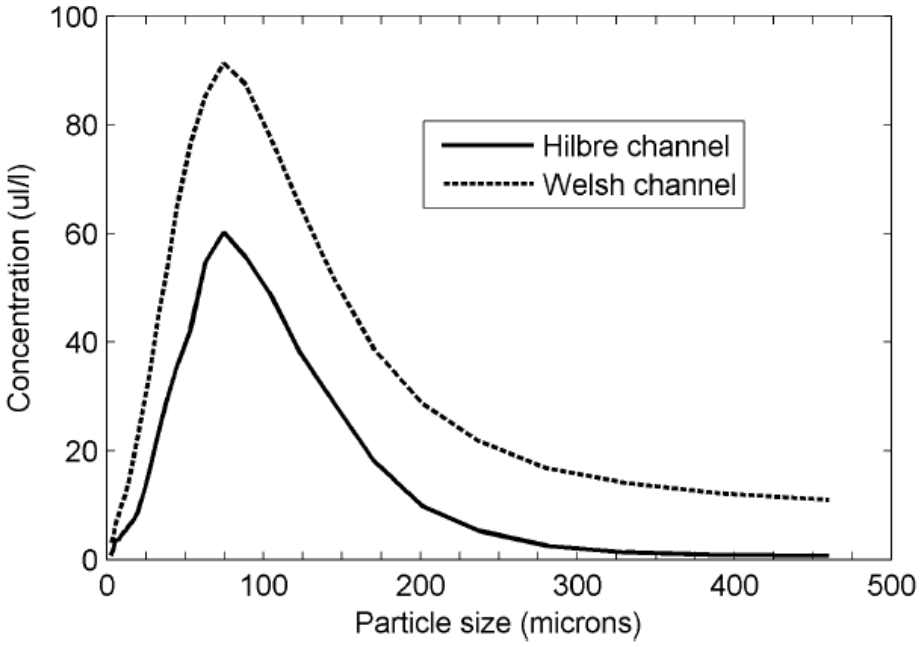

Figure 3.8: Measured suspended sediment size distribution (Bolaños and Souza, 2010).

3.2.3 Suspended sediments

The Dee estuary presents high concentrations of suspended particulate matter (SPM). Turner et al. (1994) measured surface suspended sediment concentration of about 40 $mg{\cdot}l^{-1}$ using samples taken inside the estuary before the bifurcation of the main channel. More recently, Bolaños and Souza (2010) reported volumetric concentrations of nearly 3000 $\mu l{\cdot}l^{-1}$ in the Hilbre channel. The authors also found a dominance of fine particles of about 70 μm in both channels (Fig. 3.8) which represents the limit between silt and sand. This is in agreement with the sediment fraction below 63 μm found by Turner et al. (1994) from bed samples in percentages between 23% and 62%.

In a tidally dominated estuary such as the Dee, concentration and transport of SPM would typically strongly be related to the tidal cycles. Observations by Bolaños et al. (2009) showed that SPM concentrations are controlled by flood-ebb phases and spring-neap cycles and also differences in bottom stress were found between the Welsh and Hilbre channels which seem to affect the SPM concentration. Highest SPM concentration is found during spring tides and high currents in flood and ebb. Measurements by Bolaños and Souza (2010) in the Hilbre Channel showed that SPM concentration is well correlated with the spring-neap tidal cycle. Although, there was no clear relationship between SPM maxima and quarter-diurnal current maxima during flood and ebb phases.

Regarding sediment transport, the Dee Estuary is a depository of sediments. The sources of the suspended sediments appear to be fluvial from the river discharge, resus-

pension and sediment import from offshore. According to Turner et al. (1994), sediment from a fluvial origin seems to have the lowest contribution and most of the sediment has a marine origin. An analytical model of Heaps (1972) applied to Liverpool Bay predicts residual flows northward on surface and southward near the bed. This was firstly ratified by Simpson and Sharples (1991) using a numerical model and observations, confirmed by Verspecht et al. (2009b) with 5 years observations, and by Polton et al. (2011) using both observations and modelling. These results support the phenomenon of sediment being transported into the estuary. A particle tracking modelling by Souza and Lane (2013) for Liverpool Bay, also shows sediment transport to the south-east, to the mouth of the estuaries Dee and Mersey. In addition, the tide in the Dee Estuary is flood dominant (Bolaños and Souza, 2010) and leads to a net transport of sediments towards the estuary. This suggests that sediment transport is responsible for the estuary accretion, i.e. a net transporter of sediment. Estuary sediment infilling due to tides has been also identified through particle size distributions from cores in saltmarshes by Rahman and Plater (2014). These authors found sedimentation during the last 50-100 years in upper saltmarshes as the response to sea level rise while lower saltmarshes have been accreted during the last 30 years. However, measurements by Moore et al. (2009) indicate that accretion rates are diminishing and may be leading the estuary to a stage of geomorphologic equilibrium. There is evidence of flow from the estuary as bed load to the north-west (Fig. 3.5) and according to Holden et al. (2011) it is possible that sediments from the Dee Estuary contribute to the accretion of the Sefton coast to the north of the estuary.

The Dee estuary comprises vast areas of salt marshes, tidal flats and channels. According to the Liverpool Bay sea bed sediment distribution, the north-west of the estuary entrance consists of muddy sand and gravelly muddy sand (Barne et al., 1996). This seems to be the source of sediments which are transported to the south-east by bed residual currents and flowing to the estuary through both channels (Bolaños and Souza, 2010) and causing its accretion (Moore et al., 2009). The presence of fine sediments lead to a cohesive behaviour that further complicates the understanding of sediment transport in the estuary. For example, flocculation of sediments plays an important role in sediment deposition which depending on tidal currents results in accretion of the upper part of the Dee Estuary (Rahman and Plater, 2014).

Thurston (2009) carried out a study of SPM concentration in the Hilbre Channel. After harmonic analysis, the author found an important presence of two size classes: $\sim$50 μm and between 300-400 μm in the quarter-diurnal frequency. Small flocs coincided with periods of fast currents during flood and ebb while coarse flocs reached a maximum concentration $\sim$30 minutes before slack waters suggesting particle aggregation during slow current conditions. Thurston (2009) also found a link between SPM and turbulent properties (production and dissipation of turbulent kinetic

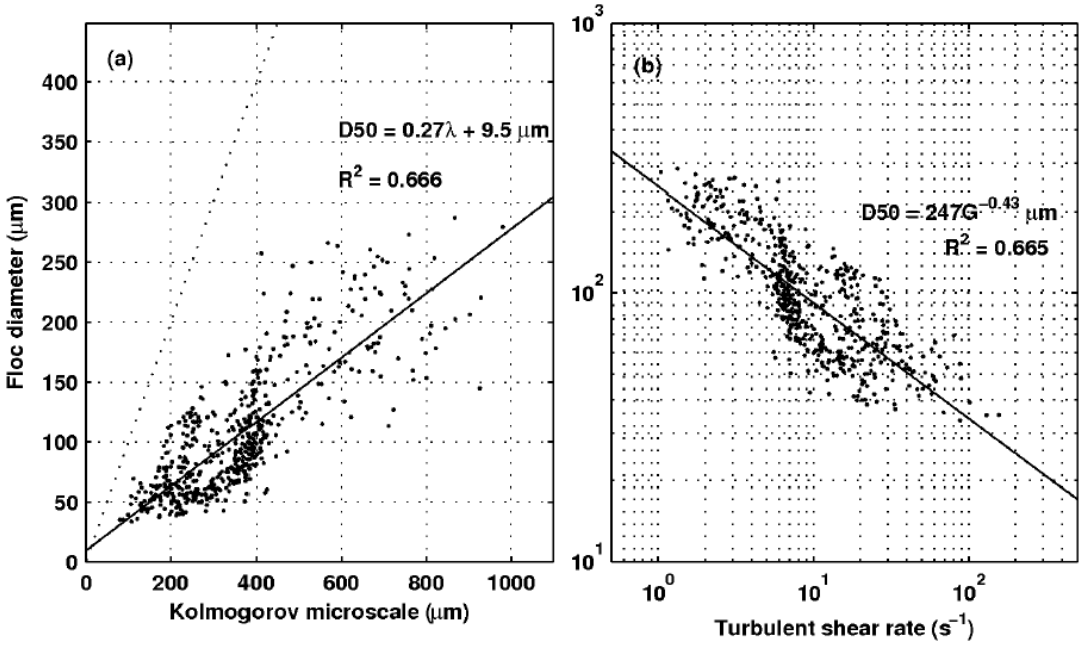

Figure 3.9: Observations by Thurston (2009) in the Hilbre Channel showing: a) median floc diameter $D50$ smaller than the Kolmogorov microscale, in this figure denoted by λ, and b) the inverse relationship between floc size and turbulent shear rate G.

energy) in which flocculation seems to happen during periods of weak turbulence and dis-aggregation during periods of intense turbulence. The relationship between median grain size and turbulence properties was also confirmed by the author using the Kolmogorov microscale of turbulence and the shear rate (Fig. 3.9).

Despite the dominance of fine sediments in the Dee Estuary and the anthropogenic changes to its morphology, a few studies exist regarding suspended sediments and flocculation. The study of Thurston (2009) is focusing on turbulence in the Hilbre Channel while the work of Bolaños and Souza (2010) is limited to present the data availability and no further analisys or explanation was presented. A good knowledge of the sediment transport and therefore of the flocculation in the Dee Estuary is needed to identify future problems and help in the management of the resources. The present study focuses on the flocculation process of suspended particulate matter and their relationship with different hydrodynamic regimes. Observations in the Welsh channel are used to investigate the effect of the strong tidal currents and waves on the flocculation of cohesive sediments. The findings of the effect of the turbulence due to currents are used to propose a formulation for the particle settling velocities and implemented in a numerical model. The behaviour of the cohesive sediments is also analised under the effect of turbulence produced by waves and currents.

Chapter 4

Methodology

This chapter explains how the study of hydrodynamics and flocculation in the Dee Estuary was carried out in the present work. The initial step is to identify whether the flocculation is indeed occurring. The first section describes (i) how the aggregation and break-up of particles were measured and (ii) the processing of velocity observations to obtain the related hydrodynamics and turbulent properties. The second section illustrates the numerical models used as a first approximation to reproduce the observations.

4.1 Observations

4.1.1 Particle size and volume concentration

Flocculation is the process of floc aggregation and break-up (Dyer, 1986; Winterwerp and van Kesteren, 2004) and therefore it is necessary to understand the variations in particle size (Winterwerp, 1998). A number of studies have been made in laboratory with either artificial or natural particles(e.g. Tambo and Watanabe, 1979; van Leussen, 1994; Verney et al., 2011). The main disadvantage of artificial particles in the laboratory is that unlike natural flocs their properties cannot change. An alternative is to use natural particles from field samples. However, floc characteristics start to change once the sample is taken in the field as they can be disaggregated by stirring during transport and handling or, on the contrary, by enhancing flocculation due to the steady conditions of the recipient sampler. A second important problem in the laboratory is to generate turbulent characteristics that adequately simulate real field conditions. In spite of these difficulties, important advances have been achieved and formulations to describe the flocculation process have been proposed (e.g., van Leussen, 1994; Winterwerp, 1998; van Rijn, 2007b; Manning, 2008). Nevertheless, floc behaviour seems to depend on local conditions, see for example Khelifa and Hill (2006) and Strom and Keyvani (2011), hence the need of simultaneous *in situ* measurements of floc aggregation-break-up and hydrodynamic conditions.

The measurements of suspended flocs can be done using images or light diffraction.

Time series using these techniques give the change of floc size. A camera takes the images of flocs as they pass through a flow chamber (e.g., Mikkelsen et al., 2006; Baugh and Manning, 2007; Graham and Nimmo-Smith, 2010; Reynolds et al., 2010). The recorded images are saved for post-processing to identify and count suspended material. Such a system seems to work well for biological purposes such as identification of organisms (Benfield et al., 2007). However, the main disadvantage is that flocs may be modified during their passage into the flow chamber, because of change to turbulent conditions, in turn affecting floc aggregation and break-up. The acoustic backscatter signal of suspended particles has been used for non-cohesive sediments to obtain concentration and grain size (e.g., Hay and Sheng, 1992; Thorne and Hanes, 2002; Thorne and Hurther, 2014). However, the application of acoustics to flocs is still at development stage because the relationship between sound and flocs is not well known (MacDonald et al., 2013). The LISST (Laser In Situ Scattering and Transmissometry) uses a light diffraction technique in a less invasive system than cameras and more reliable than acoustics-based instruments. The LISST is therefore one of the most widely used instruments to measure the size of suspended particles (e.g., Fugate and Friedrichs, 2002; Ellis et al., 2004; Fettweis et al., 2006; Davies et al., 2012; Markussen and Andersen, 2013; Amoudry et al., 2014).

The LISST measures grain size and volume concentration in approximately 100 ml of water (Fig. 4.1a). A collimated laser beam enters the water where light is diffracted by each particle at a certain angle to the optical axis of a lens. The angle and the lens focal length determine a radius sensed by a detector with 32 rings. Each ring represents a range of angles increasing logarithmically and associated with a particular size class (Fig. 4.1b). The size is then calculated assuming scattered light corresponds to that of spherical particles, and the LISST is able to measure 32 different size classes (more details in Agrawal and Pottsmit, 2000). Laboratory comparisons using artificial particles has shown good agreement between LISST and holographic camera across most of the size classes (Davies et al., 2011). A comparison between LISST, Coulter granulometer and camera system in laboratory was undertaken by Reynolds et al. (2010). The authors compared results from field samples and artificial particles, finding good agreement between them. A completely *in situ* deployment in two different sites with both a LISST and a camera system was carried out by Mikkelsen et al. (2005) and although systems have different ranges for measuring particle size, a good comparison was observed in the overlapping region between 144.43 μm and 460.27 μm. However, some LISST limitations have been identified by different authors. Davies et al. (2012) found that the effect of particles larger than the LISST maximum resolvable size produces unrealistic peaks of concentrations in the range of 250-400 μm. Styles (2006) found differences in LISST resulting concentrations depending on salinity values between 2-10 ppt, with an effect also in the larger size classes. Near-surface field observations by

Reynolds et al. (2010) showed peaks of concentration on 2 μm class which were not present in the laboratory, which was attributed to the effect of natural light during measurements.

In this study, a LISST-100C, measuring grain sizes from 2.7 to 460.1 μm, was deployed in a mooring array at 1.5 m above bottom in the Welsh Channel (Fig. 4.2). The sampling rate was one sample every 40 seconds during a 20-minute period every hour, which were then averaged to obtain hourly data. The median grain size (D_{50}) was obtained from the entire grain distribution as a single representative value of the floc size. Thus, the LISST allowed observations of the changes in grain size and volume concentration in hourly time series from 12 February to 8 March on 2008.

In order to quantify the material in suspension in terms of mass, near bottom water samples were taken hourly during the first two days of the deployment from a research vessel using a CTD rossete on 12-13 February 2008. The volume of each sample was measured and then filtered in pre-weighted 47 mm diameter filters of 1.2 μm mesh size, dried and weighted again. The difference in weight gave the mass of suspended particulate mater and together with the filtered volume results in the mass concentration of SPM. This technique is used to calibrate the output signal of optical instruments which have a linear relationship with SPM mass concentration (i.e. Optical Backscatters, Transmissometers, LISST). A linear regression can be used to convert instrument response to mass concentration. LISST data at times of water samples were used to find a calibration relationship to convert volume to mass concentration for the entire record of the LISST data.

The regression analysis between volume and mass concentration is shown in figure 4.3. Two data points are clearly outside the trend (triangles in fig 4.3) and may be the result of several factors: measurement errors by the instrument, water sample handling, occasional events at the time of measurements and sample collection. These data were not taken into account in the analysis. The minimum values were 354.1 $\mu l \cdot l^{-1}$, corresponding to 18.5 $g \cdot m^{-3}$ while maximum values were 1887.4 $\mu l \cdot l^{-1}$ and 138.1 $g \cdot m^{-3}$. The resulting linear relationship is:

$$C_m = 0.07 C_v - 0.65 \tag{4.1}$$

with a coefficient of determination R^2=0.88 and 14 degrees of freedom. This relationship is used to convert the LISST volume concentrations into mass concentrations.

One of the important properties of the flocs is their settling velocity (Winterwerp, 1998). It controls how fast a suspended floc settles and therefore how long the floc remains in the water column. A longer time leads to an increase in the relative importance of horizontal advective transport. The floc fall velocity has been measured (e.g. Tambo and Watanabe, 1979; Fennesy et al., 1994; Mikkelsen et al., 2007) or calculated from other variables (e.g. Winterwerp, 1998; Fugate and Friedrichs, 2002; Markussen

a

b

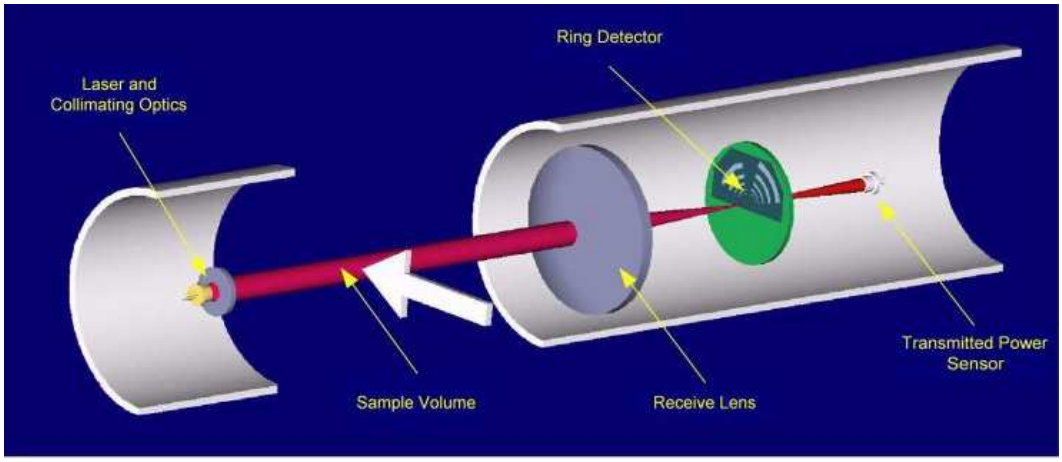

Figure 4.1: a) Photograph of a LISST Instrument, it has 0.13 m diameter and 0.87 m length. b) The lasser light is transmitted, from the left side in the picture, and the particles in the sample volume diffract the light in small forward angles which are sensed by a multiring detector (SEQUOIA, 2013).

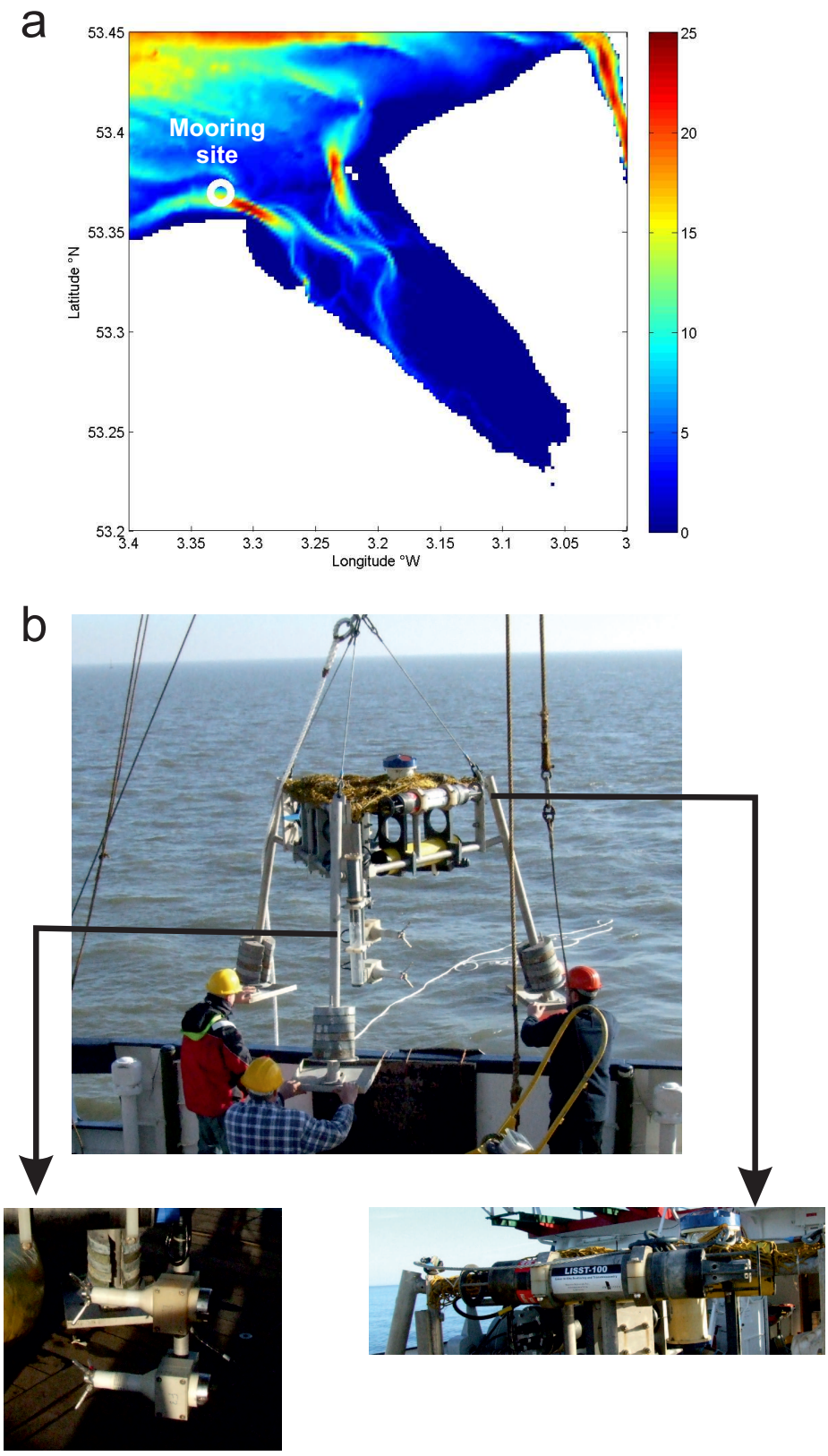

Figure 4.2: a) Mooring position in Welsh Channel, white circle b) Instrumented tripod with inserts showing ADV (left) and LISST (right). Photographs courtesy of Dr. Richard Cooke.

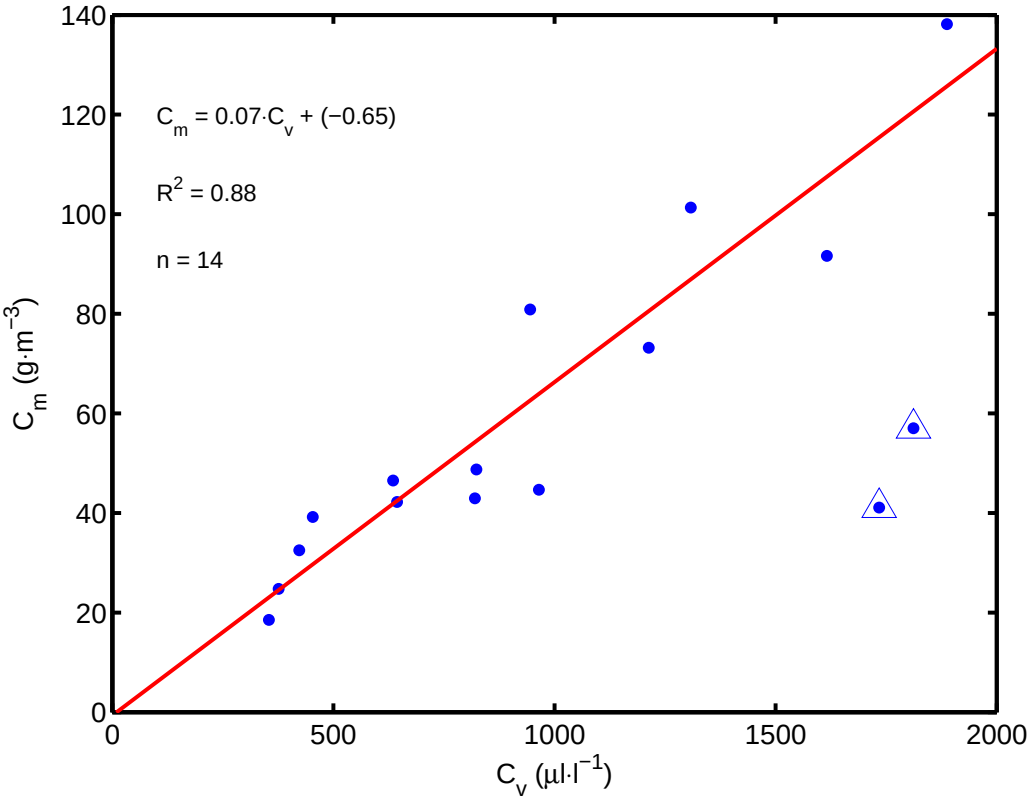

Figure 4.3: LISST volume concentrations (C_v) and mass concentrations (C_m) from water samples (blue points). Data outside the trend, marked also with triangles, are not included in the regression analysis. The line is the result of the linear relationship between the two variables.

and Andersen, 2013). A typical technique uses a tube or column where a SPM sample is left to settle and either sub-samples or images are taken at time intervals for processing to obtain particle fall velocity. More recent instruments like the LISST-ST incorporates this technique using a settling tube over the measurement volume (e.g. Ahn, 2012). Nevertheless, issues have been pointed out with regards to the long time each measurement requires (24 h) (van Wijngaarden and Roberti, 2002), the methodology to calculate settling velocities (Pedocchi and García, 2006), additional effects such as circulation inside the measuring chamber which can break the flocs (Winterwerp and van Kesteren, 2004), and it has moving parts that can become jammed. An alternative which combines holographic images and LISST is been developed by Graham and Nimmo-Smith (2010) in a less intrusive and more automated system.

As stated above, settling velocities can be also calculated from other variables (e.g., Metha, 1986; Winterwerp, 1998; van Rijn, 2007b). The basis and variables used in each formulation are as different as the formula itself, from laboratory-only data to field observations. For example, Metha (1986) proposes a power law of the concentration of cohesive sediments, van Rijn (2007b) uses a proportional relation between a flocculation factor ϕ_{floc}, a hindered factor ϕ_{hs}, and a settling velocity of single suspended particles in clear water $W_{s,o}$, and Winterwerp (1998) modifies the Stokes law to include fractal theory applied to flocs. The Stokes law has been widely applied to flocs in other studies (e.g., McCave, 1984; Mikkelsen and Pejrup, 2001). A generic result across a number of different studies is that settling velocity increases as floc size increase. However, no single formulation seems to apply across all natural conditions and a rather wide scatter of data is obtained, as shown by Strom and Keyvani (2011). The authors compiled a number of data available in the literature, including both from field and laboratory studies, and only a few of them showed a clear trend between floc size and settling velocity (Fig. 4.4). Therefore, it is still a topic of investigation to find a formula suitable to all real, variable natural conditions in estuaries.

In practice, studies are commonly restricted by available resources, which often restricts the actual choice of technique or formulation. In particular, settling velocities can only be calculated from the variables that are measured *in situ*. The formulations mentioned previously and described in section 2.3.1 are also restricted either by the variables they use or by a number of assumptions. Following from constraints on the available data and trying to minimize assumptions, the classical Stokes Law was used because it only requires floc size (D_{50}) and effective density (ρ_e):

$$W_s = \frac{g\rho_e D_{50}^2}{18\mu} \tag{4.2}$$

where g is gravitational acceleration, μ is water kinematic viscosity. Taking into account that the observations are in the applicability range of the Stokes law (i.e., $Re_s < 1$), the effective density is the only variable to be estimated. Nevertheless,

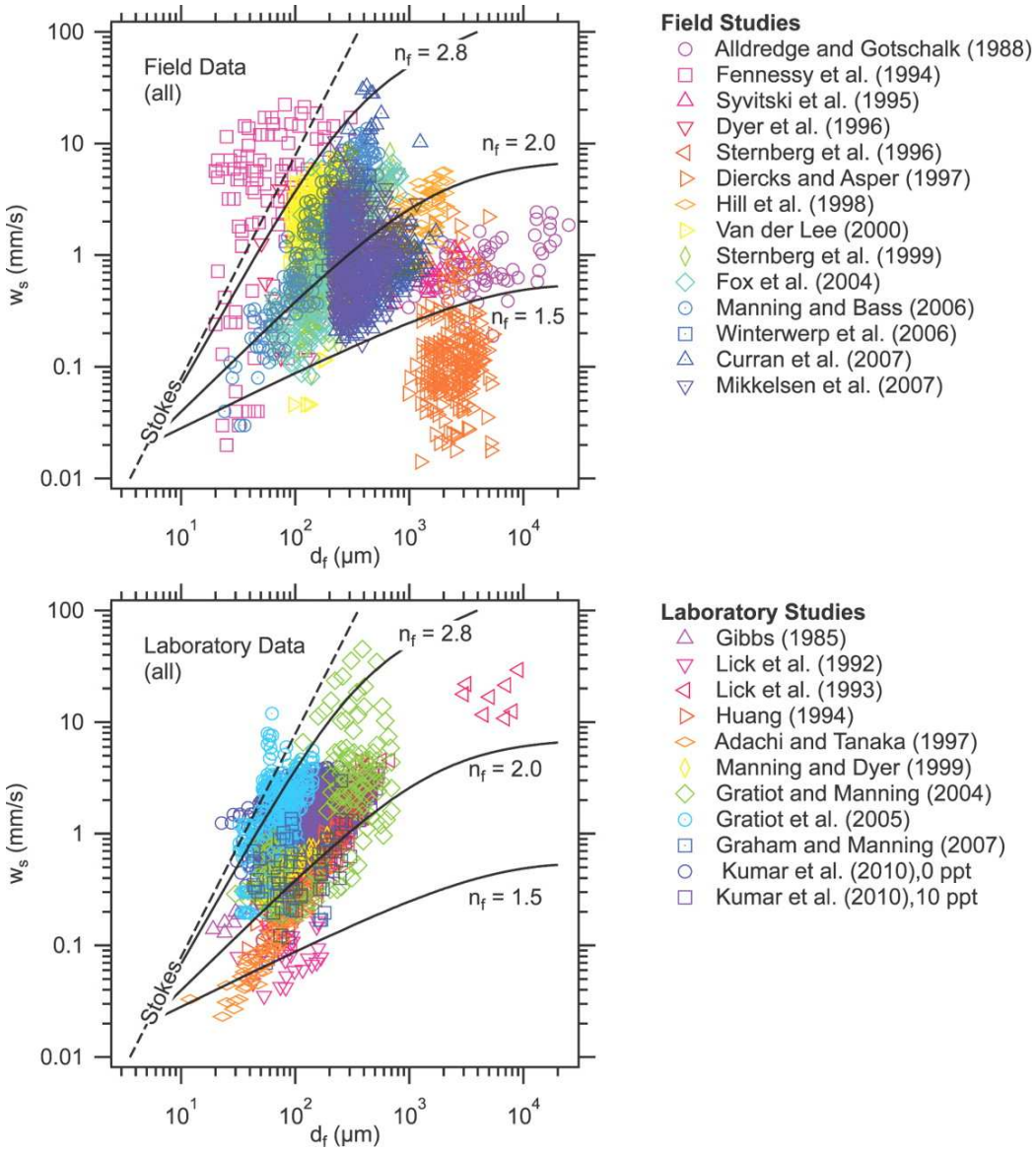

Figure 4.4: From Strom and Keyvani (2011) showing a compilation of floc settling velocities obtained in different studies distinguished with symbols and colors. Where n_f is fractal number and d_f is floc diameter. References of the studies used are available in cited paper.

comparisons with the following literature available formulations by Winterwerp (1998) and Khelifa and Hill (2006) are also carried out:

$$W_s = \frac{\alpha}{18\beta}\frac{(\rho_s - \rho_w)g}{\mu}{D_p}^{3-n_f}\frac{{D_{50}}^{n_f-1}}{1+0.15Re^{0.687}} \tag{4.3}$$

and

$$W_s = \frac{1}{18}\theta g\frac{(\rho_s - \rho_w)}{\mu}{D_p}^{3-F}\frac{{D_{50}}^{F-1}}{1+0.15Re^{0.687}}\phi \tag{4.4}$$

In equation 4.3 α and β are shape coeficients, ρ_s and ρ_w are sediment and water density respectively, μ is water dynamic viscosity, D_p is primary particle diameter and D_{50} is median particle diameter. In this formulation flocs are considered as fractals and n_f is the corresponding fractal number for a specific study site. In equation 4.4, Khelifa and Hill (2006) consider the fractal number as variable (F) and depends on floc sizes. McCave (1984) proposed a relationship between effective density and floc size as:

$$\rho_e = 30.856{D_{50}}^{-1.3} \tag{4.5}$$

Effective densities obtained with equation 4.5 are used to calculate settling velocity with the Stokes law. The comparison of these three methods and the results of this study are presented in section 5.4.5.

The effective density has been related to the floc size via a range of assumptions (e.g., McCave, 1984; Gibbs, 1985; Khelifa and Hill, 2006). However, these rely on experimental data and assumptions without general applicability. An example of the different results by different authors can be found in Khelifa and Hill (2006) and is reproduced in figure 4.5.

In the present work the effective density was obtained from LISST volume concentrations (VC) and mass concentration from water samples (M_p). If flocs are the most important part of the suspended particles, the effective density ρ_e can be obtained following Mikkelsen and Pejrup (2001):

$$\rho_e = \rho_f - \rho_w \tag{4.6}$$

where ρ_f and ρ_w are floc and water density respectively, and floc density can be defined as:

$$\rho_f = \frac{M_f}{V_f} = \frac{M_p + M_w}{V_p + V_w} = \frac{M_p}{V_p + V_w} + \frac{M_w}{V_p + V_w} \tag{4.7}$$

where the total floc mass (M_f) consist of the particle and water masses (M_p and M_w) and total floc volume of particle and water volume (V_f and V_w). Rearranging:

$$\frac{M_f}{V_f} - \frac{M_w}{V_p + V_w} = \frac{M_p}{V_p + V_w} \tag{4.8}$$

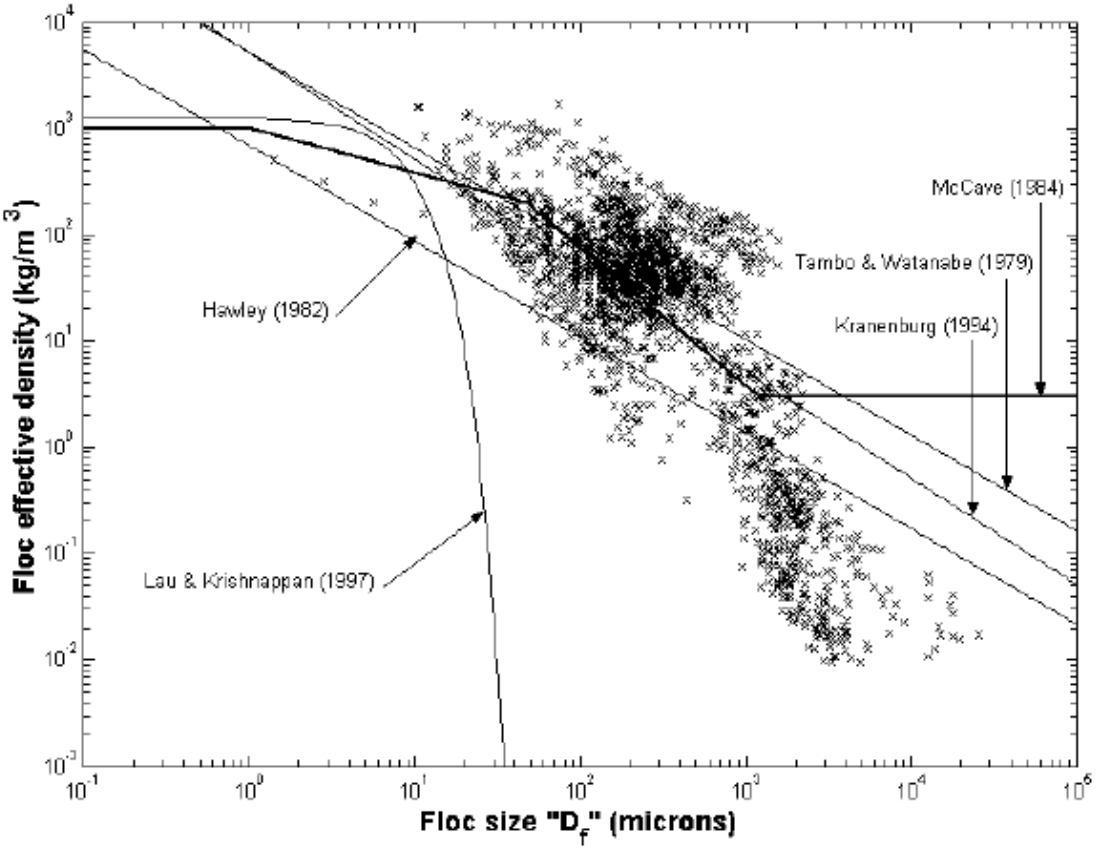

Figure 4.5: Comparison of floc effective densities from Khelifa and Hill (2006) showing data in symbols and results of models in lines. Where D_f is floc diameter. References of the studies used are available in cited paper.

if water volume is much larger than particle volume ($v_w >> V_p$), then:

$$\frac{M_f}{V_f} - \frac{M_w}{V_w} \approx \frac{M_p}{VC} \tag{4.9}$$

where the left hand side is $\rho_f - \rho_w$, therefore:

$$\rho_e \approx \frac{M_p}{VC} \tag{4.10}$$

and time series of effective density can be calculated and used in the Stokes law.

In order to assess the methodology applied, a comparison with three different approaches was made but focusing on the use of available observations in this study (Section 5.4.5). The first, and most simple, is that of McCave (1984) which is based on obtaining floc effective density as a function of a power of the median grain size as $\rho_e = D_{50}^{-1.3}$ and calculates W_s using Stokes law. The second approach is the widely used Winterwerp (1998) relation, as mentioned before, it modifies the Stokes law and applies fractal theory to calculate settling velocities. Finally, although derived from Winterwerp (1998), the formulation proposed by Khelifa and Hill (2006) was chosen because it adds a degree of complexity by taking into account a variable fractal number (see section 2.3.1 for details of three models).

4.1.2 Current velocity and turbulent properties

The current velocity and pressure at 0.3 mab (metres above bed) were measured using an Acoustic Current Velocimeter (ADV) installed on the same instrumented tripod as the LISST (Fig. 4.2) with a sampling rate of 16 Hz in bursts of 20 minutes every hour and recording for the same period as the LISST. The ADV uses the Doppler effect by emitting two known frequency short pulses of sound which propagates through water. As the sound passes through a sample volume, the particulate matter reflects the acoustic energy in all directions and some travels to a receiver in the ADV which measures the change in phase in a technique called pulse-coherent processing (SonTek, 2002). This phase change is related to the velocity of the particles via the well-known doppler effect. Using three receivers, the ADV is then capable of measuring three dimensional current velocity (Fig. 4.6).

It is common to find spike noise in the ADV due to Doppler signal aliasing and air bubbles. The noise in ADV data used in this work was removed using a despiking algorithm based on a three dimensional phase space method of Mori et al. (2007) which is based on the method of Goring and Nikora (2002). An example is shown in figure 4.7.

In an initial analysis, the data without the influence of waves were taken into account to observe sediment dynamics under the effect of currents only. Turbulent Reynolds stresses were calculated for each burst using:

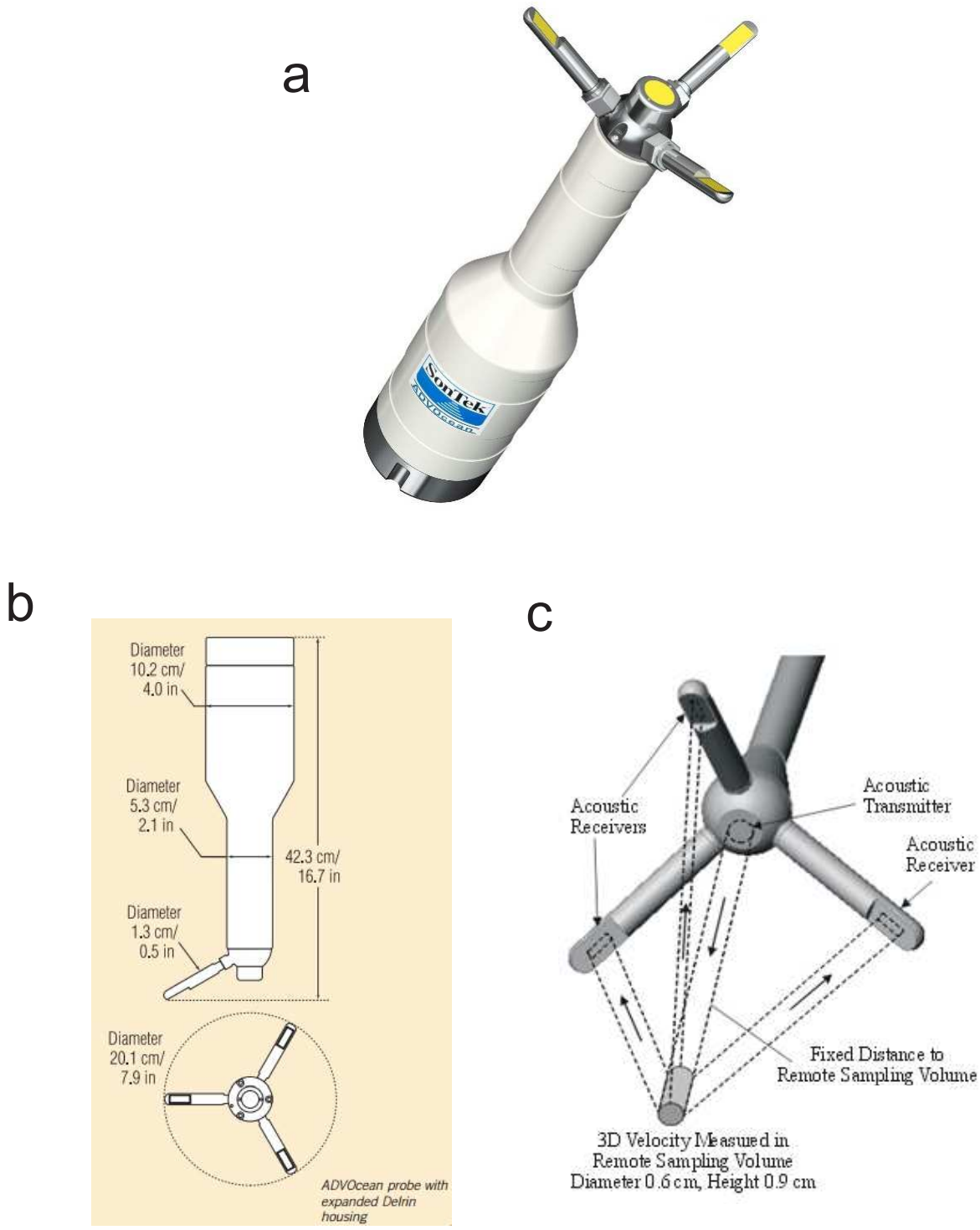

Figure 4.6: a) Photograph of an ADV, b) dimensions and c) sensor configuration.

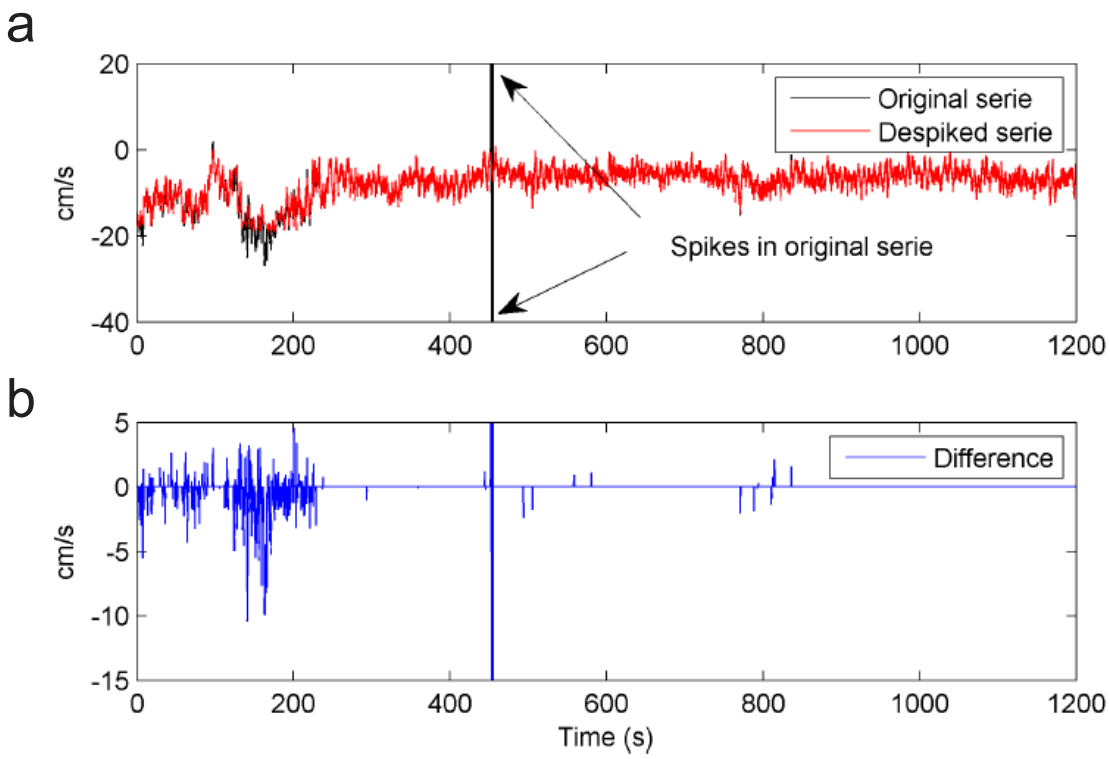

Figure 4.7: Example from Bolaños and Souza (2010), a) time series of one burst of horizontal current velocity magnitude showing the original series in black with a spike in burst number 450 and the resulting series in gray after using the despiking algorithm and b) difference between original and despiked series.

$$\tau = \rho\sqrt{\overline{u'w'}^2 + \overline{v'w'}^2} \tag{4.11}$$

where ρ is fluid density, u', v' and w' are velocity fluctuations, and the overbar indicates time average.

A further analysis was made to the entire set of data in order to compare the effect of turbulent stress from currents and waves on sediment dynamics. The fast sampling rate for velocity and pressure allowed calculation of wave parameters using the PUV method (Gordon and Lohrmann, 2001):

$$S_{\eta p} = \left(\frac{\cosh\ kh}{\cosh\ k(h+z)}\right)^2 \frac{S_p}{\rho_w^2 g^2} \tag{4.12}$$

$$S_{\eta u} = \left(\frac{\sinh\ kh}{\cosh\ k(h+z)}\right)^2 \frac{S_u}{\omega^2} \tag{4.13}$$

where $S_{\eta p}$ and $S_{\eta u}$ are surface spectra using pressure and velocity spectra, respectively, S_p and S_u, k is wave number, h is mean water level relative to the seabed, z is vertical distance relative to the mean water level, ω is wave angular frequency (defined as 2πf, where f is frequency in cycles per second), ρ_w is water density and g is gravity. The wave number was obtained from the wave dispersion relation (Fenton and McKee, 1990):

$$\omega = \sqrt{gk\tanh kh} + kU\cos\alpha \tag{4.14}$$

where the second term on the right hand side is a modification to account for the presence of a mean current U with an angle α with the waves (Bolaños and Souza, 2010). The wave direction D_w is obtained using:

$$D_w = \arctan 2(S_{pu}, S_{pv}) \tag{4.15}$$

where $\arctan 2$ is fourth quadrant arctangent of the real parts of the cross-spectra between pressure-east velocity component (S_{pu}) and pressure-north velocity component (S_{pv}). Spectral energy integration was used to calculate the zeroth moment M_o and obtain the significant wave height (H_s) as:

$$H_s = 4\sqrt{M_o} \tag{4.16}$$

The peak period (T_p) is taken as the period with highest energy in the wave spectra. Wave orbital velocities can be obtained following the linear approach:

$$U_o = \frac{a_w\omega}{\sinh kh} \tag{4.17}$$

where a_w is wave amplitude ($H_s/2$), and the value of k is calculated using the iterative Newton-Raphson method given by Wiberg and Sherwood (2008). Madsen

(1994) proposed an iterative method to obtain shear velocities from waves, currents and combined waves and currents. It uses the wave orbital velocity, wave angular frequency, the direction of wave propagation, current direction, current velocity and the bottom roughness. The method is based in a spectral wave-current model applied to simple periodic plane waves. The wave-current shear velocity u_{*cw} is obtained as:

$$u_{*cw}^2 = C_\mu u_{*w}^2 \tag{4.18}$$

where u_{*w} is the shear velocity from waves and:

$$C_\mu = (1 + 2\mu|cos\phi_{cw}| + \mu^2)^{1/2} \tag{4.19}$$

with:

$$\mu = \left(\frac{u_{*c}}{u_{*w}}\right)^2 \tag{4.20}$$

where the angle between waves and currents ϕ_{cw} is defined as:

$$\phi_{cw} = \phi_c - \phi_w \tag{4.21}$$

with ϕ_c and $\phi_w = D_w$, the direction of propagation of currents and waves respectively obtained from the PUV analysis.

Using the wave friction factor f_w concept:

$$u_{*w}^2 = \frac{1}{2} f_w U_o^2 \tag{4.22}$$

The wave friction factor is obtained based on the relative roughness and is approximated with the following formulas:

$$f_w = C_\mu exp\left\{7.02\left(\frac{C_\mu U_o}{k_N \omega}\right)^{-0.078} - 8.82\right\} \tag{4.23}$$

$$\text{for } 0.2 < C_\mu U_o / k_N \omega < 10^2$$

and:

$$f_w = C_\mu exp\left\{5.61\left(\frac{C_\mu U_o}{k_N \omega}\right)^{-0.109} - 7.3\right\} \tag{4.24}$$

$$\text{for } 10^2 < C_\mu U_o / k_N \omega < 10^4$$

where k_N is the Nikuradse number taken as $k_N = 30 z_o$ with $z_o = 2.5 D_{50}$ (Amoudry and Souza, 2011a) and D_{50} the median grain size.

The current shear velocity u_{*c} is calculated using:

$$u_{*c} = \frac{u_{*cw}}{2} \frac{\ln(z_r/\delta_{wc})}{\ln(\delta_{wc}/z_o)} \left(-1 + \sqrt{1 + \frac{4\kappa \ln(\delta_{wc}/z_o)}{(\ln(z_r/\delta_{wc}))^2} \frac{U_{zr}}{u_{*cw}}} \right) \tag{4.25}$$

where U_{zr} is velocity magnitude at height z_r, κ is the von Kármán constant (=0.4) and δ_{wc} is the wave boundary layer thickness, which Madsen specified as:

$$\delta_{wc} = \begin{cases} 2\kappa u_{*cw}/\omega & \text{for } C_\mu U_o/k_N\omega > 8 \\ k_N & \text{for } C_\mu U_o/k_N\omega < 8 \end{cases} \tag{4.26}$$

The iterative method starts with $\mu = \mu(0) = 0$ and $C_\mu = C_\mu(0) = 1$ in equations 4.19 and 4.20, respectively. Using equations 4.23 or 4.24, $f_w = f_w(0)$ is obtained and $u_{*w} = u_{*w}(0)$ with equation 4.22, and then $u_{*cw} = u_{*cw}(0)$ from equation 4.18. The value of $u_{*cw}(0)$ is used to find δ_{wc} in 4.26 which is applied in equation 4.25 to obtain the first value of $u_{*c} = u_{*c}(0)$. The value of μ can be updated with $u_{*c}(0)$ and $u_{*w}(0)$ in equation 4.20. The procedure is repeated until convergence is achieved.

Once shear velocities are calculated using Madsen (1994) method, bottom shear stresses from waves and currents are obtained using:

$$\tau_w = \rho u_{*w}^2 \tag{4.27}$$

$$\tau_c = \rho u_{*c}^2 \tag{4.28}$$

$$\tau_{cw} = \rho u_{*cw}^2 \tag{4.29}$$

where τ is turbulent stress, ρ is fluid density, subscripts w, c, cw are for waves, currents and combined waves and currents, respectively. It is important to note that the method of Madsen (1994) is based in a model which applies several assumptions, such as a representative periodic wave, and has limitations. The most important limitation is the correct determination of the wave boundary layer thickness δwc, which is strongly related to the bottom roughness. The model also enhances the importance of the near bottom orbital velocity, which has the greatest effects on the bottom shear stress and therefore is also dependent on an good determination of U_o. Nevertheless, Madsen (1994) method was chosen to calculate the different contributions of currents and waves because of the rigorous derivation of the wave characteristics. Results of the use of this model should be considered qualitative of the current-wave magnitude contributions rather than quantitative like the turbulent stresses calculated using equation 4.11 although both should show similar behaviour. Unlike Reynolds stresses, which are calculated from observations at 0.3 mab, bed shear stresses for currents and waves are the result of a theoretical model.

In order to study the role of turbulent properties related to floc behaviour, four variables were obtained. Turbulent kinetic energy *TKE* including currents and waves can be calculated from velocity fluctuations as:

$$TKE = \frac{1}{2}(\overline{u'^2} + \overline{v'^2} + \overline{w'^2}) \tag{4.30}$$

Dissipation of turbulent kinetic energy ϵ is then estimated following the inertial dissipation method. This method assumes that wave numbers at which turbulence is produced are well separated from wave numbers at which *TKE* is dissipated by viscosity and this range is called the inertial range, where the flux of energy from high to low wave numbers must be equal to the dissipation range if no sources or sinks of *TKE* are present (Huntley, 1988; Souza et al., 2011). Following Tennekes and Lumley (1972) and Voulgaris and Trowbridge (1998), the turbulent spectrum of the horizontal velocity component $E_u(k)$ is :

$$E_u(k) = \frac{9}{55}\alpha\epsilon^{2/3}k^{-5/3} \tag{4.31}$$

and the turbulent spectrum for the vertical velocity used in this study E_w is obtained as:

$$E_w(k) = \frac{4}{3}E_u(k) \tag{4.32}$$

where α=1.5 is the Kolmogorov constant and k is wave number. The spectra obtained from current velocities needs to be expressed as wave number spectra k where the Taylor hypothesis or also called frozen turbulence concept is applied. Following this theory, eddies of length L (diameter) advected beyond a fixed sensor by a mean flow U have an apparent frequency given by U/L and the link between frequency and wavenumber leads to k=$2\pi f/U$ (Tennekes and Lumley, 1972). In addition, equations 4.31 and 4.32 are only valid in the inertial subrange $k_u\kappa z > 1.8$ (Voulgaris and Trowbridge, 1998). Surface gravity waves could coincide with part of the inertial subrange. In this case Green (1992) applies a linear technique using the coherence between total velocity and the sea surface elevation to filter the waves in the spectrum. For this study, this filtering was not needed because there was no overlap between waves and turbulent ranges, and examples are included in the results section.

Once ϵ is known, the Kolmogorov microscale of turbulence (η) and the turbulent shear parameter (G) were obtained following:

$$\eta = \left(\frac{\nu^3}{\epsilon}\right)^{1/4} \tag{4.33}$$

$$G = \left(\frac{\epsilon}{\nu}\right)^{1/2} \tag{4.34}$$

The inertial dissipation method used to obtain the turbulent kinetic energy dissipation assumes (Tennekes and Lumley, 1972): a) that wave numbers at which turbulence production and dissipation occur are well separated, b) the Taylor's hypothesis of frozen turbulence, c) high Reynolds numbers, and d) isotropic turbulence. If any of these assumptions being invalid could lead to errors in further calculations.

The inertial sub-range

In a turbulent flow the energy is transfered and dissipated from large to small eddies and these to each time smaller eddies until reaches the molecular level and kinetic energy is dissipated by viscosity in the called energy cascade (Richardson, 1922). However, if there is no energy input from the mean flow and also no loss because of viscosity, the cascade of energy is conservative and the transfer of energy from large to small scales is constant (Tennekes and Lumley, 1972). This constant part is the inertial sub-range in the turbulent spectrum $E(k)$, which must exist for the first assumption to be valid. In the inertial sub-range, the spectrum has a slope of approximately -5/3. Figure 4.8a shows an example of a turbulent spectrum showing the inertial sub-range and a reference line with the -5/3 slope. It can be seen that for this case the approximation is valid although there is no specific criterion to decide whether the resulting spectrum is a good estimation. Figure 4.8b presents the time series for the entire study period and shows the limits of the inertial sub-range in white lines. Although the upper limit is outside the range of wave numbers, the limit at about 0.15 m^{-1} is clearly visible. The energy from the highest waves is in the range of lower wave numbers with no overlap with the inertial sub-range.

An example of a complete tidal cycle of the turbulent spectrum is shown in figure 4.9. The beginning of the cycle exhibits good agreement with the slope of -5/3 which corresponds from the end of the flood to high water slack (9:00-12:00) and is also a period of low values of dissipation (see fig. 6.5b). Therefore, the dissipation rate of turbulent kinetic energy at this period is low. The next five hours (13:00-17:00) are characterized by a peak in energy and almost conserving the -5/3 slope, except in some cases (14:00-15:00) at high wave numbers. It is clear that the last three hours (18:00-20:00) exhibit the higher differences, with the -5/3 slope coinciding with the lowest expected energy of the tidal cycle because of the end of the ebb phase and the lowest values of ϵ. In fact, the vertical scale for the spectrum corresponding to 19:00 has been changed in order to plot the complete spectrum. This means that maybe the estimation of dissipation at these stages of the tidal cycle is not valid.

Taylor's hypothesis: frozen turbulence

The Taylor's hypothesis assumes that there is no change in the turbulent fluctuations during the time the measurements are taken, i.e. the eddy properties remain constant

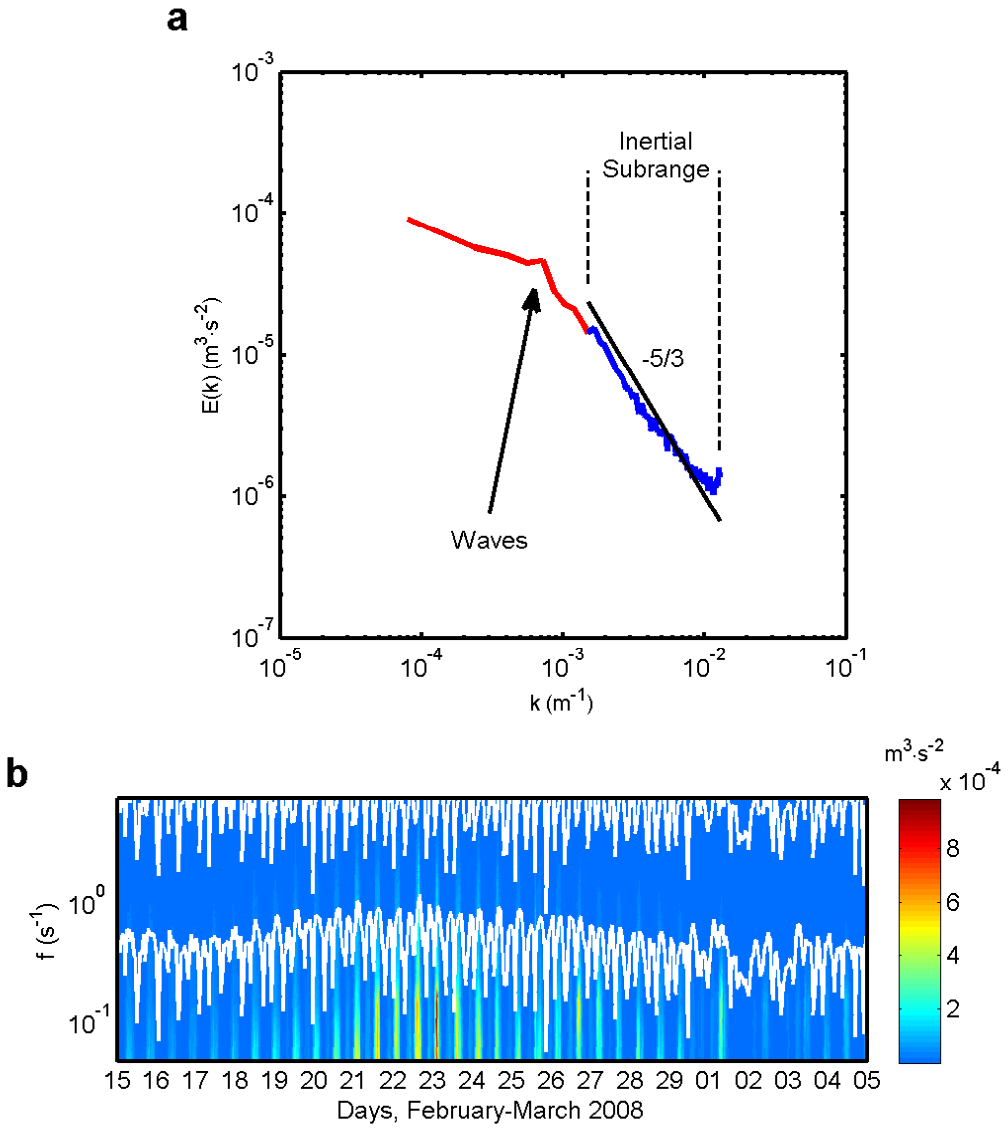

Figure 4.8: a) Example of turbulent spectrum using the ADV observations corresponding to the burst at 9:00 in 22 February, 2008. The complete spectrum consists of red and blue lines. The blue line is the part of the spectrum in the inertial sub-range, as indicated, which is used to calculate the dissipation of turbulent kinetic energy ϵ. The black line with a slope of -5/3 has been plotted for reference. The arrow points to the peak in the frequency of the waves showing that for this case are outside of the inertial sub-range. b) Complete time series of turbulent spectrum in terms of frequency throughout the study period. White lines indicate the inertial sub-range.

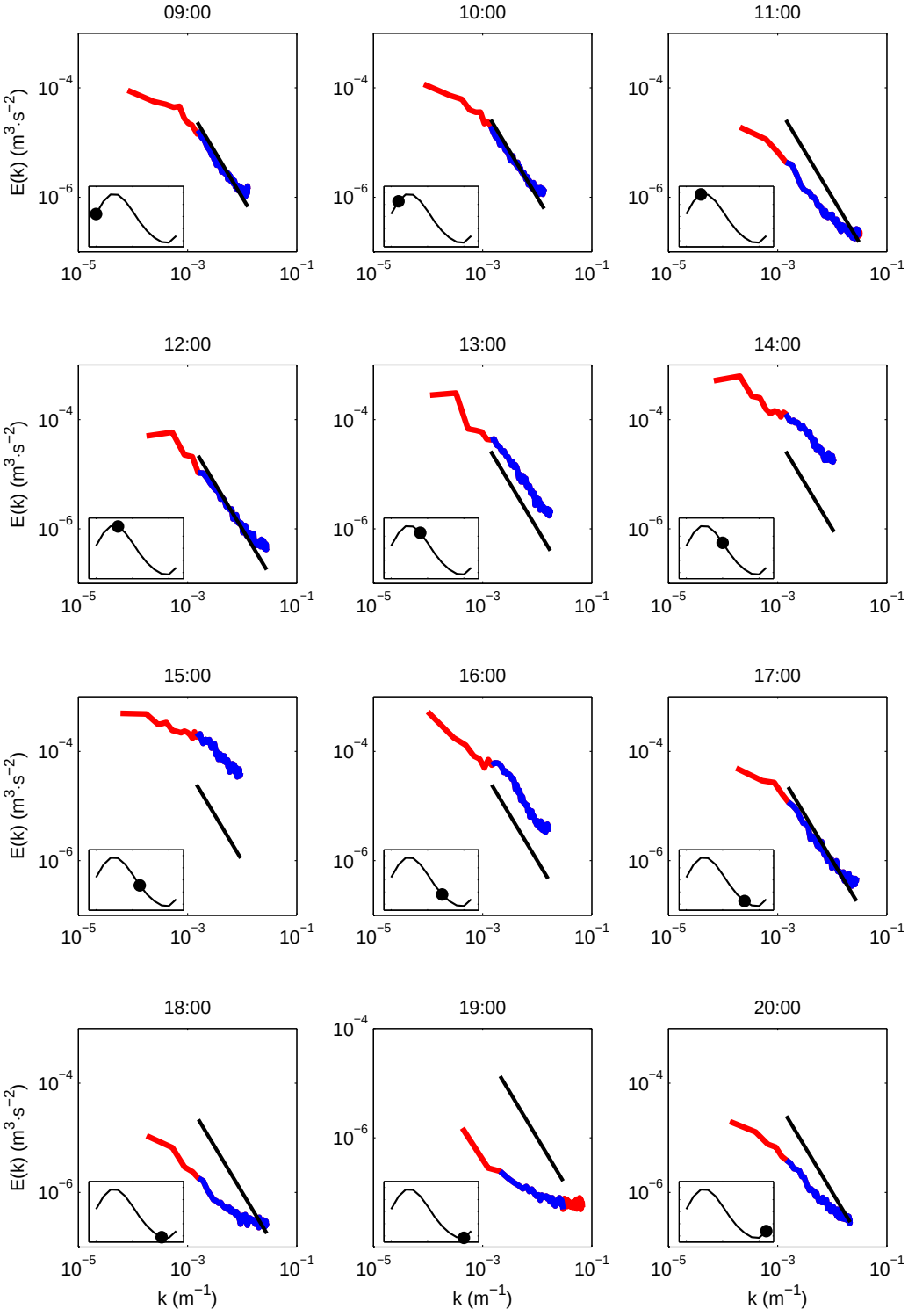

Figure 4.9: Example of turbulent spectrum results for a complete tidal cycle from hourly bursts taken by the ADV in 22 February, 2008. The complete spectrum consists of lines red and blue, the latter in the inertial sub-range, and the black line has a slope of -5/3 for reference. Small inner plots show the depth elevation for the tidal cycle and the black point indicates the specific elevation at which the burst was taken. Notice the change in scale at 19:00.

while it is advected by a mean velocity field past the sensor. A rough approximation would be the ratio $w'/\overline{U_H} \ll 1$. Where w' is the vertical velocity fluctuation and U_H the horizontal mean velocity. Figure 4.10 shows the ratio $w'/\overline{U_H}$ along with water depth for the three regimes. The obtained ratio $w'/\overline{U_H}$ is always lower than 0.5, with small semidiurnal variability. Ratio minima occurred during the flood while maxima during the ebb phase. There is no pattern coinciding with the periods when the slope of the inertial sub-range approximate the -5/3 value.

Reynolds number

For the estimation of the Reynolds number, the following relations were used:

$$Re = \frac{\kappa U_* z}{\nu} \tag{4.35}$$

where κ is the von Kármán constant (0.4), z is the height of the sensor, in this case the ADV, ν is kinematic viscosity ($1.4\times10^{-6}\mathrm{m}^3\cdot\mathrm{s}^{-1}$ at 8°C) and U_* is defined as:

$$U_* = \left(\frac{\tau_{cov}}{\rho}\right)^{1/2} \tag{4.36}$$

Resulting Reynolds numbers are shown in figure 4.11. The values during ebb phases are in general larger than the critical value Re_{cr} of 3000 used in the literature as a proof that the flow is fully turbulent (Huntley, 1988; Stapleton and Huntley, 1995; Sherwood et al., 2006) with the highest values during the "currents-waves" regime and lowest values around 1000, and consistent within the three hydrodynamic regimes. Even though most of the results are below the critical value Re_{cr}, the inertial sub-range with a $k^{-5/3}$ region on the spectrum can still be present at Re values lower than Re_{cr} (Huntley, 1988). The magnitude of the Reynolds numbers obtained for the Welsh Channel is similar to that found by Sherwood et al. (2006), with similar behaviour, higher values coinciding with periods of high turbulent stresses in a combined forcing of currents and waves. This means that low Reynolds numbers can be obtained from observations and the inertial dissipation method is may still be valid, even though Re results are lower than the critical value.

Isotropic turbulence

The assumption of isotropic turbulence implies that there is no preferential direction of the turbulent velocity fluctuations in the inertial sub-range. Theory proposed by Kolmogorov states that in the energy cascade from large to small eddies, the process of turbulence production from large eddies with corresponding orientation vanishes and, on average, the turbulence is isotropic (Green, 1992) and is called local isotropy. This is due to the loss of information in a long series of small steps and therefore only large eddies contain information about a preferential direction. Contrasting results have been

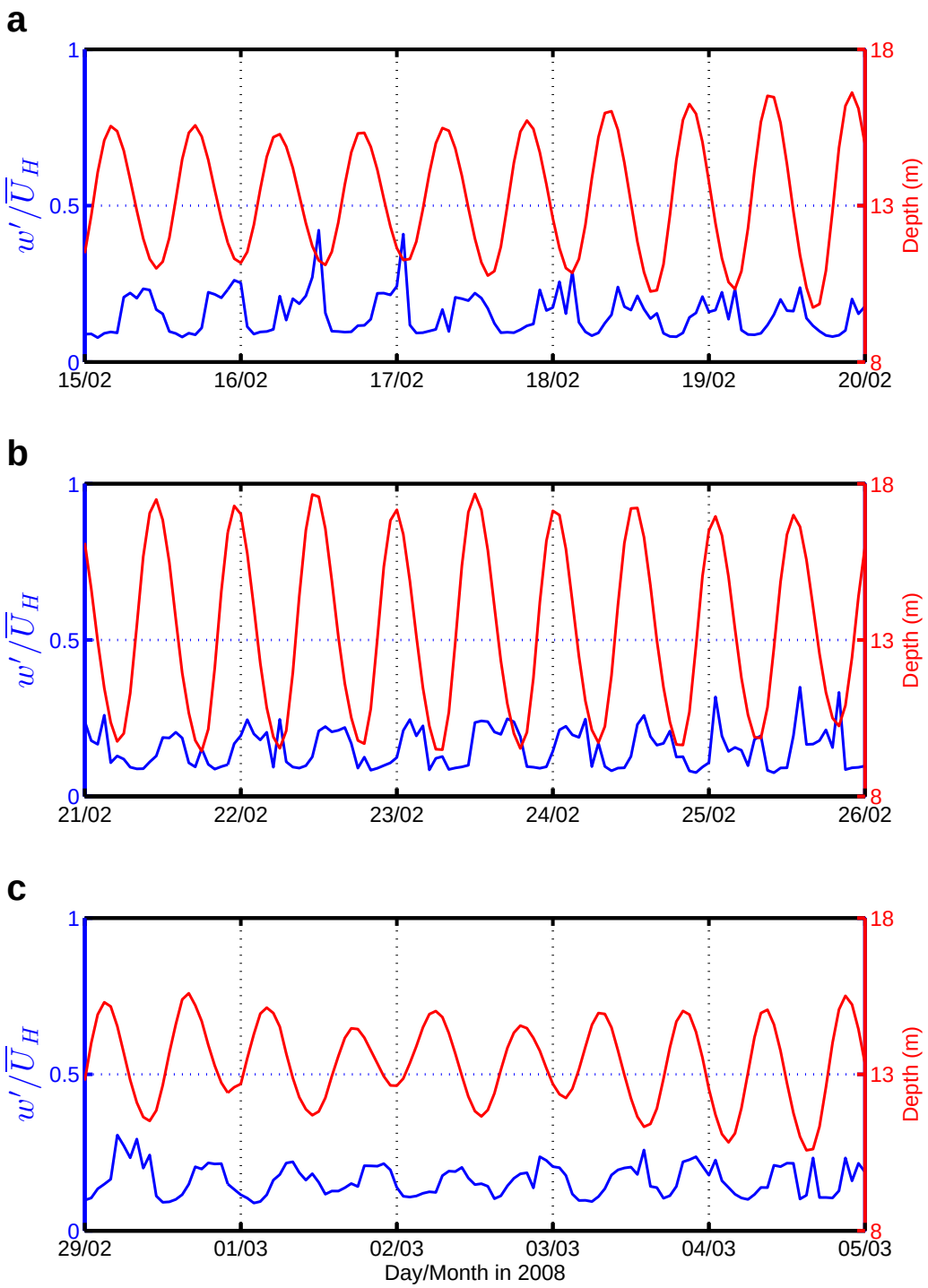

Figure 4.10: Ratio $w'/\overline{U_H}$ as a rough approximation to test the validity of the application of Taylor's hypothesis along with water depth. a) "Current only" regime, b) "combined currents-waves" regime, and c) "wave dominant" regime.

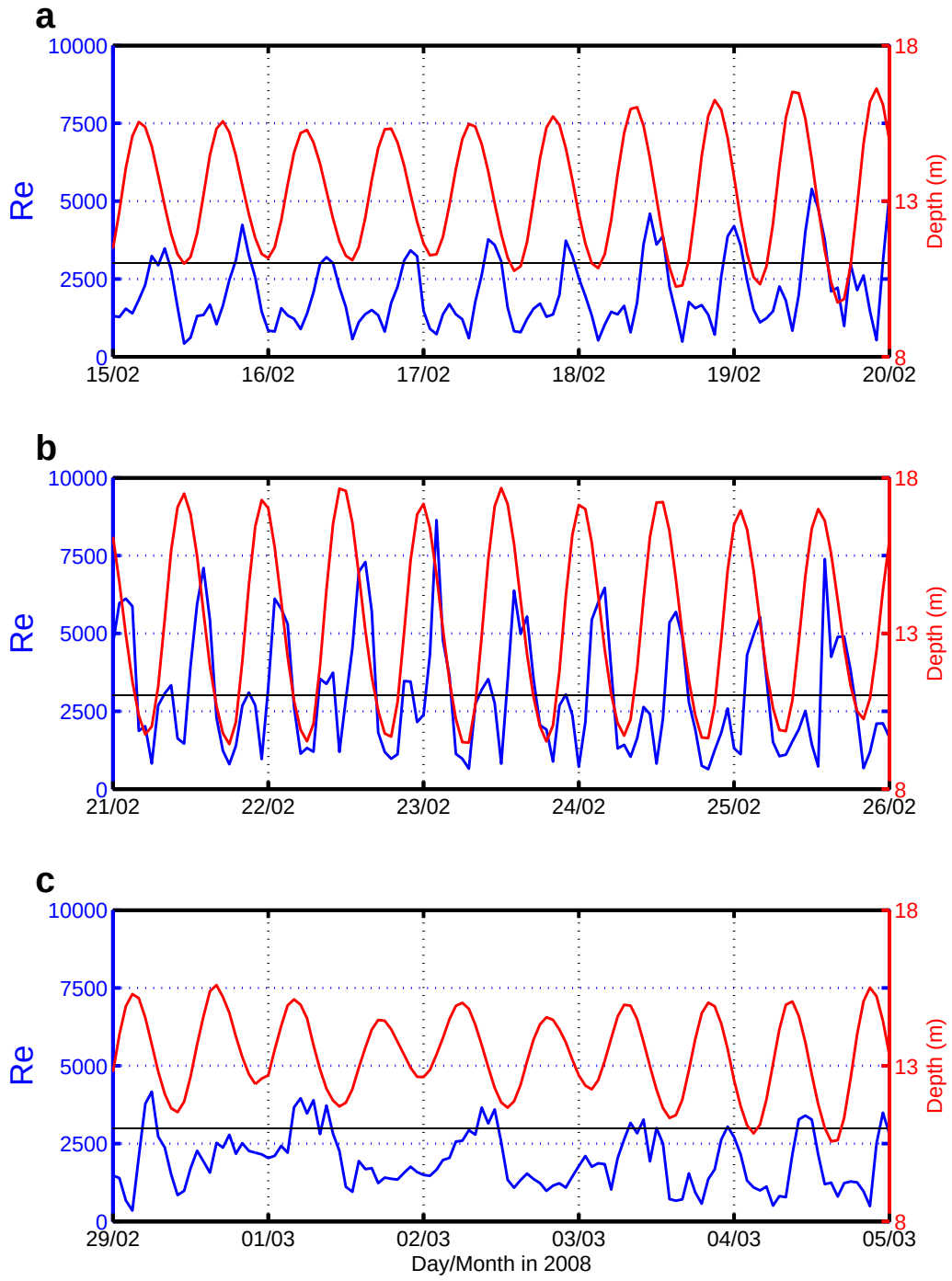

Figure 4.11: Reynolds numbers calculated as $Re = (\kappa U_* z)/\nu$ along with water depth, with a black line denoting a critical Reynolds value of 3000. a) "current only" regime, b) "combined currents-waves" regime and c) "wave dominant" regime.

obtained in studies to test this hypothesis in different flows (Saddoughi and Veeravalli, 1994 and references there in). In the Welsh Channel, a situation of isotropic turbulence could occur during low water slack, when the high turbulence has been produced at the end of the ebb phase and there is no horizontal advection. However, this would be inconsistent with the test results for the other assumptions. On the other hand, it is possible that local isotropy is valid because of the small scale of the flocs, which are in the order of μm, with the largest flocs of about 450 μm.

4.2 Numerical models

4.2.1 Hydrodynamics

The hydrodynamic model POLCOMS (Proudman Oceanographic Laboratory Coastal Ocean Modelling System) solves the incompressible, hydrostatic, Boussinesq equations of motion (Holt and James, 2001). The governing equations are formulated in spherical polar coordinates: χ (eastward), ϕ (northward) and σ (vertical), where $\sigma = (z-\zeta)/(h+\zeta)$ with z the Cartesian vertical coordinate, h reference water depth and ζ the elevation above the reference water level. An Arakawa B-grid (Arakawa, 1972) is used for the horizontal discretization in which elevation and scalar quantities are evaluated at each grid cell corner, while velocity and flux components are evaluated at the center of each grid cell. An example of the grid used by POLCOMS is shown in figure 4.12a for horizontal and figure 4.12b for vertical.

A time-splitting technique is used to calculate barotropic and baroclinic components and the velocities are thus divided into a depth varying and depth independent parts, respectively $u = \bar{u}(\chi,\phi,t) + u_r(\chi,\phi,\sigma,t)$ and $v = \bar{v}(\chi,\phi,t) + v_r(\chi,\phi,\sigma,t)$ for the eastward and northward components. The depth averaged equations are (Holt and James, 2001):

$$\begin{aligned}\frac{\partial \bar{u}}{\partial t} &= f\bar{v} - \frac{1}{R\cos\phi}\left[g\frac{\partial \zeta}{\partial \chi} + \frac{1}{\rho_0}\frac{\partial P_a}{\partial \chi}\right] \\ &\quad + \frac{1}{H}\left(F_S - F_B\right) + NLB_\chi \end{aligned} \tag{4.37}$$

and:

$$\begin{aligned}\frac{\partial \bar{v}}{\partial t} &= -f\bar{u} - \frac{1}{R}\left[g\frac{\partial \zeta}{\partial \phi} + \frac{1}{\rho_0}\frac{\partial P_a}{\partial \phi}\right] \\ &\quad + \frac{1}{H}\left(G_S - G_B\right) + NLB_\phi \end{aligned} \tag{4.38}$$

The depth varying governing equations are:

$$\begin{aligned}\frac{\partial u_r}{\partial t} &= -L(u) + fv_r + \frac{uv\tan\phi}{R} - \frac{1}{R\cos\phi}\left.\frac{\partial \psi}{\partial \chi}\right|_z \\ &\quad + D(u) - \frac{1}{H}\left(F_S - F_B\right) - NLB_\chi \end{aligned} \tag{4.39}$$

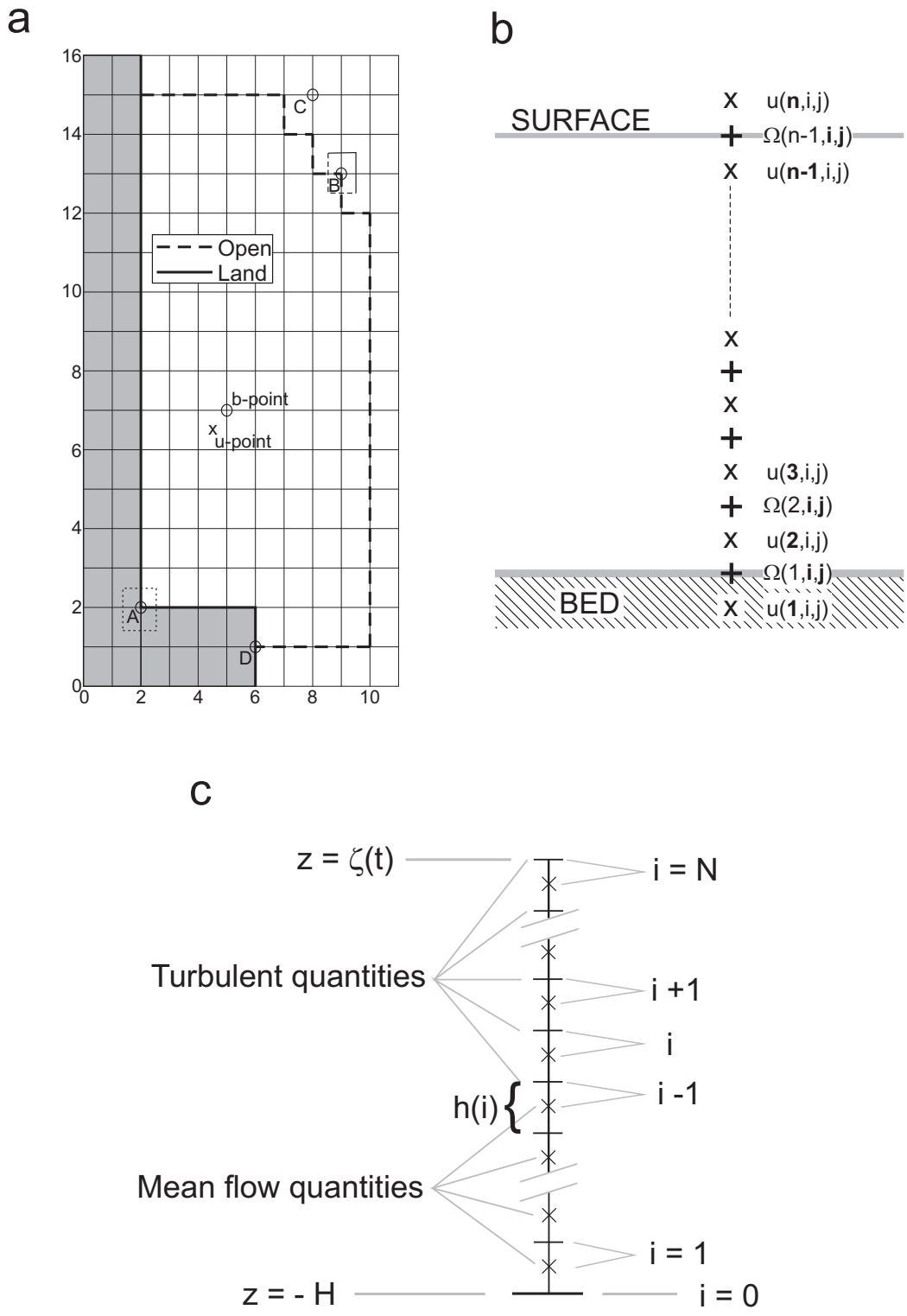

Figure 4.12: Hydrodynamic model POLCOMS horizontal (a) and vertical (b) discretization, and vertical discretization used by the turbulence model GOTM (c).

and:

$$\frac{\partial v_r}{\partial t} = -L(v) - fu_r - \frac{u^2 \tan\phi}{R} - \frac{1}{R}\left.\frac{\partial \psi}{\partial \phi}\right|_z + D(v) - \frac{1}{H}\left(G_S - G_B\right) - NLB_\phi \tag{4.40}$$

with f the Coriolis parameter, R the earth radius, P_a the atmospheric pressure, ρ_0 the reference density (ρ_0=1027 kg·m^{-3} for seawater) and $H = h + \zeta$ the total water depth. ψ relates to the buoyancy following:

$$\psi = H \int_0^\sigma b d\sigma \tag{4.41}$$

where the buoyancy $b = b_0 + b'$ consists of the potential buoyancy b_0 and a term b' accounting for the variation of compressibility with temperature and salinity:

$$b_0 = g\frac{\rho_0 - \rho\left(T, S, P\right)}{\rho_0} \tag{4.42}$$

and:

$$b' = g\frac{-0.004564\sigma H - \rho'}{\rho_0} \tag{4.43}$$

in which $\rho\left(T, S, P\right)$ is taken from the UNESCO equation of state and $\rho'(T, S, p)$ following Mellor (1991).

The depth averaged non-linear and buoyancy terms in equations 4.37 to 4.40 are given by:

$$NLB_\chi = \int_{-1}^{0}\left[-L(u) + \frac{uv\tan\phi}{R} - \frac{1}{R\cos\phi}\left.\frac{\partial \psi}{\partial \chi}\right|_z\right] d\sigma \tag{4.44}$$

and:

$$NLB_\phi = \int_{-1}^{0}\left[-L(v) + \frac{u^2\tan\phi}{R} - \frac{1}{R}\left.\frac{\partial \psi}{\partial \phi}\right|_z\right] d\sigma \tag{4.45}$$

Advection of a quantity a is expressed as:

$$L(a) = \frac{u}{R\cos\phi}\frac{\partial a}{\partial \chi} + \frac{v}{R}\frac{\partial a}{\partial \phi} + \Omega\frac{\partial a}{\partial \sigma} \tag{4.46}$$

where the vertical velocity Ω is found by:

$$\Omega = -\frac{\sigma}{H}\frac{\partial \zeta}{\partial t} - \frac{1}{HR\cos\phi} \times \left[\frac{\partial}{\partial \chi}\left(H\int_0^\sigma u d\sigma\right) + \frac{\partial}{\partial \phi}\left(H\cos\phi\int_0^\sigma v d\sigma\right)\right] \tag{4.47}$$

The equations for depth-averaged currents and free surface elevation are solved following a forward-time centered-space technique while advective terms use a piecewise parabolic method (Holt and James, 2001).

The turbulent stresses and turbulent fluxes in the depth varying governing equations are modelled following turbulent viscosity and turbulent gradient diffusion hypotheses,

and the corresponding terms have been replaced by the following diffusion term for any quantity, a:

$$\mathcal{T}(a) = \frac{1}{H^2}\frac{\partial}{\partial\sigma}\left(K_z^a\frac{\partial a}{\partial\sigma}\right) \tag{4.48}$$

where K_z^a can be the eddy viscosity, when a refers to velocities or the eddy diffusivity when a is a scalar quantity.

The terms F_S, G_S and F_B, G_B are the two components of respectively the surface and bottom stresses. The surface stresses are given in terms of the wind velocity at 10 m (U_w, V_w):

$$(F_S, G_S) = c_s\frac{\rho_a}{\rho_0}(U_w, V_w)\sqrt{U_w^2 + V_w^2} \tag{4.49}$$

where the friction coefficient is:

$$c_s = 0.63 + 0.66\sqrt{U_w^2 + V_w^2}. \tag{4.50}$$

The equation for the free surface is:

$$\frac{\partial\zeta}{\partial t} = -\frac{1}{R\cos\phi}\left(\frac{\partial H\bar{u}}{\partial\chi} + \frac{\partial H\cos\phi\bar{v}}{\partial\phi}\right) \tag{4.51}$$

4.2.2 Turbulence model

Turbulence has been included in several ways by different authors. Winterwerp (1998) inccorporates the effects of turbulence through a rate of coagulation between particles in a turbulent fluid and the time scale of the turbulent eddies. In a later study, the same author used an equation for the evolution of the floc size, applied a Reynolds decomposition, and a dissipation parameter for the break-up-aggregation process and a flocculation function (Winterwerp, 2002). A dissipation parameter which depends on the turbulent dissipation rate in both aggregation and break-up parts of the flocculation process is used for some studies (e.g., Winterwerp, 1998; Flesch et al., 1999; Ditschke and Markofsky, 2008). Most of the proposed formulations need to obtain variables strongly dependant on the turbulent kinetic energy and the turbulent dissipation rate. Also, to determine the turbulent eddy diffusivity it is necessary to take into account the turbulent viscosity hypothesis (Larsen et al., 2009). Although taking a different approach to the turbulent kinetic energy, Bowers (2003) tried to explain the spatial and seasonal variability of surface suspended sediments on the Irish Sea. At present, it is possible to compute turbulence properties from field data obtained with several instruments and investigate their relationship with suspended sediments (e.g., Jago et al., 2006). Nevertheless, the measurements are restricted to the study site and therefore it is important to include turbulence models.

The turbulence model GOTM (General Ocean Turbulence Model) is a one-dimensional water column model for the hydrodynamic and thermodynamic processes related to vertical mixing (Umlauf et al., 2012). It solves the one-dimensional versions of transport equations of momentum, salt and heat and also needs to calculate K_z^a. In the present work, K_z^a represents turbulent eddy viscosity ν_t and sediment diffusivity K_z^s. These, in analogy to molecular viscosity, are assumed as the product between a typical velocity scale of turbulence q and a typical length scale l. The velocity q can be related to the average turbulent kinetic energy as $k = q^2/2$. Thus, turbulent eddy viscosity ν_t and sediment diffusivity K_z^s can be expressed as:

$$\nu_t = c_\mu l k^{1/2} \tag{4.52}$$

$$K_z^s = c_\mu^s l k^{1/2} \tag{4.53}$$

where dimensionless quantities c_μ and c_μ^s are stability functions.

The main characteristic of GOTM is the number of options (turbulence closure models) already implemented to obtain q (or k) and l scales. In this work the turbulence model is used with a $k-\varepsilon$ closure scheme where ε is the turbulent dissipation rate (Rodi, 1987). This model uses differential transport equations for k and ε. For turbulent kinetic energy it is (Amoudry and Souza, 2011a):

$$\frac{\partial k}{\partial t} = \mathcal{T}(k) + \mathcal{P} + \mathcal{G} - \varepsilon \tag{4.54}$$

where:

$$\mathcal{P} = \nu_t M^2 \tag{4.55}$$

is shear production with M^2 in σ coordinates as:

$$M^2 = H^{-2}\left[\left(\frac{\partial u}{\partial \sigma}\right)^2 + \left(\frac{\partial v}{\partial \sigma}\right)^2\right] \tag{4.56}$$

and:

$$\mathcal{G} = -K_z^s N^2 \tag{4.57}$$

is buoyancy production with N^2 as:

$$N^2 = H^{-1}\frac{\partial b}{\partial \sigma} \tag{4.58}$$

where b is buoyancy and $H = h + \zeta$. For ε:

$$\frac{\partial \varepsilon}{\partial t} = \mathcal{T}(\varepsilon) + \frac{\varepsilon}{k}(C_{\varepsilon 1}\mathcal{P} + C_{\varepsilon 3}\mathcal{G} - C_{\varepsilon 2}\varepsilon) \tag{4.59}$$

The transport terms $\mathcal{T}(k)$ and $\mathcal{T}(\varepsilon)$ are defined in equation 4.48 with diffusivities given by:

$$K_z^k = \frac{\nu_t}{\sigma_k} \tag{4.60}$$

and:

$$K_z^\varepsilon = \frac{\nu_t}{\sigma_\varepsilon} \tag{4.61}$$

The vertical discretization used by GOTM is showed on figure 4.12c.

4.2.3 Sediment module

A sediment module is included in POLCOMS and consist of an advection-diffusion equation for concentration C of suspended sediment of different size classes (i):

$$\frac{DC_i}{Dt} = \mathcal{T}(C_i) + \frac{W_{s,i}}{H}\frac{\partial C_i}{\partial \sigma} + S_{c,i} \tag{4.62}$$

where the left-hand side is material derivative which includes horizontal advection, $\mathcal{T}(C_i)$ is sediment transport by turbulence diffusion, $W_{s,i}$ is settling velocity of the class i and last term is an optional source and sink of sediments. Turbulence diffusion is closed by the turbulence model assuming sediment diffusivity is equal to buoyancy diffusivity. The module has the capability to include different characteristics for each sediment class (density, diameter, settling velocity, morphology factor and a source factor). Also, critical erosion bed shear stress, erosion rate and properties of the sea bed (thickness, porosity, age) are user defined. The performance of the coupling of POLCOMS, GOTM and the sediment module can be found in several studies (Amoudry and Souza, 2011b; Amoudry et al., 2014).

4.2.4 Numerical setup

Simulations for the Irish Sea with 1.8 km resolution were used to obtain boundary conditions of temperature, salinity, elevation and currents for the Liverpool Bay domain. Atmospheric forcing was obtained from the UK Met Office Northwest European Continental Shelf Model which has ∼12 km resolution and consisted of atmospheric pressure, air temperature, relative humidity and cloud cover every three hours and hourly wind velocity at 10 m. Initial conditions were 35 UPS, 7°C for the hydrodynamic model. Daily averaged freshwater river supply was included from data of the Centre of Ecology and Hydrology. Tidal harmonics of 15 components were also taken into account. Wetting and drying were considered inside the Dee Estuary with bathymetry obtained from digitized charts and LIDAR surveys. The sigma coordinates were defined with 10 equidistant vertical levels and 180 m for the horizontal grid size. Values for the stability functions in the closure scheme of GOTM were 0.52 and 0.73, respectively. In

the sediment module, one class was used and the erosion rate was set to 1.25×10^{-5} kg·m^{-2}·s^{-2} with a critical value of 0.18 Pa. The models were set to run from January and February 2008, with January used to spin-up hydrodynamics and turbulence. The first 10 days of February are used to spin-up the sediment module. A variable SPM settling velocity was implemented and is explained in chapter 5.

4.3 Frame effect

Given the intrusive nature of most of the instruments and *in situ* measuring techniques mentioned previously, an effect of these on the actual measurements may reasonably be expected. An example is the modification of the flow field by the instruments and the structure they are mounted on (Bolaños et al., 2011). Figure 4.13a presents observations of current velocity from an ADV by Bolaños et al. (2011); the authors show the modification of the vertical velocity by the frame as a linear trend between vertical and horizontal velocities. According to numerical modelling of Bolaños et al. (2011), important effects on the velocities and turbulent kinetic energy are expected near a simulated object but may remain negligible near the bottom. In particular, negative frame-generated vertical velocities can reach 10% of the horizontal velocity in the case of Bolaños et al. (2011).

In the case of the present study the instruments were mounted on a tripod 1.8 m high, the triangle formed by its base of approximately 1.5 m on each side, and the bigger components of the instruments on the upper part, which represent major obstacles to the flow. The observations of velocities from the bottom-mounted ADV are shown in figure 4.13b in units of cm/s in order to be compared with the results of Bolaños et al. (2011). Vertical velocities have both upward and downward directions (positive and negative values). Although upward vertical velocities reach more than 15 cm/s and represent about 33% of the horizontal velocities, downward velocities are also important, reaching about 20% in relation to horizontal velocities. This suggests that either the frame has no effect on the observations of the Welsh Channel or the effect is not distinguishable. The differences in velocity magnitudes are due to flood and ebb tidal phases and are discussed in section 7.2. Other disturbances have been found due to the legs of the frame by Shaw et al. (2001) but in the present work the measurement volume was not near the legs of the frame. The effect of the scouring due to the frame legs over the bottom could be another important factor. If the scour is important, it could contribute to changes on the bed boundary layer, bed roughness, resuspension of sediments, and as a consequence, their flocculation. Measurements of the scour in the Welsh Channel exhibited a pit of about 0.15 m (Bolaños et al., 2011) and are therefore not considered as important for the measurements of this study.

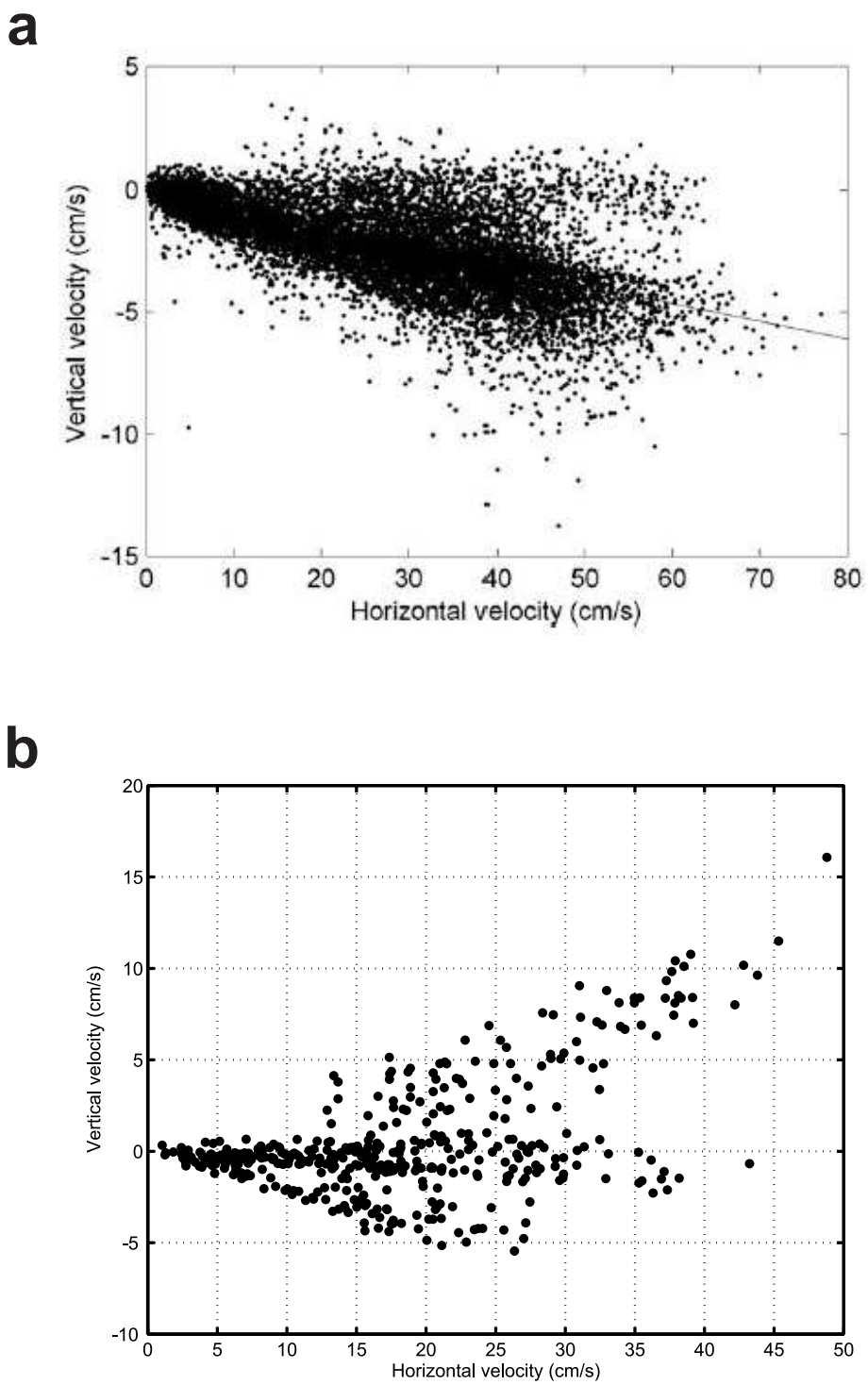

Figure 4.13: Horizontal versus vertical current velocities. a) An example of the effect of the frame in ADV data. Persistent negative downward velocity can be attributed to the frame (Bolaños et al., 2011). b) Observations in the Welsh Channel of this study where there is no evidence of the frame effect.

Chapter 5

Parameterization of flocculation as function of turbulent stress for a "current only" regime

The observations for the present study allowed an initial approach which took into account only the effects of currents on the flocculation process. Figure 5.1 shows time-series of (a) water depth, (b) current speed, and (c) significant wave height observations taken with the ADV and the river discharge (d).

The entire study period covered almost two neap-spring cycles showing semi-diurnal tides and tidal ranges of four and eight metres during neaps and springs, respectively. There was a clear difference between the two neap tidal cycles with the latter presenting lower ranges and stronger asymmetry than the former. Current velocity also showed the fortnightly period and quarter-diurnal variability, with maximum velocity of 0.53 $m{\cdot}s^{-1}$ during spring tides. Ebb currents exhibited stronger magnitudes than flood currents, with maximum differences of $\sim$0.1 $m{\cdot}s^{-1}$ during springs. However, the second period of neap tides exhibited a completely different behaviour than the first neap, and not related with either flood or ebb phases.

The significant wave height record showed the important presence of waves from 21 February. Before this date, waves were less than 0.1 m high and therefore their effect on the flocculation process is negligible compared with current velocity. For this study, the period with the lowest wave height is called "current only". During this period of observations, from 12 to 21 February, important near-bed current speed of 0.15 $m{\cdot}s^{-1}$ was achieved on neap tides. From 21 February, three periods of high waves were present: the first with almost 1.5 m height coinciding with stronger currents on springs around 22 February, the second with waves higher than 1.5 m during mid-tides around 27 February. The highest and sustained waves of almost 2 m height happened during the second neap cycle. The end of the record also showed waves of about 1 m height.

There was no significant freshwater supply from the river as the discharge diminished

from 40 to 20 $m^3 \cdot s^{-1}$ during the first half of the period, after which it increased but barely achieved 50 $m^3 \cdot s^{-1}$ and decreased again to about 40 $m^3 \cdot s^{-1}$ in the last part of the study period.

This chapter focuses on the "current only" period which took place between 15 and 22 February. Observations are presented and a turbulent stress based model, as is commonly used, is proposed as a first approach to parameterise the flocculation process. This model is implemented within the sediment module and the results obtained from modelling with the coupling of POLCOMS-GOTM are also shown.

5.1 Grain size

Measurements taken with LISST instrument showed clear changes in the grain size of the flocs depending on tidal phase. Figure 5.2 shows two bursts as examples of the typical grain size behaviour of near-bed suspended sediment found in the Welsh Channel. In figure 5.2a the circles mark times at which samples were taken and the filled circle marks the sample used in this example. The first case corresponds to an ebb cycle with, fast near-bed current of 0.2 $m \cdot s^{-1}$. The volume concentration of fine flocs, between 74 and 88 μm, increased throughout the 20 minutes sample time from 49 to 77 $\mu l \cdot l^{-1}$ while concentration of coarse flocs remained below 20 $\mu l \cdot l^{-1}$ (Fig. 5.2c). Averaging of the 20 minutes sample results in unimodal distribution with the highest concentrations in grains between 20 and 200 μm with a maximum concentration of 60 $\mu l \cdot l^{-1}$ in the 80 μm size class, whereas coarse flocs over 200 μm remained below 20 $\mu l \cdot l^{-1}$ (Fig. 5.2e). On the contrary, during slack waters with a current velocity of 0.04 $m \cdot s^{-1}$ (Fig. 5.2b), fine flocs around 100 μm diminished to concentrations of $\sim$20 $\mu l \cdot l^{-1}$ and coarse flocs increased and achieved a maximum of 79 $\mu l \cdot l^{-1}$ in the 330 μm size class at approximately 10 minutes of the sampling period (Fig. 5.2d). However, it is important to note that the concentration of flocs smaller than 330 μm is significant. Overall in figure 5.2f, it can be seen that maximum concentrations above 40 $\mu l \cdot l^{-1}$ were present between the 300 and 400 μm size classes but concentrations of approximately 30 $\mu l \cdot l^{-1}$ around the 200 μm size class were also important. This floc behaviour during fast and slow currents was repeated throughout the entire observation period, although in different magnitudes, and is presented below for this section of the study.

Figure 5.3 shows the time-series of LISST observations between 15 and 22 February. The relationship between median grain size and tidal phase is shown in Figure 5.3a. Tidal range changed from neap to spring tides, increasing from about 4 m to 8 m at the end of this period. Similar to the tide, a fortnightly modulation seems to be present in D_{50} but, conversely to the tide, the grain size is large during neap tides ($\sim$170) μm and small during spring tides ($\sim$60 μm). Minimum values of D_{50} of about 50 μm are found at the end of the record during spring tides while maxima of more than 200 μm were commonly found during neap tides. Quarter-diurnal frequency cycles are also present

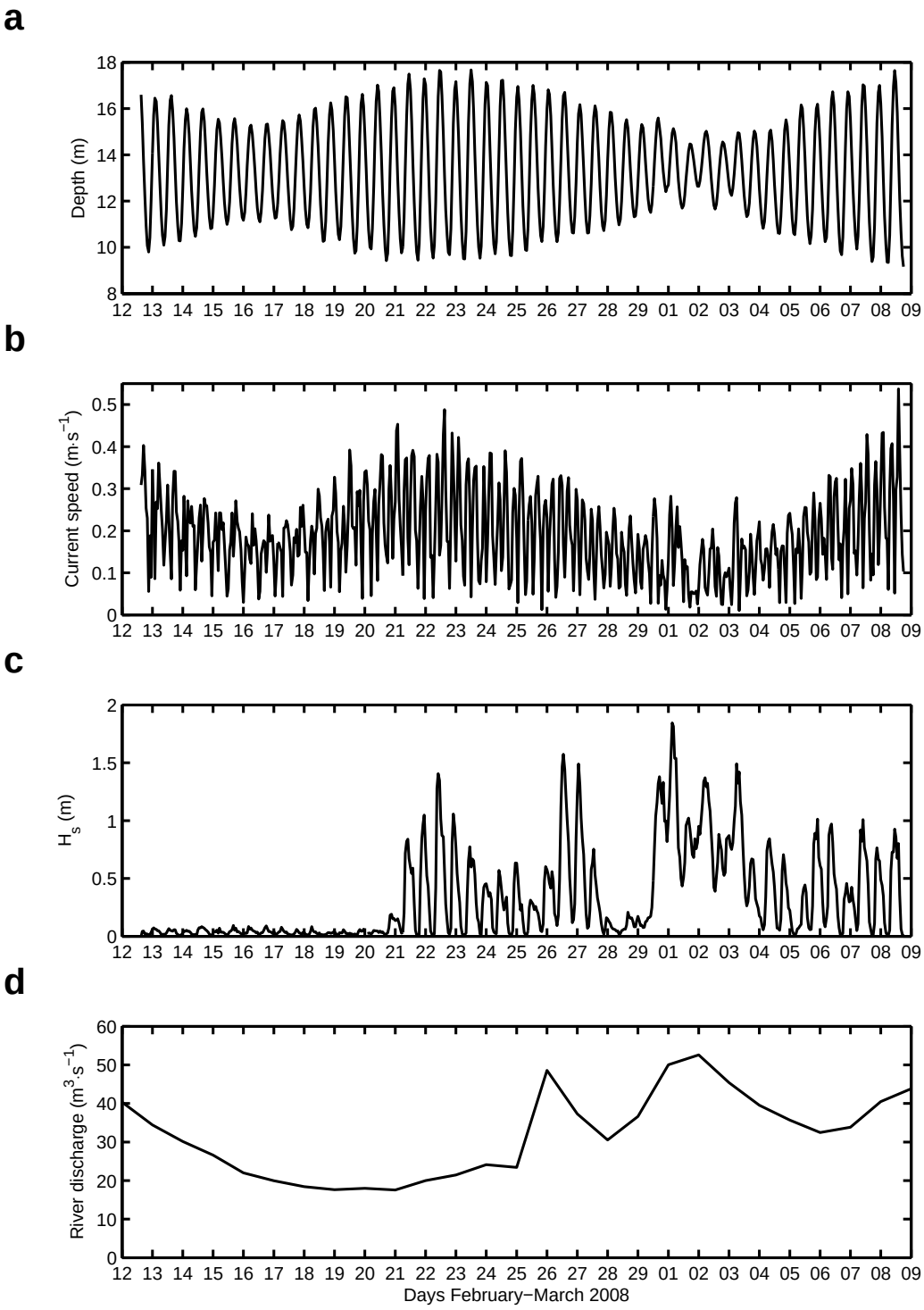

Figure 5.1: Time-series in Welsh Channel. a) Water depth, b) horizontal current speed, c) significant wave heigth and d) river discharge.

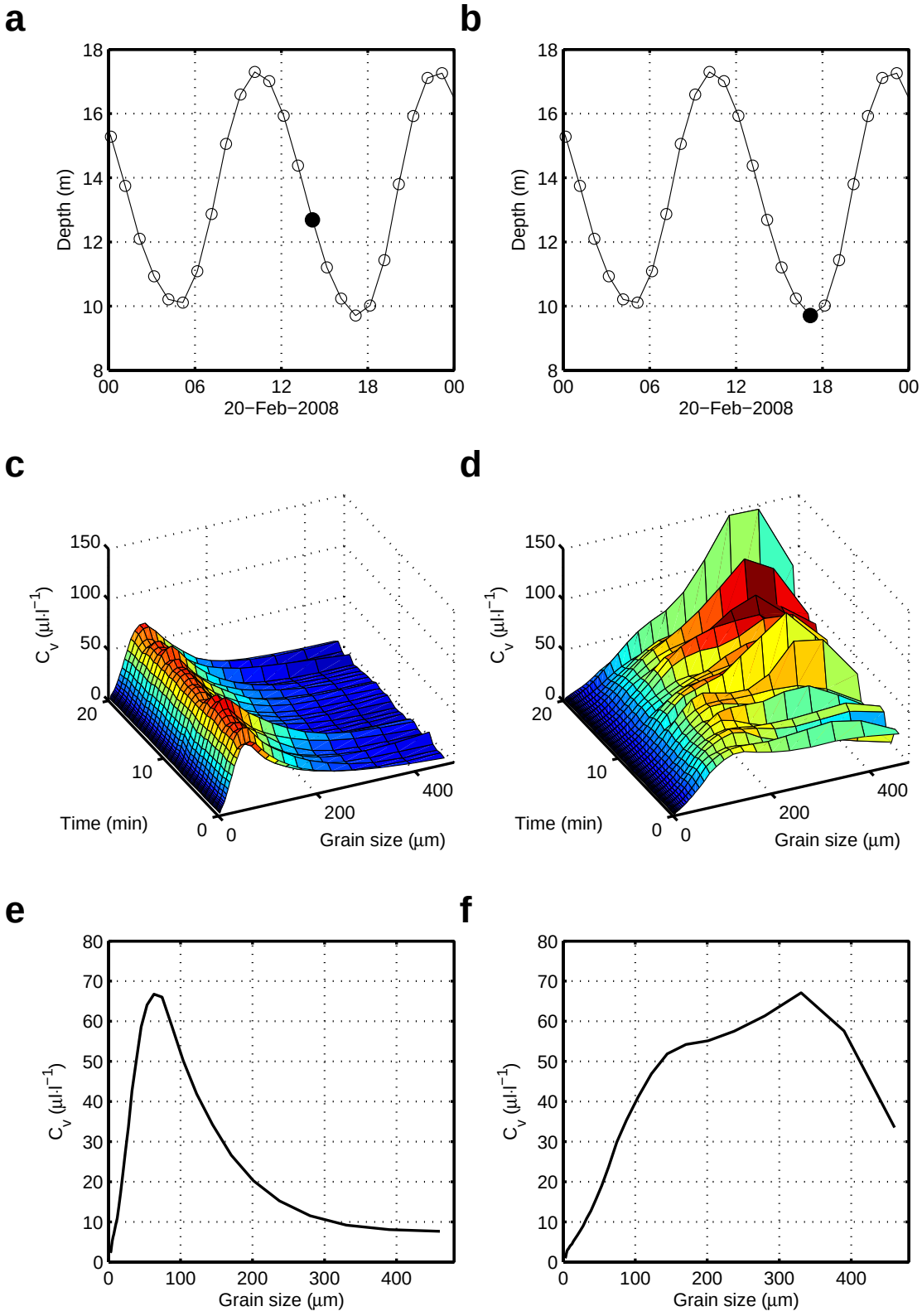

Figure 5.2: Example of two bursts of grain size taken with the LISST instrument. a) and b): the circles mark the time and the depth (line) at which the grain size samples were taken. Filled circles are the samples used as examples. c) and d): time-series of grain size during the 20 minute sample time for the two examples. e) and f): mean grain size for the two examples.

in D_{50}, with maxima at slack water and minima during maximum flood and ebb. During neap tides, higher values were achieved after the ebb than after the flood phase. The grain size spectrum is plotted in figure 5.3b on a logarithmic scale and in terms of mass concentration. The calibration used to convert from volume concentration LISST output C_v to mass concentration C_m is presented further. The behaviour described in the previous paragraph can be seen for this period of observations, with high concentrations of both fine and coarse flocs but during strong and weak currents, respectively. The maximum observed concentration value was about 9 g·m^{-3} for sediment of 122 μm size and occurred on the 21st February at 16:00. High concentrations of sediment of about 100 μm were present during flood and ebb periods. High concentrations of coarse particles, about 350 μm, were recorded during slack waters although magnitudes were lower than for flood and ebb. This behaviour was observed even during neap tides when suspended sediment concentrations were smaller overall. Figure 5.4 shows specific periods including entire tidal cycles during neaps and spring tides in order to better visualise the details of the changes in floc size. Note the strong diference in concentration magnitude which lead to the use of diferent scales. In figure 5.4a the scale is linear while in 5.4b is logarithmic. The most important feature of neap tides (Fig. 5.4a) is the high concentration of small flocs during flood and ebb and of big flocs during low water slack. However, given the small magnitude of concentrations, this result must be qualitative. In spring tides (Fig. 5.4b) the high concentrations of small flocs is clear during the ebb phase and the change to high concentration of big flocs seems to take place immediately without any floc settling as during neap tides.

An important assumption in the present study is that the observations of floc size and current velocities were measured at the same level over the bottom. At the height of the LISST the turbulent kinetic energy is lower than the measured near the bottom at the height of the ADV. Therefore, figures in Chapter 6 should have a smaller range in turbulent properties. Depending on the response of the system to the resuspension, there would be a time lag of energy and LISST measurements. For example, at maxima of energy (stress or TKE), flocs are resuspended, disaggregated and transported upward in the water column. If the vertical transport is fast enough, they will be recorded in the LISST coinciding with the maximum of energy. However, if the vertical movement is slow, the size of the flocs could be recorded at the next reading. If the time lag remains during the tidal cycle, it would be possible to find like a tail of floc sizes increasing after the energy has reached a minimum because of flocs either remain in aggregation step or falling from upper zones of the water column. An interesting case would be to obtain LISST measurements near the bottom, at the height of the ADV. Probably the floc grow at low shear stress mentioned by Dyer (1989) could be recorded and is also maybe the connection part in, for example, figure 6.9 at low energy where there seems to be a gap. The observations of this research seem to be fast enough for the

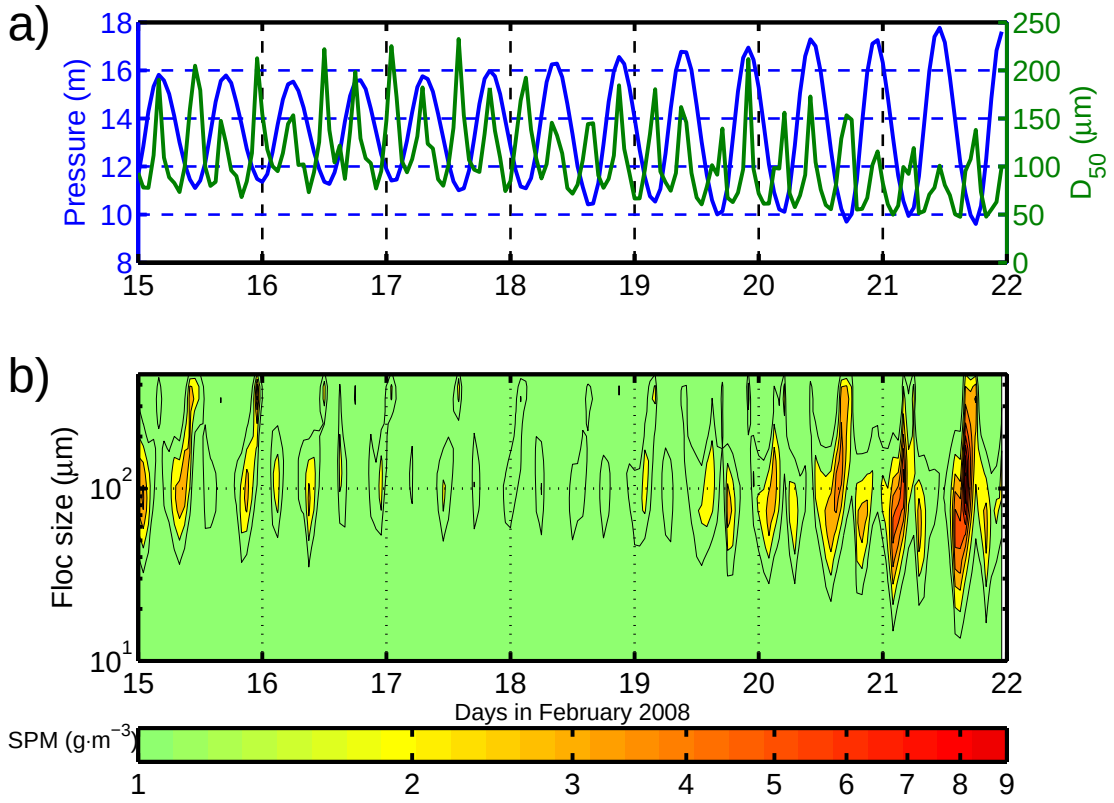

Figure 5.3: LISST observations of grain size. a) Depth (blue line) and median grain size D_{50}(green line). b) Contours of mass calibrated concentrations on a logarithmic scale ($log_{10}C_m$) for each grain size during the study period.

assumption of same level to be valid.

5.2 Settling velocities from observations

The effective density following equation 4.10, from the LISST volume concentration and from the mass concentration, is shown in figure 5.5a. This effective density is used in the Stokes law relation (eq. 4.2) along with the observed LISST median grain size to calculate settling velocities (see figure 5.5b). Turbulent stresses calculated using equation 4.7 with ADV measurements are also shown in figure 5.5c. These three variables exhibit related behaviour. During neap tides, higher variability in effective density and settling velocity is found corresponding to lowest variability in turbulent stresses. Conversely, during spring tides, turbulent stresses show the largest variability while for effective density and settling velocity the opposite is observed. Quarter-diurnal variability and flood-ebb asymmetries are both noticeable in the three variables, with the largest differences for turbulent stresses. The quarter-diurnal variability is characterized by maxima in effective density coinciding with low values of settling velocity and high values of turbulent stresses. However, important differences are found between

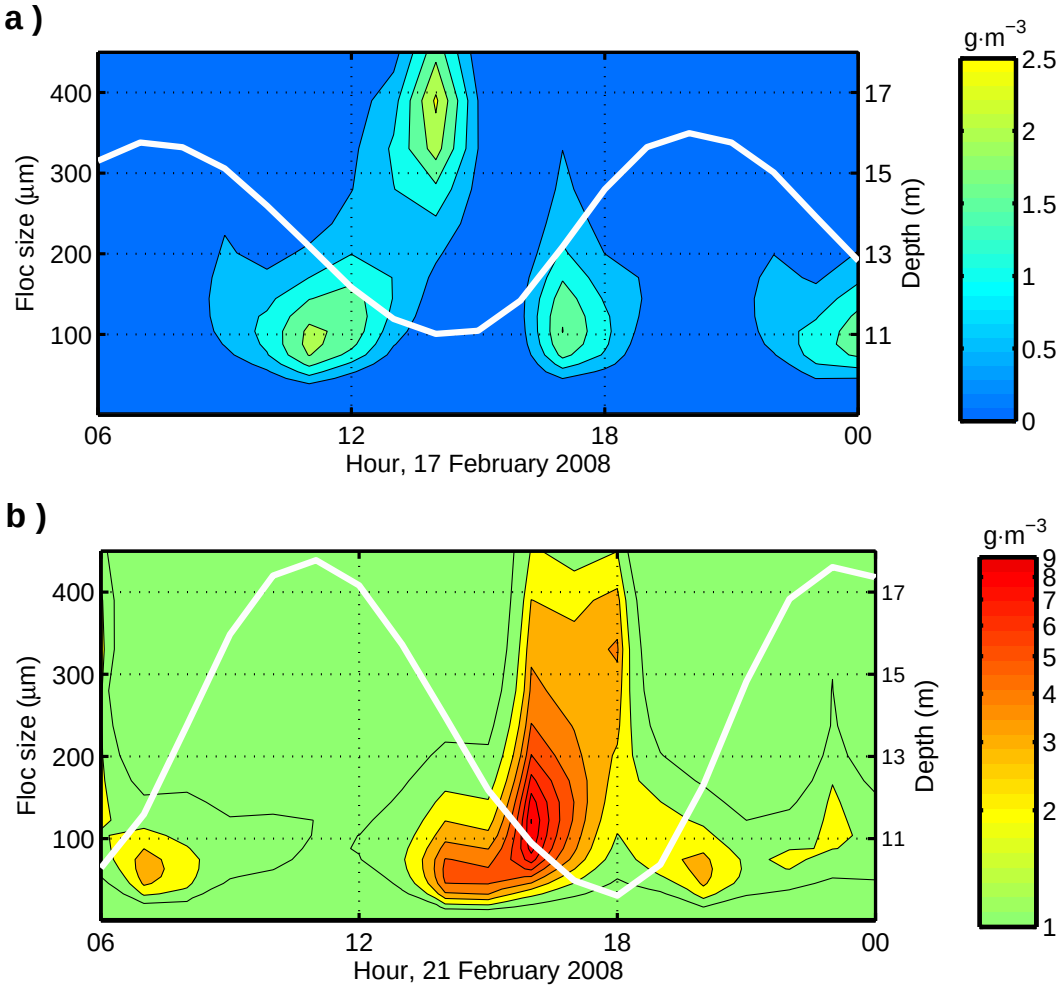

Figure 5.4: Specific periods extracted from figure 5.3 showing tidal cycles during neap (a) and spring (b) tides. Note the difference in scales used to better illustrate the particular details of each period. For neap tides (a) the scale is linear while for spring tides $log_{10}C_m$ has been used. The white line is water depth and corresponds to the right axis scale. During neap tides, high concentrations of small flocs happened in ebb and flood phases while high concentrations of big flocs were present in low water slack with periods of low concentrations between these phases and high water slack. Nevertheless, the concentrations in general were low during the entire period and may be in the range of error the measurements. During spring, there is a clear signals of high concentrations of small flocs during ebb and of big flocs during low water slack.

flood-ebb phases and slack waters. During neaps, extreme values (minima and maxima) of effective density show sharp peaks during flood and high slack waters whereas moderate peaks are present during ebb and low water slack. These sharp peaks diminish through spring tides and vanish during the last two days of the record. For settling velocities during neaps, the lowest values are found during the ebb rather than flood, but largest differences occur between slack waters. Maxima of settling velocity are present over weak currents but largest values are reached throughout low water slack with differences of about 1 mm·s^{-1} on day 16. During spring tides these differences are not clear for both extreme values of W_s. Maxima of turbulent stresses happen over flood and ebb cycles, with the latter reaching 80% more than the values of the former. This proportionality difference is maintained through spring tides. No clear differences are present for turbulent stresses during slack waters when values are nearly zero.

During neap tides, maxima of ρ_e of almost 66 kg·m^{-3} are reached with almost constant W_s values of about 0.35 mm·s^{-1} despite the fact that turbulent stresses increase from ∼0.2 Pa to more than 1 Pa on flood and ebb, respectively. Clear asymmetries in maxima of W_s and minima of ρ_e are present during slack waters in neap tides, with minimum values of turbulent stress. Maximum values of settling velocity of more than 1.5 mm·s^{-1} are obtained after the ebb and coinciding with low effective densities. Nevertheless, lowest values of ρ_e, including the minimum 60.42 kg·m^{-3}, after flood coincide with high W_s values but not as high as after ebb phases.

Through spring tides, asymmetries between flood and ebb are still clear in ρ_e and τ but with lower magnitude in the former and higher in the later. While effective density difference was about 0.5 kg·m^{-3}, with highest values during ebb, turbulent stress increased to ∼1 Pa and ∼5 Pa during flood and ebb, respectively, which means a change in about 4 times the values during neap tides. Maximum settling velocities diminished to less than 0.5 mm·s^{-1} without a clear pattern of flood-ebb difference.

5.3 Flocculation modelling

5.3.1 Settling velocity formulation

In figure 5.6 turbulent stress (τ) obtained from the ADV and settling velocities calculated using Stokes law are presented together with an adjusted curve. The maximum particle Reynolds number is of the order of 10^{-1} and therefore the assumption of using Stokes law is reasonable to calculate settling velocities. Some low values of turbulent stress correspond to a wide scatter of settling velocities (higher than 1.5 mm·s^{-1}) which seem to be outside the trend and therefore were not taken into account in the study. The maximum value of turbulent stress is about 5 Pa and corresponds to a minimum settling velocity of 0.1 mm·s^{-1}. The minimum value of turbulent stress of about 0.025 Pa coincides with settling velocity about 0.8 mm·s^{-1}. However, there is a wide range

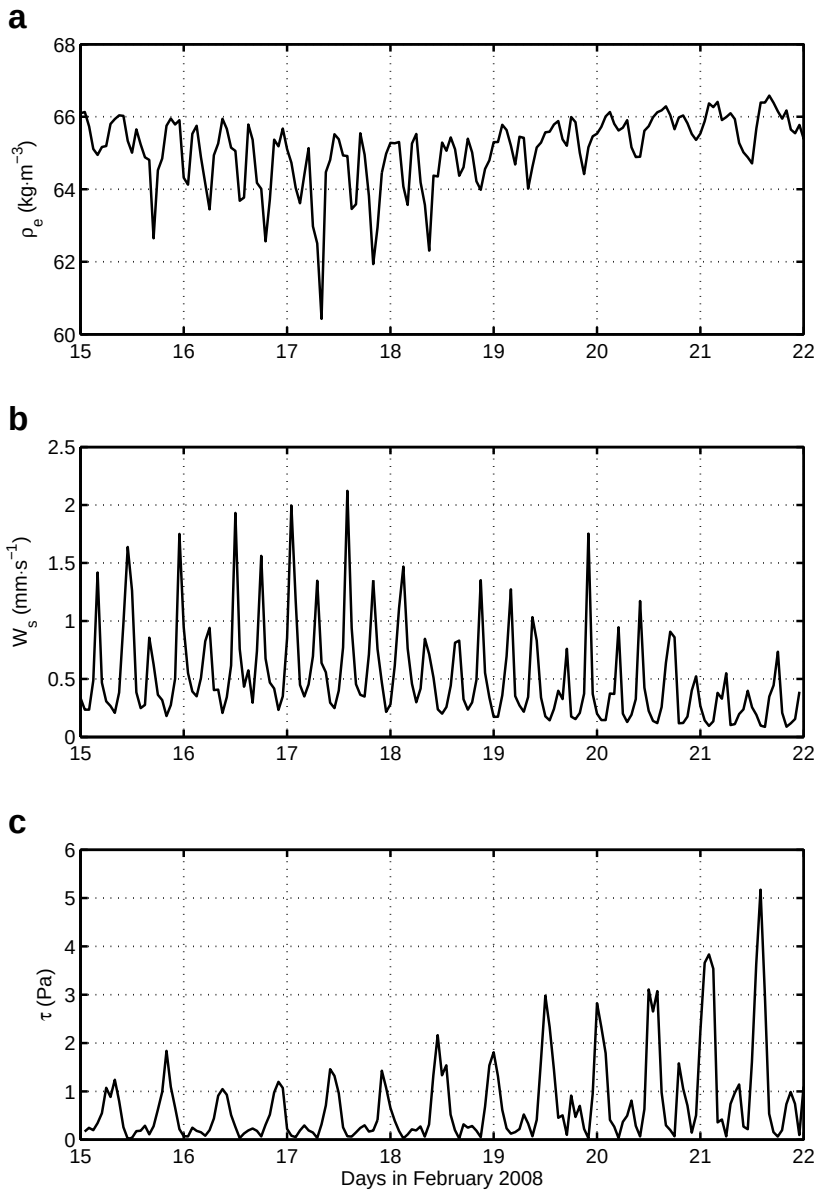

Figure 5.5: Variables calculated from observations: (a) efective density ρ_e showing the highest variability during neap tides and lowest variability during spring tides, (b) settling velocity W_s using the Stokes Law and also, the highest variability was found during neap tides, and (b) turbulent Reynolds stress τ calculated from ADV velocity data, opposed to ρ_e and W_s, the highest variability was present during spring tides.

of settling velocities for a fixed value of turbulent stress. The range of settling velocity increases as turbulent stress diminishes from τ ~5 Pa to 0.3 Pa, while the scattering of W_s cover most of the range from 0.2 to more than 1.5 mm·s^{-1}.

The aim is to represent the observed trend by an expression that can easily be implemented into the three-dimensional model. The simplest option is, in a semi-logarithmic plot such as in figure 5.6, a straight line, but only the section corresponding to τ between ~0.1-1 Pa seems to follow a linear distribution. A straight line formulation would result in negative settling velocities as turbulent stresses increase. Another option is a power law but this results in infinite settling velocities when $\tau = 0$. A polynomial formulation adds non-existing variability in the observations. Therefore, a formulation according to the natural behaviour of flocs is needed. In terms of floc size, when the range of τ is 0.1-1 Pa, flocs aggregate or break-up in approximate proportion to the decrease or increase in turbulent stress values. However, as τ diminishes from 0.1 Pa, the rate of floc growth also diminishes, otherwise they would aggregate to unrealistic sizes. On the other hand, as τ increases beyond 1 Pa, floc break-up rate diminishes and converges to a constant value. This means either flocs have reached the minimum size or τ is not enough to break them apart into smaller sizes. A formula is proposed that satisfies floc behaviour and the following mathematical constraints: finite and non-zero settling velocities as stress becomes either infinitely large or small, continuity, and derivability. The simplest mathematical expression to match these criteria follows the following form:

$$W_s = W_{s,0} + W_{s,m}\, e^{-\tau/\tau_{cf}} \tag{5.1}$$

where $W_{s,0}$ represents the settling velocity of smallest flocs, $W_{s,m}$ is such that $W_{s,0}+W_{s,m}$ is the maximum settling corresponding to minimum stress, and τ_{cf} a critical stress value denoting how quickly the observed settling rates decrease with increasing turbulent stress. Fitting the above expression to the observations leads to the following values: $W_{s,0} = 0.25$ mm·s^{-1}; $W_{s,m} = 0.89$ mm·s^{-1}; and $\tau_{cf} = 0.19$ Pa. The maximum settling velocity is then 1.14 mm·s^{-1}. The high variability of the calculated settling velocities against the simple modeled curve results in a high value of the root mean square error (RMSE) of 0.3 mm·s^{-1}.

5.3.2 Comparison of modelled results and observations

Comparison between model results and observations is presented in figure 5.7. The water depth (Fig. 5.7a) shows that the study period mostly covers neap tide conditions. Tidal amplitude during the study period ranges from approximately 5 m to 9 m. Differences between model and observations are small over the entire period and the semi-diurnal tide is well predicted.

The turbulent stresses are qualitatively well predicted by the model (Fig. 5.7b)

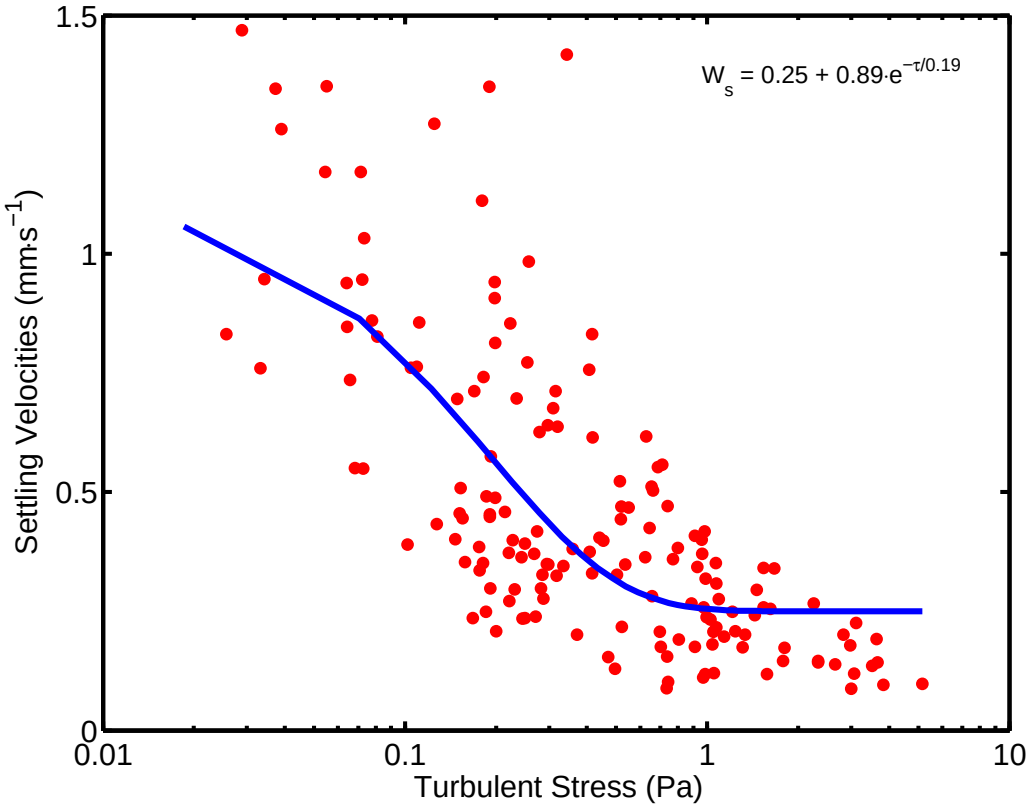

Figure 5.6: Turbulent stresses from the ADV and settling velocities obtained from Stokes Law using sediment samples and LISST data. Solid line is the adjusted curve to the exponential formulation shown at the upper right corner. Data with W_s higher than 1.5 mm·s^{-1} were not taken into account. The root mean square error (RMSE) for the fitted curve is 0.3 mm·s^{-1}.

although quantitatively under-predicted. As expected, the neap to spring evolution, the quarter-diurnal variability with maxima during flood and ebb periods and the corresponding asymmetry (i.e., high stress during ebb and low stress during flood) are all reproduced by the model. Quantitatively, the model performs well during most of flood periods, although for ebbs the predicted magnitude is lower than observations, with larger relative differences during neap tides. The maximum turbulent stress found from observations is 5.1 Pa while the model maximum is 2.8 Pa, both occurring during spring tides at 14:00 on day 21. The coefficient of determination between calculated and predicted turbulent stresses is R^2=0.75 with 95% of confidence interval.

As expected, settling velocities obtained with the model are in good agreement with observations, which is a direct consequence of prescribing the settling rate in the model following equation 5.1. Nevertheless, there are still some discrepancies in the high and low values. Observed settling velocities (Fig. 5.7c) show large intratidal variations during neap tides (15 to 18 February), with values ranging from approximately 0.25 to 2.1 mm·s^{-1}. As the tidal range increases after 18 February, these intratidal variations in settling rates are reduced and W_s remains between 0.09-0.3 mm·s^{-1}. In comparison, the modelled settling rates are restricted by equation 5.1, and the resulting values range from 0.25 to 1.14 mm·s^{-1}. Modelled fall velocities also have a lower range during spring tides, therefore reproducing the observed trend. The quarter-diurnal variations are qualitatively well captured by the model, even though maximum settling values are underestimated around neap tides and asymmetry in settling rate between high water and low water is not reproduced. It is important to note that maximum settling velocities, both modelled and observed, coinciding with slack water, and minimum stress values. Such discrepancy on the maximum settling rates would therefore not be caused by the disagreement in maximum stress values (Fig. 5.7b). Maximum observed settling velocity of 2.12 mm·s^{-1} was found at 14:00 on day 17 while model maximum is 1.12 at 13:30 on day 16, both maxima occurring during neap tides. The minimum observed settling velocity of ∼0.09 mm·s^{-1} was found at 15:00 on day 21 whilst the model minimum is 0.25 mm·s^{-1} at 14:00 on day 21, both during spring tides.

The model reproduces reasonably well the general variability of SPM concentration during the study period (Fig. 5.7d). Lowest concentrations are found during neaps and highest concentrations during spring tides. However, during most of the first three days of the record, the model underestimates observed concentrations. Maximum values are 123.2 g·m^{-3} and 148.5 g·m^{-3} for observed and modelled concentrations, respectively on the last ebb cycle on day 21. The quarter-diurnal variability is captured by the model for the entire record and tidal asymmetry is reproduced for most of the period. During the first three days, a tidal asymmetry is obtained in the model but the maxima are found during the flood while they are found during ebb cycles in the observations. From the end of day 17, observed ebb peaks are higher than flood and the model qualitatively

reproduces this difference of maximum concentrations even though it overestimates its magnitude. There is a timing difference between the maximum flood concentrations for which the model values are about one hour late.

Figures 5.8 and 5.9 show model results of near bed suspended sediment concentration during neap and spring tides, respectively. As expected, there are differences in magnitude of more than about 350 $g \cdot m^{-3}$. Although the concentrations during neap tides are low, it is clear the decrease from the ebb phase (11:00) until the low water slack (15:00) when concentrations are minima and the next hour increase again with the start of the flood. A similar pattern but with higher magnitude happens during spring tides. However, the sediment transport is clearly visible as an increase in concentration before low slack water. Even though current speed is diminishing at hours 16:00 and 17:00, an increase in concentrations happens at the mouths of the estuaries which is maybe sediment being transported from the estuaries. At 18:00 the current speed is in a minimum and concentration starts to diminish. These figures represent only examples of the model results to show how different regions affect each other and the suspended sediment in one cell is the result of the movement of sediment in other cells. In a three-dimensional model like the used in the present study, vertical effects are also present. It is possible that part of the differences between observed and modelled concentrations are due to sediment transport.

5.4 Cohesive sediment dynamics in the Dee Estuary

5.4.1 Floc size variability

In this study the changes in grain size are used to identify the flocculation process. Typical floc size changes in the Welsh Channel are shown in figure 5.2. Strong current periods (flood and ebb) cause turbulent stresses over the sea bed and thus produce resuspension of small flocs and break-up of large flocs, resulting in higher concentrations of fine sediments (Figs. 5.2 and 5.3a). The presence of coarse sediment in low concentrations during flood and ebb phases may be the result of the same re-suspension process or flocculation by inter-particle collision due to high concentration of suspended sediments. Once the strong currents diminish, turbulent stresses also decrease and suspended small flocs begin to settle. When slack waters are reached and turbulent stresses are negligible, the aggregation process occurs and large concentrations of big flocs are found. Nevertheless, there is still an important concentration of small flocs, which may be due to the settling of flocs resuspended to higher parts in the water column during previous high turbulent stress periods. The same floc behaviour is found throughout the study period but important changes in magnitude take place depending on tidal cycles. This has also been found for several places with similar hydrodynamic characteristics (e.g. Jago et al., 2006; Badewien et al., 2009; Bartholomä et al., 2009).

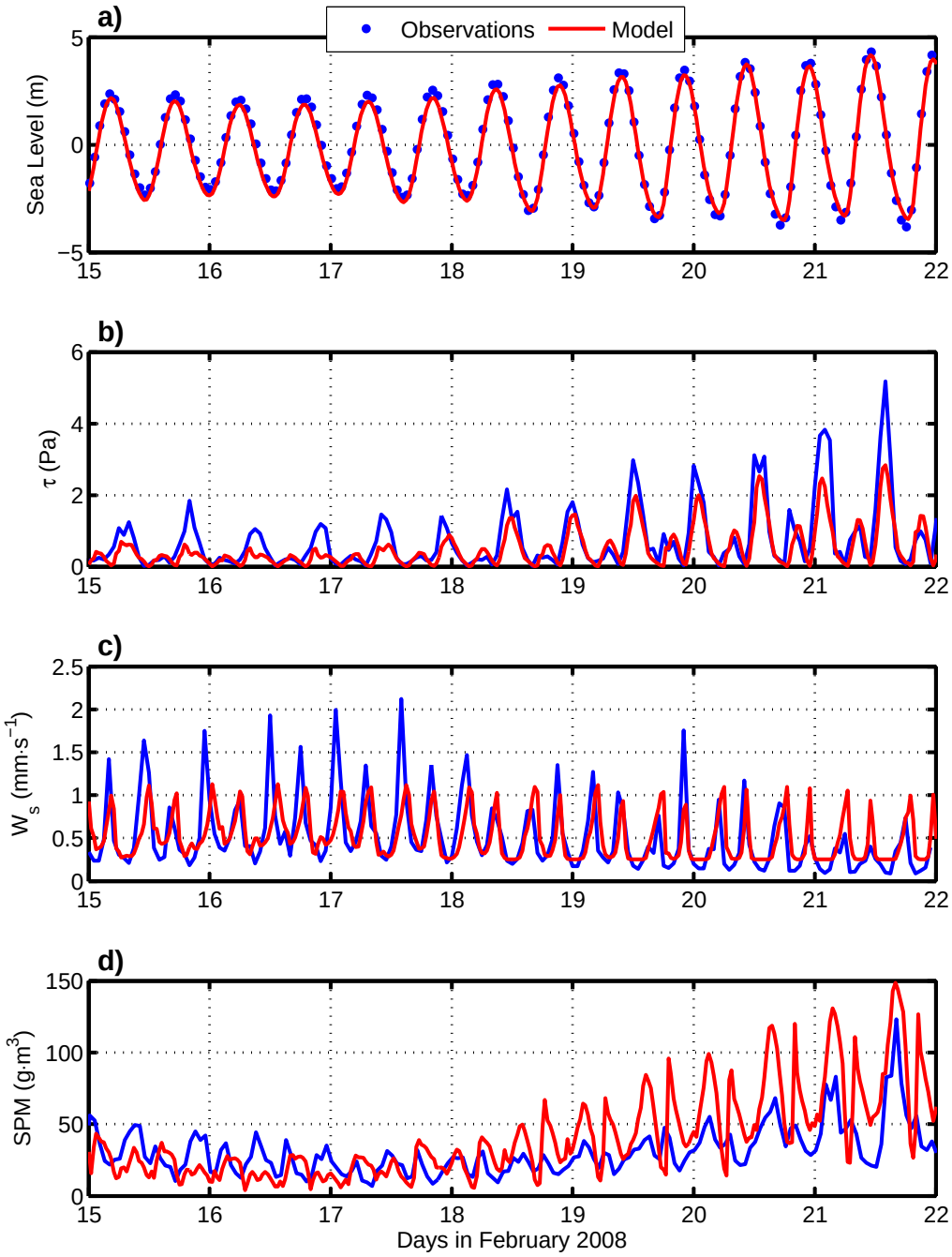

Figure 5.7: Comparison between observations (blue points and lines) and model results (red lines). a) Sea level, observations from LISST pressure sensor. b) Turbulent stress from current measurements and modeled results. c) Settling velocities computed with Stokes law and obtained using the proposed model formulation. d) Total observed mass concentrations from LISST and predicted concentrations including flocculation effect.

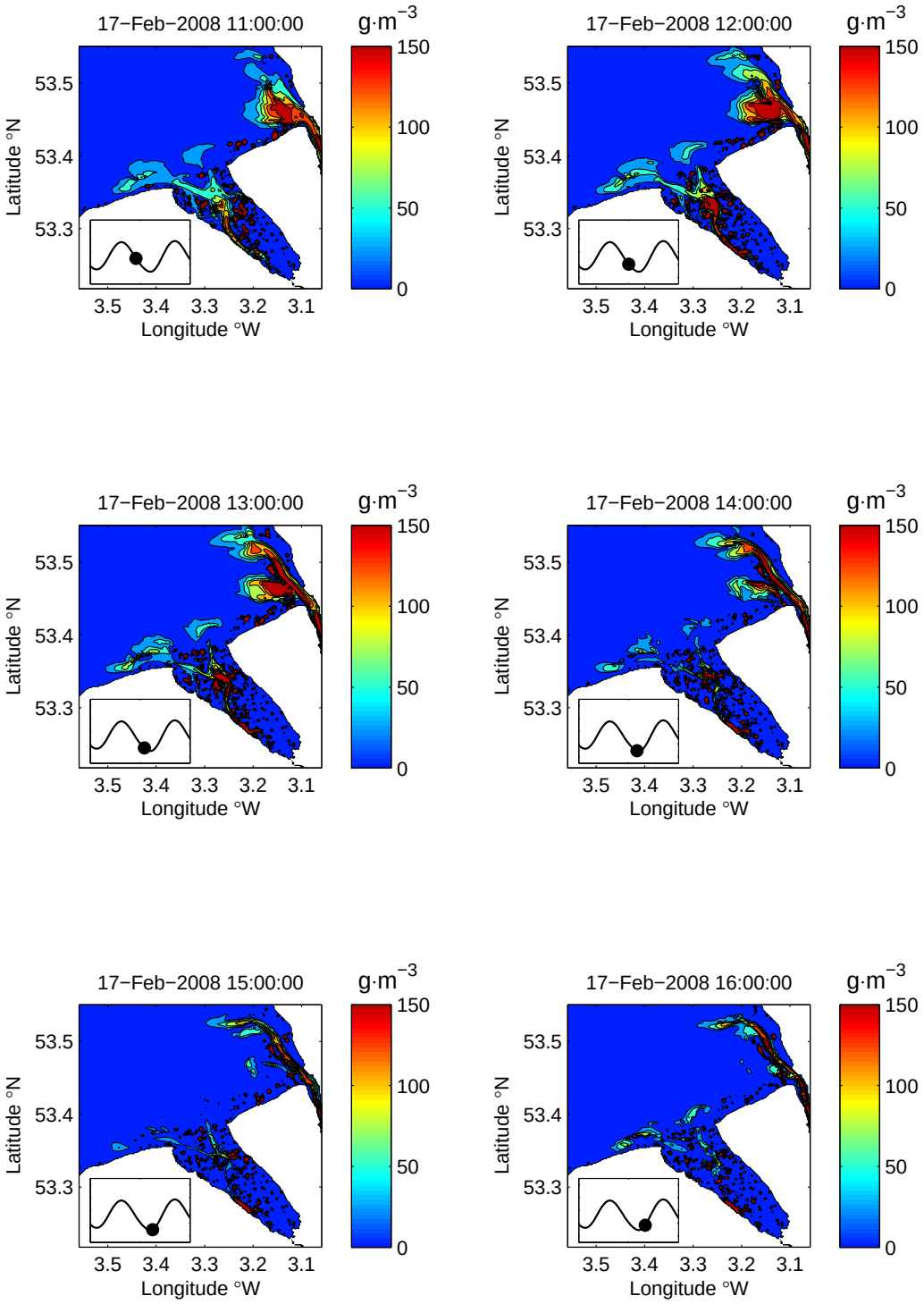

Figure 5.8: Near bottom horizontal distribution of suspended particulate matter in the Dee estuary during neap tides. Obtained from numerical models POLCOMS, GOTM and a sediment module including the formula 5.1 for the changes in floc settling velocity.

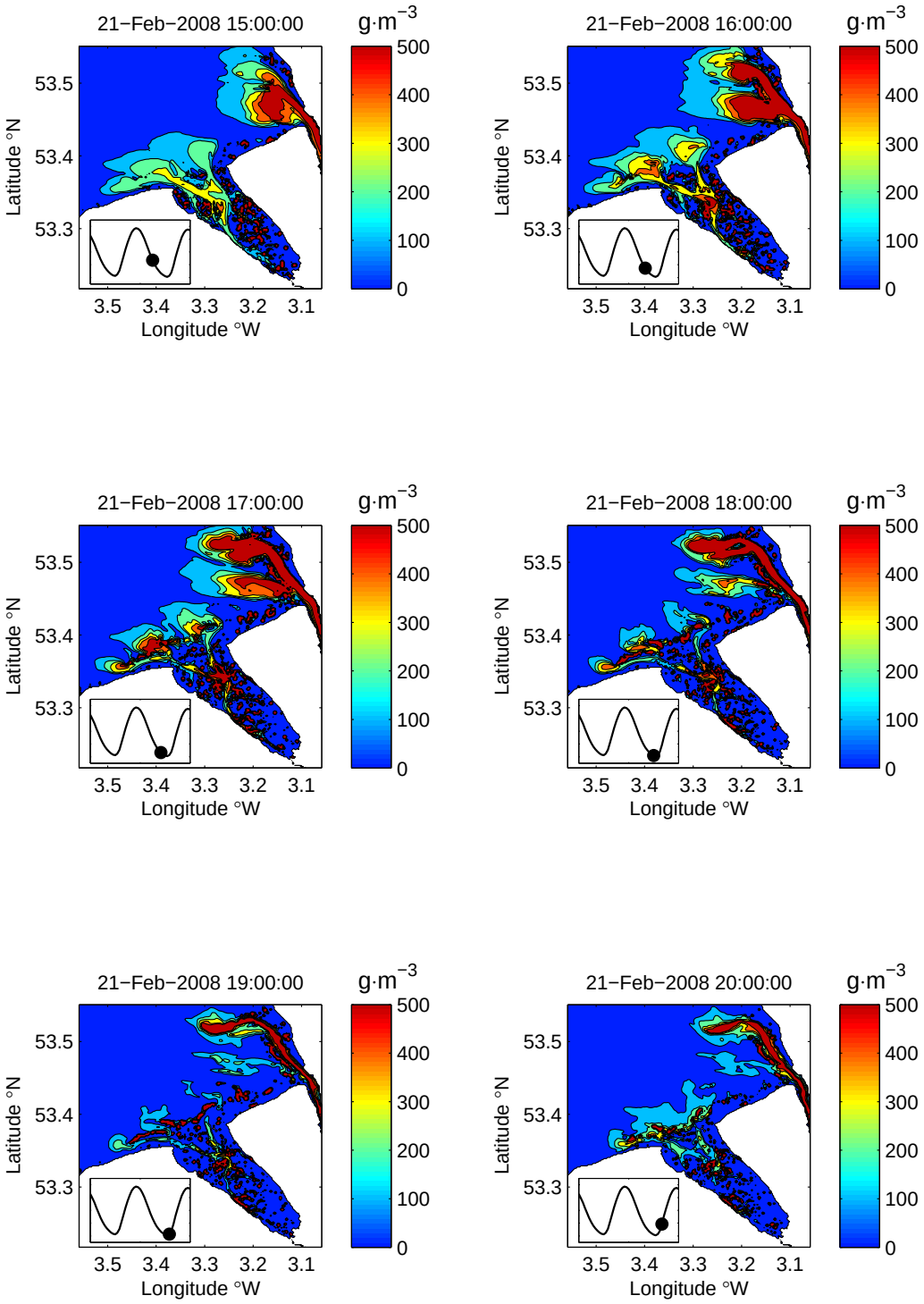

Figure 5.9: Near bottom horizontal distribution of suspended particulate matter in the Dee estuary during spring tides. Obtained from numerical models POLCOMS, GOTM and a sediment module including the formula 5.1 for the changes in floc settling velocity.

In particular the changes in grain size in figure 5.3 show differences in floc size maxima and minima between spring and neap tides. During neaps, the turbulent stresses are lower, and the break-up process is not as strong as during spring tides. As a consequence, the minimum median grain size is about 75 μm around neap tides while it is 50 μm around spring tides. This spring-neap grain size variability has also been found by several authors (e.g. Fettweis et al., 2006; Bartholomä et al., 2009). Another feature is a difference in the range of grain sizes of $\sim$160 μm during neaps and $\sim$50 μm during springs. Therefore, the aggregation process seems to be more important during neaps.

There is, in particular during neap tides, an asymmetry in maximum floc sizes between low and high water, bigger flocs being found at low water. This is not due to asymmetry in turbulent stress values between ebb and flood as these two asymmetries occur at different phases of the tide. Instead, a possible explanation would be that flocs of different origin are advected during ebb and flood: during the ebb, fine particles would be advected from the salt marshes or the upper-estuary (e.g. Amoudry et al., 2014), while during flood the observed flocs would be of marine provenance. The different origin of particles may result in different settling velocities for similar low turbulent stress values due to different sediment characteristics. For increased tidal range (i.e., not during neap tides), the magnitude of turbulent stresses is higher (fig 5.7b), which leads to reduced asymmetry in W_s because there is not enough time with low enough turbulent stresses for the sediments to aggregate.

The floc size variability has been found in several studies. Badewien et al. (2009) reported changes in grain size from about 20 to 400 μm and Jago et al. (2006) found about 50 to 150 μm of median grain size. Krivtsov et al. (2008) measured grain size in Liverpool Bay and found highest concentrations of particles bigger than 200 μm, which is in agreement with the size of big flocs encountered in this study. These features have been found by Jago et al. (2007) and Krivtsov et al. (2008) in sites near the area of this study. Flocs are bigger on neap tides due to longer residence time in the water column and low turbulent stresses. On the other hand, during spring tides turbulent stresses prevents the formation of big flocs.

5.4.2 Treatment of flocs as fractal structures

Fractal theory states that primary particles and flocs are related by a fractal dimension or number in the range of 1-3 (Kranenburg, 1994). According to Kranenburg (1994), a fractal number of 1 means that flocs are very fragile and a number of 3 corresponds to compact aggregates. A precise determination of the floc fractal number is important because it also provides an indication of the strength of cohesive forces for the flocs of the study site and their tendency to aggregate or break-up. Following Kranenburg (1994) and Winterwerp (1998):

$$C_m = \rho_s C_v \left(\frac{D_p}{D_{50}} \right)^{3-n_f} \tag{5.2}$$

To use the known quantities C_m from water samples, D_{50} and C_v from LISST taken on 12-13 February (see section 4.1.1). Equation 5.2 may then be rearranged into a linear relationship:

$$C_m = \rho_s {D_p}^{3-n_f} \left(\frac{C_v}{D_{50}^{3-n_f}} \right) \tag{5.3}$$

in which different n_f values are used and result in a linear relationship for each floc fractal number. The best relationship is then:

$$C_m = 0.0008 \frac{C_v}{D_{50}^{0.6}} \tag{5.4}$$

corresponding to a fractal number of 2.4 and is shown in figure 5.10. The coefficient of determination is R^2=0.95 and units of mass concentration are shown in kg·m^{-3} to be consistent with units of density. Therefore, the corresponding value for the factor $\rho_s \cdot {D_p}^{3-n_f}$ is 0.0008. The floc fractal number of 2.4 obtained from observations in the present study is in the range expected (1-3).

5.4.3 Effective density

In the present study, the values of effective density used in equation 4.1 are implicitly inferred by the conversion of LISST volume concentrations into mass concentrations. These results are in the range reported by Mikkelsen and Pejrup (2001) for different sites. The effective density has been related to the floc size via a range of formulations (e.g., McCave, 1984; Gibbs, 1985; Khelifa and Hill, 2006; Maggi, 2007). In order to compare against different methods, the work of McCave (1984) and Khelifa and Hill (2006) are selected because of the different degree of complexity. For the first case, McCave (1984) proposed to calculate the effective densities as a function of median grain size according to:

$$\rho_e = 30.856 {D_{50}}^{-1.3} \tag{5.5}$$

Khelifa and Hill (2006) obtain effective densities as function of a variable fractal number which, in turn, depends on median grain size D_{50} and primary particle size D_p as:

$$\rho_e = (\rho_s - \rho_w) \left(\frac{D_p}{D_{50}} \right)^{F-3} \phi \tag{5.6}$$

where ϕ depends on the size of the primary particles that form flocs. The variable fractal number F is defined by:

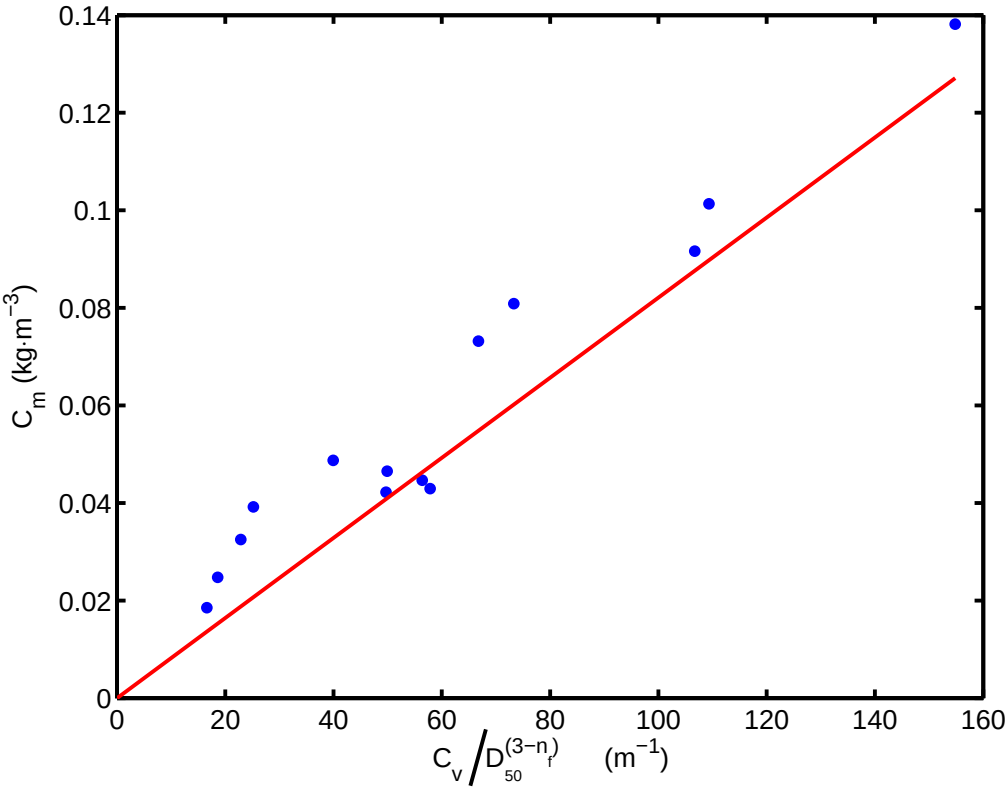

Figure 5.10: Regression to find the fractal number for the study site based on measured quantities. The best relationship of the form C_m=0.0008($C_v/{D_{50}}^{0.6}$) corresponds to a fractal number n_f=2.4, with R^2=0.95

.

$$F = \alpha_{kh}\left(\frac{D_{50}}{D_p}\right)^{\beta} \tag{5.7}$$

with the following boundary conditions:

$$F = \begin{cases} 3 & \text{at } D_{50} = D_p \\ F_c & \text{at } D_{50} = D_{fc} \end{cases} \tag{5.8}$$

where the maximum F value (3) is reached when the flocs have the same size as the primary particles while it takes its minimum value F_c when the flocs have a characteristic size D_{fc}. Thus $\alpha_{kh} = 3$ and β is obtained as:

$$\beta = \frac{log(F_c/3)}{log(D_{fc}/d)} \tag{5.9}$$

For the comparison with the results of this study, a characteristic floc size $D_{fc} = 250$ μm, $D_p = 5$ μm and $F_c = 2$ were used.

Figure 5.12 shows the comparison of effective densities obtained with the different methods explained before. There is a clear difference between the magnitudes obtained from this study and those obtained from the two other methods. In this comparison, there is little change in effective densities using the relation C_m/C_v, in which values are between 60.5-66.5 kg·m^{-3} describing an almost constant value for data on 15-22 February. Results using the McCave (1984) and Khelifa and Hill (2006) methods change by one order of magnitude from about 40 to 450 kg·m^{-3} and show the same behaviour. Larger values are obtained from the Khelifa and Hill (2006) method, with the difference increasing as floc size decreases. Small floc sizes result in effective densities of ∼300 and ∼400 kg·m^{-3} while large flocs are ∼35 and ∼40 kg·m^{-3} using McCave (1984) and Khelifa and Hill (2006) methods, respectively.

There is a small dynamical range if the samples taken on 12-13 February are used. Mass concentrations obtained during these days are the direct result of water samples and not from calibration. Median grain size and effective density varies between 50 and 200 μm and between 46 and 86 kg·m^{-3}, respectively. This small effective density range is an unexpected result but is a fact obtained from independent observations of filtered water samples and volumetric measurements. The even smaller range after calibration for the period 15-22 February is a result of the decreasing mass and volume concentrations during neap tides. These values of effective density seem to be specific of the Dee Estuary and the Welsh Channel. Todd (2014) calculated effective densities for the Hilbre Channel and found strong differences consisting in a smaller dynamical range during winter than during spring (Fig. 5.11). The difference was attributed to a higher biological activity during the spring season. Therefore, the small range of effective densities in the Welsh Channel is maybe a result of low organic content.

The low values of effective density make very difficult the comparison of the results of this study with those of McCave (1984) and Khelifa and Hill (2006). Results of these

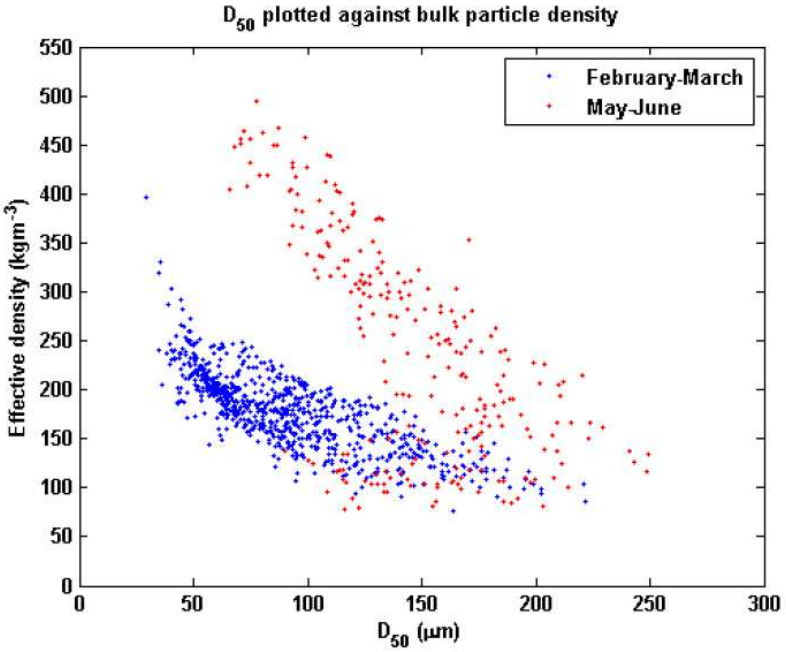

Figure 5.11: Effective densities against median grain size for the Hilbre Channel as obtained by Todd (2014). A small range of effective densities is present during winter season while during spring organic content seems to play an important role in floc grow.

authors have been derived based on several data sets covering a very wide dynamical range for both D_{50} and ρ_e. Nevertheless, it has to be noted that the fractal number calculated in the previous section ($n_f = 2.4$) implies that $\rho_e \propto D^{-0.6}$, which is qualitatively similar to other expressions such as McCave (1984), i.e. ρ_e is proportional to a negative power of floc size. However, effective densities using only samples (12-13 February) in the relation $\rho_e = C_m/C_v$ can also be used to estimate a fractal number. Using these densities in the Stokes law and the median grain size, a relationship between W_s and D_{50} can be found following the proportionality relation $W_s \propto D_{50}^{n_f-1}$ (Winterwerp, 1998). The relationship is shown in figure 5.13 and the corresponding value for the floc fractal number is 2.8, which means the flocs are even more compact in comparison with the 2.4 value found previously. This value is probably more adequate because it takes into account the floc size.

5.4.4 Floc settling velocities

The settling velocities obtained from equation 4.1 are in broad agreement with values reported by several authors. For example, Winterwerp et al. (2006) and Manning et al. (2010) found W_s between 0.1-2 mm·s^{-1} for grain sizes between 50 and 200 μm, while van Rijn (2005) reported settling velocities between 0.06 to 1 mm·s^{-1} for the Mersey Estuary, which is a nearby estuary (approximately 10 to 20 km to east of the Dee Estuary).

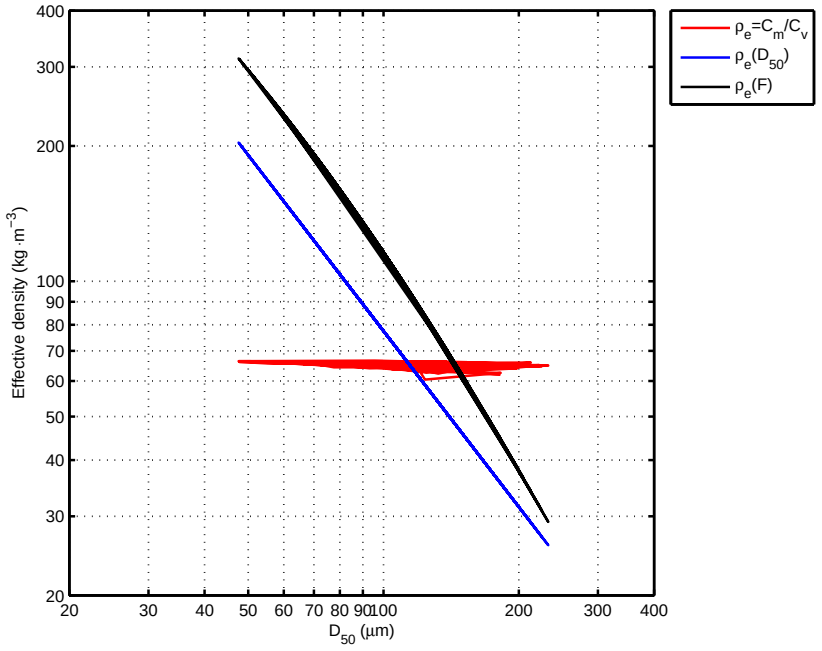

Figure 5.12: Comparison between results of this study and other authors for effective density. Red line is ρ_e=C_m/C_v and is plotted against D_{50} for this study, blue line is ρ_e=$30.856{D_{50}}^{-1.3}$ (McCave, 1984) and in black line is the effective density calculated as a function of variable floc fractal number which, in turn, depends on floc size D_{50} (Khelifa and Hill, 2006).

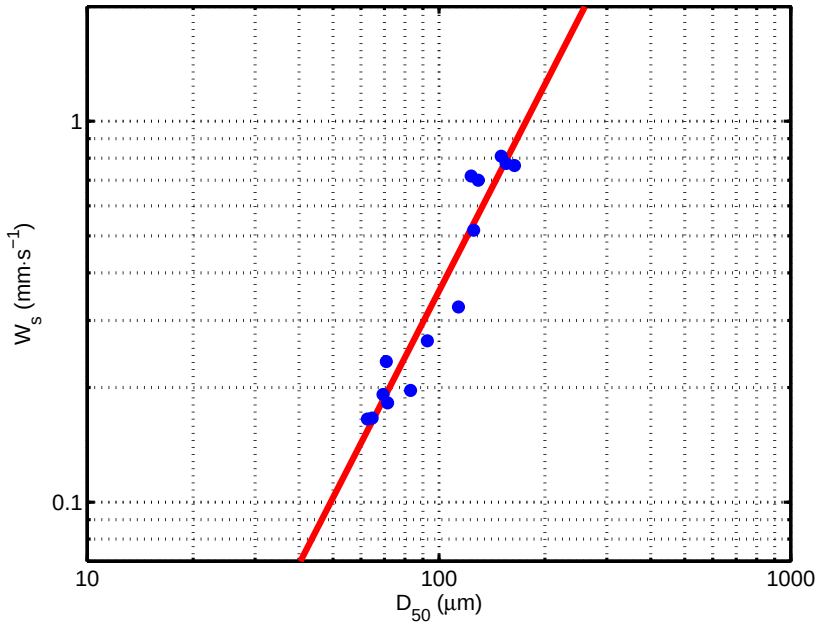

Figure 5.13: Relationship between settling velocity and floc size. Effective density used in Stokes law obtained using only the samples taken during the days 12 and 13 February 2008 (blue points). The effective densities were in the range 46-86 kg·m^{-3}. The red line corresponds to $W_s \propto \mathrm{D}^{n_f-1}$ with n_f=2.8.

A relationship between grain size and shear stress has been described conceptually by Dyer (1989). For low shear stress, aggregation occurs due to inter-particle collisions until a threshold size is achieved. This results in floc size increasing with low shear stress until a maximum size is achieved and break-up of flocs becomes more important, and floc size then decreases with increasing shear stress. This behaviour has been found for turbulent stresses and floc settling velocity (instead of shear stress and grain size) using a settling chamber (e.g. Winterwerp et al., 2006; Manning, 2008). Winterwerp et al. (2006), numerically, found maximum or critical settling velocity at intermediate values of turbulent stress. However, if the water column increases, higher values of the maximum settling velocity are found at lower values of turbulent stress. At turbulent stress values very close to zero, there is no maximum settling velocity as its value would be infinite (equilibrium settling velocity).

Results of this study show, from observations, that the highest settling velocities (or largest flocs) correspond to the lowest values of turbulent stress. However, the big flocs are the result of aggregation as turbulent stress is diminishing rather than increasing, i.e. the grain size changes from microflocs to macroflocs and not from primary particles. In addition, the water depth of about 14 m enables the flocs growth to achieve an equilibrium settling velocity (Winterwerp et al., 2006). These results have also been found in experiments with mud (e.g. van Leussen, 1994; Verney et al., 2011). Another feature found in this study at low values of turbulent stresses is the high variability of settling velocities, which has also been reported in experiments with mud by Winterwerp (1998) and by Verney et al. (2011) for high variability of floc median diameter at low values of shear rate. This may be due to a high sensitivity of W_s to the environment conditions (Winterwerp, 1998) or to a longer aggregation time because of the low collision rates (Verney et al., 2011). The observations also showed settling velocities decreasing as turbulent stresses increase, which coincides with the behaviour described by Dyer (1989) after the grain size threshold at low values of shear rate. In fact, the relationship between shear rate and maximum settling velocities found by van Leussen (1994) is in qualitatively good agreement with the semi-empirical formulation for W_s proposed in this study.

Several relations have been proposed in the literature to obtain the settling velocities of flocs, with different degrees of complexity and variables involved. These include simple power relationship with MPS concentration (Metha, 1986) and more complicated formulations including variable fractal theory (Maggi, 2007). However, as formulations become more complete and dependent on multiple variables, the requirements of field data increase and the implementation in a numerical model becomes more complex. The flocculation process is affected by turbulent stresses, differential settling, Brownian motion, concentration, salinity and biology factors (Fugate and Friedrichs, 2003). For estuaries and coastal zones, Brownian motion and differential settling are negligible

(Winterwerp, 2002). Salinity is important if there are values lower than three PSU, which would be at the river-estuary transition zone. In this study it is assumed that the biology effects are negligible in winter and flocculation depends on turbulent stresses and concentration only. In the Dee estuary turbulence plays an important role in the changes of grain size (see fig. 5 in Amoudry and Souza, 2011a), and therefore in the settling velocity. Thurston (2009) found strong relationships of grain size with the Kolmogorov microscale, which can be related to the turbulent stress itself.

The proposed fall velocity formula in this investigation is based on the behaviour of observed quantities and depends only on turbulent stresses computed simultaneously with suspended sediment calculations. The formulation describes high settling velocities or big flocs formed because of the aggregation of smaller flocs during periods of low turbulent stresses or slack waters. As current increases, turbulent stresses also increase and the break-up process begins to disrupt the flocs and their size diminishes. If turbulent stresses continue increasing, flocs continue breaking apart until a minimum size is achieved. Also, the formulation has mathematical advantages, i.e., near zero values of turbulent stress results in a settling velocity close to a defined value given by the sum 0.25+0.89, and very high turbulent stresses result in a constant value of 0.25. These features also have physical meaning because flocs cannot either aggregate to an indefinite size or break apart below a minimum size. It is also considered that the formula is suitable as a first approximation to model the flocculation process.

5.4.5 Comparison with other models for settling velocity

Settling velocities calculated following equation 4.1 imply: (i) validity of the Stokes law and (ii) knowledge of both ρ_e and D_{50}. In this study, D_{50} is directly obtained from the LISST measurements and ρ_e inferred by the calibration of LISST volume concentration into mass concentration. Other approaches could be employed for obtaining the effective density. As mentioned in the previous section, a number of expressions can be used to relate the effective density to the floc size, and could therefore be used to calculate the settling velocity from our observational data. A comparison is carried out with different methods which, in order of complexity, are by: (i) McCave, 1984, (ii) the widely used formulation of Winterwerp (1998) and (iii) Khelifa and Hill, 2006. It is important to note that calculations must use available data and minimise assumptions. McCave (1984) also uses the Stokes law (Eq. 4.1) with ρ_e obtained as explained in section 5.4.3. Following Winterwerp (1998), settling velocity including fractal number is:

$$W_s = \frac{\alpha}{18\beta}\frac{(\rho_s - \rho_w)g}{\mu} {D_p}^{3-n_f} \frac{{D_{50}}^{n_f-1}}{1 + 0.15Re^{0.687}} \tag{5.10}$$

From Kranenburg (1994), the effective density can be estimated by:

$$\rho_e = (\rho_s - \rho_w) {D_p}^{3-n_f} {D_{50}}^{n_f-3} \tag{5.11}$$

which can be rearranged to obtain a value using the average of known variables (ρ_e, D_{50}, n_f):

$$\frac{\rho_e}{{D_{50}}^{n_f-3}} = (\rho_s - \rho_w) {D_p}^{3-n_f} = 0.2662 \tag{5.12}$$

Reordering the equation 5.10:

$$W_s = (\rho_s - \rho_w) {D_p}^{3-n_f} {D_{50}}^{1.4} \left[\frac{g}{18\mu(1 + 0.15Re^{0.687})} \right] \tag{5.13}$$

where $(\rho_s - \rho_w) {D_p}^{3-n_f}$ is a known constant (eq. 5.12), $\alpha = \beta = 1$ if flocs are assumed to have spherical shape and $n_f = 2.4$ (section 5.4.2). Thus, equation 5.13 takes the following form using observations of this study:

$$W_s = 0.2662 {D_{50}}^{1.4} \left[\frac{g}{18\mu(1 + 0.15Re^{0.687})} \right] \tag{5.14}$$

The settling velocity formulation of Khelifa and Hill (2006) is:

$$W_s = \frac{1}{18} \theta g \frac{(\rho_s - \rho_w)}{\mu} {D_{50}}^{3-F} \frac{{D_p}^{F-1}}{1 + 0.15Re^{0.687}} \phi \tag{5.15}$$

where F is the variable floc fractal and the following assumptions are used: $\rho_s = 2300$ kg·m^{-3}, $\rho_w = 1020$ kg·m^{-3}, $\phi = 1$ and $\theta = 1$.

In contrast to effective density, settling velocities show the opposite behaviour with smallest ranges for the McCave (1984) and Khelifa and Hill (2006) formulations and larger ranges for the Stokes and Winterwerp (1998) methods (Fig. 5.14). Even tough all results show neap-spring and quarter-diurnal variability, the differences in magnitudes are important. Stokes settling velocities show the highest variability and are already described in section 5.2. Settling velocities using equation 5.14 (Winterwerp, 1998) show similar variability as those from Stokes, with smallest differences in the minima and largest differences in maxima during neap tides. The maximum W_s values are about 1.2 and 1.9 mm·s^{-1} for Winterwerp (1998) and Stokes, respectively. Nevertheless, these maximum differences diminish throughout spring tides and are negligible on the last day of the record. Results of W_s following McCave (1984) show less variability, with a range between 0.4 and 0.7 mm·s^{-1} during neap tides diminishing to about 0.35-0.5 mm·s^{-1} during spring tides. Flood-ebb and slack waters differences in this case are not as large as in previous methods. Settling velocities using the Khelifa and Hill (2006) model show the smallest range but conversely to all other models, during neap tides the range is slightly smaller than during spring tides, with values about 0.5-0.7 mm·s^{-1} and 0.35-0.6 mm·s^{-1}, respectively. As in the previous case, differences in extreme values corresponding to flood-ebb and slack waters are not as clear as in the first two cases.

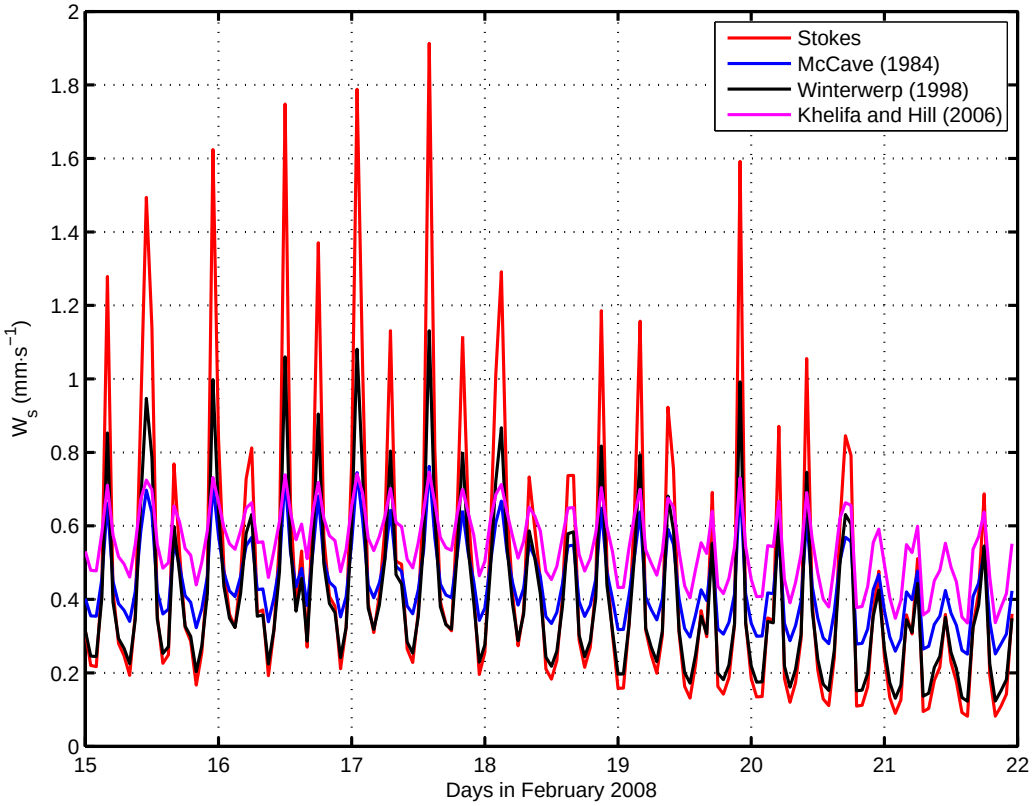

Figure 5.14: Comparison of settling velocities obtained from different methods: i) using observations of this study in the Stokes law (eq. 4.1), ii) applying McCave (1984) method for floc effective densities as a function of floc size and also Stokes law, iii) calculated with a modification of the Stokes law with a constant fractal number by Winterwerp (1998) and iv) based on the formulation by Winterwerp (1998) but with variable fractal number (Khelifa and Hill, 2006).

As expected, settling velocities obtained in this study and those using eq. 5.14 are similar because both methods are based on Stokes law. The main advantage of the method used in this study is the use of observations to calculate (ρ_e) or apply (D_{50}) in the Stokes law, while the main disadvantage of the model of Winterwerp (1998) seems to be the floc fractal number estimation.

5.4.6 Flocculation and hydrodynamics

Turbulent stresses obtained in this study from observations with the ADV are of similar order of magnitude as some previously reported (e.g. Winterwerp et al., 2006; Baugh and Manning, 2007). Based on quantities obtained from observations, the turbulent stress asymmetries (Figs. 5.5c and 5.7) have a clear relationship with corresponding minima of settling velocities. Higher values of τ during the ebb lead to a more efficient break-up and smaller flocs are present with slightly lower settling velocities than during the flood period. During neap tides the model reproduces this feature very well, with

similar minima of calculated and modelled W_s values. During spring tides, maximum turbulent stresses are well predicted but corresponding minima of modelled settling velocities are limited by the formulation. This result implies that some processes may either not be well reproduced or may not be taken into account in the model. Calculated settling velocity maxima coincided with low values of turbulent stresses, and the highest W_s values happened during neap tides and seem to be related to the asymmetries between previous flood or ebb periods. This could be due to an enhancement of floc growth in successive periods of low turbulent stress and more availability of suspended sediment after the ebb by either advection from the estuary or local resuspension. Modelled settling velocities have maximum values with minimum turbulent stresses and highest W_s during neap tides. However, there is no clear asymmetry as in observed data.

The stress asymmetries are interpreted as being due to barotropic and baroclinic processes. However, processes like strain-induced periodic stratification and internal tidal asymmetry (tidal straining) can play an important role in estuarine circulation (Burchard and Hetland, 2010). Giddings et al. (2011) found the variability of advection and straining during flood and ebb strongly related to stratification, mixing and longitudinal dispersion. According to Simpson et al. (2005), tidal straining has been found to control the structure and intensity of turbulent stresses on both ebb and flood, with higher values in the lower half of the water column. Also, stress asymmetries are also related to the sediment dynamics. The internal tidal asymmetry has been mentioned as responsible for the estuarine turbidity maximum in the Columbia River (Jay and Musiak, 1994). Burchard et al. (2008) found an important contribution from tidal straining to net sediment transport in the Wadden Sea. Tidal current asymmetry with ebb dominance and no river discharge has been reported as the main factor for sediment transport (Bartholomä et al., 2009). In the Dee Estuary there is a contribution from the river, greater than that of Simpson et al. (2005), and strong tidal currents. This seems to enhance stratification and enable asymmetries in turbulence production (Bolaños et al., 2013). Nevertheless, Bolaños et al. (2013) show that the POLCOMS-GOTM model predicts accurately barotropic processes but not the baroclinic part, which leads to an underestimation of the current tidal asymmetries.

There are time lags between observed and modelled results. For turbulent stresses (Fig. 5.3.2b) the time difference is mainly during flood periods, with modelled values delayed with respect to observations. Modelled settling velocities lag observations by about one hour throughout the study period for both ebb and flood periods (Fig. 5.3.2c). Modelled suspended sediment concentrations display a similar lag mostly during floods around neap (Fig. 5.3.2d). These results could be related to the time lags of the hydrodynamic model which can be seen in a comparison of modelled and observed density anomaly in fig. 5.15. Observations show stratification at the end of ebb periods

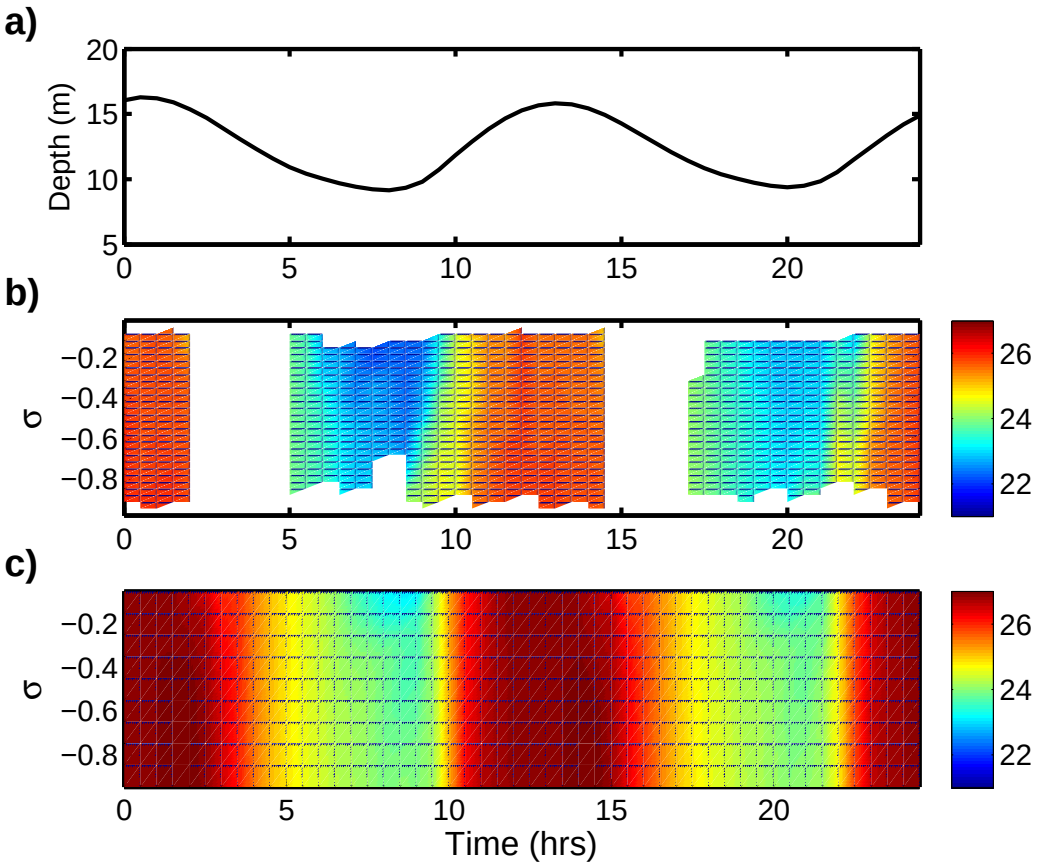

Figure 5.15: Welsh Channel model predictions and observations during two tidal periods. a) Measured sea level, b) Vertical distribution of observed density anomaly (kg·m^{-3}), c) Vertical distribution of modeled density anomaly (kg·m^{-3}). Vertical axes in (b) and (c) are in σ-coordinates used in the models.

(stronger during the first) while modelled stratification is weak and the response is delayed. Then, stratification seems to affect the timing of predicted settling velocities and concentrations.

Another difference in the predicted and calculated W_s and SPM is the magnitudes during spring tides. In this cycle the floc concentration may be an important factor while during neap cycles the timing factor is most significant. Also, settling velocities in the second half of the record have a flat shape when turbulent stresses have minimum values. This is a result of the minimum limit established by the settling velocity formulation, and the comparison suggests a different minimum value. These factors can be taken into account to improve model predictions. In general, the performance of the models (POLCOMS, GOTM and the sediment module accounting for flocculation) is good on the time scale at which they were applied.

Chapter 6

Turbulence as a common approach on flocculation through currents and waves regimes

The classical relationship between turbulence, represented by stresses or shear rate, and flocculation, represented by floc size or settling velocity, displays significant uncertainty as indicated by the large scatter of data (see Section 5.3). This behaviour is found in this study (Fig. 5.6) and has also been found in the literature (e.g., Winterwerp, 1998; Fugate and Friedrichs, 2003; Verney et al., 2011; Strom and Keyvani, 2011; Wang et al., 2013). Despite the clear trend shown by the observations in figure 5.6, it is evident that there are other effects or forcing processes involved which cause the large variability of settling velocities for a given value of turbulent stress. For example, flocculation is complicated by the presence of gravity waves which can modify the turbulence field (Winterwerp and van Kesteren, 2004; Braithwaite et al., 2012; Fettweis et al., 2012). It is also possible that turbulent stresses are not the best turbulent property to describe the floc behaviour. Previous work has identified a hysteresis effect on flocculation which maybe explains the dispersion of data (Dyer, 1986; Verney et al., 2011). In this chapter, the more complex situation of floc behaviour under the effect of different hydrodynamic regimes (currents and waves) is investigated. It specifically investigates various relationships between floc size and turbulent properties, separating both in terms of wave-current regime and tidal phase (flood or ebb).

The analysis of the observations is divided in three distinctive regimes shown in figure 6.1. The first part, from 15 February to 20 February, occurs during neap tides, has a wave height of about 0.1 m and a bottom current speed of up to 0.28 $m{\cdot}s^{-1}$, and is therefore considered as a **"current only"** regime. The second part, from 21 February to 26 February, has a bed current speed of nearly 0.5 $m{\cdot}s^{-1}$ because the spring tides, which coincide with waves between 0.5 and 1.4 m in height, and it is thus defined as a **"combined currents-waves"** regime. The third part is again during neap tides from 29 February to 5 March but with current speed lower than the previous neap tide

period (less than 0.2 $m{\cdot}s^{-1}$) and the highest waves of the entire record (nearly 2 m height) which characterise this period as a **"wave dominant"** regime.

6.1 The floc size spectrum

The entire distribution of floc sizes measured by the LISST during the three sets of observations is shown in figure 6.2. Volume concentrations have been converted to mass concentrations, as explained in section 4.1.1, using the calibration equation 4.1. The change in floc sizes during the "current only" regime has been described in section 5.1 and is repeated in figure 6.2a in order to be compared with the other regimes (note the different scale to be consistent with figures 6.2b and 6.2c). In summary, the "current only" regime is characterized by high concentrations of flocs of about 75 μm during strong currents and 350 μm during weak currents.

The "combined currents and waves" regime (Fig. 6.2b) presents the highest concentrations out of the three regimes for both small and large flocs, and floc behaviour is similar as in the "current only" case. In particular, the concentration of large flocs increases in comparison with that of the "current only" case and the highest concentration of the three regimes corresponds to flocs of about 325 μm on 24 February. It is possible that this concentration is not the highest of the study period because there is a gap in the LISST measurements on 23 February due to a concentration higher than the instrument measuring range. In these cases the instrument records zero concentration values. The only case in which high concentrations are not found is during slack high water when concentrations seem to be of the same magnitude as during the "current only" case. In addition to the highest concentrations, the presence of waves and currents seems to enhance the floc break-up process, with the smallest flocs found during this regime.

Figure 6.2c shows the "wave dominant" regime. In this case, concentrations are generally low and the behaviour is not as clear as in previous cases. The highest concentration during this regime, of flocs of about 100 μm on 1st March seems to be the response of break-up due to waves, while the high concentration of large flocs of about 350 μm is due to a short period without waves on the same day. The rest of the record presents low concentrations for the entire floc size spectrum and in particular during days 1 to 3 before noon when waves were highest. Probably the most important feature of the "wave dominant" regime is that floc aggregation is almost suppressed and floc break-up is not as strong as expected, which means the flocculation process is maybe in an equilibrium phase.

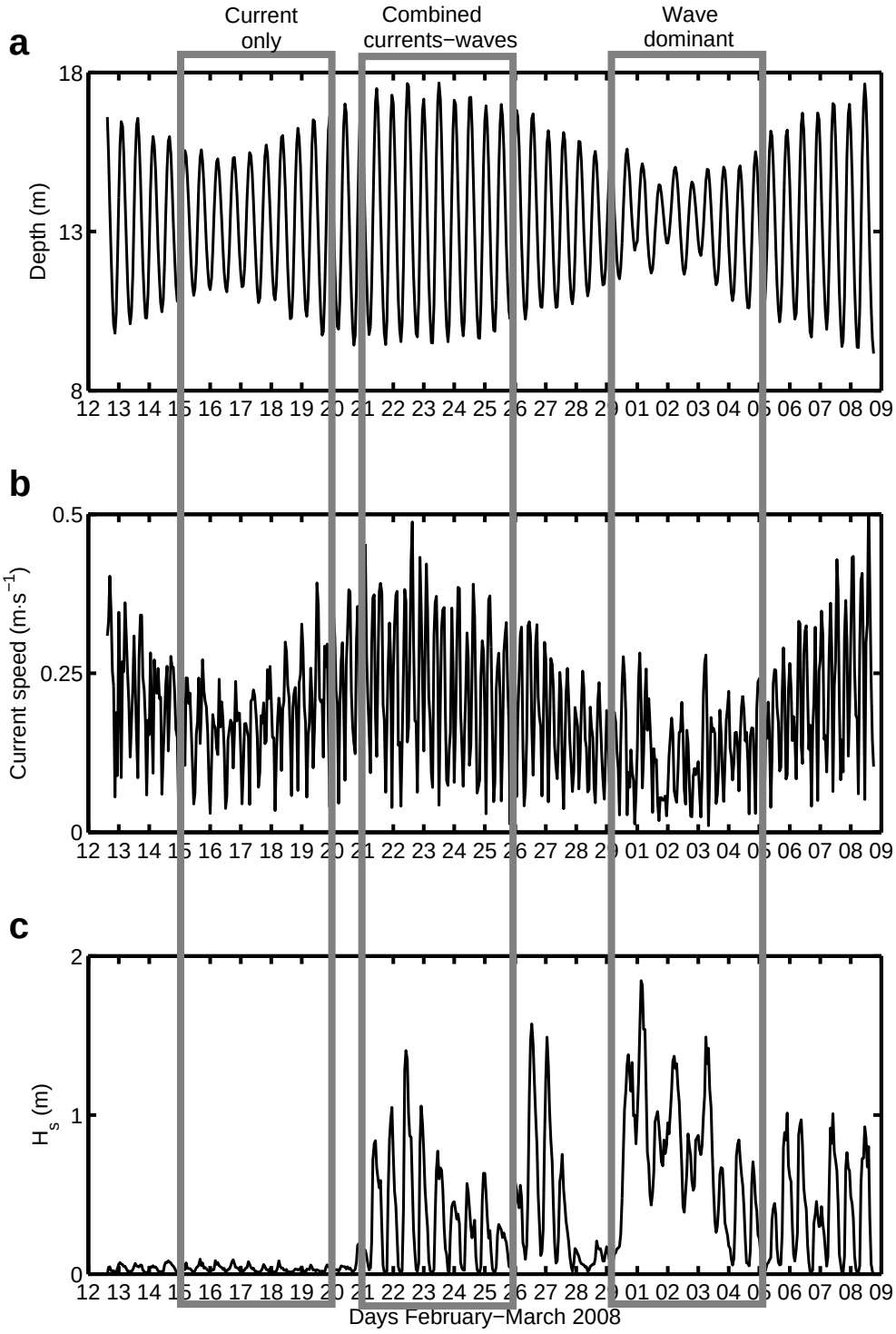

Figure 6.1: Separation of observations into three hydrodynamic regimes. The gray rectangles mark the five days taken into account for each regime: (i) "current only" during 15-20 February, (ii) effect of "combined currents-waves" throughout 21-26 February and (iii) the "wave dominant" regime from 29 February to 5 March. a) Water depth (metres), b) horizontal bed current speed (m·s^{-1}) and c) significant wave height (metres).

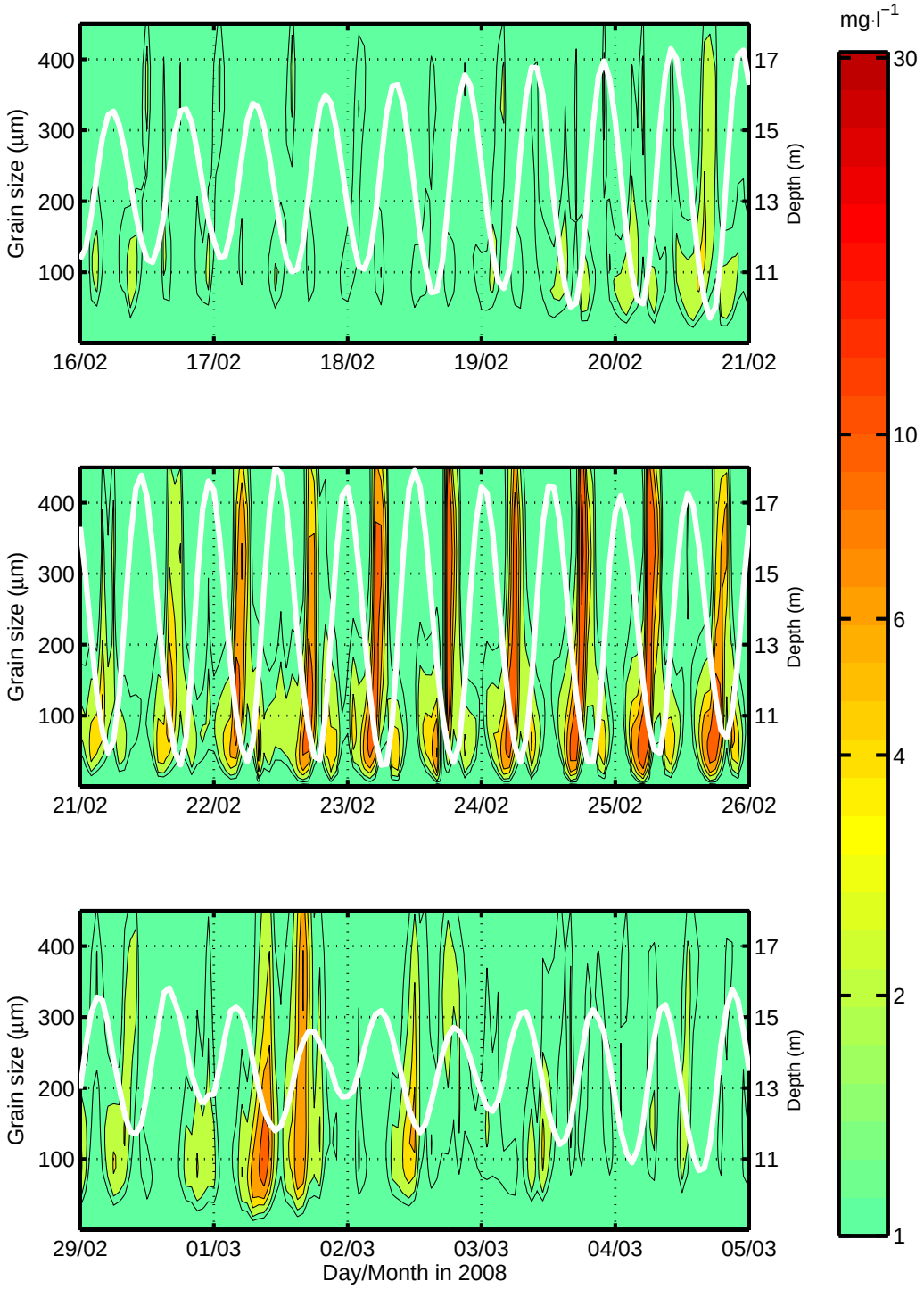

Figure 6.2: Grain size spectrum for the three hydrodynamic regimes as measured by LISST and water depth (white line). a) "current only" regime, b) "combined currents and waves" regime, and c) "wave dominant" regime.

6.2 Time series

6.2.1 Turbulent stresses and flocculation

Chapter 5 presented turbulent stresses and floc sizes from a classical point of view for the "current only" regime. In this section, we present a comparison between the three regimes for the time series of floc size and bottom shear stress from currents (τ_c) and waves (τ_w), which are obtained following the method by Madsen (1994), explained in section 4.1.2 (eqs. 4.18-4.29). It is important to note that in chapter 5, Reynolds turbulent stresses were calculated using equation 4.11 with current velocity fluctuations at 0.3 mab. Figure 6.3 presents the time series for τ_c, τ_w and D_{50} for the "current only" regime in panel a, for the "combined currents-waves" regime in panel b, and for the "wave dominant" regime in panel c. As the "current only" regime has been discussed in chapter 5, this section is focused in the other two regimes. For the combined regime (Fig 6.3b) turbulent stresses from waves are as important as turbulent stresses from currents. In particular, during the first two days of this regime, stresses reach more than 0.75 Pa on 22 February. Like current stresses, wave stresses are tidally modulated and are actually in phase with current stresses with the same quarter-diurnal variability persistent throughout the entire period. This wave-tidal modulation has been found in the Hilbre Channel, in the northeast channel of the Dee Estuary mouth, by Bolaños et al. (2013). Asymmetries in maxima of floc sizes present larger differences than during the "current only" regime. In this regime, flocs exhibit the smallest sizes (50 μm) of the three regimes and the largest flocs barely reach 150 μm, in particular during the first two days. During the last two days, wave stresses diminish and floc size behaviour becomes similar to that of "current only" regime although the size of the small flocs remains in 50 μm. The resulting floc size variability is the highest of the three regimes, with a range of 50-225 μm.

The "wave dominant" regime is shown in figure 6.3c where turbulent stresses from waves reach more than 2 Pa, and those from currents remain about 0.5 Pa as in previous regimes. In this case the tidal modulation of τ_w found during the combined regime is almost lost, as is the quarter-diurnal variability for large values of wave turbulent stresses. Floc sizes seem to have a low variability and remain around a value of 75 μm during the highest τ_w magnitudes. Even though floc break-up is clearly the dominant factor in this regime, aggregation is still present, as can be seen after periods of high τ_w at for example 12:00 on 2 March. It is important to note that this regime presents the highest turbulent stresses but these are not enhancing the floc break-up and keep an almost constant floc size value.

In summary, for the time series of floc size and turbulent stresses: (i) the "current only" regime has the highest floc size variability with clear floc aggregation and break-up, (ii) during "combined currents-waves" effect floc break-up becomes dominant and

aggregation diminishes, and (iii) when stresses from waves are more important seems to be a balance of the aggregation and break-up processes. There is a question that arises from these results about why the highest turbulent stresses from waves do not coincide with the smallest flocs.

Differences between the "combined currents-waves" and "wave dominant" regimes are maybe explained in terms of the resuspension of sediments from the bottom to the entire water column. The currents-waves regime is characterized by enhancement of the conditions of the "current only" regime, with higher concentrations of small and large flocs during high and low turbulent energetic periods, respectively. The combined effect of wave and current turbulent stresses resuspends flocs from the seabed, small flocs are taken to upper parts of the water column and large flocs are disaggregated and recorded as small flocs. Since both waves and currents are in phase, the decrease of turbulent stresses enhances the aggregation of suspended flocs which are also measured in high concentrations. The "wave dominant" regime presents a more complex process. In this case turbulent stresses from waves are the highest of the entire record and therefore the highest expected erosion, resuspension and flocculation of the three regimes. Nevertheless, concentrations are lower and floc sizes not smaller than the currents-waves regime during the highest turbulent stresses periods. A possible explanation of the differences in concentration is that during high energy conditions suspended sediments could be dispersed over the entire water water column and thus not recorded by measurements at a given level. This implies that during the currents-waves regime the high concentrations are limited to the lower part of the water column. Measurements of Bartholomä et al. (2009) and model results of Stanev et al. (2006) showed higher concentrations through the water column in conditions of high waves than during calm periods. Souza et al. (2001) measured and modeled the resuspension events due to two hurricanes up to 30 m above the bottom in 70 m total depth at their study site.

Floc size changes seem to be also related to their distribution in the water column. A possible process could be that at the beginning turbulence resuspends small flocs, as turbulence continues these flocs are easily taken to upper parts of the water column while at the bottom bigger flocs are resuspended, broken-up and measured as small flocs. The process continues if turbulent stresses remain high and increase the concentration of fine sediments over the entire water column and not only in the lower parts. In the lower part of the water column, a possible "steady state" could be achieved, as described by Puls et al. (1988) based on field observations with a settling tube. According to Puls et al. (1988), during the "steady state" large flocs are continuously disaggregated and aggregated, which could explain the almost constant floc size during the higher energy events of the "wave dominant" regime. The authors state that flocs in upper parts of the water column are subjected to less turbulent conditions and therefore aggregate to bigger flocs and fall to high energy lower parts of

the water column where they break apart and are again raised to the upper parts. It is possible that flocs at the measurement height during the "wave dominant" regime are flocs in the process of falling as aggregates and therefore not as small as during the currents-waves regime. Another possible explanation for the slightly bigger flocs is that during the "wave dominant" regime, turbulence firstly erodes small flocs and continues the erosion effect over the seabed where flocs could be larger, more compact than the firstly eroded flocs, and thus more energy is needed for them to be disaggregated, these measured flocs are therefore slightly larger than the first suspended flocs. These flocs are not resuspended by the turbulent current stresses because the duration of the effect on the seabed is not as long as the wave turbulent stresses.

Nevertheless, different results have been found by several authors regarding floc size and concentration in the presence of waves. modelling results of Stanev et al. (2007) show that vertical gradients of horizontal velocities are important in the distribution of SPM in the water column and in the increase in concentration of fine SPM, which could be the case of the currents-waves regime in this study. Observations of Braithwaite et al. (2012) show the presence of a storm during their study with an increase in concentration and floc size (see figure 2 of cited paper). According to the authors, during part of their study period, the floc size was the result of the local effect of turbulence while during the other part particles were resuspended in shallow waters due to a storm and advected to the measuring site. Observations by Fettweis et al. (2012) included three storm periods and during two of them the floc sizes were not as small as during the calm period. However the smallest flocs of the study were found during a storm from a different direction. Agrawal and Traykovsky (2001) also reported three storm periods and the storm with the highest stresses coincided with low concentration and small floc size while the other two showed the opposite behaviour. The authors suggested tidal currents are important to take the flocs to higher parts of the water column which is in agreement with the model results of Stanev et al. (2007). Therefore, there are two possible processes occurring during the "wave dominant" regime: (i) small flocs resuspended in the entire water column with a "steady state" at the measurement height, and (ii) resuspension confined near the bottom due to a lack of horizontal gradients.

There is evidence in the present study of large flocs that could be the result of high concentrations in the water column. Focusing on the "wave dominant" regime and after the high waves (12:00 on 3 March), there is a period of floc size variability in the range of 100 to 200 μm which is larger than the small floc size during high waves. Although the turbulent stresses from currents and waves are the lowest, in comparison to the "current only" regime, the variability trend remains in the same range. This led to the assumption that flocs remain in suspension after the high waves period and the system slowly returns to a state of "current only", as can be seen in the last extreme

values of D_{50} on 4 March (Fig. 6.3c). If, on the contrary, the high concentration of flocs is near the bottom, large flocs would settle first after the high wave period.

6.2.2 Turbulent properties

As stated in the previous chapter, turbulence is the main physical factor for resuspension and flocculation of particles. In the case of this particular study, turbulence can be generated in three ways: (i) currents, (ii) waves and (iii) the combined effect of both currents and waves. In Chapter 5 the effects of currents on the flocculation process were analysed and a first approach was presented, with the turbulent stresses as the main forcing factor and the main control of floc settling velocities. However, different turbulent variables have been used in the literature to investigate the behaviour of cohesive sediments. This section compares three of the more widely used variables, from which other turbulent properties can be obtained, in order to study their variability throughout the three flow regimes: turbulent stresses, turbulent kinetic energy and dissipation rate. The comparison of turbulent stresses in this section includes the values obtained from the covariance method (Eq. 4.11), denoted as τ_{cov}, and from the wave analysis, taking into account waves and currents τ_{max} (Eq. 4.29). It is important to note that τ_{cov} and τ_{max} are calculated using different methods as explained in section 4.1.2. Turbulent kinetic energy *TKE* is calculated for the three regimes from the fluctuations of the current velocity record (Eq. 4.30) and is often used to calculate current turbulent stresses applying the relation $\tau = C_1 \cdot TKE$, where $C_1 = 0.19$ is an empirical constant. Dissipation rate ϵ is obtained using the inertial method (Section 4.1.2). It is important to notice that ϵ is used to calculate relevant parameters such as the Kolmogorov microscale η and the shear rate G. It is therefore particularly important to study the variability of the primary sources (i. e. τ_{cov}, *TKE*, ϵ) and also their differences between hydrodynamic regimes.

Figures 6.4, 6.5 and 6.6 show the time series for turbulent stresses, turbulent kinetic energy and dissipation rate along with water depth for "current only", "combined currents-waves" and "wave dominant" regimes, respectively. During the "current only" regime (Fig. 6.4), the expected increase in magnitude of all variables from neap to spring tides is clearly visible, as is the quarter-diurnal variability. The most striking feature is the asymmetry between flood and ebb tidal phases. The asymmetries showed by turbulent stresses and *TKE* are of similar magnitude. However, for the dissipation rate the differences between the flood and ebb maxima are larger and a change in the vertical scale of the plot from linear to logarithmic is necessary. In fact, it could be argued that ϵ only shows semidiurnal variability. The "combined currents-waves" regime shows an expected increase in magnitude because of the spring tides and waves. The quarter-diurnal variability is also present and, with the increase in magnitude, ϵ also shows four maxima per day. Turbulent stresses are in phase but the asymmetries

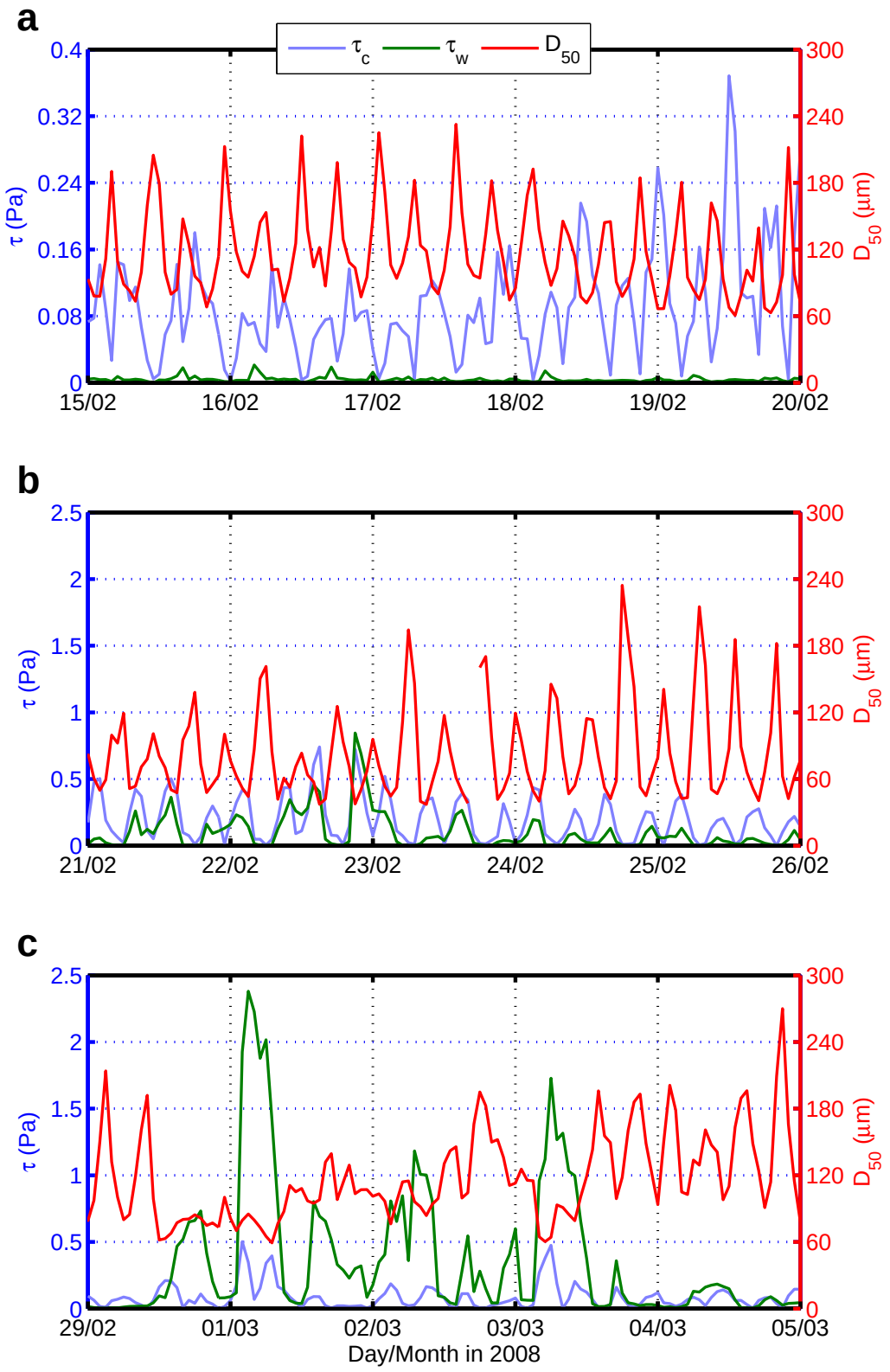

Figure 6.3: Turbulent stresses from currents (τ_c), waves (τ_w), and median grain sizes (D_{50}) for each hydrodynamic regime. a) "current only" regime, b) "combined currents and waves" regime and c) "wave dominant" regime. Notice the change in turbulent stresses vertical scale in a).

shown by τ_{max} seem to be not as large as asymmetries of τ_{cov}. For *TKE* during this regime the differences between flood and ebb are lower than during the "current only" regime. The change in *TKE* magnitude for the flood is from several times in the "current only" case to less than a half the magnitude of ebb in the "combined currents-waves" regime. An important difference between τ_{cov} and *TKE* during this regime is the time of the maximum peaks. For example, the maximum τ_{cov} occurred on day 23 while for *TKE* it was on day 25. This contrasts with their behaviour during the "current only" regime when times and magnitudes followed the same pattern (Figs. 6.4a and 6.4b).

It is obvious that during the third regime the waves are the most important forcing, but how are the turbulent properties affected by the waves? Figure 6.6 shows a comparison of the effect of waves on the turbulent variables considered in this study. In figure 6.6a the magnitude of τ_{cov} is lower than during the "combined currents-waves" regime (Fig. 6.5a) since this period happens during neap tides and reaches a minimum at the end of the neaps. The presence of maxima of τ_{cov} coinciding with maxima of τ_{max} are evidence of forcing from currents. In contrast to τ_{cov}, maxima of τ_{max} during this regime are larger than in the currents-waves regime and follow the height of the waves. A time lag between maxima of turbulent stresses is present, with peaks of τ_{max} occurring approximately 2 hours before the peaks of τ_{cov}. The turbulent kinetic energy (Fig. 6.6b) almost follows the time series of τ_{max} during this regime. Important differences of turbulent stresses and *TKE* during the "wave dominant" case are that the asymmetries found in the currents-waves regime are almost lost and the frequency of the maxima changes from quarter-diurnal to semidiurnal. For dissipation rate (Fig. 6.6c) the magnitude also decreases, it still has the quarter-diurnal variability and asymmetries are clearest than in previous regimes. Therefore, for the "wave dominant" regime turbulent stresses obtained with the covariance method seem to have part of the wave information since it almost follows the time series of turbulent stresses from the wave analysis. In contrast, *TKE* captures the features shown by τ_{max}. Unlike τ_{cov} and *TKE*, dissipation rate only decreases the variability shown in previous regimes. The implications of these results for floc behaviour will be investigated in the next section.

6.3 Turbulent controls of flocculation

In order to investigate the relationship between floc size and either turbulent stresses, or *TKE* or ϵ, a comparison was carried out, taking into account all the observations of the three regimes described above. The reason for including the entire data set was to find whether a single variable can be used to explain the floc behaviour throughout the three different hydrodynamic regimes. Figure 6.7 shows the scattering of observations and all the distributions show an inverse relationship with floc size. However, τ_{cov} and *TKE* have the simplest relationship since only one population of data can be distinguished. On the other hand, in τ_{max} and ϵ at least two populations can be identified which

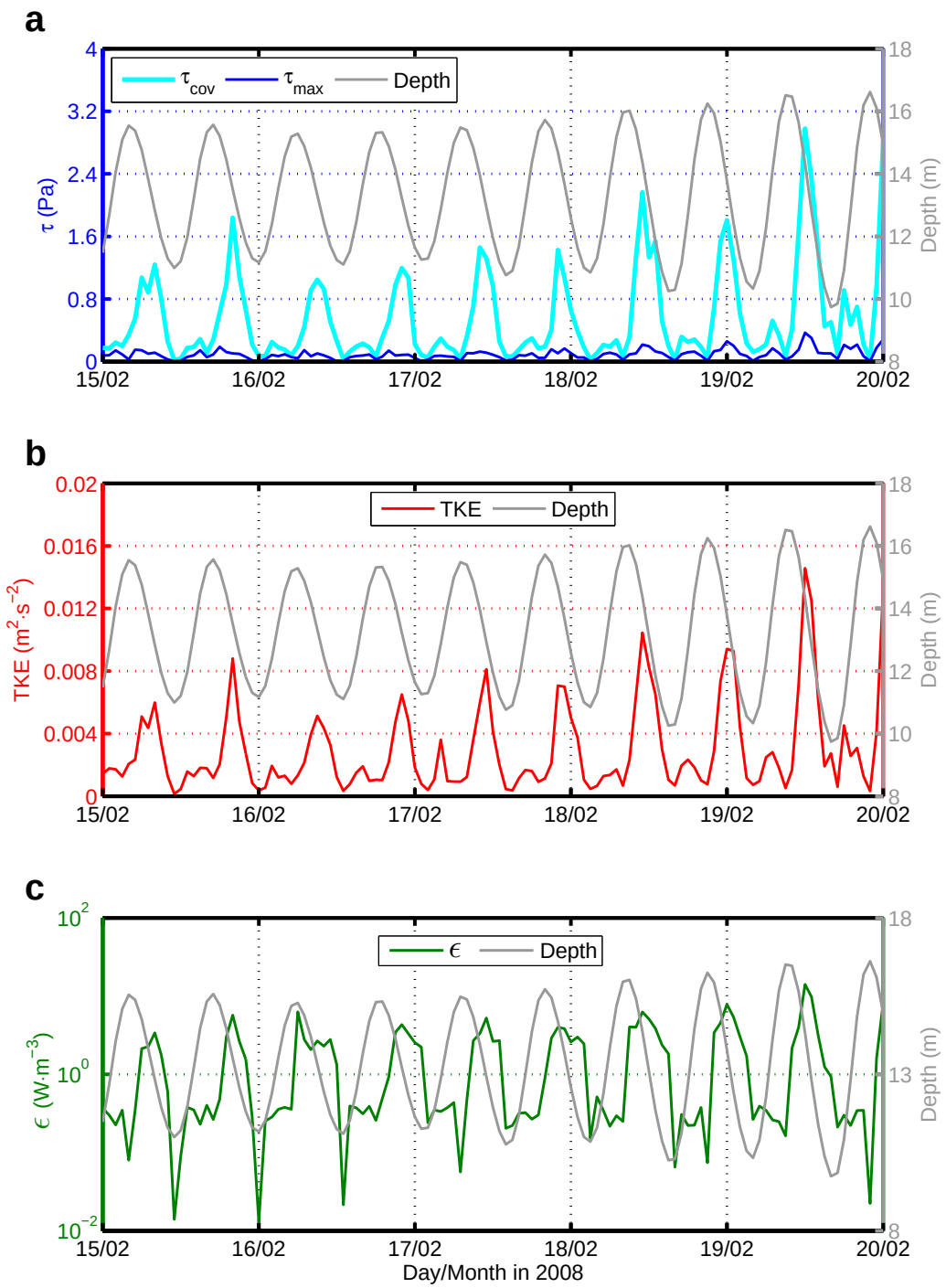

Figure 6.4: "Current only" regime: a) turbulent stresses using the covariance method (τ_{cov}) and maximum bed stresses from the currents and waves analysis (τ_{max}), b) turbulent kinetic energy from Reynolds decomposition of current velocity record, and c) dissipation of turbulent kinetic energy (ϵ) from the turbulent spectrum analysis.

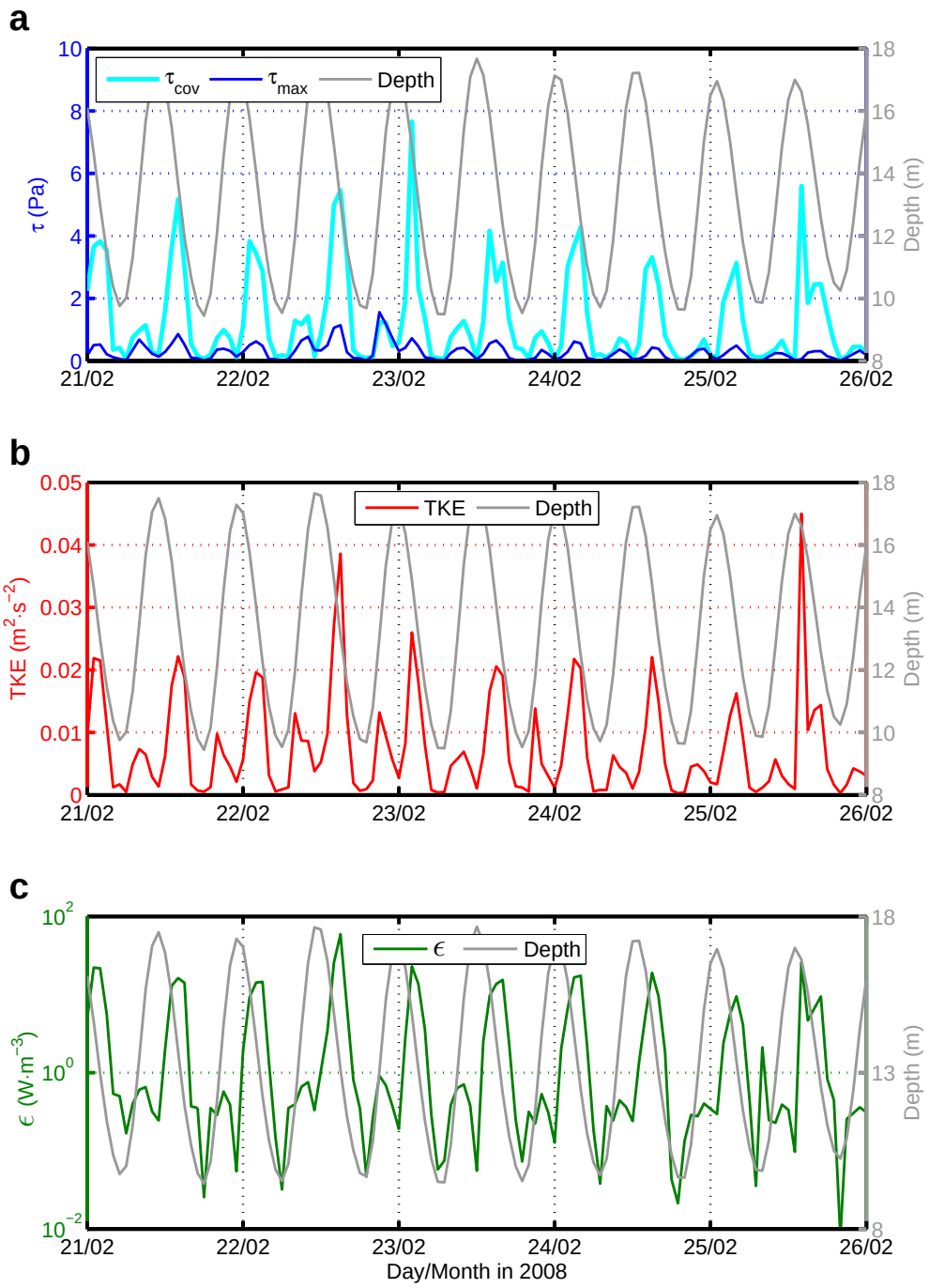

Figure 6.5: "Combined currents-waves" regime: a) turbulent stresses using the covariance method (τ_{cov}) and maximum bed stresses from the currents and waves analysis (τ_{max}), b) turbulent kinetic energy from Reynolds decomposition of current velocity record, and c) dissipation of turbulent kinetic energy (ϵ) from the turbulent spectrum analysis.

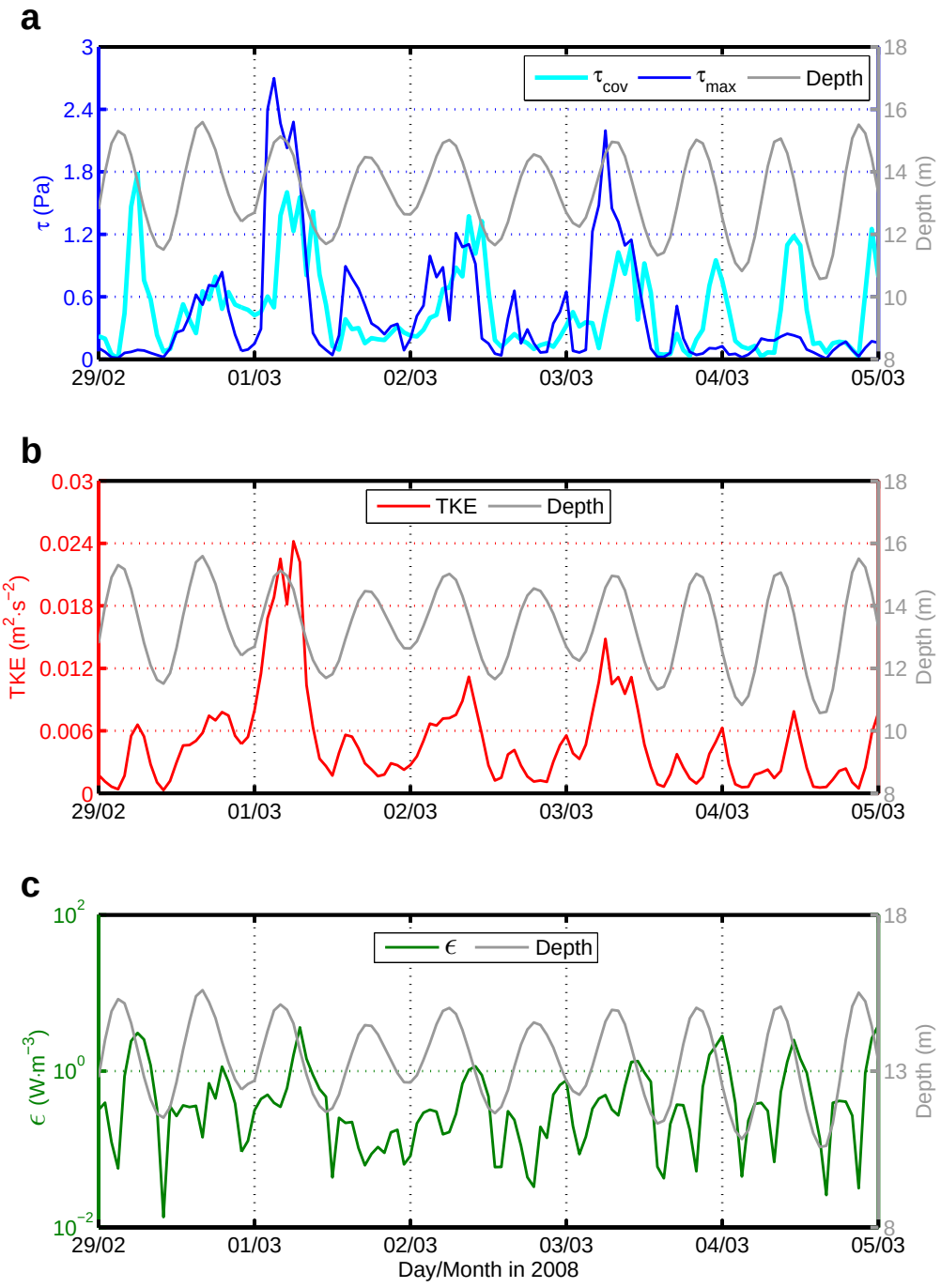

Figure 6.6: "Wave dominant" regime: a) turbulent stresses using the covariance method (τ_{cov}) and maximum bed stresses from the currents and waves analysis (τ_{max}), b) turbulent kinetic energy from Reynolds decomposition of current velocity record, and c) dissipation of turbulent kinetic energy (ϵ) from the turbulent spectrum analysis.

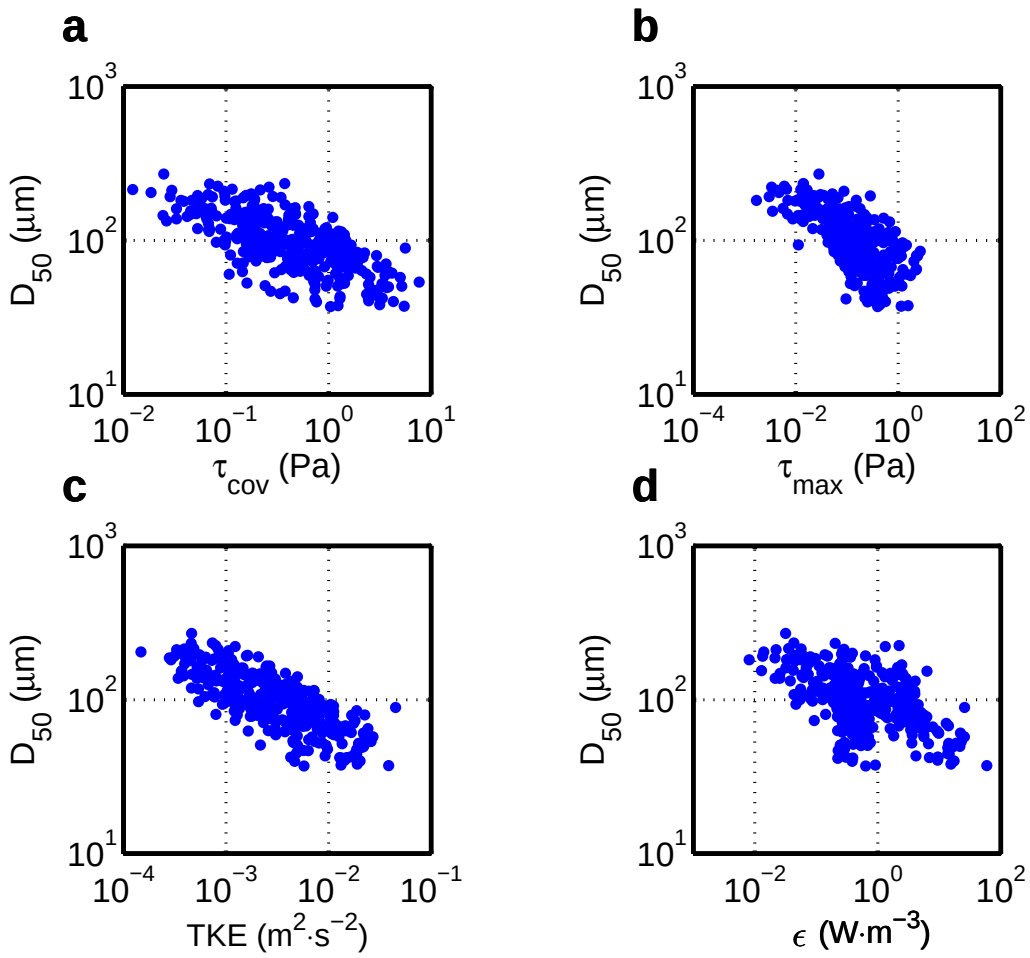

Figure 6.7: Dispersion diagram comparison showing the relationship of different variables with median grain size (D_{50}) including the entire data set for the three regimes: a) turbulent stresses using a covariance method (τ_{cov}), b) maximum bed shear stresses from the currents and waves analysis (τ_{max}), c) turbulent kinetic energy (TKE) from Reynolds decomposition of current velocity record, and d) dissipation of turbulent kinetic energy (ϵ) from the turbulent spectrum analysis.

would lead to a more complex formulation to describe the behaviour. Furthermore, a lower scatter of points is obtained when relating D_{50} to TKE, which would result in a decrease in the uncertainty when a curve fitting is applied to the data. Despite the clear relationship, the variability of the observations remains high since changes in floc size of approximately half an order of magnitude are common for a given value of TKE. For other variables the floc size range is even higher. These results suggest that TKE would give better results if used to describe floc size changes. To further analyze this hypothesis, in the next sections values of τ_{cov} and TKE are divided into the three hydrodynamic regimes and flood and ebb phases. In addition, to observe the effects of the dissipation rate ϵ on other variables, the same analysis is carried out for the Kolmogorov microscale η and shear parameter G.

6.3.1 Turbulent stresses τ_{cov}

The entire set of observations relating D_{50} to τ_{cov} is shown in figure 6.8a displaying the high scatter of data mentioned before. Figures 6.8b to 6.8d show flood and ebb phases in different colours. Some features are clearly visible in these figures. For τ_{cov} the range of each regime is different. The "current only" regime has the largest variability, the "currents-waves regime" is characterized by the highest values of the three regimes, while the "wave dominant" case seems to be almost limited in the observed minimum values (0.1 Pa) and the maxima almost achieve the values of the "current only" regime. Floc sizes are mainly different in their minimum values. The smallest flocs during the "current only" and "wave dominant" regimes are of about 60 μm diameter, while the smallest flocs in the "currents-waves regime" are about 40 μm according to the highest values of τ_{cov} for this case. The most important feature is that the relationship follows the same pattern during flood and ebb phases. These tidal phases show only a shift in the pattern but the distribution remains the same and the magnitude of the shift seems to be similar for the three regimes. Unlike the "current only" regime, "currents-waves" and "wave dominant" regimes present a wide scatter of data that would lead to an increase in the errors of floc size estimations as function of τ_{cov}.

6.3.2 Turbulent kinetic energy *TKE*

In order to find a simple and useful variable to explain the wide scatter of data and variability during different hydrodynamic regimes, the turbulent kinetic energy *TKE* and floc size was used with the floc size observations. Figure 6.9 shows the results for the three regimes and flood and ebb tidal phases. Turbulent kinetic energy and floc size show a single population for all the data, as shown in figure 6.9a. An inverse relationship is present with low *TKE* values of about 0.0003 $m^2 \cdot s^{-2}$ and large values of D_{50} of about 200 μm. Turbulent kinetic energy increases and results in a decrease of floc sizes with values of 0.03 $m^2 \cdot s^{-2}$ and 40 μm respectively. Figures 6.9b, 6.9c and 6.9d show the "current only" regime, combined "currents-waves" regime, and the "wave dominant" regime, respectively. As in previous section, flood and ebb tidal phases are also distinguished in the figures. All regimes show the same behaviour, with differences in magnitudes and tidal phases. For the "current only" regime in figure 6.9b the difference between flood and ebb is clear in the change of *TKE* magnitude, with high energy present during ebb phases. It is of relevance to note that despite the difference in *TKE*, floc sizes reach the same range on both flood and ebb phases. The difference in turbulent kinetic energy between tidal phases is lower in the case of the combined "currents-waves" regime shown in figure 6.9c. The range of floc sizes is also similar for both tidal phases. The "wave dominant" regime in figure 6.9d is the only exception in which there is no difference between tidal phases. This result demonstrates the possibility to describe floc size using simple equations of a power of the turbulent

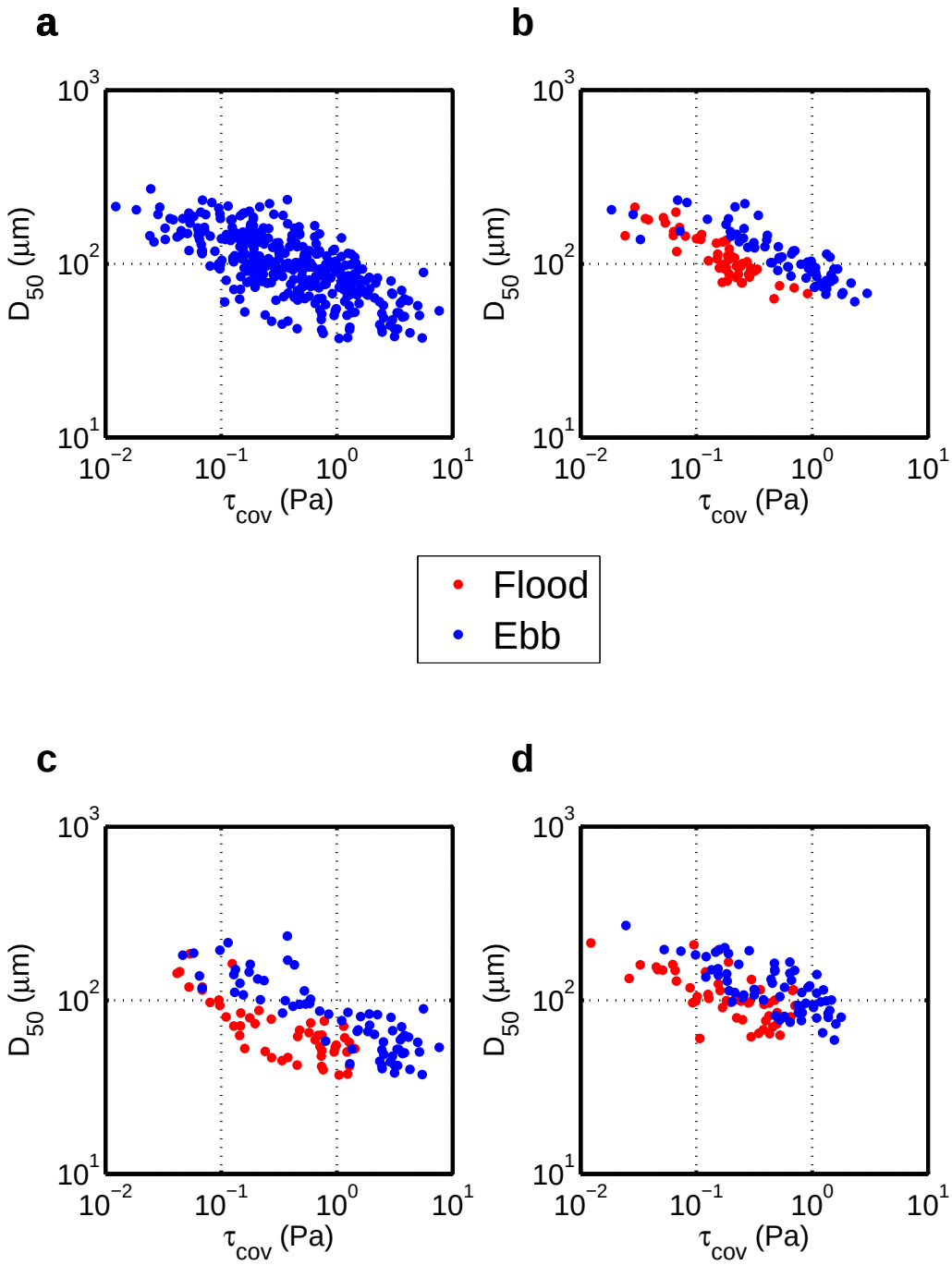

Figure 6.8: Median grain size as a function of turbulent stresses from the covariance method for a) all three regimes, b) "current only" regime, c) combined "currents and waves" regime and d) "wave dominant" regime.

Table 6.1: Comparison of coefficients, R^2 and Root Mean Square Error (RMSE) values of the forms D_{50}=A·$(TKE)^B$ and D_{50}=A·$(\tau_{cov})^B$ resulting of curve fittings for the three hydrodynamic regimes and tidal phases.

		TKE			***τ_{cov}***		
		Flood	Ebb	Flood and Ebb	Flood	Ebb	Flood and Ebb
"current only"	A	7.06	18.33	21.89	59.14	93.37	87.21
	B	-0.41	-0.31	-0.26	-0.34	-0.27	-0.20
	R^2	0.66	0.75	0.55	0.77	0.73	0.51
	RMSE	113.3	116.4	113.9	113.7	115.6	113.2
Currents - waves	A	8.97	15.46	14.56	48.87	78.31	66.44
	B	-0.35	-0.31	-0.29	-0.29	-0.30	-0.23
	R^2	0.70	0.80	0.67	0.63	0.73	0.48
	RMSE	71.2	87.0	79.3	70.2	84.5	76.47
Wave dominant	A	26.10	21.65	23.71	71.57	94.72	89.82
	B	-0.24	-0.30	-0.27	-0.23	-0.26	-0.18
	R^2	0.47	0.81	0.62	0.44	0.55	0.32
	RMSE	106.8	121.5	114.6	106.5	119.4	112.4
All data	A	17.81			77.68		
	B	-0.29			-0.24		
	R^2	0.58			0.48		
	RMSE	101.9			100.3		

kinetic energy of the form: D_{50}=A·$(TKE)^B$.

A test was carried out adjusting curves to the data distributions of figures 6.9 and 6.8. The resulting coefficients of determination, R^2, are shown in table 6.1 in order to compare the use of TKE and τ_{cov} for the description of floc size, as well as how the regime and tidal separation improves their relationship. Except for the flood phase during the "current only" regime, the use of turbulent kinetic energy produces the best fits to the data according to R^2 values. Improvements from 2% ("current only"-ebb) to 26% ("wave dominant"-ebb) and of 30% for the "wave dominant" regime and both phases are reached using TKE. The minimum R^2 difference is obtained in the "current only" regime, it increases in the combined regime and is maximum in the "wave dominant" regime, which emphasizes the important role of the waves in the process. Turbulent kinetic energy appears to be a better predictor of floc size than the widely used turbulent stresses or turbulent shear rate (e.g. Winterwerp et al., 2006; Manning et al., 2010; Kombiadou and Krestenitis, 2012). This also seems to be particularly true in the presence of waves.

6.3.3 Turbulent shear parameter G

Another commonly used property to assess the turbulence effect on the flocculation process is the shear parameter G, which is a measure of the turbulent shear rate in the flow and therefore strongly related to floc sizes. Figure 6.10 shows a comparison of D_{50} versus G data for the three regimes. The entire data set is plotted in figure 6.10a

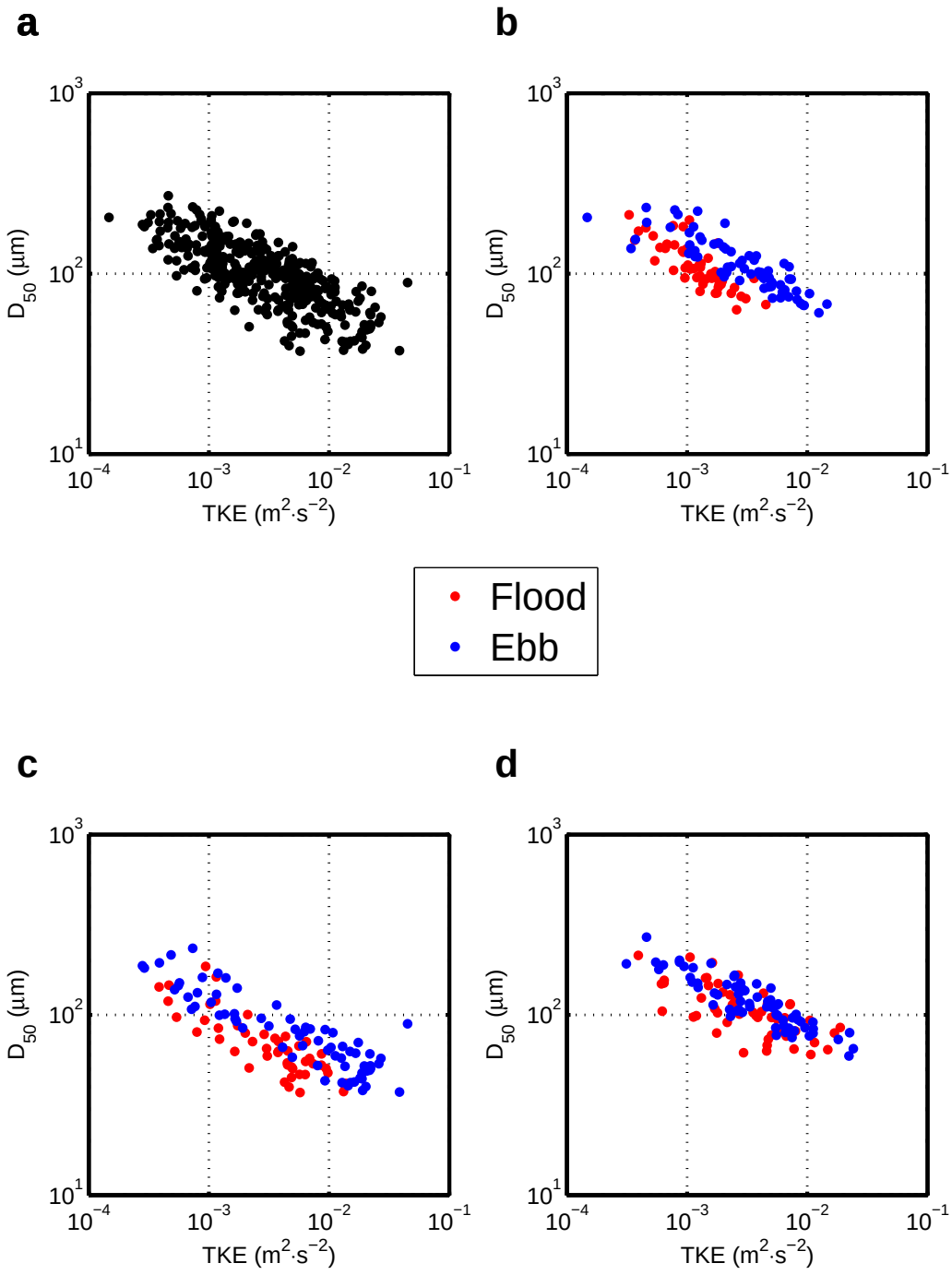

Figure 6.9: Turbulent kinetic energy *TKE* and median grain size D_{50} separated according to hydrodynamic regimes and tidal phases. a) All observations, b) "current only" regime, c) "combined currents and waves" regime and d) "wave dominant" regime. Red and blue points for flood and ebb, respectively.

where values of G range over 2-200 s^{-1} and floc sizes across 3-300 μm. Despite the wide scatter of data, two populations can be distinguished. A large population with, as expected, an inverse relationship showing small floc sizes for high values of shear rate and increasing floc size with decreasing shear rate (floc break-up and aggregation, respectively). A small population appears almost in the middle of the afore-mentioned population, with values of G between 10 and 20 s^{-1}. In order to study this behaviour in more detail, a separation between the three regimes and between flood and ebb phases is shown in figures 6.10b to 6.10d. The "current only" regime is plotted in figure 6.10b and the first feature to notice is the difference between populations during flood and ebb. Flood periods are characterized by an almost constant shear rate between 10 and 20 s^{-1}, which does not seem to be related to changes in floc size until it diminishes to less than 10 s^{-1} and floc size increases. During ebb periods the inverse relationship between turbulent shear and floc size is clear but a spread of data is present when the shear rate is lower than 40 s^{-1}. In figure 6.10c the "combined currents-waves" regime shows a clear relationship during ebb periods, with the largest values of G and D_{50} of the three regimes. However, during flood the relationship is not clear: there are changes in floc size with small changes in shear rate. Although G values are larger than those of the "current only" regime, the behaviour is similar. The only changes in floc size that seem to be related with shear rate occur when D_{50} is larger than about 80 μm. During the "wave dominant" regime in figure 6.10d there is a wide spread of data without any clear difference between flood and ebb phases or different populations. Although the relationship between shear rate and floc size is still present, is not as clear as in previous regimes. Differences between the three regimes and flood and ebb tidal phases are present but there is no single relationship for all the cases.

The turbulent shear parameter G follows the behaviour reported by different authors during the ebb and part of the flood (e.g. Mietta et al., 2011; Verney et al., 2011; Wang et al., 2013). The part with high scatter of data for the "current only" regime corresponds to large flocs and mainly low values of G, which is expected because of the random nature of floc formation during low energy periods, and has also been found in other studies (Winterwerp, 1998; Verney et al., 2011). The "currents-waves" regime has a more defined pattern and the scatter of data of the previous regime is not found. Instead, a clear aggregation and disaggregation behaviour is present. Higher scatter of data is found during the "wave dominant" case and both flood and ebb phases. Turbulent shear rate is widely used to relate either floc size or settling velocities with turbulence. However, in the present study, turbulent shear seems to have a strong effect during ebb periods, disrupting the flocs when its values are large and allowing aggregation when it diminishes. Nevertheless, during flood periods, floc sizes change without an important effect from turbulent shear. This means that the flocculation process is still happening during flood phases even though the low variability in turbulent shear

rate and this low variability is sufficient for aggregation and break-up of flocs. In addition, the shear rate depends on the dissipation of turbulent kinetic energy ϵ, which means that turbulence during ebb periods is larger than during flood, with differences that reach an order of magnitude as in the "current only" regime. This result leads to the conclusion that, for the Dee Estuary and winter season, turbulent shear rate is not a good parameter for representing the observations in all regimes and tidal phases.

6.3.4 Kolmogorov microscale of turbulence η

The smallest eddies in the turbulent flow are represented by the Kolmogorov microscale η, which is assumed to be related to the size of flocs. As in the previous section, the observations of D_{50} are separated between the three regimes and tidal phases and are shown with the Kolmogorov microscale in figure 6.11. The entire data set is plotted in figure 6.11a showing values of η between 80 and 800 μm, while D_{50} presents lower values beetween 30 and 300 μm. Two populations are also present but with a wider scatter of data than in the previous section, which are clearly distinguishable in the smallest flocs below and above a Kolmogorov microscale value of 200 μm. These different populations are more clearly visible when different regimes and tidal phases are taken into account. Figure 6.11b shows the separation of data for the "current only" regime. During flood, the Kolmogorov microscale presents an almost constant value of about 300 μm for flocs in the range of 50-150 μm. Only for flocs larger than 150 μm is the Kolmogorov microscale larger than 300 μm. During ebb, a linear relationship is present between η and D_{50}, with a wide scatter of data at values larger than 150 and 90 μm for the Kolmogorov microscale and floc size, respectively. During the "combined currents-waves" regime (Fig. 6.11c), a behaviour similar to that of the previous regime is observed for both flood and ebb, but the smallest flocs have sizes of about 40 μm, and there is no scatter of data during ebb as was the case in the "current only" regime. The results for the "wave dominant" regime in figure 6.11d show a less evident linear relationship and smaller differences between flood and ebb because of the scatter of the data. In addition, this regime shows the lowest variability of the three regimes for both η and D_{50}. The Kolmogorov microscale also depends on turbulent diffusivity and the similar results of this property and those of the turbulent shear rate are not surprising and rather expected. The additional information is that flocs cannot grow in size to achieve the Kolmogorov microscale and this effect does not depend of either hydrodynamic regime or tidal phase.

The size of the flocs of this study is smaller than the Kolmogorov microscale of turbulence which has also been found in a number of studies (e.g. Braithwaite et al., 2012; Fettweis et al., 2006; Cross et al., 2013; Son and Hsu, 2011) and also in the Dee Estuary by Thurston (2009). However, flocs larger than the Kolmogorov microscale of turbulence are also found (e.g. Cross et al., 2013). Flocs smaller than the Kolmogorov

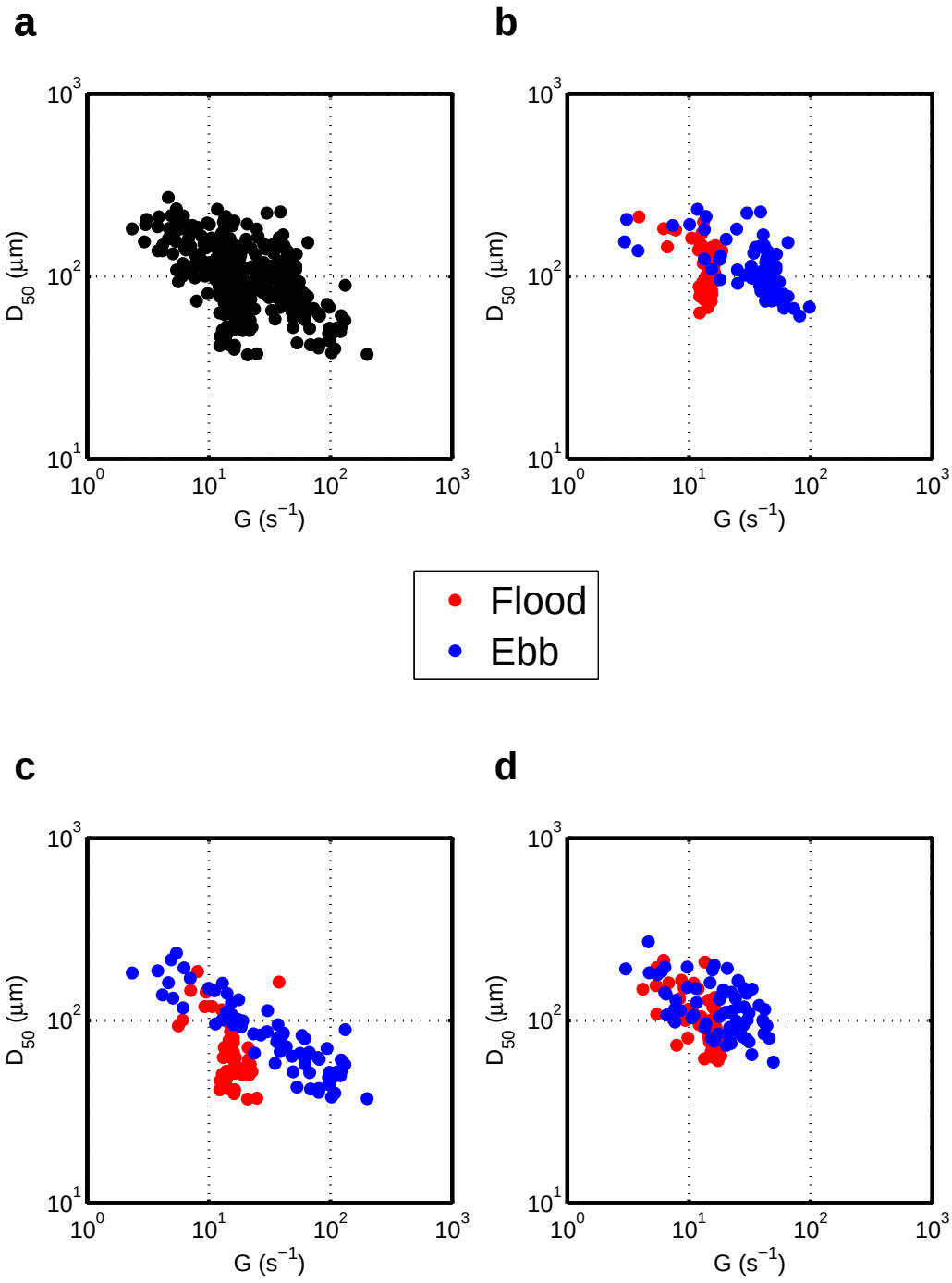

Figure 6.10: Turbulent shear rate G and median grain size D_{50} separated according to hydrodynamic regimes and tidal phases. a) All observations, b) "current only" regime, c) "combined currents and waves" regime and d) "wave dominant" regime. Red and blue points for flood and ebb, respectively.

microscale are mainly composed of inorganic matter while larger flocs are related to extrapolymeric substances due to biologic activity which increase the aggregation of particles. In the Dee Estuary, there is evidence of large flocs due to this process during spring season (Todd, 2014). This is also supported by the slight difference between the floc size and the Kolmogorov microscale, which means that the latter can be easily exceeded. This may be a feature of the flocs in the Dee Estuary because studies in different locations have shown values of η larger than the floc size, from η of several times the floc size (e.g. Braithwaite et al., 2012) to one order of magnitude (e.g. Fettweis et al., 2006). In addition, Fugate and Friedrichs (2003) investigated three estuaries and found different relationships for each site.

6.3.5 Flood and ebb tidal phases

The scatter of data still present when observations are divided into flood and ebb phases is maybe due to the hysteresis effect. This is one of the most important and scarcely mentioned features of the cohesive sediment behaviour. The effect can be seen in the relationship of a number of different variables: turbulent stresses, SPM concentration, current speed, Reynolds stresses, turbulent kinetic energy and median grain size (e.g. Dyer, 1986; Fettweis et al., 2012; Wang et al., 2013). It has been stated that the effect is due to a time lag in the response between different variables. Braithwaite et al. (2012) obtained better correlations between floc size and the Kolmogorov microscale using time lags ranging over 30-60 minutes. Using field samples in laboratory, Verney et al. (2011) reproduced the turbulent stresses of an hypothetical symmetric tidal cycle, i.e. equal turbulent shear rate during flood and ebb phases. Despite the controlled conditions, the authors found a hysteresis effect and concluded that was due to different time scales of aggregation and disaggregation to achieve an equilibrium floc size. After the results of Verney et al. (2011) it is not difficult to visualize the degree of complexity that hysteresis adds to floc behaviour taking into account the common tidal asymmetries present in estuaries.

The flood and ebb behaviour of the present study is similar to results presented by Fettweis et al. (2012). The authors showed periods of neap tides without the effect of waves with clear difference between the flood and ebb periods, while during storms the observations showed high scatter with a slight difference between tidal phases (see figure 8 in cited paper). A particular behaviour is observed in the present study for the turbulent shear rate and the Kolmogorov microscale during flood, which does not have the same variability as during the ebb. This is due to the strong asymmetries in turbulent dissipation, since both G and η depend on ϵ, which shows lower values during flood. *TKE* also shows asymmetries but differences are not as large as for ϵ. Asymmetries in *TKE* are found in observations (Sottolichio et al., 2011) and modelling (Stanev et al., 2006). These results illustrate an important difference between *TKE* and

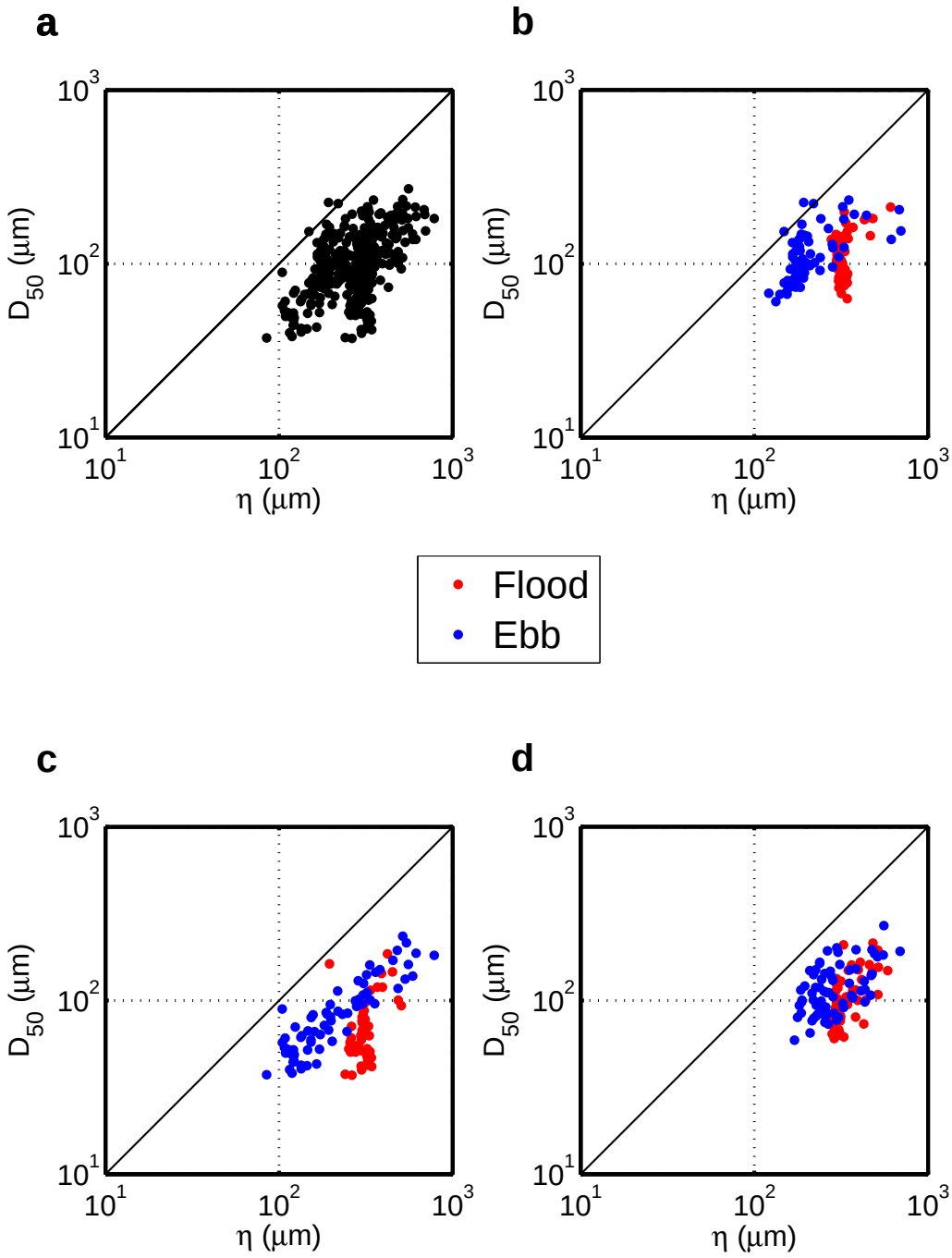

Figure 6.11: Kolmogorov microscale η and median grain size D_{50} separated according to hydrodynamic regimes and tidal phases. a) All observations, b) "current only" regime, c) "combined currents and waves" regime and d) "wave dominant" regime. Red and blue points for flood and ebb, respectively.

ϵ. Since both variables are obtained from ADV observations, *TKE* is an almost direct calculation provided that Reynolds decomposition can be applied to high frequency current velocity measurements. In contrast, the inertial method to obtain ϵ requires a number of assumptions. The weakness of the Reynolds decomposition is the possible misalignment of the vertical and horizontal axis of the sensor (Huntley, 1988), but assuming the beam noise levels of the ADV sensors are ientical, measurements are not affected by misalignments (Voulgaris and Trowbridge, 1998). On the other hand, the inertial method for obtaining ϵ is insensitive to this misalignment but instead the errors could be produced if any of the assumptions is not correct for the study (Voulgaris and Meyers, 2004). An analysis of these assumptions is carried out in section 7.4.

Chapter 7

Discussion

This overall study focuses on the turbulence-induced flocculation in a channel of a hypertidal estuary. However, flocculation, or aggregation and break-up of flocs, is a complex process affected by a number of different variables and other processes which, in turn, are difficult to measure and therefore to study. Important aspects of the results are discussed in the following sections including analyses already carried out in the present investigation and some phenomena not previously considered. Important points about floc properties, how are they measured and the implementation of their behaviour in numerical models are examined here. Section 7.2 shows the hysteresis in the scatter behaviour of the flocs of the Welsh channel. The relationship between turbulent stresses and turbulent kinetic energy is taken into account in section 7.3. An evaluation of the assumptions for obtaining the dissipation of turbulent kinetic energy is carried out in section 7.4. Finally, the relationship between the results of this study and the accretion of the Dee Estuary is explored in the last section (7.5).

7.1 General remarks

7.1.1 Floc properties

The characteristics of aggregates present difficulties in their analysis since there is no generally accepted methodology to measure them accurately. Maybe the most important properties for cohesive sediments are settling velocity and effective density. Floc effective density has mostly been calculated in two ways, as mentioned in chapter 5 (e.g. McCave, 1984; Mikkelsen and Pejrup, 2001). Settling velocities can be obtained from experiments in the laboratory (e.g. Gibbs, 1985; Graham and Nimmo-Smith, 2010) and the field and then effective density is calculated using Stokes Law (Dyer and Manning, 1999). In the field, *in situ* settling tubes (e.g. Jones et al., 1998), combination of settling chambers and video cameras (e.g. van Leussen, 2011) and laser diffraction (e.g. Ahn, 2012) have been used to obtain settling velocities. Fugate and Friedrichs (2002) calculate settling velocities of the fast floc populations as a balance between settling and turbulent dispersion. A number of different studies have been compiled by

Strom and Keyvani (2011), displaying a wide spread for the relationship between settling velocity and floc size, which may be due to the site-specific flocculation behaviour or different instruments being used. Most of the field studies in this comparison used video systems and settling columns to measure floc settling. A key issue with these systems is related to the use of a settling column, which is an intrusive device and may be a better classification of the technique as a semi-field system. Uncertainties in the calculation of effective densities and settling velocities have been pointed out by Fettweis (2008): i) instrument inaccuracy, ii) imprecision of observations, and iii) the statistical nature of the variables (primary particle size, density, and floc size).

The methodology used in the present study is based on measurements and calibration of the LISST instrument. The current velocity measurements have been taken with an acoustic doppler velocimeter at a high frequency rate that allowed the calculation of turbulent fluctuations. Suspended sediment concentrations used for calibration are based on water samples. These instruments and techniques are widely used and their accuracy is well known. Therefore, derived floc properties of effective density and settling velocity are considered reliable. Nevertheless, based on the studies in the literature, the findings should be considered specific to the Welsh Channel and for the winter 2008 season.

7.1.2 Measurements

In order to understand the behaviour of cohesive sediments a range of measurements have to be taken to obtain at least current velocity, turbulent properties, volumetric and gravimetric concentration of suspended sediments, allowing the calculation of floc effective density and floc settling velocity. The development of non-intrusive instruments is needed for reliable measurements in the field. Three dimensional measurements would help to gain knowledge of the flocculation process throughout the water column. In particular, vertical profiles of grain size are much needed to study and confirm or reject the presence of larger flocs in upper parts of the water column than near the bottom, as has been shown by Fugate and Friedrichs (2003). This behaviour has been suggested as a result of the effect of the pycnocline on the optic response of the LISST (Styles, 2006). Also, horizontal coverage is important to study the advection of flocs to determine their origin, i.e. marine or saltmarsh. Sediment samples from the bed surface are needed to verify its composition and, if possible, its degree of consolidation which has influence on the resuspension (Dyer, 1986). The measurement techniques and devices are designed to avoid external disturbance, however, an assessment of these possible effects should be made. Long-term measurements over tidal to seasonal time scales are needed to investigate the changes in floc size. The biology factor is assumed negligible in the present study, although it seems to be important during spring and summer seasons (Todd, 2014). The measurements under laboratory-controlled conditions also give

an insight of the behaviour of the flocculation process. However, the experiments must include as many real variables as possible. Different settling velocities were obtained by van Leussen (1994) using artificial particles and natural sediments in laboratory experiments. Verney et al. (2011) were able to reproduce the hysteresis effect with the simulation of the tidal cycle of turbulent stresses. Even though laboratory results help to understand the floc behaviour, the differences with real conditions should be considered when the results are being compared against real conditions. In addition, complete and realistic observations would help to diminish the number of assumptions about floc behaviour.

The analyses in the present investigation are based on observations longer than a fortnightly period, which allowed coverage of three different hydrodynamic regimes, including the effect of waves, and the study of differences in floc behaviour between them. This is the basis of the proposed semi-empirical formulation for the floc settling velocity during the "current only" regime (Section 5.3.1). However, these results are based in the calibration fitting presented in figure 4.3 in which some assumptions have been made. The first issue is related to the measurements, mass concentrations were obtained from filtered water samples that not strictly were taken at the same height over the bottom. The second assumption and the most important is the linear regression between the two variables of volume and mass concentration, which means that their relationship throughout the measuring period remained without any change, meaning that the floc density was constant, at least during this calibration period, and independent of the floc size. It is probable that an error exists, but it would be difficult to estimate because there is no method to measure the floc effective density. Even when the field work is not always as planned, a better approach to diminish the error could be to take samples for calibration during neap tides when small changes in grain size are expected.

7.1.3 Numerical modelling

The next step after obtaining reliable measurements is how to represent floc size and their variability. One of the options is the fractal theory. Some aspects of this theory applied to flocs are discussed in section 5.4.2 and is an approximation to the complex structure that determines some floc properties such as density, permeability of the sea bed, yield strength and porosity (Kranenburg, 1994). Cohesive sediments have been also separated into macroflocs and microflocs, each with a different formulation to describe their relationship with corresponding settling velocities (Manning, 2008). Nevertheless, the observations do not always clearly present two populations, therefore the use of one formulation or the other becomes difficult. A description of floc size into four modes has also been suggested by Fettweis et al. (2012). In addition, the performance of a proposed formulation is needed to verify the correct reproduction of the observations and this

enable prediction. This aspect is not often taken into account and tests are carried out using short observation periods, sometimes of the order of 1 or 2 tidal cycles (e.g. Winterwerp, 2002; Baugh and Manning, 2007). This is due to costs and time limitations but the formulations are still been considered applicable to different conditions (e.g. Braithwaite et al., 2012). The implementation of a proposed formulation in a numerical model to predict floc behaviour is another important challenge. The formulation has to be easy to implement and suitable for different study areas. Some measurements are needed to calibrate and adjust the model, but this becomes difficult if the formulation has a number of free parameters. For example, the formulation of Winterwerp (1998) requires previous knowledge of grain size, effective density, fractal number and shape; this information is needed to obtain the settling velocities of the flocs. In addition, it also has 4 empirical calibration coefficients. In a modified version of the formulation of Winterwerp (1998), a variable fractal dimension is proposed with 7 empirical coefficients by Son and Hsu (2011). Calibration coefficients, time-limited and one-level observations make difficult the implementation of the formulations in three-dimensional models, which should be the aim for obtaining sediment transport predictions.

Floc and turbulent properties from observations in the Welsh Channel allowed a formulation to be proposed for settling velocity depending on one variable, turbulent stress, as a proxy of the changes in grain size. Therefore, the formulation can be easily implemented in the numerical model and depends on a variable also obtained with the numerical turbulence model. Results show that good approximations can be achieved but more information is needed to compare the three-dimensional model results with observations at different levels of the water column and longer time scales than the 7 days used for the "current only" regime. In addition, the root mean square error of the proposed formulation (3 mm·s−1, see figure 5.6) is high in comparison with the range of the settling velocities calculated from observations (0.25-1.5 mm·s−1). However, this is not surprising given the high scattering of settling velocity values from observations. Specifically, this means that the formulation is underestimating or overestimating the observations. The worst case occurs when turbulent stress is high because the calculated settling velocities showed the minimum scattering and the fitted curve is not throughout the points. Minima of turbulent stress coincided with the highest scattering of settling velocities and therefore, modelled values resulted in even settling velocities lower than the maxima of those calculated. The effect in model predictions is clearly seen in figure 5.7c, where minima are overestimated and maxima are underestimated.

7.2 Flood and ebb particle behaviour: hysteresis

The effect of hysteresis is present in the results of this study and seems to play an important role in the flocculation process. Observations of grain size show a wide scatter in the relationship with different turbulent variables. Two different populations

have been identified for flood and ebb phases but there is still a scatter of data that seems to be related to a hysteresis effect. Figure 7.1 shows two examples of this effect in the Welsh Channel during the period of this study. In figure 7.1a the tidal cycle shown corresponds to a neap tide and starts with the flood phase (red circle) at low energy conditions. The floc size diminishes as the energy increases until the system reaches maximum energy and have a minimum for median grain size. When the energy decreases, the floc size increases but with a small shift, with values slightly greater than those when the energy was increasing. The start of the ebb phase (blue circle) was recorded one hour later and the behaviour is similar. In figure 7.1c a spring tidal cycle is shown and the behaviour is the same as before except that the shift after the maximum during the ebb phase is in the opposite direction than for the neap tide case. The hysteresis effect has been identified by different authors (Dyer, 1986; Verney et al., 2011; Fettweis et al., 2012) and has been attributed to a time lag in the response of the floc size. This particular feature seems to add another variable to the flocculation process since the size of the flocs at the end of one phase is important for the beginning of the next phase, i.e., the effect of the turbulence will be different on flocs of slightly different sizes and also small changes in turbulence will have a different effect. These can be seen in consecutive tidal cycles, when hydrodynamic conditions are similar but the resulting floc distribution is different. This feature would need to be taken into account in particular for long-term studies when a high magnitude is expected due to the variability of the conditions.

In the Welsh Channel, the first characteristic of the behaviour of the floc size with respect to turbulent properties is their inverse relationship, the second feature is the shift between tidal phases and the third is the hysteresis phenomenon, which appears to be responsible for the wide scatter of observations during the same tidal phase. The difference in grain size observed during flood and ebb is maybe due to the origin of the sediments. During flood, sediments from the Liverpool Bay are expected to arrive at the Welsh channel. The fine part of these sediments maybe consits of large and strong flocs. Because the effect of the currents in deeper waters is not as strong as inside the shallow estuary, flocs have the time grow and consolidate if they reach the bottom. Unlike the flocs of the bay, flocs from the inner parts of the estuary are expected to be smaller and weaker. However, they also can reach larger sizes because they are more prone to aggregation due to more concentration and turbulence. Figures in section 6.3 show clearly two populations that react in the same way but with diferent magnitudes of energy.

7.3 Turbulent stress and turbulent kinetic energy

A good relationship between turbulent kinetic energy and median grain size was obtained in section 6.3.2. This is proposed as a better predictor of floc size instead of

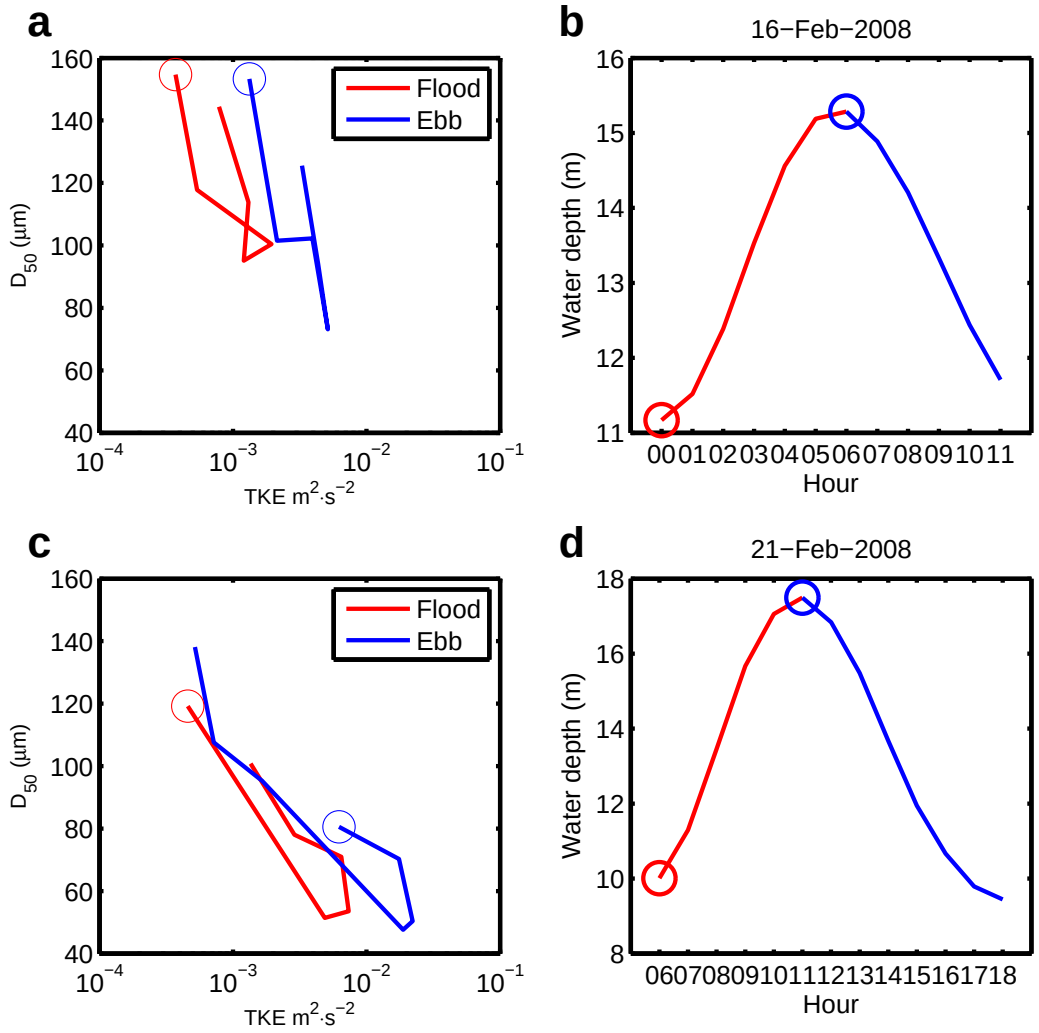

Figure 7.1: a) and c), examples of hysteresis effect between turbulent kinetic energy and median floc size in the Welsh Channel. b) and d) water depth corresponding to phases shown. In all plots, the circles mark the initial point in the respective flood and ebb phase.

more complicated formulations (e.g. Khelifa and Hill, 2006) or the widely used turbulent stress-floc size relationship (e.g. Winterwerp et al., 2006). Nevertheless, turbulent kinetic energy and turbulent stresses are often related as (Pope, 2000):

$$\tau = C_1 TKE \tag{7.1}$$

with C_1 obtained after a linear fit between τ and TKE and typically taking a value of 0.19. Using the results obtained for these variables in this study, it is possible to evaluate this relationship. Figure 7.2 shows the values obtained using the entire set of data and for the three regimes independently. The best results are obtained for the "current only" case, with a value of 0.2 for the constant C_1 (Fig. 7.2b). A value of 0.16 was found for the "combined currents-waves" regime (Fig. 7.2c) and for the entire data set (Fig. 7.2a), although with highest determination coefficient for the "currents-waves" case. Results indicate a poor relationship when waves are the dominant factor (Fig. 7.2d), with a determination coefficient of 0.42. This illustrates an increasing effect of the waves as they become dominant during the study period. Besides the low values of turbulent kinetic energy during flood phase, already seen in chapter 6, no other significant feature is seen in these relationships.

The value of 0.2 for the "current only" case is in the range reported by other authors (Soulsby, 1983; Kim et al., 2000; Verney et al., 2006; Souza and Lane, 2013). Lower values can also be obtained (Gordon and Dohne, 1973) and could be due to surface-wave motion (Soulsby, 1983), which may be the case of the present study with C_1 decreasing until reaching the lowest value when the waves are dominant. High values of turbulent stresses calculated using the proportionality relation of equation 7.1 were obtained by Verney et al. (2006), which coincided with waves generated by barges and vessels in the Seine Estuary. Based on figure 7.2b and 7.2c for the Dee Estuary, the proportionality relation is adequate in conditions of "current only" and "combined currents and waves", considering a lower value of C_1 in this latter case, but fails profoundly in the regime when waves are dominant. This has implications for calculating the turbulent stresses when waves are the dominant forcing and it is possible to quantify the different turbulent stress contributions with the method explained in section 4.1.2. A method to obtain the turbulent kinetic energy by Soulsby and Humphery (1990) is based on splitting the velocity spectrum to obtain the variances of both turbulent fluctuations and waves. Thus, the equation for the turbulent kinetic energy is also used ($TKE = 0.5(\overline{u'^2} + \overline{v'^2} + \overline{w'^2})$). This method has been successfully used by different authors (Stapleton and Huntley, 1995; Williams et al., 1999; Verney et al., 2007).

However, the advantage of the high sampling rate of the ADVs is that turbulent fluctuations can be obtained almost directly from the observations and avoid extra calculations, and therefore sources of error due to turbulent stresses and turbulent kinetic energy are obtained separately. In addition, the most important result is that

the use of *TKE* seems to better represent the floc behaviour throughout the three regimes and may produce better predictions when implemented in a numerical model.

7.4 Asymmetries of turbulent dissipation

An important feature of the results of turbulent kinetic energy dissipation ϵ between flood and ebb phases is the strong asymmetry as shown in section 6.2.2. In figures 6.4c and 6.5c the differences between tidal phases are larger than in figure 6.6c when waves are the dominant forcing. This behaviour seems to be a consequence of the tidal asymmetry of the current velocity, although the strong differences in dissipation values are a striking characteristic. The logarithmic scale in the vertical axis of the aforementioned figures helps to show that actually there is a small variability in dissipation behaviour during ebb phases. In Figure 7.3 a linear version is plotted to show more clearly the differences between tidal phases. In all three regimes the dissipation rate is very low during the flood phase while during ebb the magnitude reaches almost 60 $\mathrm{W{\cdot}m^{-3}}$. The magnitude of ϵ increases from neap tides to the beginning of spring tides during the "current only" regime (Fig. 7.3a), reaches its maximum values during spring tides in the "combined currents-waves" regime (7.3b), and exhibits the lowest values when waves are dominant in the second neap tide period (Fig. 7.3c). Only during this latter regime are the differences between flood and ebb not as high as in the other regimes because of the low values during ebb. Higher turbulent dissipation during ebb than during flood was also found by Thurston (2009) in the Hilbre Channel of the Dee Estuary. The author found that dissipation during the ebb phase was higher than during flood for all measurements taken at 0.3, 0.6 and 0.9 metres above the sea bed. Strong dissipation asymmetries have also been found by Simpson et al. (2002) in Liverpool Bay, with values of approximately $1{\times}10^{-4}$ $\mathrm{W{\cdot}m^{-3}}$ during high water slack (after flood) and values of approx $1{\times}10^{-2}$ $\mathrm{W{\cdot}m^{-3}}$ at any other time of the tidal cycle. The observations of Simpson et al. (2002) were taken in a water column of 35 m depth and current velocities of approximately 0.1 $\mathrm{m{\cdot}s^{-1}}$ which explains the differences in dissipation magnitude in comparison with the results of this study.

According to the turbulence energy spectral analysis, most of the estimations of turbulent kinetic energy dissipation are valid, but also suggests that some data at the end of the ebb phase are doubtful. This is clear in the example of turbulent velocity spectrum in figure 4.9 at hours 18:00 and 19:00. This coincides with the lowest estimations of dissipation, as can be seen in figures 6.4-6.6. Unfortunately, there are no quantitative criteria to accept or reject these observations. For this investigation, low estimations of dissipation appear to be outside a valid range, and a value of 0.1 $\mathrm{W{\cdot}m^{-3}}$ is applied as a lower limit. Figure 7.4 shows the resulting Kolmogorov microscale, η, and shear parameter, G, distinguishing between calculations from ϵ above and below the lower limit value, points and open circles, respectively. It can be seen that the

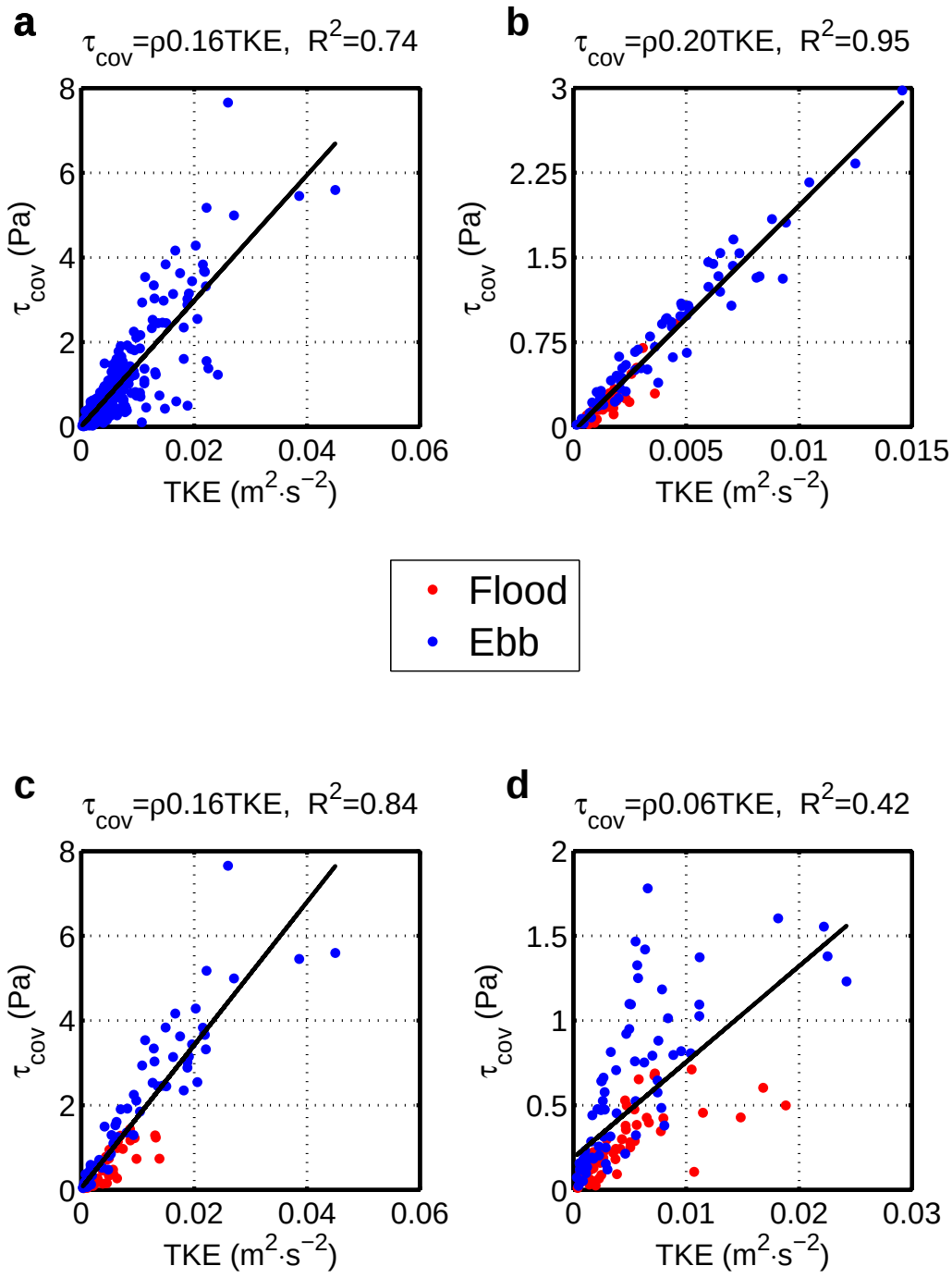

Figure 7.2: Turbulent kinetic energy and turbulent stresses from currents, calculated using equations 4.30 and 4.11 respectively, are related as $\tau_{cov}=\rho C_1 TKE$. a) Using the entire data set, b) "current only" regime, c) "combined currents-waves" regime and d) "wave dominant" regime. ρ=1025 kg·m^{-3}.

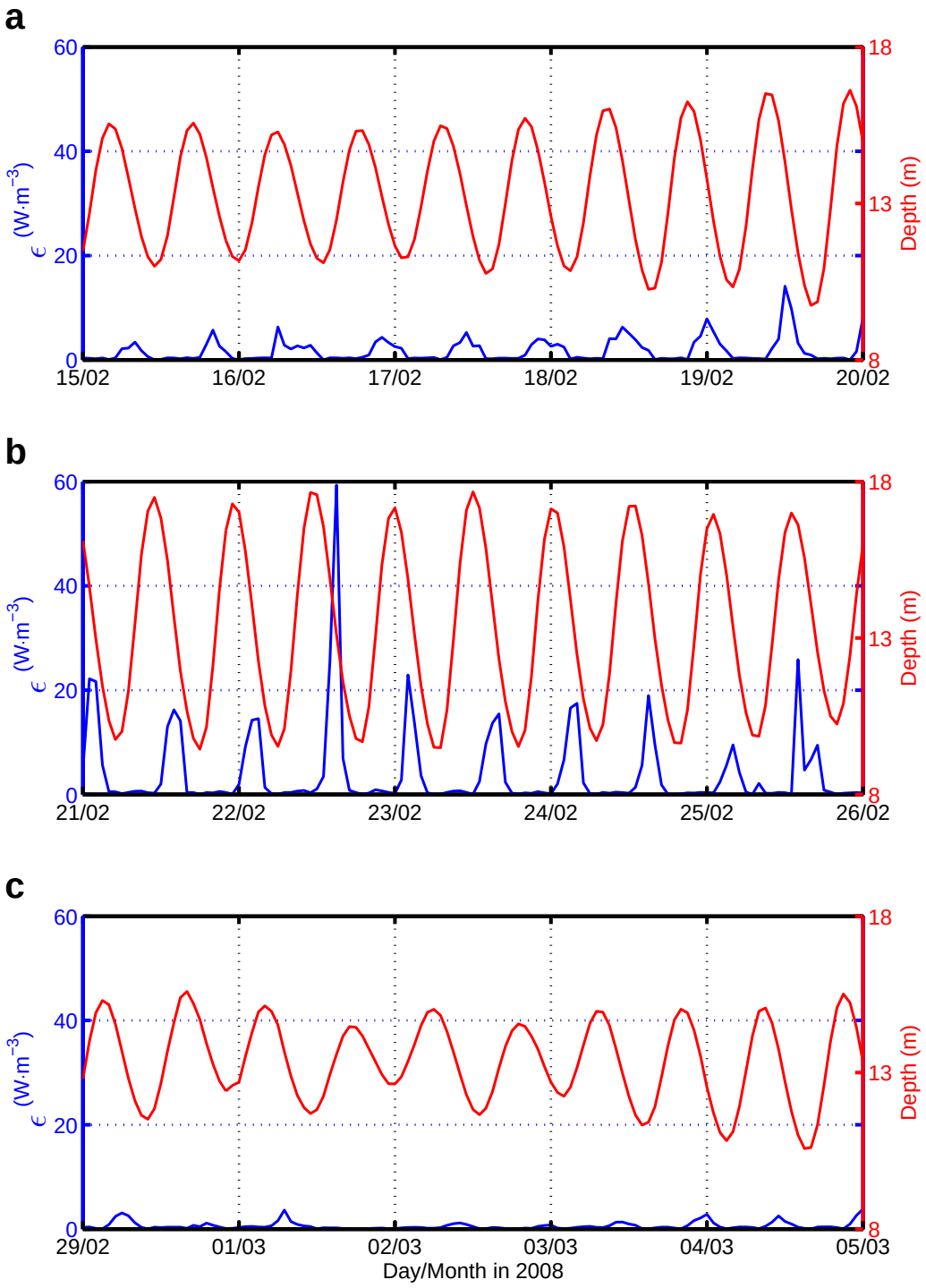

Figure 7.3: Dissipation ϵ and water depth for a) "current only" regime, b) "combined currents-waves" regime and c) "wave dominant" regime.

greater effect is in the flood phase, with greatest data scattering at high and low values of G and η, respectively, corresponding to dissipation values below the limit. The flood phase without these data exhibits now only one distribution but maintains its contrasting behaviour in comparison with the ebb phase. Even though some results for the ebb phase are below the dissipation limit, the behaviour remains unaffected. Also, the populations described by the "wave dominant" regime appears not to be affected. Therefore, the presence of two different populations during flood and ebb phases remains supported by these results.

The strong asymmetries in dissipation calculations appear not to be related to data validity. The magnitude of the difference in dissipation between flood and ebb phases seems to be due to higher moment calculations. Tidal currents are slightly stronger during the ebb than during the flood. The initial difference between flood and ebb is maybe due to velocity shear. The differences become greater when obtaining turbulent stresses, greater again in the calculation of turbulent kinetic energy, and the inequality reaches almost two orders of magnitude in the dissipation calculations during spring tides with the combination of effects of currents and waves.

7.5 Flocculation in the Dee Estuary

An interesting and remaining question is how the floc behaviour contributes to the sediment transport in the Dee Estuary. In particular, the Dee is accreting (e.g. Moore, 2009) and there is a general sediment transport pathway to the south-east corner of Liverpool Bay, due amongst other effects to baroclinicity (e.g. Souza and Lane, 2013). The importance of baroclinic effects is due to the freshwater supply to Liverpool Bay from the rivers Mersey, Dee and Ribble. Yet, fine sediment availability seems to be limited in the bay according to the sea bed sediment distribution (Fig. 3.3). Therefore, it is not clear whether the low river discharge from the Dee is enough to drive a similar behaviour in the Welsh Channel as in Liverpool Bay. Based on the observations of the present investigation, it is suggested that throughout the Welsh Channel the import and export of sediments is in equilibrium and an explanation of the possible mechanism is given below. A combination of flocculation and periodic stratification seem to be the main factors preventing a dominant sediment transport in the Welsh Channel. Since there is no information about what occurs in the water column regarding suspended sediments and flocculation, hereafter the conditions in the upper part of the water column are inferred.

A convenient start is the high water slack (HWS) because it presents the most stable and simple conditions of the tidal cycle. During this period the water column is mixed, with near zero turbulent stresses and negligible resuspension of sediments from the sea bed. The suspended sediment concentration (SPM) in the lower half of the water column consists mainly of fine sediments, and the aggregation and break-up of flocs

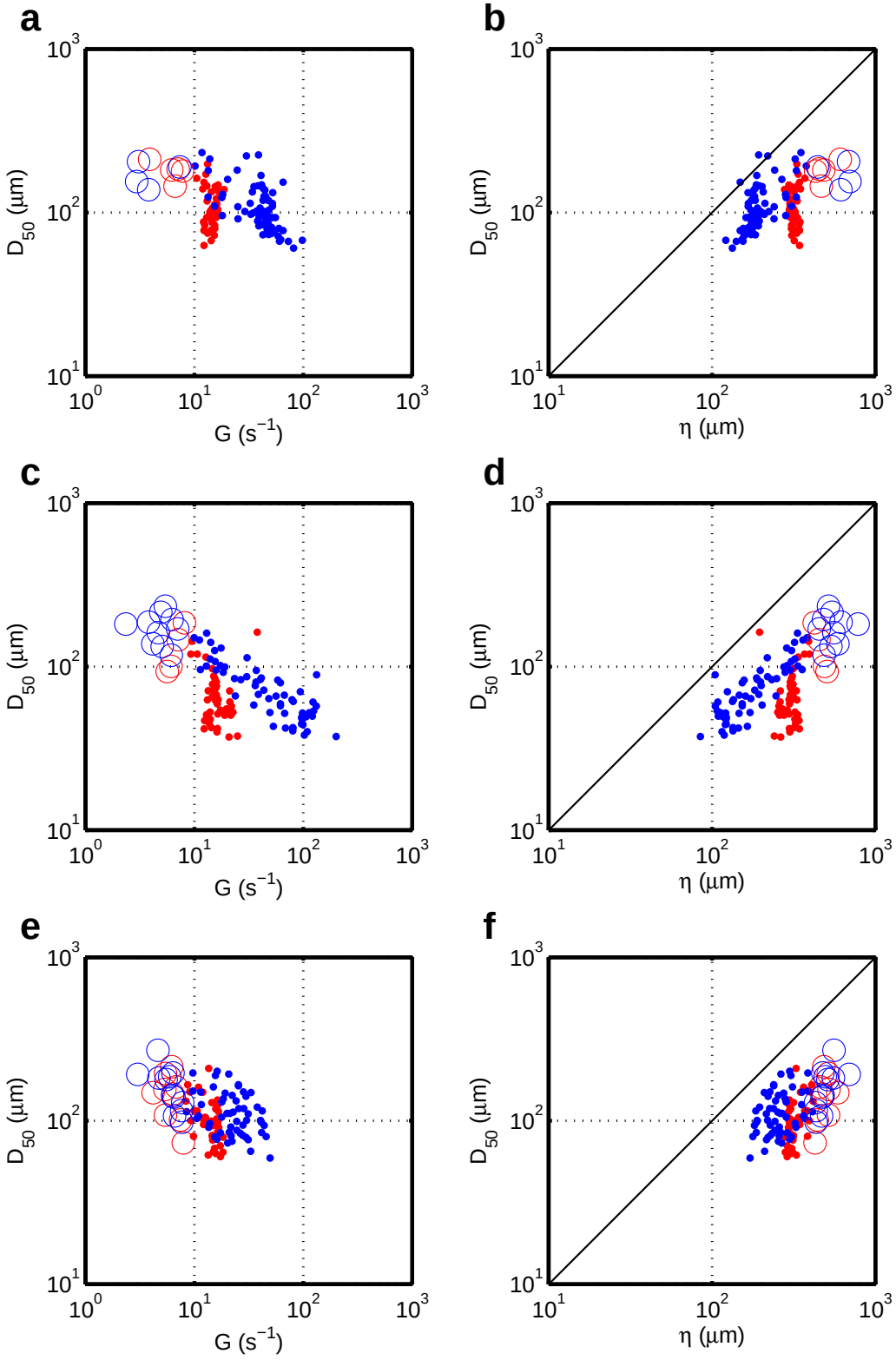

Figure 7.4: Turbulent shear rate G and Kolmogorov microscale η versus median grain size D_{50}. Points and open circles are results of $\epsilon \geq 0.1$ and $\epsilon < 0.1$ W·m^{-3}, respectively. Blue and red colors are ebb and flood data, respectively. a) and b): "current only" regime, c) and d) "combined waves-currents" regime, and e) and f) "wave dominant" regime.

are low. Although near the sea bed the SPM concentration is low, aggregation is still present, as has been seen in observations of this study. Under these HWS conditions, the upper part of the water column must have negligible SPM and therefore also negligible floc aggregation and break-up.

The ebb phase also presents mixed conditions, although dominant brackish water is flowing from the estuary with the highest turbulent stresses of the tidal cycle, with also the greatest resuspension of sediments from the sea bed. Under these conditions, flocs of different sizes are resuspended and subjected to considerable break-up while aggregation remains negligible. The SPM in the upper part of the water column likely consists also of small flocs in high concentrations. Aggregation probably remains low, unlike break-up which must affect flocs even at this height of the water column.

During low water slack (LWS) the stratification starts but its influence is not yet important. Turbulent stresses at LWS fall to negligible values, as well as the sediment resuspension. These low energy condition enhances the deposition of flocs near the sea bed and thus suspended flocs in the lower part of the water column consist of flocs that reached the upper part of the water column during the ebb phase. The low energy conditions near the bottom and sufficient floc concentrations enhance aggregation while the break-up remains negligible. The upper part of the water column is likely characterised by low SPM concentration with predominantly small flocs, aggregation is consequently low and break-up negligible.

The flood phase must be split into stratified and mixed portions. Although during the period of stratification the turbulent stresses are important, they are not as high as those during the ebb phase. Hence resuspension is low and consists of small flocs. Unlike LWS there is no floc contribution from upper parts of the water column because of either low concentrations at the previous phase or the stratification preventing flocs from settling. Under these moderate energy conditions the aggregation and break-up remain limited in the lower part of the water column, while the upper part is likely dominated by the more freshwater with low SPM concentration, fine flocs, low aggregation and negligible break-up effect. The second part of the flood phase presents mixed conditions and is the decelerating part of the current, with turbulent stresses decreasing. The characteristics of this part are similar to HWS, with low SPM concentration in the lower part of the water column and consisting of small flocs. The contribution from upper parts of the water column is also of small flocs but in low concentration because these are the flocs falling from the brackish water during the stratification period. Aggregation and break-up are low in the lower part of the water column while they are negligible in the upper part due to the low concentrations and turbulence. These last conditions are the same as those during HWS and the cycle starts again.

The above sequence is affected by the presence of waves. Although resuspension and flocculation is clear in the observations of this study during the “wave dominant”

regime (Fig. 6.2c), their magnitudes were not as high as during spring tides (Fig. 6.2b). However, events with higher waves with greater effects are possible. It is difficult to estimate a realistic net sediment transport with the present observations but a rough approximation is given by the tidal asymmetries. Todd (2014) used vertically-averaged current velocities for the Hilbre Channel, which is located at the north-east of the Dee Estuary mouth. The author used averages for the ebb and flood velocities and reported a difference of 0.1 $m{\cdot}s^{-1}$ with flood dominance. Using the near-bed ADV current observations of this study, a difference of about 0.02 $m{\cdot}s^{-1}$ is obtained for the Welsh Channel with ebb dominance. Although this is a rough approximation, it suggests that transport of sediment towards the estuary is in the Hilbre Channel. In addition, it is necessary to assess in the Welsh Channel other processes such as bed sediment characteristics which has been shown to be important for the Hilbre Channel (Amoudry et al., 2014).

Based on the results of this study, the sediment dynamics in the Welsh Channel during winter conditions appear to be dominated by: resuspension by turbulence, rapid settling of sediments because of flocculation during low slack water, and horizontal advection of fine sediments during flood due to longer time in the water column. In the presence of waves as the dominant forcing factor, aggregation and break-up of flocs seem to be in equilibrium.

7.6 Key findings

In the present investigation long term measurements have been used in order to study the factors that govern the flocculation process in a hypertidal estuary. The period of study allowed include floc size, concentration and turbulent properties from tidal phases to a fortnightly cycle. In addition, hydrodynamic regimes accounting for the effects of only current velocity, the combined effect of currents and waves and in wave dominant regime could also be analysed. The response of the flocculation to these regimes was clearly obtained as changes in floc size in relation with turbulence. Even though some long-term studies can be found in the literature, no clear relationship with the hydrodynamic regimes has been shown. The study by Bartholomä et al. (2009) reported only a few characteristics of the floc size during part of their measurements, although identified seasonal changes in floc size. Braithwaite et al. (2012) found a possible response of the grain size to the effects of a storm only during the last two days of their study and no clear relation during the previous seven days. Unlike the results of the present study, changes in floc size were not found by Fettweis et al. (2012) in measurements during storms. However, the authors identified the difference in floc behaviour between flood and ebb phases, but no further analysis was made. Although these differences together with the hysteresis effect have been recognized in earlier studies (e.g. Dyer, 1989), the effects have been only taken into account as a

time lag of the floc response to tidal forcing (e.g. Braithwaite et al., 2012. More recently, laboratory experiments which simulated the tidal oscillations also found these effects (Verney et al., 2011). The results of the present study show clear differences when observations are separated in tidal phases and explain part of the high scattering commonly found in observations. In addition, these differences still remain in high energetic periods with the combined forcing of waves and currents and only vanished if waves are the dominant effect.

The numerical modelling in the present study shows that a simple formulation for the floc behaviour can be implemented with reasonable results in reproducing the original observations. Probably the main advantage of the formulation is that only depends on one variable, which can be calculated from commonly measured current velocity and is also calculated in numerical models. In general, existing formulations need a previous knowledge of floc properties, require parameterisations and calibration of coefficients, see for example, table 1 in the study by Son and Hsu (2011). An issue with formulations trying to include many factors is the lack of knowledge of their temporal and spatial variability. Nevertheless, some formulations have been implemented in 3D numerical models (e.g. section 2.7), but need a proper comparison to assess their accuracy. The proposed formulation of this investigation has been made as a first approximation of the flocculation process. According to the results of chapter 6, the use of turbulent kinetic energy instead of turbulent stress would provide better simulations of floc behaviour. Moreover, further improvement should be achieved if the differences found for hydrodynamic regimes and tidal phases are included.

Chapter 8

Conclusions

In order advance knowledge in the understanding of the flocculation process in a hypertidal estuary, a set of observations of grain size, volume concentration, mass concentration and current velocities were used to obtain turbulent properties and study their relationships with the phenomenon of flocculation in the Dee Estuary. With the only exception of mass concentration, the variables were obtained from a mooring deployed at the Dee Estuary in the Welsh Channel. Mass concentration was obtained from water samples from a research vessel at the study site which allowed the calibration of volume concentration from the mooring site to mass concentration. There was no evidence of the effects of the mooring frame on the measurements. Observations should be only considered characteristic of the study period, February-March 2008.

The first characteristic of the observations was the presence of three different hydrodynamic regimes. The first case had waves of about 0.1 m height, therefore their influence on the sea bed is negligible and for this study is called the "current only" regime. The second regime coincided with spring tides and nearly 1.5 m height waves: "currents-waves" regime. The feature of the last case was the presence of the highest waves of the study period and happened during neap tides, and hence is called "wave dominant" regime. The first part of this chapter (Sections 8.1 and 8.2) is focused in the results of the "current only" regime while the next two sections (8.3 and 8.4) refer to all three regimes.

8.1 Turbulent stress from currents and flocculation

This part of the study covered the period from a neap tide to the beginning of spring tide between the days of 15-22 February in 2008. Near-bed current velocities exhibited quarter-diurnal variability with slight ebb dominance, with magnitudes reaching almost 0.3 $m \cdot s^{-1}$. Calculated turbulent stresses reached a maximum value of more than 5 Pa with also quarter-diurnal variability in phase with current velocity maxima. Strong asymmetries between maxima during flood and ebb phases were present, with differences increasing from almost 1 Pa during neap tides to 5 Pa during spring tides.

From the grain size distribution, high concentrations of flocs smaller than 100 μm were observed during maxima of turbulent stresses. Flocs of about 350 μm were present in high concentrations during low water slack. Large flocs were also present during high water slack but in low concentrations. Median grain size obtained from grain size measurements also showed quarter-diurnal variability, with maxima in phase with minima of turbulent stresses while grain size minima coincided with maxima of turbulent stresses. The median grain size range during neap tides was about 100-200 μm while for spring tides was diminished to 50-120 μm.

The observations showed the presence of flocculation during the "current only" regime. Highly energetic periods were characterised by the break-up of flocs, with high concentrations during the ebb and slightly lower concentrations during the flood as a result of asymmetries in turbulent stress maxima. Disaggregation of small flocs is also increased with the increase of turbulent stresses from neap to spring tides and results in the lower median grain size during the beginning of the spring tide. Conversely, floc aggregation happened during periods of low turbulent stresses. Even though floc aggregation is important during slack waters, the concentration of large flocs is higher during low water slack. The period of neap tide allowed aggregation of flocs resulting in the high median grain size range mentioned earlier. An hysteresis effect during flood and ebb phases seems to result in the wide scatter of observations. Periodic stratification after low water slack followed by a velocity shear in the Welsh Channel is considered the probable process responsible for the tidal asymmetries and, therefore, the floc behaviour.

8.2 Semi-empirical formulation for floc behaviour

Using observations of mass and volume concentrations, floc effective densities ρ_e were calculated and, in turn, used with median grain size data in the Stokes law to obtain floc settling velocities W_s for the observations between 15-22 February 2008. As expected, low effective densities and large settling velocities were obtained for large flocs while high effective densities and low settling velocities were calculated for small flocs. Effective densities range from about 60-66 $\mathrm{kg{\cdot}m^{-3}}$ while settling velocities reached more than 2 $\mathrm{mm{\cdot}s^{-1}}$. Maxima and minima of both ρ_e and W_s coincided with corresponding values of turbulent stresses. Large flocs with low ρ_e and high W_s were present during low energy periods, and vice versa for the high energy conditions. The neap to spring variability was also obtained for settling velocities and effective densities. Since the neap tide showed larger flocs than the spring tide, W_s was also higher during neap tides.

A semi-empirical relationship between turbulent stresses τ_{cov} and W_s for this period of observations was obtained with the form:

$$W_s = 0.25 + 0.89e^{-\tau_{cov}/0.19} \tag{8.1}$$

The formulation describes the floc behaviour taking into account that W_s is high (large flocs) when turbulent stresses are low while W_s diminishes (small flocs) as τ_{cov} increases. The important features of the formula are that it is mathematically and physically correct: (i) it cannot result in infinite values of W_s if τ_{cov} is near to or zero, which represents a growth limit for floc size and (ii) the minimum value of W_s is constant if τ_{cov} is too large, which also is a limit for the small floc size. An advantage of the proposed formulation is that only depends on one variable.

The formulation was implemented in the coupled hydrodynamic and turbulence numerical models POLCOMS-GOTM which include a sediment transport module. Quarter-diurnal and neap-spring variability of settling velocities and suspended sediment concentration is reproduced qualitatively by the model. The model reproduces W_s reasonably well during most of the period of the study but underestimates the maxima during neap tides. The suspended sediment concentration is underestimated during neap tides and overestimated during spring tides. Model results present a delay of about one hour which seems to be related with the modelled stratification.

In order to find the fractal number n_f for the flocs in the Dee Estuary, observations of mass and volume concentration, and median grain size were used in a linear relationship for different values of the fractal number. The fit with the highest R^2 value of 0.95 was found for n_f =2.4. However, different values of the fractal number in the range of 1-3 also showed high R^2 values. Unrealistic settling velocities were obtained using different values of fractal number.

Three different formulations to obtain settling velocities were tested to compare with the results of this study: (i) McCave (1984) based on a different way to calculate floc effective density; (ii) Winterwerp (1998) using fractal theory; and (iii) Khelifa and Hill (2006) using a variable fractal number. Results using formulations of McCave (1984) and Khelifa and Hill (2006) show low settling velocity variability which seems to be unrealistic. Results using the formulation of Winterwerp (1998) are in general agreement with the settling velocities calculated in this study, with differences in maxima (higher in this study).

8.3 Flocculation under the effects of currents and waves

For the purpose of comparison between the three hydrodynamic regimes, five days for each were selected as the most representative: 15-20 February for "current only", 21-26 February for "combined curents-waves" and 29 February to 5 March for the "wave dominant" regimes. Turbulent stresses from currents and waves were calculated separately to see their independent contribution to the forcing. The first regime showed negligible

values of turbulent stresses from waves τ_w of about 0.02 Pa while from currents τ_c the values reach more than 0.16 Pa and a maximum of nearly 0.4 Pa. An increase in magnitude during the second regime was found with similar values from both currents and waves of about 0.5 Pa. During the "wave dominant" regime, τ_w exceeded τ_c by a factor of four, reaching almost 2.5 Pa during the period of highest waves while turbulent stresses from currents remained in general lower than 0.5 Pa.

During the "combined currents-waves" regime, the quarter-diurnal variability of turbulent stresses and median grain size mentioned for the "current only" case in section 8.1 is still present because of the tidal modulation of waves. The increase in turbulent stresses in the second regime resulted in an increase in resuspension and floc disaggregation, with greater resuspension and break-up during peak ebb. The smallest floc sizes of the entire study period were found during this regime, with values of about 40 μm. Floc aggregation during slack waters was higher after ebb than after flood. As expected, the flocculation process during the third regime was due to waves. During this "wave dominant" regime, the quarter-diurnal modulation was lost and the variability was related to the wave turbulent stresses. An important result was the low median grain size variability even though the concentration was significant. During the period of highest τ_w, the values of D_{50} range between 60-90 μm. This suggests a nearly "steady state" of the flocculation process due to floc aggregation in a level of low turbulent stress in the water column and the now large flocs fall to regions of higher turbulent stress where they are disaggregated again.

8.4 Flocs and turbulent properties

Turbulent variables were also calculated for the three regimes in order to study their relationships with floc behaviour and to seek for a better descriptor of the changes in floc sizes through the processes of aggregation and break-up. Turbulent kinetic energy *TKE* and dissipation rate ϵ presented quarter-diurnal variability and asymmetries between flood and ebb, with the latter the dominant magnitude, for the "current only" and "currents-waves" regimes. Differences of *TKE* between flood and ebb were higher during the "current only" regime than during "combined currents-waves" regime. For these two regimes, differences of ϵ between flood and ebb were about four orders of magnitude as a consequence of very low minima occurring mostly during low slack waters. The behaviour of *TKE* during the "wave dominant" regime was strongly in phase with turbulent stresses from waves, with maxima coinciding with those of τ_{max}. In the "wave dominant" regime, ϵ presented quarter-diurnal behaviour as expected because the energy from waves is not included in the calculation of dissipation. Asymmetries were also present but with less variability than previous regimes.

Dissipation rate ϵ was used to obtain the Kolmogorov microscale of turbulence η and the shear rate G. Relationships between τ_{cov}, *TKE*, η and G with median grain size D_{50}

were analysed separating into regimes and the flood and ebb phases. In general inverse relationships were found. These were clear in scatter plots of TKE and τ_{cov} against D_{50} with higher data scatter in the case of τ_{cov}. Flood and ebb followed the same behaviour but were clearly distinguished with a shift that diminished throughout regimes. The best relationship was found between TKE and D_{50}, suggesting the possibility to describe floc size changes based on turbulent kinetic energy rather than turbulent stresses with the use of a simple power formulation of the form:

$$D_{50} = A(TKE)^B \tag{8.2}$$

The use of TKE also avoids the use of the formulation $\tau{=}\rho 0.2(TKE)$, which is sensitive to the presence of waves, at least for purposes like in the present study.

Relationships between η and G with median grain size showed two different behaviours related with flood and ebb phases. In general, median grain size was smaller than the Kolmogorov microscale. During the ebb, η had an inverse relationship with D_{50} while the flood was characterised by low variability in η with changes in floc size in the range of changes during ebb. For the shear rate and median grain size, the expected inverse relationship was found during ebb while a similar behaviour to that for η was obtained during flood. These results suggested a flocculation process present in ebb phases and changes in floc size during flood are due to other processes, which is inconsistent with results of τ_{cov} and TKE, or it was not possible to observe flocculation using η and G during flood phase.

Since η and G depend on dissipation rate, analyses of the different assumptions to obtain ϵ were carried out. No unequivocal evidence to invalid results was found, with the exception of the minima of ϵ occurring mostly at low slack waters. None of the behaviours described for η and G change after identifying possibly erroneous data.

8.5 Future work

Spatial and temporal coverage of measurements of grain size are needed to improve our knowledge of the flocculation process. Observations at different sites of the Dee Estuary will help to characterise the dynamics of the fine sediments and identify the possible changes in beaviour along the estuary and also confirm the presence of a lateral shear in the Welsh Channel, which could have implications for the transport of flocs. Although the strong variability takes place near the bottom, there is evidence that important processes are happening in upper parts of the water column. Therefore, measurements of grain size are needed throughout the water column. Instruments like the LISST are able to achieve this goal through profiling from a vessel but assesment of the possible effects of the pycnocline should be taken into account. Data from the water column is necessary for comparison with numerical model results. Temporal resolution

is needed to study the changes in floc behaviour during a tidal phase and the hysteresis effect which results in the scattering of data. The proposed formulation of grain size depending on turbulent kinetic energy should be implemented in the numerical model to confirm the improvements in predictions even in the presence of waves.

Bibliography

Agrawal, Y., Pottsmit, H. 2000. Instruments for particle size and settling velocity observations in sediment transport, *Marine Geology*, 168:89–114.

Agrawal, Y., Traykovsky, P. 2001. Particles in the bottom boundary layer: Concentration and size dynamics through events, *J. Geophys. Res.*, 106(C5):9533–9542.

Ahn, J. 2012. Size distribution and settling velocities of suspended particles in a tidal embayment, *Water Research*, 46:3219–3228, doi:10.1016/j.watres.2012.03.038.

Al-Ani, S., Dyer, K., Huntley, D. 1991. Measurement of the influence of salinity on floc density and strength, *Geo-Marine letters*, 11(3-4):154–158.

Álvarez, L. G. 2010. Bottom boundary layer properties in the Upper Gulf of California derived from velocity profiles, *Ciencias Marinas*, 36:285–299.

Amoudry, L. O., Bell, P. S., Thorne, P. D., Souza, A. J. 2013. Toward representing wave-induced sediment suspension over sand ripples in rans models, *J. Geophys. Res.*, 118(5):2378–2392.

Amoudry, L. O., Ramírez-Mendoza, R., Souza, A. J., Brown, J. M. 2014. Modelling-based assessment of suspended sediment dynamics in a hypertidal estuarine channel, *Ocean Dynamics*, 64:707–722, dOI 10.1007/s10236-014-0695-8.

Amoudry, L. O., Souza, A. J. 2011a. Deterministic coastal morphological and sediment transport modeling: A review and discussion, *Rev. Geophys.*, 49:1–21, rG2002, doi:10.1029/2010RG000341.

Amoudry, L. O., Souza, A. J. 2011b. Impact of sediment induced stratification and turbulence closures on sediment transport and morphological modelling, *Continental Shelf Research*, 31:912–928.

Arakawa, A. 1972. *Design of the UCLA general circulation model*, Tech. rep., University of California, Los Angeles.

Archer, A. 2013. World's highest tides: Hypertidal coastal systems in North America, South America and Europe, *Sedimentary Geology*, 284-285:1–25, doi:10.1016/j.sedgeo.2012.12.007.

Arkema, K., Guannel, G., Verutes, G., Wood, S., Guerry, A., Ruckelshaus, M., Kareiva, P., Lacayo, M., Silver, J. 2013. Coastal habitats shield people and property from sea-level rise and storms, *Nature Climate Change*, 3:913–918, dOI:10.1038/nclimate1944.

Badewien, T. H., Zimmer, E., Bartholomä, A., Reuter, R. 2009. Towards continuous long-term measurements of suspended particulate matter (SPM) in turbid coastal waters, *Ocean Dynamics*, 59:227–238.

Barne, J., Robson, C., Kaznowska, J., Doody, J., Davidson, N. 1996. *Coasts and seas of the United Kingdom, Region 13*, Joint Nature Conservation comitee.

Bartholomä, A., Kubicki, A., Badewien, T. H., Flemming, B. W. 2009. Suspended sediment transport in the German Wadden Sea—seasonal variations and extreme events, *Ocean Dynamics*, 59:213–225.

Baugh, J. V., Manning, A. J. 2007. An assesment of a new settling velocity parameterisation for cohesive sediment transport modeling, *Continental Shelf Research*, 27:1835–1855.

Benfield, M., Grosjean, P., Culverhouse, P., Irigoien, X., Sieracki, M., Lopez-Urrutia, A., Dam, H., Hu, Q., Davis, C., Hansen, A., Pilskaln, C., Riseman, E., Schultz, H., Utgoff, P., Gorsky, G. 2007. RAPID: Research on Automated Plankton Identification, *Oceanography*, 20:172–187.

BGS. 1996. *British Geological Survey. Coasts and seas of the United Kingdom. Region 13 Northern Irish Sea: Colwyn Bay to Stranraer, including the Isle of Man*, chap. 2.2 Offshore geology, pages 24–28, Peterborough, Joint Nature Conservation Committe.

Bolaños, R., Amoudry, L. O., Doyle, K. 2011. Tides effects of instrumental bottom tripods on process measurements, *Journal of Athmospheric and Ocean Technology*, 28:827–837.

Bolaños, R., Brown, J. M., Amoudry, L. O., Souza, A. J. 2013. Tidal, Riverine and Wind Influences on the Circulation of a Macrotidal Estuary, *Journal of Physical Oceanography*, 43:29–50, dOI: 10.1175/JPO-D-11-0156.1.

Bolaños, R., Moate, B., Souza, A. J. 2009. Measuring suspended sediment and its wave and turbulence forcing in the dee estuary, in Mizuguchi, M., Sato, S., eds., *Coastal Dynamics 2009: Impacts of human activities on dynamic coastal processes, Japan. World Scientific*, vol. 43, page 12, paper 119.

Bolaños, R., Souza, A. J. 2010. Measuring hydrodynamics and sediment transport processes in the Dee Estuary, *Earth Syst. Sci. Data*, 2:157–165.

Bowers, D. G. 2003. A simple turbulent energy-based model of fine suspended sediments in the Irish Sea, *Continental Shelf Research*, 23:1495–1505.

Braithwaite, K., Bowers, D., Nimmo-Smith, W., Graham, G. 2012. Controls on floc growth in an energetic tidal channel, *J. Geophys. Res.*, 117:1–12, doi:10.1029/2011JC007094.

Brown, J., Amoudry, L., Souza, A., Rees, J. 2013. *Particle tracking study in the Mersey Estuary*, Research and Consultancy Report 40, National Oceanography Centre.

Brown, J. M., Bolaños, R., Souza, A. J. 2014. Process contribution to the time-varying residual circulation in tidally dominated estuarine environments, *Estuaries and Coasts*, 0:0–0, dOI 10.1007/s12237-013-9745-6.

Brown, J. M., Souza, A. J., Wolf, J. 2010. An 11-year validation of wave-surge modelling in the Irish Sea, using a nested POLCOMS-WAM modelling system, *Ocean Modelling*, 33:118–128, doi:10.1016/j.ocemod.2009.12.006.

Burchard, H., Föser, G., Staneva, J. V., Badewien, T. H., Riethmüller, R. 2008. Impact of Density Gradients on Net Sediment Transport into the Wadden Sea, *Journal of Physical Oceanography*, 38:566–587, dOI: 10.1175/2007JPO3796.1.

Burchard, H., Hetland, R. D. 2010. Quantifying the contributions of tidal straining and gravitacional circulation to residual circulation in periodically stratified tidal estuaries, *Journal of Physical Oceanography*, 40:1243–1262, dOI: 10.1175/2010JPO4270.1.

Cahoon, D., Hensel, P., Spencer, T., Reed, D., McKee, K., Saintila, N. 2006. 12 coastal wetland vulnerability to relative sea-level rise: Wetland elevation trends and process control, in Verhoeven, J., Beltman, B., Bobbink, R., Whigham, D., eds., *Wetlands and Natural Resource Management*, vol. 19 of *Ecological Studies*, pages 271–292, Springer-Verlag Berlin Heidelbe.

Cohen, J., Small, C., Mellinger, A., Gallup, J., Sachs, J. 1997. Estimates of coastal populations, *Science*, 278:1211–1212.

Cross, J., Nimmo-Smith, W., Torres, R., Hosegood, P. 2013. Biological controls on resuspension and the relationship between particle size and the kolmogorov length scale in a shallow coastal sea, *Marine Geology*, 343:29–38.

Dagg, M., Benner, R., Lohrenz, S., Lawrence, D. 2004. Transformation of dissolved and particulate materials on continental shelves influenced by large rivers: plume processes, *Continental Shelf Research*, 24:833–858.

Davidson, N., Buck, A. 1997. *An inventory of UK estuaries. Volume 1. Introduction and methodology*, Peterborough, Joint Nature Conservation Committee.

Davies, E., Nimmo-Smith, W., Agrawal, Y., Souza, A. 2011. Scattering signatures of suspended particles: an integrated system for combining digital holography and laser difraction, *Optics Express*, 19(25):25489–25499.

Davies, E., Nimmo-Smith, W., Agrawal, Y., Souza, A. 2012. Lisst 100 response to large particles, *Marine Geology*, 307-310:117–122, doi:10.1016/j.margeo.2012.03.006.

Davies, J. 1964. A morphogenic approach to world shorelines, *Zeitschrift der Geomorphologie*, 8:127–142.

Ditschke, D., Markofsky, M. 2008. A time-dependent flocculation model, in *Sediments and Ecohydraulics: INTERCOH 2005*.

Dyer, K., Manning, A. 1999. Observation of the size, settling velocity and effective density of flocs, and their fractal dimensions, *Journal of Sea Research*, 41:87–95.

Dyer, K. R. 1986. *Coastal and Estuarine Sediment Dynamics*, John Wiley & Sons, pp 342.

Dyer, K. R. 1989. Sediment processes in estuaries: future research requirements, *J. Geophys. Res.*, 94(C10):14327–14339.

Eisma, D., Bale, A., Dearnaley, M., Fennessy, M., van Leussen, W., Maldiney, M., Pfeiffer, A., Wells, J. 1996. Intercomparison of *in situ* suspended matter (floc) size measurements, *Journal of Sea Research*, 36(1/2).

Ellis, K. M., Bowers, D. G., Jones, S. E. 2004. A study of the temporal variability in particle size in a high-energy regime, *Estuarine, Coastal and Shelf Science*, 61:311–315.

Evans, G., Prego, R. 2003. Rias, estuaries and incised valleys: is a ria an estuary?, *Marine Geology*, 196(3-4):171–175.

Fairbanks, R. 1989. A 17,000-year glacio-eustatic sea level record: influence of glacial melting rates on the younger dryas event and deep-ocean circulation, *Nature*, 342:637–642.

Fennesy, M. J., Dyer, K. R., Hunley, D. A. 1994. Inssev: An instrument to measure the size and settling velocity of flocs in situ, *Marine Geology*, 117:107–117.

Fenton, J., McKee, W. 1990. On calculating the lengths of water waves, *Coastal Engineering*, 14:499–513.

Fettweis, M. 2008. Uncertainty of excess density and settling velocity of mud flocs derived from in situ measurements, *Estuarine, Coastal and Shelf Science*, 78:426–436, doi:10.1016/j.ecss.2008.01.007.

Fettweis, M., Baeye, M., Lee, B., Chen, P., Yu, J. 2012. Hydro-meteorological influences and multimodal suspended particle size distributions in the belgian nearshore area (southern north sea), *Geo-Marine letters*, 32:123–137, dOI 10.1007/s00367-011-0266-7.

Fettweis, M., Francken, F., Pison, V., Van den Eynde, D. 2006. Suspended particulate mater dynamics and aggregate sizes in a high turbitidy area, *Marine Geology*, 235:63–74.

Flesch, J. C., Spicer, P. T., Pratsinis, S. E. 1999. Laminar and turbulent shear-induced flocculation of fractal aggregates, *AIChE Journal*, 45(5):1114–1124.

Fredsøe, J., Deigaard, R. 1992. *Mechanics of coastal sediment transport*, vol. 3 of *Advanced Series on Ocean engineering*, World Scientific.

Fugate, D., Friedrichs, C. 2002. Determining concentration and fall velocity of estuarine particle populations using adv, obs and lisst, *Continental Shelf Research*, 22:1867–1886.

Fugate, D., Friedrichs, C. 2003. Controls on suspended aggregate size in partially mixed estuaries, *Estuarine, Coastal and Shelf Science*, 58:389–404.

Geertz, L., Maris, T., Meire, P. 2012. *An interestuarine comparison for ecology in TIDE - The Scheldt, Elbe, Humber and Weser*, Study in the framework of the interreg ivb project tide, University of Antwerp. Ecosystem Management Research Group, Antwerp, Belgium, 89 pages.

Gibbs, R. J. 1985. Estuarine Flocs: Their Size, Settling Velocity and Density, *J. Geophys. Res.*, 90(C2):3249–3251.

Giddings, S. N., Fong, D. A., Monismith, S. G. 2011. Role of straining and advection in the intratidal evolution of stratification, vertical mixing, and longitudinal dispersion of a shallow, macrotidal, salt wedge estuary, *J. Geophys. Res.*, 116:1–20, doi:10.1029/2010JC006482.

Gordon, C., Dohne, C. 1973. Some observations of turbulent flow in a tidal estuary, *J. Geophys. Res.*, 78(12):1971–1978.

Gordon, L., Lohrmann, A. 2001. Near-shore doppler current meter wave spectra, in Edge, B., Hemsley, J., eds., *Ocean wave measurement and analysis*, Fourth International Symposium on Ocean Wave Measurement and Analysis, pages 33–43, ASCE, doi: 10.1061/40604(273)4.

Goring, D., Nikora, V. 2002. Despiking acoustic doppler velocimeter data, *Journal of Hydraulic Engineering*, 128(1):117–126, 10.1061/(ASCE)0733-9429(2002)128:1(117).

Graham, G. W., Nimmo-Smith, A. M. 2010. The application of holography to the analysis of size and settling velocity of suspended cohesive sediments, *Limnol. Oceanogr.: Methods*, 8:1–15.

Grasmeijer, B., Chu, A., van Rijn, L. 2011. Application and comparison of two different fine cohesive sediment transport models in DELFT3D, in Wang, P., Rosati, J., Roberts, T., eds., *The Proceedings of the Coastal Sediments 2011*, vol. 1, pages 1741–1754, WorldScienific.

Green, M. 1992. Spectral estimates of bed shear stress at subcritical reynolds numbers in a tidal boundary layer, *Journal of Physical Oceanography*, 22:903–917.

Halliwell, A. 1973. Residual drift near the sea bed in Liverpool Bay: an observational study, *Geophys. J. R. astr. Soc.*, 32:439–458.

Hansen, D., Rattray, J. 1966. New dimensions in estuary classification, *Limnology and Oceanography*, XI(3):319–326.

Hay, A. E., Sheng, J. 1992. Vertical profiles of suspended sand concentration and size from multifrequency acoustic backscatter, *J. Geophys. Res.*, 97(C10):15661–15677.

He, Q., Tang, J., Cheng, J. 2008. A study of *in situ* floc size in turbidity maximum, Yangtse Estuary, China, in *Sediments and Ecohydraulics: INTERCOH 2005*.

Hinrichsen, D. 1998. *Coastal waters of the world: trends, threats, and strategies*, Washington, D.C. : Island Press, c1998., 276 pages.

Holden, V., Worsley, A., Booth, C., Lymbery, G. 2011. Characterisation and sediment-sourde linkages of intertidal sediment of the UK's north Sefton coast using magnetic and textural properties: findings and limitations, *Ocean Dynamics*, 61(12):2157–2179.

Holmes, R., Tappin, D. 2005. *DTI Strategic Environmental Assessment Area 6, Irish Sea, seabed and surficial geology and processes.*, Commissioned report, cr/05/057, British Geological Survey.

Holt, J. T., James, I. D. 2001. An s coordinate density evolving model of the northwest European continental shelf 1, model description and density structure, *J. Geophys. Res.*, 160(C7):14015–14034.

Howlett, E., Rippeth, T., Howarth, J. 2011. Processes contributing to the evolution and destruction of stratification in the Liverpool Bay ROFI, *Ocean Dynamics*, 61(9):1403–1419, dOI 10.1007/s10236-011-0402-y.

Huntley, D. 1988. A modified inertial dissipation method for estimating seabed stresses at low Reynolds numbers, with application to wave/current boundary layer measurements, *Journal of Physical Oceanography*, 18:339–346.

Huntley, D., Leeks, G., Walling, D., eds. 2001. *Land-Ocean Interaction*, IWA Publishing.

Jago, C. F., Jones, S. E., Sykes, P., Rippeth, T. 2006. Temporal variation of suspended particulate matter and turbulence in a high energy, tide-stirred, coastal sea: Relative contributions of resuspension and disaggregation, *Continental Shelf Research*, 26:2019–2028.

Jago, C. F., Kennaway, G. M., Novarino, G., Jones, S. E. 2007. Size and settling velocity of suspended flocs during a *Phaeocystis* bloom in the tidally stirred Irish Sea, NW European shelf, *Marine Ecology Progress Series*, 345:51–62.

Jay, D. A., Musiak, D. 1994. Particle trapping in estuarine tidal flows, *J. Geophys. Res.*, 99:20445–20461.

Jones, S. E., Jago, C. F., Bale, A. J., Chapman, D., Howland, R. J. M., Jackson, J. 1998. Aggregation and resuspension of suspended particulate matter at a seasonally stratified site in the southern North sea: physical and biologic controls, *Continental Shelf Research*, 18(11):1283–1309.

Kaiser, M., Attrill, M., Jennings, S., Thomas, D., Barnes, D., Brierley, A., Geert-Hiddink, J., Kaartocallio, H., Polunin, N., Raffaelli, D. 2011. *Marine Ecology*, 2nd edn., Oxford University Press.

Khelifa, A., Hill, P. S. 2006. Models for effective density and settling velocity of flocs, *Journal of Hydraulic Research*, 44(3):390–401.

Kim, S., Friedrichs, C., Maa, J., Wright, L. 2000. Estimating bottom stress in tidal boundary layer from acoustic doppler velocimeter data, *Journal of Hydraulic Engineering*, 126(6):399–406.

Kombiadou, K., Krestenitis, N. Y. 2012. Fine sediment transport model for river influenced microtidal shelf seas with application to the thermaikos gulf, *Continental Shelf Research*, 36:41–62.

Kranenburg, C. 1994. The fractal structure of cohesive aggregates, *Estuarine, Coastal and Shelf Science*, 39:451–460.

Krivtsov, V., Howarth, M. J., Jones, S. E., Souza, A. J., Jago, C. F. 2008. Monitoring and modelling of the irish sea and liverpool bay: An overview and spm case study, *Ecological Modelling*, 212:37–52.

Krone, R. 1962. Flume studies of the transport of sediment in estuarial shoaling processes, Final Report Hydraulic Engineering Laboratory and Sanitary, Engineering Research Laboratory, university of California, Berkeley, USA.

Larsen, L. G., Harvey, J. W., Crimaldi, P. 2009. Morphologic and transport properties of natural organic floc, *Water Resources Research*, 45:1–13.

Lee, B., Toorman, E., Fettweis, M. 2014. Multimodal particle size distributions of fine-grained sediments: mathematical modeling and field investigation, *Ocean Dynamics*, 64:429–441, dOI 10.1007/s10236-014-0692-y.

van Leussen, W. 1988. Aggregation of particles, settling velocity and mud flocs: A review, in Dronkers, J., van Leussen, W., eds., *Physical Processes in Estuaries*, page 560, Springer-Verlag.

van Leussen, W. 1994. *Estuarine macroflocs and their role in fine-grained sediment transport*, Ph.D. thesis, University of Utrecht, The Netherlands.

van Leussen, W. 2011. Macroflocs, fine-grained sediment transports, and their longitudinal variations in the Ems Estuary, *Ocean Dynamics*, 61:387–401, dOI 10.1007/s10236-011-0384-9.

MacDonald, I., Vincent, C., Thorne, P., Moate, B. 2013. Acoustic scattering from a suspension of flocculated sediments, *J. Geophys. Res.*, 118:2581–2594.

Madsen, O. 1994. Spectral wave-current bottom boundary layer flows, in Edge, B., ed., *Proceedings of the 24th International Conference on Coastal Engineering*, pages 384–398, ASCE, Kobe, Japan.

Maerz, J., Verney, R., Wirtz, K., Feudel, U. 2011. Modeling flocculation processes: Intercomparison of a size class-based model and a distribution-based model, *Continental Shelf Research*, 31:S84–S93, doi:10.1016/j.csr.2010.05.011.

Maggi, F. 2005. *Flocculation dynamics of cohesive sediment*, Ph.D. thesis, Delft University of Technology.

Maggi, F. 2007. Variable fractal dimension: A major control for floc structure and flocculation kinematics of suspended cohesive sediment, *J. Geophys. Res.*, 112(C07012):1–12.

Maggi, F. 2009. Biological flocculation of suspended particles in nutrient-rich aqueous ecosystems, *Journal of Hydrology*, 376(1-2):116–125, doi:10.1016/j.jhydrol.2009.07.040.

Manning, A. 2008. The development of algorithms to parameterise the mass settling flux of flocculated estuarine sediments, in Kusuda, T., Yamanishi, H., Spearman, J., Gailani, J., eds., *Sediments and Ecohydraulics: INTERCOH 2005*, pages 193–210, Elsevier B.V.

Manning, A. 2012. *TR167-Enhanced UK Estuaries database: explanatory notes and metadata*, Tech. Rep. DDY0427-RT002-R02-00, HR Wallingford.

Manning, A., Baugh, J., Spearman, J., Whitehouse, R. 2010. Flocculation settling characteristics of mud: sand mixtures, *Ocean Dynamics*, 60:237–253.

Manning, A., Dyer, K. 1999. A laboratory examination of floc characteristics with regard to turbulent shearing, *Marine Geology*, 160:147–170.

Marker, M. 1967. The Dee estuary-its progressive silting and salt marsh development, *Trans. Inst. Br. Geogr.*, 41:65–71.

Markussen, T., Andersen, T. 2013. A simple method for calculating in situ floc settling velocities based on effective density functions, *Marine Geology*, 344:10–18.

McCave, I. N. 1984. Size spectra and aggregation of suspended particles in the deep ocean, *Deep Sea Research*, 31(4):329–352.

McKee, B., Aller, R., Allison, M., Bianchi, T., Kineke, G. 2004. Transport and transformation of dissolved and particulate materials on continental margins influenced by major rivers: benthic boundary layer and seabed processes, *Continental Shelf Research*, 24:899–926.

Mellor, G. 1991. an equation of state for numerical models of oceans and estuaries, *Journal of Athmospheric and Ocean Technology*, 8:609–611.

Metha, A. 1986. Characterization of cohesive sediment transport processes in estuaries, in Metha, A., ed., *Estuarine Cohesive Sediment Dynamics*, pages 290–325, Springer-Verlag, berlin.

Mietta, F., Chassagne, C., Verney, R., Winterwerp, J. 2011. On the behavior of mud floc size distribution: model calibration and model behavior, *Ocean Dynamics*, 61:257–271, dOI 10.1007/s10236-010-0330-2.

Mikkelsen, O. A., Hill, P., Milligan, T. 2006. Single-grain, microfloc and macrofloc volume variations observed with a lisst-100 and a digital floc camera, *Journal of Sea Research*, 55:87–102, doi:10.1016/j.seares.2005.09.003.

Mikkelsen, O. A., Hill, P., Milligan, T. 2007. Seasonal and spatial variation of floc size, settling velocity, and density on the inner Adriatic Shelf (Italy), *Continental Shelf Research*, 27:417–430, doi:10.1016/j.csr.2006.11.004.

Mikkelsen, O. A., Hill, P., Milligan, T., Chant, R. 2005. In situ particle size distributions and volume concentrations from a lisst-100 laser particle sizer and a digital floc camera, *Continental Shelf Research*, 25:1959–1978, doi:10.1016/j.csr.2005.07.001.

Mikkelsen, O. A., Pejrup, M. 2001. The use of a LISST-100 laser particle sizer for in situ estimates of floc size, density and settling velocity, *Geo-Marine letters*, 20:187–195.

Monismith, S., Burau, J., Stacey, M. 1996. *San Francisco Bay: the ecosystem*, chap. Stratification dynamics and gravitational circulationin northern San Francisco Bay, pages 123–155, American Association for the Advancement of Science.

Moore, R. 2009. *Hydrodynamic and morphometric modelling of a macro-tidal estuary: the Dee Estuary of NW England*, Ph.D. thesis, University of Liverpool.

Moore, R., Wolf, J., Souza, A., Flint, S. 2009. Morphological evolution of the dee estuary, eastern irish sea, uk: A tidal asymmetry approach, *Geomorphology*, 103:588–596, doi:10.1016/j.geomorph.2008.08.003.

Mori, N., Suzuki, T., Kakuno, S. 2007. Noise of acoustic doppler velocimeter data in bubbly flows, *Journal of Engineering Mechanics*, 133:122–125, doi:10.1061/(ASCE)0733-9399(2007)133:1(122).

Parker, W., Marshall, L., Parfitt, A. 1994. Modulation of dissolved oxygen levels in a hypertidal estuary by sediment resuspension, *Netherlands Journal of Aquatic Ecology*, 28(3-4).

Partheniades, E. 1965. Erosion and deposition of cohesive soils, *Journal of the Hydraulic Division*, 91.

Partheniades, E. 2009. *Cohesive Sediments in Open Channels: Properties, Transport and Aplications*, Butterworth-Heinemann/Elsevier.

Pedocchi, F., García, M. 2006. Evaluation of the lisst-st instrument for suspended particle size distribution and settling velocity measurements, *Continental Shelf Research*, 26:943–958, doi.org/10.1016/j.csr.2006.03.006.

Phelps, J., Polton, J., Souza, A., Robinson, L. 2013. Hydrodynamic time scales in a hyper-tidal region of fresh water influence, *Continental Shelf Research*, 63:13–22.

Plater, A., Grenville, J. 2010. Linking the eastern irish sea to the sefton coast, in Worsley, L., Newton, eds., *Proceedings of the conference on coastal geomorphology, biogeography and management 2008*, pages 28–54.

Polton, J., Palmer, M., Howarth, M. 2011. Physical and dynamical oceanography of Liverpool Bay, *Ocean Dynamics*, 61:1421–1439.

Pope, S. B. 2000. *Turbulent Flows*, 1st edn., Cambridge University Press, United Kingdom.

Prandle, D. 2009. *Estuaries*, Cambridge University Press.

Prandle, D., Lane, A., Manning, A. 2006. New typologies for estuarine morphology, *Geomorphology*, 81:309–315.

Pritchard, D. 1967a. Basic considerations. What is an Estuary: Physical Viewpoint, in Lauff, G., ed., *Estuaries*, pages 3–5, American Association for the Advancement of Science.

Pritchard, D. 1967b. Physical factors. Observations of Circulation in Coastal Plain Estuaries, in Lauff, G., ed., *Estuaries*, pages 37–44, American Association for the Advancement of Science.

Puls, W., Kuehl, H., Heymann, K. 1988. Settling velocity of mud flocs: results of field measurements in the Elbe and the Weser Estuary, in Dronkers, J., van Leussen, W., eds., *Physical Processes in Estuaries*, page 560, Springer-Verlag.

Pye, K., Blott, S. 2010. The use of sediment particle size data for coastal, estuarine and marine management purposes: an example from the ne irish sea, kenneth Pye Associates Ltd.

Rahman, R., Plater, A. 2014. Particle-size evidence of estuary evolution: A rapid and diagnostic tool for determining the nature of recent saltmarsh accretion, *Geomorphology*, X:X–X.

Reynolds, R. A., Stramski, D., Wright, V. M., Woźniak. 2010. Measurements and characterization of particle size distribution in coastal waters, *J. Geophys. Res.*, 115:1–19.

Richardson, L. 1922. *Weather Prediction by Numerical Processes*, Cambridge: Cambridge University Press.

van Rijn, L. 2005. *Principles of sedimentation and erosion engineering in rivers, estuaries and coastal seas*, Aqua Publications, Amsterdam, The Netherlands.

van Rijn, L. C. 2007a. Unified view of sediment transport by currents and waves. I: Initiation of motion, bed roughness, and bed load transport, *Journal of Hydraulic Engineering*, 133:649–667.

van Rijn, L. C. 2007b. Unified view of sediment transport by currents and waves. II: Suspended transport, *Journal of Hydraulic Engineering*, 133:668–689.

Rodi, W. 1987. Examples of calculation methods for flow and mixing in stratified fluids, *J. Geophys. Res.*, 92(C5):5305–5328.

Rouse, H. 1937. Modern concepts of the mechanics of fluid turbulence, *American Society of Civil Engineers, Transactions*, 102(1):463–543.

Saddoughi, S., Veeravalli, S. 1994. Local isotropy in bottom boundary layers at high Reynolds numbers, *Journal of Fluid Mechanics*, 268:333–372.

Sanford, L., Halka, J. 1993. Assessing the paradigm of mutually exclusive erosion and deposition of mud, with examples from upper Chesapeake Bay, *Marine Geology*, 114(1-2):37–57.

Sanford, L., Maa, J.-Y. 2001. A unified erosion formulation for fine sediments, *Marine Geology*, 179(1-2):9–23.

Schweim, C., Köngeter, J. 2008. Modelling erosion of fine sediments and the influence of time-variable stress and depth-variable resistance, in *Sediments and Ecohydraulics: INTERCOH 2005*.

SEQUOIA. 2013. *LISST-100X Particle Size Analyzer, User's Manual*, Sequoia Scientific, Inc., version 5.0 edn.

Shaw, W., Trowbridge, J., Williams III, A. 2001. Budgets of turbulent kinetic energy and scalar variance in the continental shelf bottom boundary layer, *J. Geophys. Res.*, 106(C5):9551–9564.

Sherwood, C., Lacy, J., Voulgaris, G. 2006. Shear velocity estimates on the inner shelf off Grays Harbor, Washington, USA, *Continental Shelf Research*, 26:1995–2008, doi:10.1016/j.csr.2006.07.025.

Simpson, J., Brown, J., Matthews, J., Allen, G. 1990. Tidal straining, density currents, and stirring in the control of estuarine stratification, *Estuaries*, 13(2):125–132.

Simpson, J., Burchard, H., Fisher, N., Rippeth, T. 2002. The semidiurnal cycle of dissipation in a rofi: model-measurement comparisons, *Continental Shelf Research*, 22:1615–1628.

Simpson, J., Sharples, H. 1991. *Coastal and Estuarine Studies*, chap. 6. Dynamically-active models in the prediction of estuarine stratification, pages 101–113, Dynamics and Exchange in Estuaries and the Coastal Zone, American Geophysical Union.

Simpson, J., Sharples, H., Rippeth, T. 1991. A prescriptive model of stratification induced by freshwater runoff, *Estuarine, Coastal and Shelf Science*, 33:23–35.

Simpson, J., Williams, E., Brasseur, L., Brubaker, J. 2005. The impact of tidal straining on the cycle of turbulence in a partially stratified estuary, *Continental Shelf Research*, 25:51–64, doi:10.1016/j.csr.2004.08.003.

Son, M., Hsu, T. 2011. The effects of flocculation and bed erodibility on modeling cohesive sediment resuspension, *J. Geophys. Res.*, 116(C03021):1–18.

SonTek. 2002. *SonTek ADVField Acoustic doppler Velocimeter Technical Documentation.*

Sottolichio, A., Hurther, N., D. Gratiot, Bretel, P. 2011. Acoustic turbulence measurements of near-bed suspended sediment dynamics in highly turbid waters of a macrotidal estuary, *Continental Shelf Research*, 31:S36–S49, doi:10.1016/j.csr.2011.03.016.

Soulsby, R. 1983. *Physical Oceanography of Coastal and Shelf Seas*, chap. 5. The bottom boundary layer of shelf seas, pages 189–266, Elsevier.

Soulsby, R., Humphery, J. 1990. *Water Wave Kinematics*, chap. Field observations of wave-current interaction at the sea bed, pages 413–428, Kluwer Academic Publishers, Netherlands.

Souza, A. 2013. On the use of the Stokes number to explain frictional tidal dynamics and water column structure in shelf seas, *Ocean Sciences*, 9:391–398, doi:10.5194/os-9-391-2013.

Souza, A., Bolaños, R., Wolf, J., Prandle, D. 2011. *Measurement Technologies: Measure What, Where, Why, and How?*, vol. 2 of *Treatise on Estuarine and Coastal Science*, Waltham: Academic Press., pp. 361-394.

Souza, A. J., Dickey, T. D., Chang, G. C. 2001. Modeling water column structure and suspended particulate matter on the middle atlantic continental shelf during the passages of hurricanes edouard and hortense, *Journal of Marine Research*, 59:1021–1045.

Souza, A. J., Lane, A. 2013. Effects of freshwater inflow on sediment transport, *Journal of Operational Oceanography*, 6(1):27–31.

Spearman, J., Manning, A. J. 2008. On the significance of mud transport algorithms for the modelling of intertidal flats, in *Sediments and Ecohydraulics: INTERCOH 2005.*

Stanev, E., Brink-Spalink, G., Wolff, O. 2007. Sediment dynamics in tidally dominated environments controlled by transport and turbulence: A case study for the east frisian wadden sea, *J. Geophys. Res.*, 112(C04018):1–20, doi:10.1029/2005JC003045.

Stanev, E., Wolff, O., Brink-Spalink, G. 2006. On the sensitivity of the sedimentary system in the east frisian wadden sea to sea-level rise and wave-induced bed shear stress, *Ocean Dynamics*, 56:266–283, dOI 10.1007/s10236-006-0061-6.

Stapleton, K., Huntley, D. 1995. Seabed stress determinations using the inertial dissipation method and the turbulent kinetic energy method, *Earth Surface Processes and Landforms*, 20:807–815.

Steers, J. 1967. Geomorphology and Coastal Processes, in Lauff, G., ed., *Estuaries*, pages 100–107, American Association for the Advancement of Science.

Strom, K., Keyvani, A. 2011. An explicit full-range settling velocity equation for mud flocs, *Journal of Sedimentary Research*, 81:921–934, dOI: 10.2110/jsr.2011.62.

Styles, R. 2006. Laboratory evaluation of the lisst in a stratified fluid, *Marine Geology*, 227:151–162, doi:10.1016/j.margeo.2005.11.011.

Tambo, N., Watanabe, Y. 1979. Physical chracteristics of flocs-I. the floc density function and aluminium floc, *Water Research*, 13:409–419.

Tennekes, H., Lumley, J. 1972. *A First Course in Turbulence*, The Massachusetts Institute of Technology.

Thorne, P., Hanes, D. 2002. A review of acoustic measurement of small-scale sediment processes, *Continental Shelf Research*, 22:603–632.

Thorne, P., Hurther, D. 2014. An overview on the use of backscattered sound for measuring suspended particle size and concentration profiles in non-cohesive inorganic sediment transport studies, *Continental Shelf Research*, 73:97–118, doi.org/10.1016/j.csr.2013.10.017.

Thurston, W. 2009. *Turbulence as a mediator of processes in a macrotidal estuary*, Ph.D. thesis, University of Leeds, School of Earth and Environment, Leeds, UK.

Todd, D. 2014. *Temporal variability of suspended particulate matter in a tidal estuary*, Ph.D. thesis, University of Bangor, Bangor, UK.

Turner, A., Millward, G., Tyler, A. 1994. The distribution and chemical composition of particles in a macrotidal estuary, *Estuarine, Coastal and Shelf Science*, 38:1–17.

Umlauf, L., Burchard, H. 2005. Second-0rder turbulence closure models for geophysical boundary layers. a review of recent work, *Continental Shelf Research*, 25:795–827.

Umlauf, L., Burchard, H., Bolding, K. 2012. *GOTM - source code and test case documentation*, Tech. rep., Leibiniz-Institute for Baltic sea Research, Warnemünde, Germany, version 4.0.

UN. 2011. World urbanizations prospects: The 2011 revision, United Nations Department of Economics and Social Affairs/Population Division, pages 318.

Valle-Levinson, A. 2010. *Contemporary Issues in Estuarine Physics*, Cambridge University Press, 315 pages.

Verney, R., Brun-Cottan, J., Lafite, R., Deloffre, J., Taylor, J. 2006. Tidally-induced shear stress variability above intertidal mudflats in the macrotidal Seine Estuary, *Estuaries and Coasts*, 29(4).

Verney, R., Deloffre, J., Brun-Cottan, J., Lafite, R. 2007. The effect of wave-induced turbulence on intertidal mudflats: Impact of boat traffic and wind, *Continental Shelf Research*, 27.

Verney, R., Lafite, R., Brun-Cottan, J. 2009. Flocculation potential of estuarine particles: The importance of environmental factors and of the spatial and seasonal variability of suspended particulate matter, *Estuaries and Coasts*, 32:678–693, dOI 10.1007/s12237-009-9160-1.

Verney, R., Lafite, R., Brun-Cottan, J., Le Hir, P. 2011. Behaviour of a floc population during a tidal cycle: laboratory experiments and numerical modelling, *Continental Shelf Research*, 31:S64–S83.

Verspecht, F., Rippeth, T., Howarth, M., Souza, A., Simpson, J., Burchard, H. 2009a. Processes impacting on stratification in a region of freshwater influence: Application to liverpool bay, *J. Geophys. Res.*, 114(C11022), doi:10.1029/2009JC005475.

Verspecht, F., Rippeth, T., Simpson, J., Souza, A., Burchard, H., Howarth, M. 2009b. Residual circulation and stratification in the liverpool bay region of freshwater influence, *Ocean Dynamics*, 59:765–779, dOI 10.1007/s10236-009-0233-2.

Voulgaris, G., Meyers, S. 2004. Temporal variability of hydrodynamics, sediment concentration and sediment settling velocity in a tidal creek, *Continental Shelf Research*, 24:1659–1683, doi:10.1016/j.csr.2004.05.006.

Voulgaris, G., Trowbridge, J. 1998. Evaluation of the acoustic doppler velocimeter (adv) for turbulence measurements, *Journal of Atmospheric and Oceanic Technology*, 15(1):272–289.

Wang, Y., Voulgaris, G., Li, Y., Yang, Y., Gao, J., Chen, J., Gao, S. 2013. Sediment resuspension, flocculation, and settling in a macrotidal estuary, *J. Geophys. Res.*, 118:5591–5608, i:10.1002/jgrc.20340.

Wiberg, P., Sherwood, C. 2008. Calculating wave-generated bottom orbital velocities from surface-wave parameters, *Computers & Geosciences*, 34:1243–1262, doi:10.1016/j.cageo.2008.02.010.

van Wijngaarden, M., Roberti, J. 2002. In-situ measurements of settling velocity and particle size distribution with the lisst-st, in Winterwerp, J., Kranenburg, C., eds., *Fine Sediment Dynamics in the marine Environment*, vol. 5 of *Proceedings in Marine Science*, pages 295–311, Elsevier.

Williams, J., Rose, C., Thorne, P., O'Connor, B., Humphery, J., Hardcastle, P., Moores, S., Cooke, J., Wilson, D. 1999. Field observations and predictions of bed shear stresses and vertical suspended sediment concentration proles in wave-current conditions, *Continental Shelf Research*, 19:507–536.

Winterwerp, J. C. 1998. A simple model for turbulence induced flocculation of cohesive sediment, *Journal of Hydraulic Research*, 36:309–326.

Winterwerp, J. C. 2002. On the flocculation and settling velocity of estuarine mud, *Continental Shelf Research*, 22:1339–1360.

Winterwerp, J. C., van Kesteren, W. G. M. 2004. *Introduction to the physics of cohesive sediment in the marine environment*, 1st edn., Elsevier, B. V., Amsterdam, The Netherlands.

Winterwerp, J. C., Manning, A. J., Martens, C., de Mulder, T., Vanlede, J. 2006. A heuristic formula for turbulence-induced flocculation of cohesive sediment, *Estuarine, Coastal and Shelf Science*, 68:195–207.

Wolf, J., Brown, J., Howarth, M. 2011. The wave climate of liverpool bay - observations and modelling, *Ocean Dynamics*, 61(5):639–655, doi:10.1007/s10236-011-0494-4.

Yuan, Y., Wei, H., Zhao, L., Yiang, W. 2008. Observations of sediment resuspension and settling off the mouth of Jiaozhou Bay, Yellow Sea, *Continental Shelf Research*, 28:2630–2643.